UNIVERSITÉ DE STRASBOURG

ÉCOLE DOCTORALE- Physique et Chimie-Physique

Institut de Chimie et Procédés pour l'Energie, l'Environnement et la Santé – UMR 7515 CNRS

THÈSE présentée par :

Dhiraj Kumar GARG

soutenue le : **14 Mars 2014**

pour obtenir le grade de : **Docteur de l'université de Strasbourg**

Discipline / Spécialité : Génie des procédés / Simulation de procédés

Numerical modeling and simulation of polymerization reactions in Coiled Flow Inverters

THÈSE dirigée par :
  M. C.A. SERRA Professeur, Université de Strasbourg
Co-encadrant :
  M. Y. HOARAU Maître de Conférences, HDR, Université de Strasbourg
RAPPORTEURS :
  Mme. N. SHEIBAT - OTHMAN Chargé de Recherches, HDR, CNRS - LAGEP Lyon
  M. S. ZHU Professeur, McMaster University (Canada)

AUTRES MEMBRES DU JURY :
  M. A. DURAND Professeur, Université de Lorraine
  M. Y. REMOND Professeur, Université de Strasbourg

Abbreviations and Notations

Abbreviations

AIBN	2,2′-Azobis(2-methylpropionitrile)
AK	Achilias & Kiparissides
AS	Analytical Solution
ATRP	Atom Transfer Radical Polymerization
BuA	Butyl Acrylate
BPO	Benzoyl Peroxide
CCS	Chiu Carrat Soong
CFD	Computation Fluid Dynamics
CFI	Coiled Flow Inverter
CFIR	Coiled Flow Inverter Reactor
CT	Coil Tube
CTR	Coil Tube Reactor
FRP	Free Radical Polymerization
FVT	Free Volume Theory
MMA	Methyl Methacrylate
NS	Numerical Solution
PBuA	Poly- Butyl Acrylate
PMMA	Poly-Methyl Methacrylate
PS	Polystyrene
PVAc	Poly- Vinyl Acetate
QSSA	Quassi Steady State Assumption
RTD	Residence Time Distribution
St	Styrene
ST	Straight Tube
STR	Straight Tube Reactor
VAc	Vinyl Acetate

Notations

A	Chain transfer agent concentration at any time t, mol/l
$A1$	A parameter of CCS model
A_H	Area for heat transfer, m^2
A_s	Proportionality parameter, $A_{s,L}, A_{s,U}, A_{s,avg}$ are lower, upper and average value respectively.
$B1$	A parameter of CCS model
B_{n-1}	$= \sqrt{\frac{8f[K_{pr}]^2 I_{n-1}}{K_d K_t}}$, Constant in the analytical solution at the beginning of $(n-1)^{th}$ time step
$C1$	A parameter of CCS model
C_A	$= \frac{K_{fa}}{K_p}$, dimensionless
C_b	Bulk monomer concentration, mol/l
C_M	$= \frac{K_{fm}}{K_p}$, dimensionless
C_{n-1}	$= 2B_{n-1} \cdot \sqrt{\frac{.[V_R]_{n-1}}{.[V_R]_0}}$, Constant in the analytical solution at the beginning of $(n-1)^{th}$ time step
Cp	Specific heat capacity of mixture, $cal/g/°C$
C_S	$= \frac{K_{fs}}{K_p}$, dimensionless
C_T	$= \frac{K_{td}}{K_{tc}}$, dimensionless
D_{eff}	Effective diffusion coefficient, m^2/s
D_{i0}	Pre-exponential factor of diffusion coefficient of chemical species i (i=M, P, I) cm^2/s
D_i	Diffusion coefficient of chemical species i (i=M, P, I) cm^2/s
D_{n-1}	$= \frac{2(K_{pr}M_{n-1})^2}{K_t K_d} e^{-C_{n-1}}$, Constant in the analytical solution at the beginning of $(n-1)^{th}$ time step
DP_n	Number averaged degree of polymerization
E_{d0}	Activation energy for dissociation rate constant, cal/mol
F_{seg}	Probability of two radicals to react when their active centers come into close proximity
G_{ij}	Binary interaction parameter for the two mixture components i and j
I	Initiator concentration, mol/l
J_{n-1}	$= \frac{4}{R_P}\left(\frac{R_T}{R_P}(1 + R_{SA}) + 1\right) \cdot \frac{\sqrt{K_t}}{K_d}\left[\frac{(2fK_d I_{n-1})^{\frac{3}{2}}}{K_{pr}M_{n-1}}\right]$, Constant in the analytical solution at the beginning of $(n-1)^{th}$ time step
K_{MH}	Mark-Mouwink constant, dl/g
$K1$	Transfer to monomer rate coefficient, $l/(mol.min)$
$K2$	Transfer to monomer rate coefficient, $l/(mol.min)$

K_d	Dissociation rate coefficient, min^{-1}
K_{d0}	Pre-exponential factor of K_d, dissociation rate coefficient, min^{-1}
K_{fa}	Transfer to CTA rate coefficient, l/(mol.min)
K_{fm}	Transfer to monomer rate coefficient, l/(mol.min)
K_{fs}	Transfer to solvent rate coefficient, l/(mol.min)
K_i	Kinetic rate constant for initiation, s^{-1}
K_p	Propagation rate coefficient, l/(mol.min)
K_p^0	Propagation rate coefficient at time $t = 0$, l/(mol.min)
K_{pr}	$= K_p + K_{fm} = (1 + C_M)K_p$, l/(mol.min)
K_t	$= K_{tc} + K_{td}$, l/(mol.min)
K_t^0	Termination rate coefficient at time $t = 0$, l/(mol.min)
K_{tc}	Termination by combination rate coefficient, l/(mol.min)
K_{td}	Termination by disproportionation rate coefficient, l/(mol.min)
$K_{t,res}$	Residual termination rate constant, l/(mol.min)
L	Kinetic chain length, $= \frac{K_{pr}M\lambda_0}{2fK_dI}$
$\bar{L}$	$= L.\left(\frac{1 - R_{MM}}{1 + R_PL}\right) = L.\left(\frac{1 - R_M}{1 + R_PL}\right)$
M	Monomer concentration, mol/l
M_{ji}	Molecular weight of jumping unit of chemical species I (i=M,P,S,I), g/mol
MW	Molecular weight, g/mol
MW_n	Number averaged chain length of polymer, g/mol
MW_w	Weight averaged chain length of polymer, g/mol
N_A	Avogadro constant, $6.023x10^{23}$, mol^{-1}
P	$= \frac{2}{(R_L + 1)} + \frac{R_T}{(R_L + 1)^2}$, Parameter in the analytical solution
PDI	Polydispersity index, dimensionless
P_n	Dead polymer chain length of n no. of monomer units
Q_{n-1}	$= \frac{2R_T}{R_P^2}.\frac{K_t}{K_d}\left[\frac{(2fK_dI_0)^2}{(K_{pr}M_n)^2}\right]$, Constant in the analytical solution at the beginning of $(n - 1)^{th}$ time step
R	Universal gas constant, 1.986 cal/mol/K
R_0	Zero order radical obtained from initiator dissociation
R_A	$= \frac{C_A}{1 + C_M} = \frac{K_{fa}}{K_{pr}}$
R_{AM}	$= \frac{C_A}{1 + C_M}\frac{A}{M} \approx \frac{C_A}{1 + C_M}\frac{A_0}{M_0}$
R_H	Hydrodynamic radius of polymer
R_L	$= R_PL$, Parameter in the analytical solution
R_M	$= \frac{K_{fm}}{K_p + K_{fm}} = \frac{K_{fm}}{K_{pr}} = \frac{C_M}{1 + C_M}$
R_{MM}	$= R_M$
R_n	Live polymer chain length of n no. of monomer units
R_P	$= R_{MM} + R_{SM} + R_{AM} = R_{MM} + R_{SA}$

R_S	$= \dfrac{C_S}{1+C_M} = \dfrac{K_{fs}}{K_{pr}}$
R_{SA}	$= R_{SM} + R_{AM}$
R_{SM}	$= \dfrac{C_S}{1+C_M}\dfrac{S}{M} \approx \dfrac{C_S}{1+C_M}\dfrac{S_0}{M_0}$
R_T	$= \dfrac{K_{tc}}{K_{tc}+K_{td}} = \dfrac{K_{tc}}{K_t} = \dfrac{1}{1+C_T}$, dimensionless
S	Solvent concentration any time t, mol/l
T	Temperature, K
T'	$= T - T_{bath}$, K
T_{bath}	Temperature of heat sink, K
T_{gi}	Glass temperature of chemical species i (i=M,P,S,I), K
U	Overall heat transfer coefficient, W/m2/K
V_m	Monomer volume, cm^3
V_f	Free volume, dimensionless
V_i^*	Specific critical hole free volume of species i (i=M,P,S,I), cm^3/g
V_R	Volume of solution at any time t, liter
V_{R0}	Initial volume of solution at t_0, liter
X_{C0}	Critical degree of polymerization for entanglement of pure polymer
a_{MH}	Mark –Houwink constant, dimensionless
a_{seg}	Parameter depending on initiator type and mixture composition
f	Initiator efficiency, dimensionless
f_s	Solvent volume fraction, dimensionless
j_c	Entanglement spacing between polymer chains
k_B	Boltzmann constant, $1.3806x10^{-23}$ J/K
r_1, r_2	Effective reaction radius, cm
r_e	Kuhn's segment length, $A°$
r_m, r_t	Radius of reaction between polymer radical and monomer
t	Time , min
x_M	Monomer conversion, dimensionless
y	$= e^{\frac{-K_d.t}{2}}$, Variable evaluated in the analytical solution
ΔH_P	Heat of reaction, cal/mol
β	Ratio of solvent volume to non-solvent volume, dimensionless
ε	Volume contraction factor corrected for solvent volume fraction, dimensionless
ε_0	Volume contraction factor without solvent volume fraction, dimensionless
ε_i	$= K_{i0}/K_{p0}$
λ_0	Zeroth order moment for live polymer chain concentration, mol/l
λ_1	First order moment for live polymer chain concentration, mol/l
λ_2	Second order moment for live polymer chain concentration, mol/l
μ_0	Zeroth order moment for dead polymer chain concentration, mol/l
μ_1	First order moment for dead polymer chain concentration, mol/l

μ_2	Second order moment for dead polymer chain concentration, mol/l
ρ	Mixture density, g/cm3
Φ	Volume fraction, dimensionless
Θ_t	Parameter defined for gel effect in CCS model
Θ_p	Parameter defined for glass effect in CCS model
δ	Average root-mean-square end-to-end distance of polymer chain, A°
η_M	Dynamic viscosity of monomer, cP
$[\eta]$	Intrinsic viscosity of the polymer, dl/g
σ	Lennard Jones radius, A°
γ	Overlap factor, dimensionless
ω	Weight fraction, dimensionless
ξ_{iP}	Ratio of the critical molar volume of the jumping unit of chemical species i to the critical molar volume of the polymer
τ	Characteristic time
Subscript	
M	Monomer
P	Polymer
S	Solvent
I	Initiator
n	At the beginning of nth time step
0	At time t=0

Acknowledgement

When I came to France, I observed the national motto of France- "Liberté, Egalité, Fraternité". The first word –"Liberté" is of paramount importance. In English, it means Liberty. Indian tradition, culture and philosophy also give similar stress to the importance of Liberty- liberation from all worldly things in following words-

"**Tamso Ma Jyotir Gamya**   (Take (me) from darkness to light)

Asato Ma Sat Gamya   (Take (me) from untruth to truth)

Mrityor Ma Amritam Gamya"   (Take (me) from death to eternity)

We can easily observe that there is desire to liberate from darkness, untruth and death and this can happen only through knowledge whose importance can well be represented from following shlok in indian philosophy-

"**Yeshaam na vidya na tapo na danam, Gyanam na sheelam na gunon na dharmah**

Tey mrityulokey bhuvi bhaar bhoota, Manushya rupen mrigash charanti"

"Those who do not have education, nor have experience, nor have a giving heart, Lack knowledge, have no patience, do not have any qualities nor have sense of duty, Such people, in this mortal world, are nothing but a burden on Earth. They are like animals (antelop) grazing in the form of Humans."

So, in pursuit of this goal of gaining knowledge, I pursued PhD which is the highest level of gaining formal knowledge on any topic although it is not an end or obstacle for gaining further knowledge throughout life. The pursuit of knowledge can only be through an honest search- search using a free, open, questioning and unbiased mind. And a Guru can help in this endeavor by developing our mind in this way and also by guiding us through the low times. That is why Guru is given a very high status in indian culture, society and philosophy as can be seen in following shlok:

"**Gurur Brahma, Gurur Vishnuhu, Guru Devo Maheshwaraha**

Guru Saakshaat Parabhrahma, Tasmai Shri Gurave Namaha"

"The true meaning of Guru is "one who dispels darkness of ignorance". Guru resembles the trinity Brahma, Vishnu and Shiva. Brahma is creator. Guru creates or inculcates knowledge in the minds of the students. Guru is Vishnu. Lord Vishnu maintains the creation. Similarly Guru helps in keeping up the knowledge. Guru is like Shiva. Shiva is the destroyer. Guru destroys or gets rid of the ignorance from the students' minds."

PhD is a multi-disciplinary approach towards any problem and is always a massive task requiring the synergetic efforts from several people to make it successful. No single person can achieve it otherwise, how-so-ever good he/she may be. So it would be highly ungreatful or rather sinful on my part not to acknowledge the direct or indirect contribution by various

persons to this great effort making it successful. So I would like to take extreme pleasure to thanks my teachers during my school and college days (they were actually educationists in true sense) which not only shaped my views towards life and science by allowing and promoting free and rational thinking in me but also educated me about the very purpose of knowledge. I would like to thank particularly to Mrs. Swati, Mrs. Aruna and Mr. Jitender (DMS) and Mr. Sudeesh (GFPS) and several other teachers during my school days for guiding me in the right direction which enabled me to be what I am and where I am today. Their teachings are like stones in the foundation- not visible from outside but always give the strength to the structure under all conditions. I would also like to thank Pr. U.K.Mandal, Dr. B.Sarkar, Pr. S.S.Sambi, (GGSIPU) Pr. Vasudeva, Pr. T.R.Rao and Pr. D.P.Rao (IITD) for not only guiding me in my professional expertise of chemical engineering but also helped in becoming a better person. I should actually thank to God for bringing Pr. C.A.Serra and Dr. Y.Hoarau as my director and co-director respectively for my PhD thesis. I shall always be grateful to them for their unconditional support and cooperation and for allowing me to think and work freely and independently during my work. It was only due to this that I could achieve whatever I could do in this PhD. Besides this, they also inculcated several good habits and views towards science in me which are definitely going to help me in future in becoming not only good scientist but also good person. I will always remain indebted to them for whatever they have done for me and given me.

Whenever I felt low in my life, I always looked at my parents. This life always motivated me and saying that my parents are my role models will not be exaggeration. I would also like to thank my parents and family for not only providing me all the moral and psychological support but also their love which never let me felt alone despite such a huge physical separation. I would also like to express my sincere thanks to my friends (especially Atul & Vikrant) who were present through various phases of my life-good and bad. Their presence lessens the bitterness of the pain and increased the sweetness of joy. I would also like to thank various friends (Srikant Reddy, Vikrant Verma, Jogender & Sunil) who provided me papers as and when required. Without their help, it would really be impossible to finish the work on time. I would also like to express my gratitude to Dambarudhar Parida, Rahul, Siddharth, Debashish, Heena and Thanuja and all friends from Strasbourg and around for providing me homely environment here far away from my home. Without this, it would have been a horrible lonely life. I would also like to thank my lab-mates especially Thibaut, Marcin and Anthony without whose help it would be impossible for me to carry out my work in lab and Strasbourg smoothly. The efforts and cooperation of secretariat, ICUBE (ex-IMFS) also cannot be forgotten and is duly acknowledged.

Place: **Strasbourg, France**

Date: **14/03/14**   **Dhiraj Kumar Garg**

Résumé de Thèse

Modélisation numérique et simulation de réactions de polymérisation

dans des réacteurs à inversion de flux

1. Introduction

Cette thèse vise à améliorer la modélisation et la simulation de la polymérisation radicalaire (FRP) aussi bien dans des réacteurs discontinus que dans des réacteurs continus. Ces améliorations ont ensuite été utilisées pour évaluer trois géométries de microréacteurs tubulaires dans différentes conditions d'alimentation à très faible nombre de Reynolds (Re ≤ 1). La modélisation de la FRP considérée ici a pris en compte successivement des paramètres thermo-physiques constants pour les fluides puis leur variation en fonction de la conversion du monomère. Les effets de ces deux approches sur les résultats de la simulation ont été observés et comparées avec les données expérimentales de la littérature pour différents monomères. Une étude plus spécifique sur les effets de diffusion obtenus en faisant varier le coefficient de diffusion des espèces réactives de façon discrète ainsi que de façon continue a également été effectuée. Les trois géométries de microréacteurs considérées furent un réacteur tubulaire droit (STR), un réacteur tubulaire hélicoïdal (CTR) et un réacteur à inversion de flux (CFIR). Les conditions d'alimentation à l'entrée du microréacteur ont été choisies telles que les flux de réactifs furent non mélangés ou parfaitement mélangés. Plusieurs monomères du plus lent au plus rapide ont été considérés au cours de cette étude : le styrène (St), le méthacrylate de méthyle (MMA) pour les réacteurs discontinus et continus, l'acrylate de butyle (ABu) et l'acétate de vinyle (VAc) seulement pour le réacteur dicontinu.

2. Solution analytique pour la polymérisation radicalaire : Développement et Validation

Dans cette thèse, l'une des principales réalisations est la dérivation d'une solution analytique exacte généralisée du modèle mathématique d'homopolymérisation radicalaire. Les étapes de la polymérisation considérées furent l'initiation, la propagation, le transfert au monomère, le transfert au solvant et aux agents de transfert, la terminaison par combinaison et par dismutation. Cela constitue un panel assez large et réaliste d'étapes tant du point de vue théorique que pratique. Les hypothèses pour le calcul furent : température constante, coefficients cinétiques constants et état quasi stationnaire (QSSA) pour les moments d'ordre zéro, un et deux de la distribution des longueurs de chaînes des polymères vivants. Le modèle mathématique fut basé sur la méthode des moments qui est très largement établie et acceptée dans ce domaine.

Les hypothèses de température constante et QSSA ne sont toutefois pas restrictives quant à l'utilisation théorique ou pratique de la solution analytique ainsi dérivée. En effet, la plupart des expériences pratiques sont conduites dans des conditions isothermes. L'hypothèse de QSSA est mise en défaut seulement pour de grands taux de conversion mais dans ce cas a un effet minime sur les prédictions. L'hypothèse de coefficients constants est de nature restrictive dans une certaine mesure, car elle permet l'utilisation de la solution seulement avant l'effet de gel. Cet effet apparait à cause de la diminution des coefficients cinétiques des réactions de terminaison et de propagation en fonction de la conversion du monomère sous l'effet de

l'augmentation de la viscosité du milieu réactionnel. Ainsi, la solution analytique dans sa forme actuelle peut être utilisée avant cet effet de gel.

La solution analytique (AS) a été validée en comparaison avec une solution numérique (NS) obtenue à partir du même modèle mathématique (Fig. 1). Cette solution analytique a permis d'identifier les raisons pour lesquelles il est plus facile de corréler et de prédire MW_n par des méthodes empiriques ou semi-empiriques mais plus difficile de prédire MW_w et l'indice de polymolécularité (PDI). Ceci est dû à la coexistence de trois cas différents pour déterminer la valeur de μ_2 (2sd moment de la distribution des longueurs de chaînes des polymères morts) sur la base de la valeur du paramètre R_L issu du développement analytique. Par souci de clarté, les résultats du modèle analytique pour ces trois cas sont comparés à la solution numérique sur la figure 2. La solution analytique a également été validée par comparaison avec des solutions numériques ainsi que des données expérimentales avant le début de l'effet de gel pour quatre cas différents de systèmes monomère-polymère tel que mentionné dans l'introduction. Seuls les résultats du MMA sont présentés ici dans la figure 3.
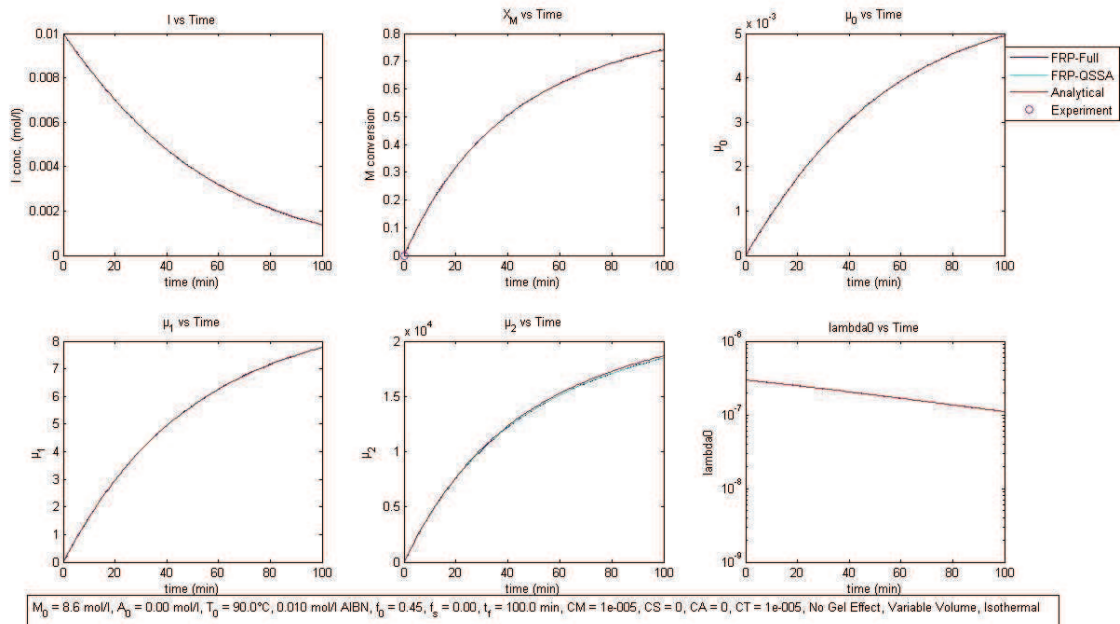
Fig. 1- Comparaison entre l'AS et la solution numérique pour le cas général de la polymérisation isotherme en masse sans processus de transferts

12
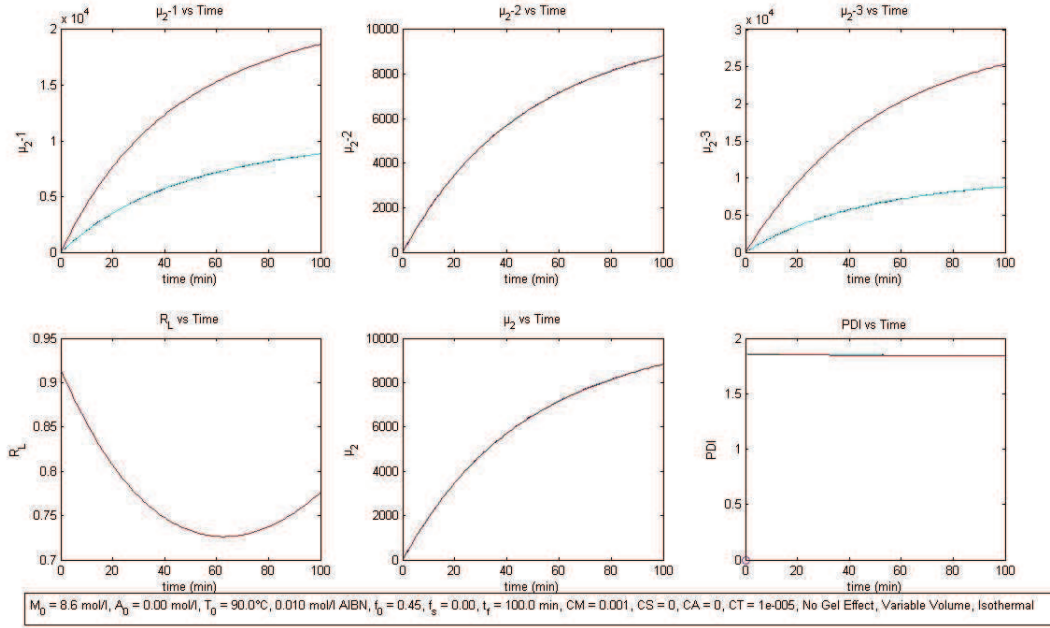
Fig. 2- Cas 2: $0.1 \leq R_L < 10$ pour le cas général de polymérisation isotherme en masse avec en considérant seulement le processus de transfert au monomère
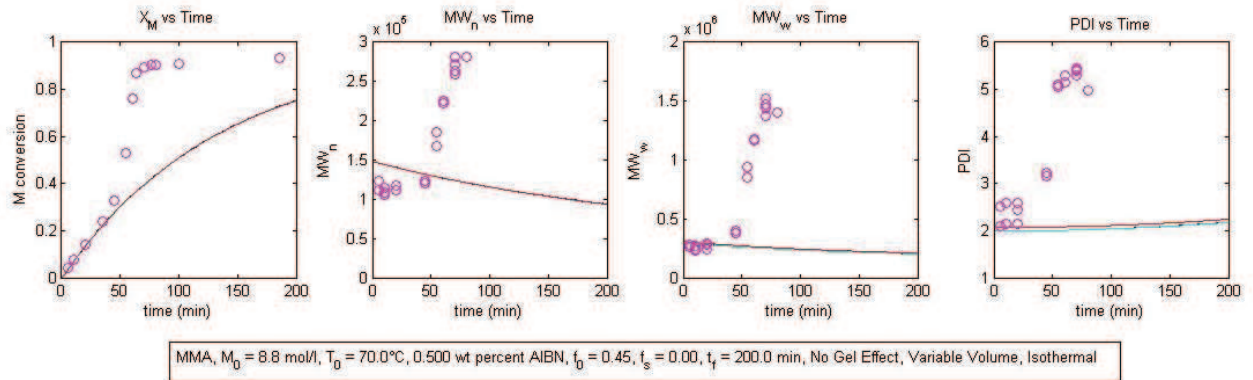
Fig. 3- Cas de la polymérisation en masse du MMA[1] $T = 70°C$

Nous avons constaté que les paramètresR_F et L apparaissant dans la solution analytique pour le cas sans effet de gel (phase I) étaient similaires aux deux paramètres β et γ^{-1} donnés par Soh *et al.*[2], qui conditionnent les effets de gel et de verre (Phase II à IV). En outre, la solution analytique a montré que ces deux paramètres affectent également les quatre phases de la réaction et qu'ils ont une signification physique importante. Deux autres paramètres, R_L et R_T, apparaissant naturellement dans la AS sont similaires à ceux donnés par Zhu *et al.*[3] pour la prédiction de l'effet de gel. Contrairement à ce qu'il était envisagé, il a également été constaté que l'équation de conservation de l'énergie était la véritable source de rigidité dans le modèle actuel sans effet de gel / verre. Nous avons également montré pourquoi et dans quelle proportion l'équation de l'énergie est sensible aux variations de température ainsi qu'au temps (c-à-d à la conversion du monomère).

La solution analytique ne nécessite que des données physiques et chimiques du système monomère / polymère étudié. Il n'y a pas de paramètres ajustables de corrélation. Seul

l'efficacité de l'amorceur doit être modifiée une seule fois pour correspondre aux données expérimentales, puis il reste constant pour le système monomère / polymère. La AS est très pratique et les seuls paramètres d'entrée nécessaires sont le temps et la température initiale. Il peut facilement être mis en œuvre dans tout programme informatique ou une simple feuille Excel contrairement aux modèles précédents[4]. Cette AS a le potentiel pour être utilisé dans diverses applications pratiques comme les modèles de contrôle de procédés, les simulations CFD etc.

3. Implémentation de l'effet de gel basé sur le modèle de Chiu, Carratt & Soong (CCS)

Il existe différents modèles de prédiction de l'effet de gel allant des modèles empiriques, semi-empiriques aux modèles semi- théoriques ou théoriques avec différents degrés de sophistication. Les deux modèles théoriques les plus utilisés sont le modèle CCS (Chiu, Carratt et Soong[5]) sur la base de la théorie de la reptation et un autre basé sur la théorie du volume libre. Ce dernier est bien plus complexe que le premier mais a l'avantage d'avoir une base théorique plus large et ne nécessite donc presque aucun paramètre ajustable. De son côté le modèle CCS nécessite un "calage" numérique des données expérimentales pour générer des valeurs réelles des variables utilisées pour chaque monomère étudié. Ainsi ces valeurs de la courbe d'ajustement peuvent ne pas être disponibles pour tous les cas souhaités et le "calage" peut être approximatif en l'absence de grande quantité de données expérimentales. Par opposition, tous les paramètres nécessaires pour la théorie du volume libre sont relatifs à différentes propriétés physiques / chimiques du monomère et de son polymère et sont donc facilement disponibles dans la littérature. Les résultats incorporant la méthode CCS pour introduire la modélisation de l'effet du gel sont présentés sur la figure 4 pour le MMA et sur la figure 5 pour le MMA avec agent de transfert. Ainsi les résultats présentés dans ce travail ont démontré la supériorité de notre solution analytique sur celle proposée par Venkateshwaran *et al.*[4] dans des conditions similaires de simulation l'effet de gel en utilisant le modèle CCS dans des conditions isothermes.
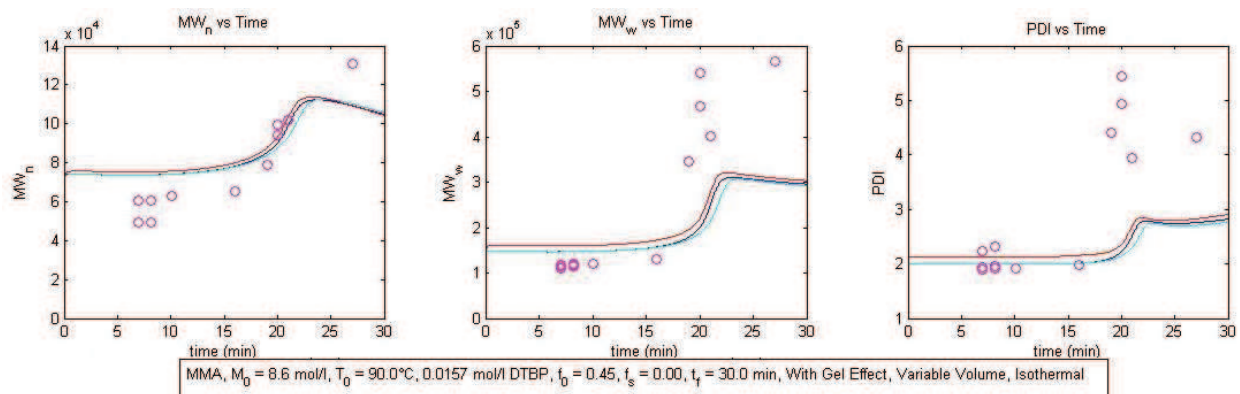
Fig. 4- Résultat du modèle CCS pour le MMA[1]- MW_n, MW_w, PDI

14
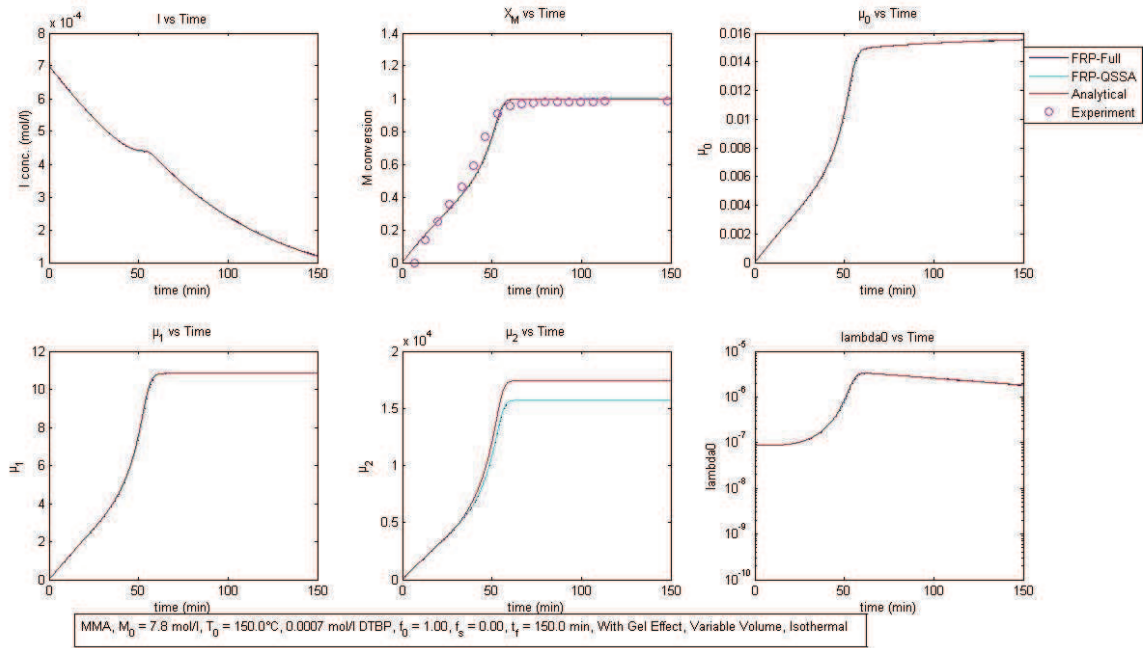
Fig. 5- Résultat du modèle CCS pour le MMA[6] avec agent de transfert-I, x_m, μ_0, μ_1, μ_2, λ_0

4. Implémentation de l'effet de gel basé sur le modèle de Achilias & Kiparissides (AK)

Les limitations concernant le modèle de CCS ont été surmontées en le remplaçant par le modèle plus évolué de Achilias et Kiparissides[7] (AK) qui en est une extension naturelle. Le modèle AK utilise la théorie du volume libre pour les effets de diffusion et par conséquent est en mesure de tenir compte également l'effet de cage (diminution de l'efficacité de l'amorceur). Il intègre aussi l'effet de la longueur de la chaîne sur les coefficients cinétiques des réactions de terminaison. Les résultats de la solution analytique basée sur le modèle AK ont été améliorés par rapport au modèle CCS et sont en bon accord avec les données expérimentales ainsi que les solutions numériques. Les résultats pour le MMA sont présentés sur la figure 6 et la figure 7. La bonne adéquation démontre la grande flexibilité de l'AS par rapport à l'intégration explicite de différents modèles d'effets de gel / verre et cage. Nous pensons qu'il serait possible d'améliorer les résultats en intégrant explicitement de meilleurs modèles quand ils sont disponibles à l'avenir ou bien d'utiliser notre AS pour le développement de nouveaux modèles.
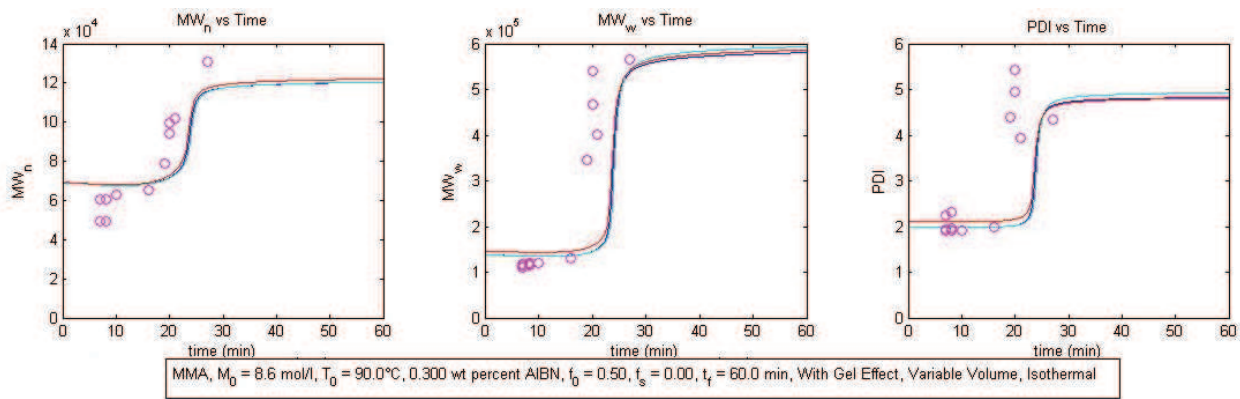
Fig. 6- Résultat avec le modèle AK pour le MMA[1]- MW_n, MW_w, PDI[13]
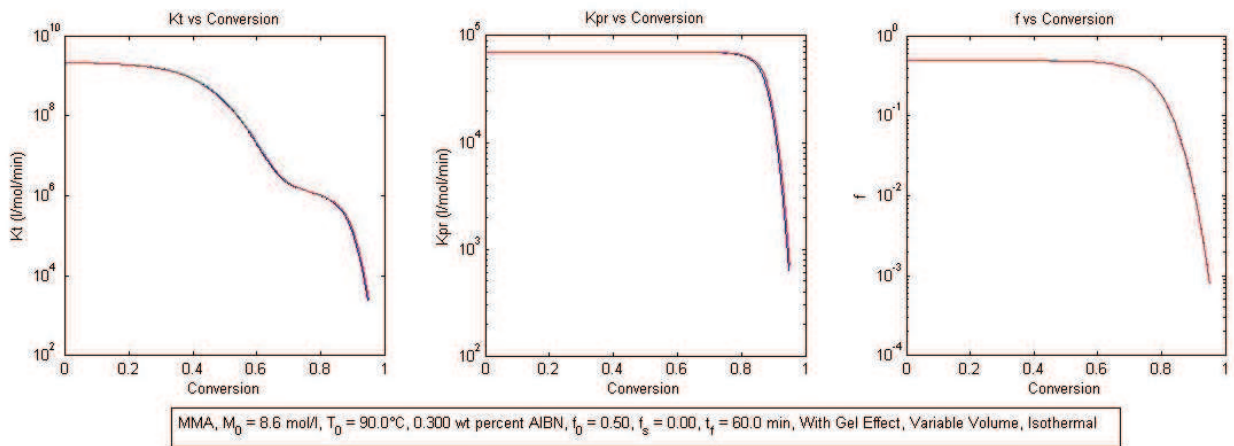
Fig. 7- Résultat avec le modèle AK pour le MMA- K_t, K_{pr}, f

5. Implémentation des effets de la variation de température

Enfin la solution analytique a été utilisée pour simuler les effets non-isothermes. Les conditions utilisées impliquèrent une vitesse finie de transfert de chaleur et l'état adiabatique, c'est à dire pas de transfert de chaleur à la paroi. Les résultats ont été obtenus en résolvant l'équation différentielle du bilan énergétique qui prit ses données d'entrée de la AS lors de l'incorporation des modèles CCS et AK. Les résultats ont été comparés avec des solutions numériques et furent en bon accord avec les données publiées dans la littérature. Les résultats du MMA dans des conditions non-isothermes sont donnés dans les figures 8 et 9. Avec cette dernière modification, la solution analytique s'est finalement avérée être meilleure en comparaison des travaux antérieurs de Ventakeshwaran *et al.*[4] pour tous les cas de figure testés.
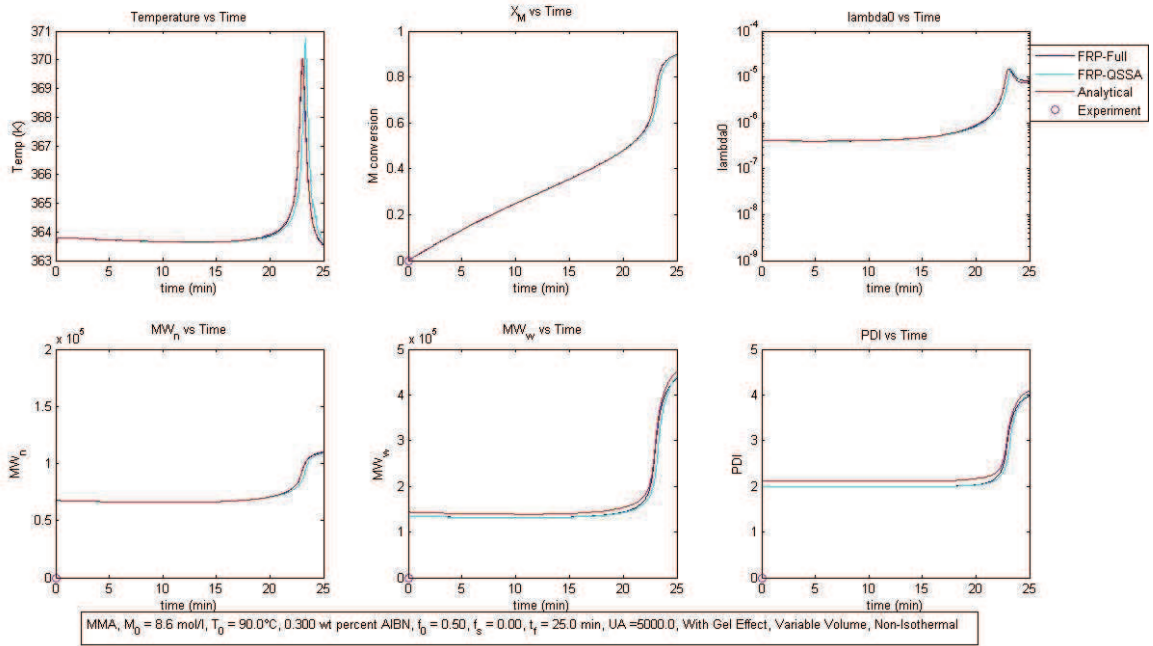
Fig. 8- MMA- Résultats obtenus pour des variations de température avec $UA = 5000\ cal/ min/K$ et prise en compte des effets de gel/verre/cage basé sur le modèle AK
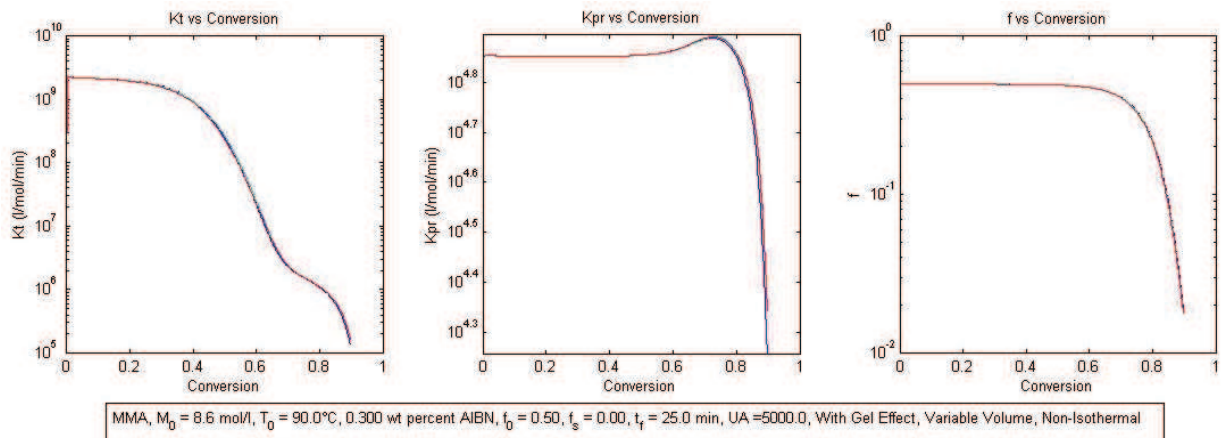
Fig. 9- MMA- Résultats obtenus pour K_t, K_{pr}, f pour des variations de température avec $UA = 5000\ cal/min/K$ et prise en compte des effets de gel/verre/cage basé sur le modèle AK

6. Conclusion sur la solution analytique

Nous avons ainsi pu démontrer la polyvalence de la solution analytique (AS) développée dans cette thèse, sa flexibilité et sa facilité d'utilisation dans des conditions pour lesquelles elle a été développée mais également pour celles pour lesquelles elle n'était pas directement applicable (par exemple les conditions non isothermes). En intégrant différents modèles explicitement (CCS, AK), la AS a vu son champ utilisation étendu pour finalement couvrir l'ensemble de la gamme de conversion du monomère.

7. Étude numérique du réacteur à inversion de flux

Dans une seconde partie, les aspects de modélisation numérique de mécanique des fluides (CFD) couplés à de la simulation de polymérisation radicalaire (FRP) dans différentes géométries de microréacteurs tubulaires ont été considérés. Un nouveau code a été écrit pour générer le CFIR avec les caractéristiques souhaitées, y compris la hauteur, le nombre de tours, le nombre de coudes etc. Ce codefonctionne bien pour n'importe quel type de maillage structuré de type butterfly, carré etc. comme indiqué sur la figure 10.

(a)   (b)
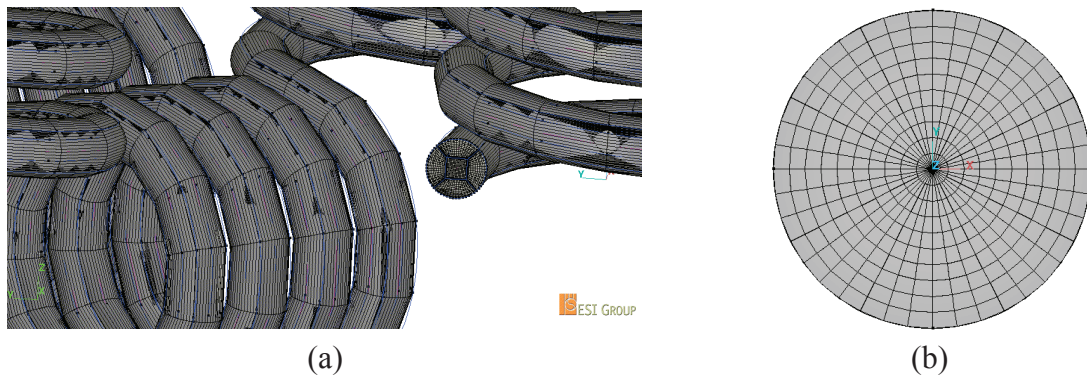
Fig. 10- Maillage du CFIR généré par notre programme : butterfly (a), maillage O(b).

Le maillage non structuré a été utilisé pour les conditions d'alimentation sans mélange du STR et du CFIR comme indiqué sur la figure 11. L'entrée est constituée de 30% de solvant avec un amorceur (section rouge) tandis que le monomère a été introduit à partir de la section de couleur verte comme représenté sur la figure 11 (a) pour le STR et la figure 11 (c) pour le CFIR. Le maillage structuré a été utilisé pour le STR, le CTR et le CFIR comme indiqué sur la figure 12.

(a)   (c)   (d)

(b)   (e)
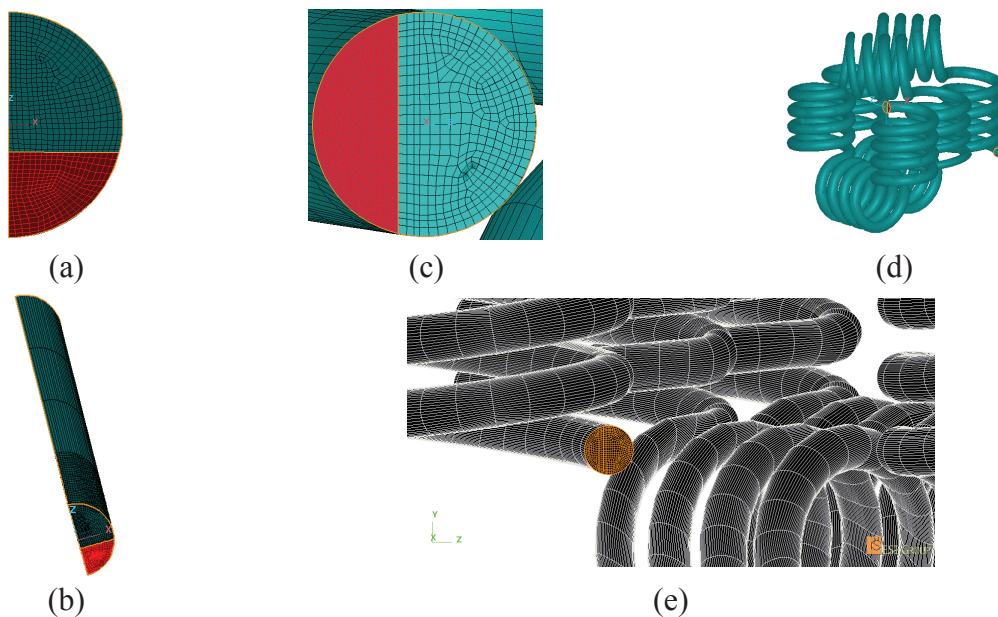
Fig. 11- Maillage non-structuré utilisé pour des conditions d'entrée non mélangée : a) entrée du STR avec 30% solvant, b) maillage volumique pour le STR, c) entrée du CFIR avec 30% solvant, d) maillage du CFIR, e) maillage détaillé du CFIR

(a) (c) (d) (e)

(b) (f) (g)
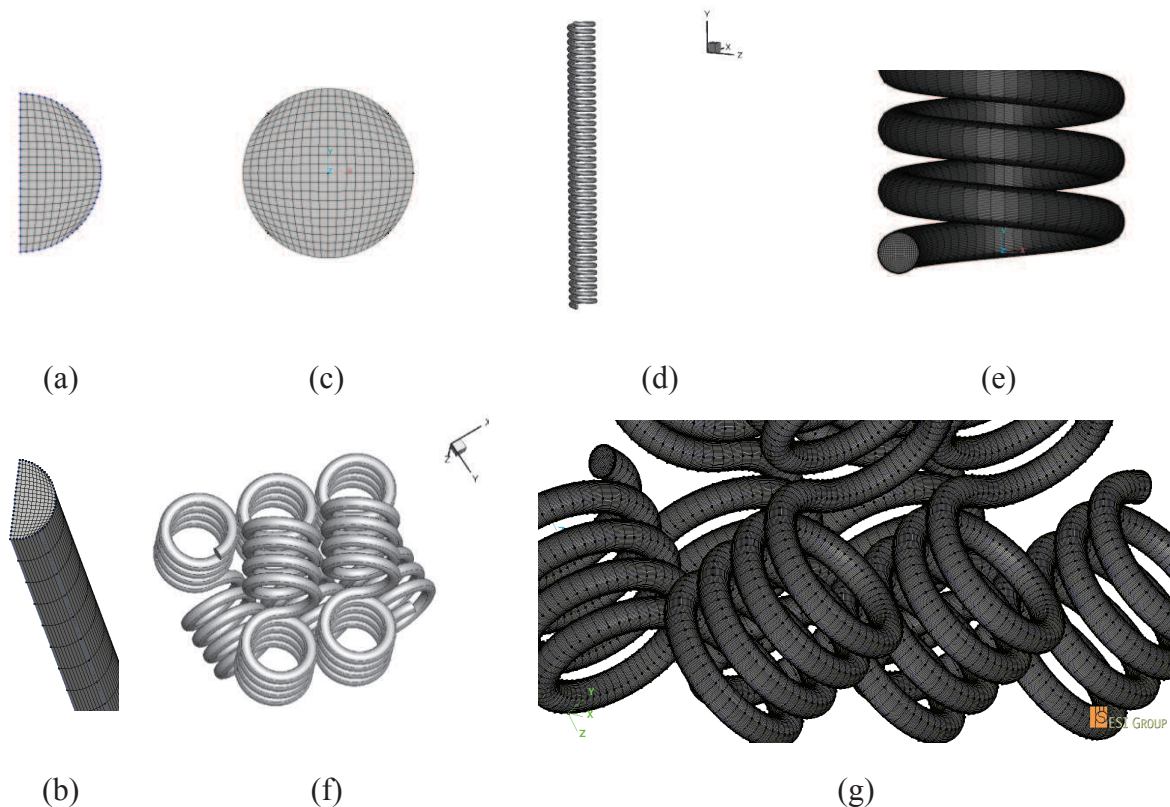
Fig. 12- a) plan de coupe pour l'entrée du STR, b) maillage du STR, c) plan de coupe pour l'entrée du CTR, d) représentation du CTR, e) maillage partiel du CFIR, f) représentation du CFIR, g) maillage complet du CFIR.

8. Nouvelle transformation

L'intégration des réactions chimiques dans la CFD a été réalisée en modélisant les espèces chimiques comme des scalaires passifs et leurs vitesses de réaction en tant que termes sources. Le scalaire passif est une quantité sans masse qui n'affecte pas le profil d'écoulement. L'utilisation de ces scalaires passifs est assez habituelle dans les simulations CFD. Mais toutes les quantités qui sont modélisés en CFD doivent obéir à la loi de conservation de la masse. Ainsi, les données correspondant à ces scalaires passifs et leurs termes sources doivent être formulés en termes de masse. Mais les données sur les espèces chimiques (modélisées comme des scalaires passifs) et de leurs termes sources (vitesse de réaction) se trouvent sous la forme molaire dans la littérature. La conversion de la forme molaire à la forme de masse pose certains problèmes et peut conduire à des erreurs dans les résultats de simulation et leur analyse. Une nouvelle transformation a été proposée pour obtenir des coefficients cinétiques adimensionnés en termes de concentration. Cela évite ainsi de devoir fournir les données sous forme massique et conserve de plus la formulation originelle des données sous forme molaire. La nouvelle transformation proposée a également gardé la forme originale des équations pour les termes source et a donc permis un codage et un débogage plus faciles. En outre, cette nouvelle transformation possède tous les avantages de la transformation de Zhu[8], tout en réduisant la rigidité de l'ensemble des équations car toutes les variables transformées ont même ordre de grandeur (Fig. 13).
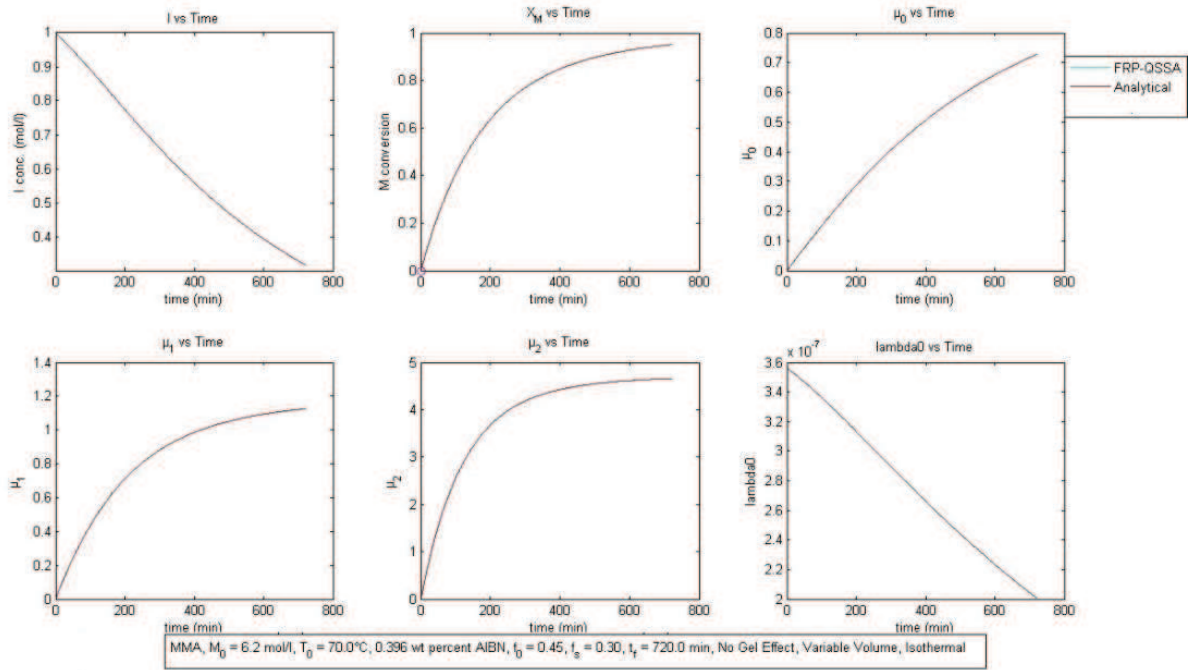
Fig. 13- Comparaison entre la solution analytique et la solution numérique FRP_QSSA en utilisant la nouvelle transformation

Les résultats obtenus en utilisant la nouvelle transformation ont été comparés avec les données publiées par Serra et al.[9] pour le STR dans des conditions similaires (Fig. 14 à Fig. 16) et également avec les données expérimentales pour CTR. La nouvelle transformation a permis d'améliorer les prédictions car les résultats prédis furent beaucoup plus proche de la réalité. Ainsi, cette nouvelle transformation est plus appropriée pour les simulations CFD de FRP.
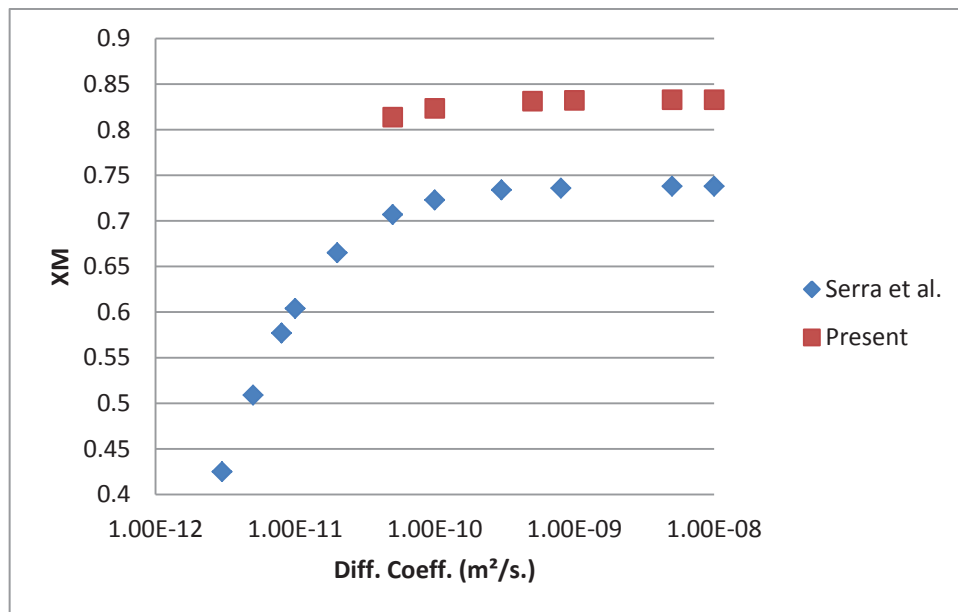
Fig. 14- Comparaison des valeurs de conversion du monomère obtenues par AS et celles prédites par Serra et al.[9]
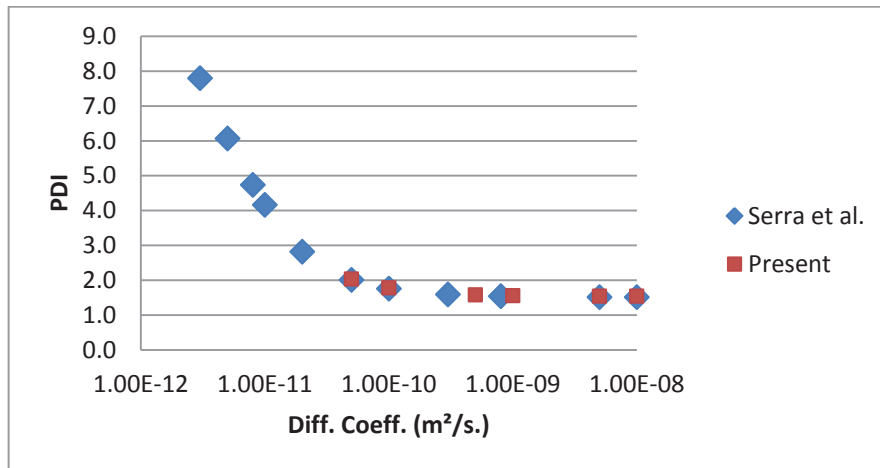
Fig. 15- Comparaison pour le *PDI* avec Serra *et al.*[9]
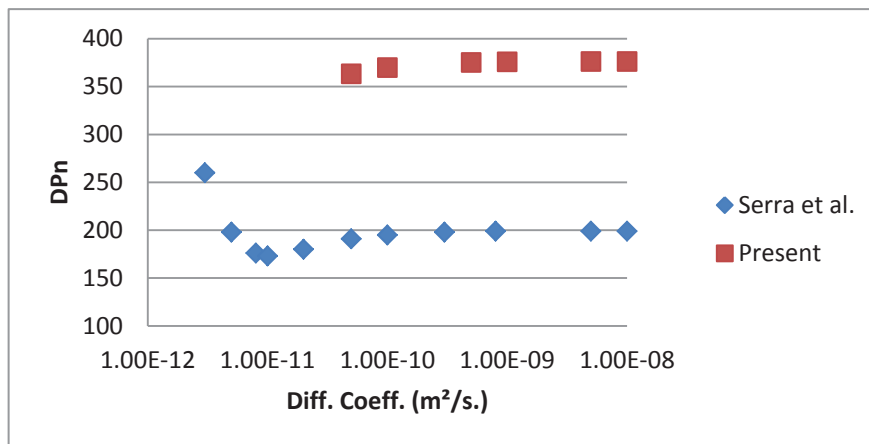
Fig. 16- Comparaison pour le *DPn* (masse moléculaire moyenne en nombre) avec Serra *et al.*[9]

9. Résultats numériques de la condition d'entrée non-mélangée

Le cas de la condition d'entrée non-mélangée du STR et du CFIR a été étudié. La nouvelle transformation a été appliquée avec des propriétés thermo-physiques du fluide constants et la variation discrète du coefficient de diffusion pour imiter l'effet de l'augmentation de viscosité. Au cours de la réaction. Les résultats ont ensuite été comparés avec les résultats publiés de Mandal *et al.*[10] dans des conditions similaires et des différences significatives ont été observées. Le travail actuel prédit une conversion plus élevée et un *DPn* supérieur pour les STR et CFIR et un *PDI* inférieur pour le CFIR. Les nouveaux résultats pour le STR et le CFIR ont clairement démontré la supériorité du CFIR sur le STR dans des conditions d'entrée non-mélangée dans le contrôle de la qualité des polymères, mais avec une conversion du monomère légèrement inférieure par rapport au STR. Les variations de la masse volumique, de la viscosité et de la conductivité thermique ont ensuite été modélisées en gardant une variation discrète de coefficient de diffusion. Les résultats obtenus furent significativement différents comparativement au cas des propriétés thermo-physiques constantes. Ces résultats ont prédit une conversion du monomère et un *DPn* supérieur tandis que le *PDI* fut prédit avec des valeurs inférieures et une tendance différente (Fig. 17).
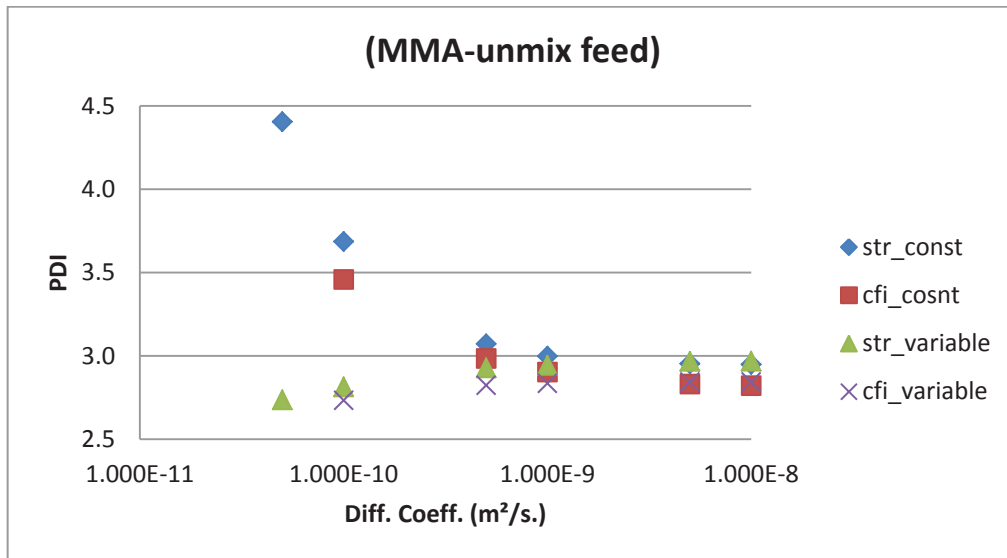
Fig. 17- Variation de l'indice de polymolécularité du poly(méthacrylate de méthyle) en fonction du coefficient de diffusion pour des propriétés thermo-physiques variables et constantes.

Encore une fois le CFIR démontre un meilleur contrôle par rapport au STR quant aux caractéristiques des polymères syntétisés. Un cas particulier de l'amélioration du mélange interne en l'absence de toute agitation mécanique dans le STR à faible coefficient de diffusion a été observé comme indiqué dans le tableau 1. Il était dû à une variation de direction de l'écoulement résultant de l'effet visqueux non-uniforme pour l'entrée sans mélange et un faible coefficient de diffusion. Cet effet n'a pas pu être observé dans le cas des propriétés thermo-physiques constantes. Ceci souligne clairement l'importance de la modélisation de la variation de la densité et de la viscosité dans le cas de la FRP pour les réacteurs continus sans mélange initial. La variation de la conductivité thermique et la variation de la température à travers la section transversale furent négligeables. On en conclut que la conductivité thermique et la température peuvent être raisonnablement supposés constantes pour ces types de réacteurs, réduisant ainsi la complexité des simulations sans introduire une erreur importante dans les résultats de la simulation.

10. Analyse numérique d'une condition d'entrée mélangée

Les effets d'une condition d'entrée parfaitement mélangée dans différentes géométries de microréacteurs ont été considérés. Une stratégie similaire à la condition d'alimentation non mélangées a été retenue, c'est à dire un cas avec les propriétés thermo-physiques du fluide constants et un autre pour lequel ces propriétés étaient variables avec à la fois une variation discrète du coefficient de diffusion. Là encore, les résultats sont différents pour les deux cas. Le cas des propriétés constantes prédit des valeurs plus faibles de toutes les caractéristiques du polymère, comme la conversion de monomère, le DPn et le PDI. La tendance de la conversion du monomère est également différente dans les deux cas (Fig. 18).

Tableau1-Distribution du scalaire7(un traceur nonréactif et nondiffusif) à la sortie du réacteur.

Coefficient de diffusion (m²/s)	STR		CFIR	
	Propriétés constantes	Propriétés variables	Propriétés constantes	Propriétés variables
5×10^{-11}				
1×10^{-10}				
5×10^{-10}				
1×10^{-9}				
5×10^{-9}				
1×10^{-8}				
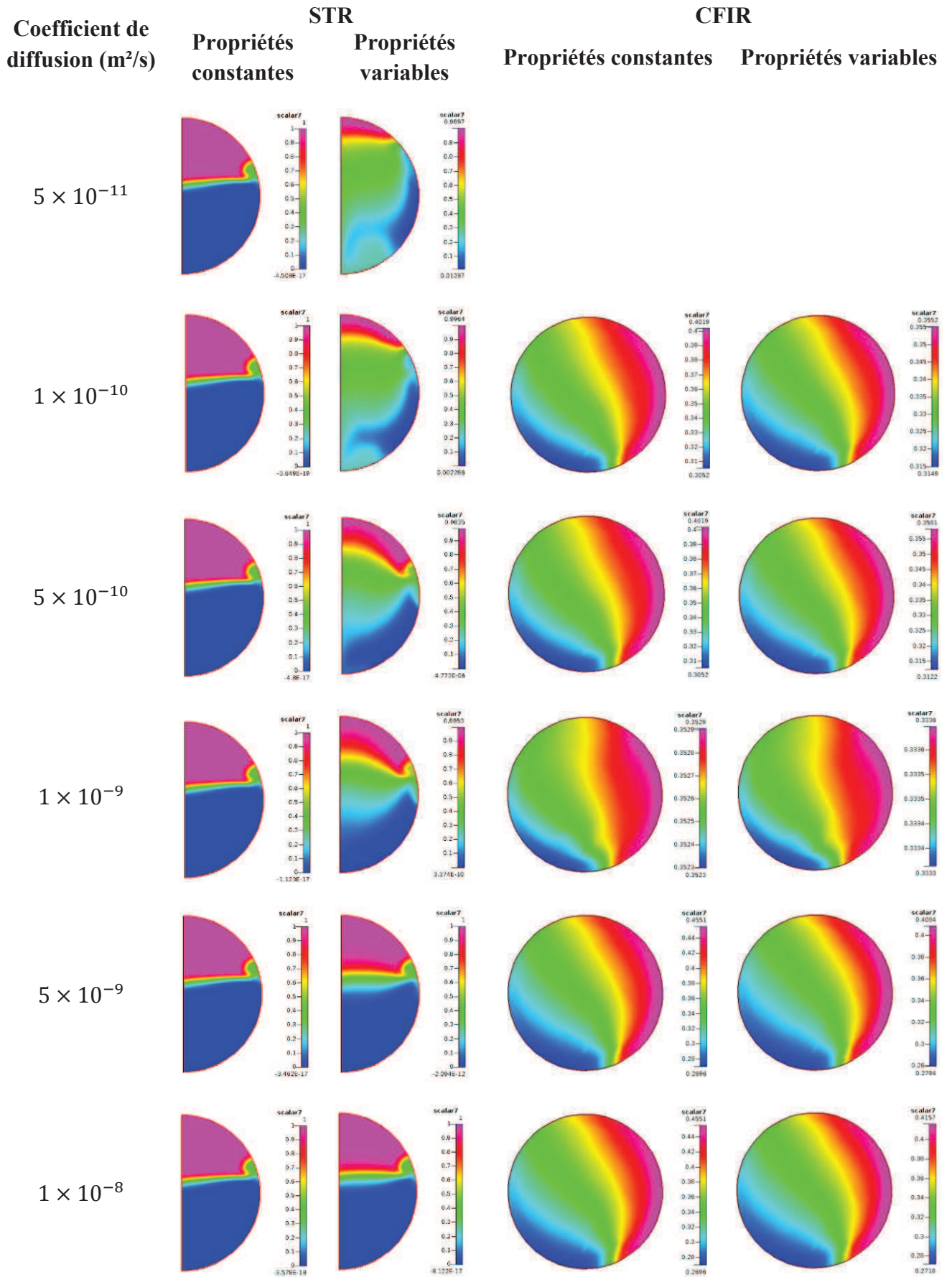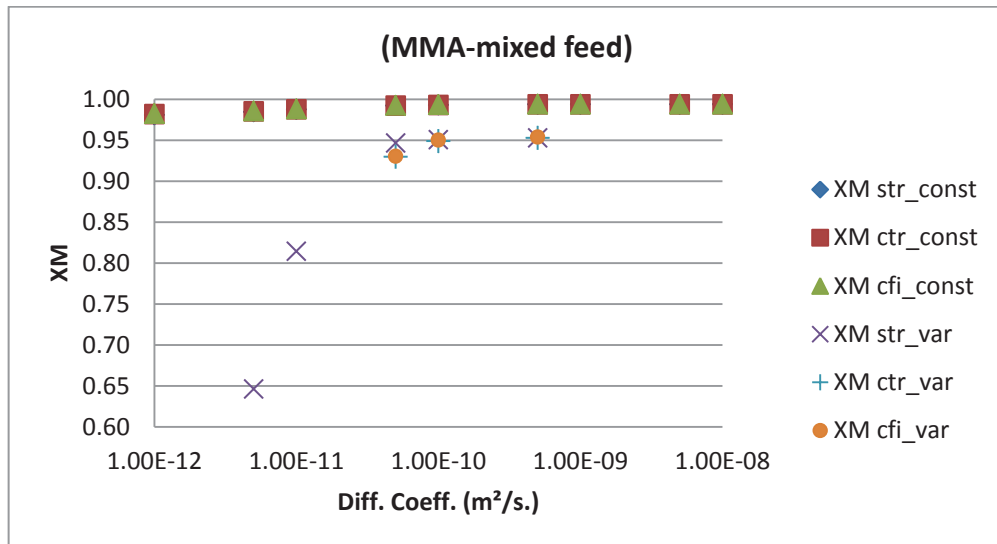
Fig. 18- Variation de la conversion du monomère (x_M) pour le STR, CTR et CFIR dans le cas de propriété thermo-physiques constantes et variables.

Pour le cas des propriétés thermo-physiques constantes, la conversion du monomère reste presque constante quelle que soit la variation du coefficient de diffusion alors que pour le cas des propriétés thermo-physiques variables, elle diminue avec la baisse du coefficient de diffusion. Les trois géométries de réacteurs ont donné des résultats similaires dans les deux conditions de propriétés constantes et variables. La figure 19 montre les résultats de la variation de la viscosité, de la chute de pression et de la masse volumique pour deux coefficients de diffusion différents. La non uniformité de la masse volumique et de la viscosité le long du CFIR, due au faible coefficient de diffusion, peut être facilement observée. Une simulation de la variation du coefficient de diffusion en utilisant la théorie de volume libre a également été faite. Les résultats étaient proches du cas des propriétés variables sauf pour le DPn. Encore une fois les variations de la conductivité thermique et de la température ont été jugés négligeables et peurent donc être supposées constantes pour des conditions d'entrée mélangées.

Coefficient de diffusion (m²/s)	5×10^{-11}	1×10^{-10}
Viscosité (kg/m/s)		
Chute de pression (N/m²)		
Masse volumique (kg/m³)		
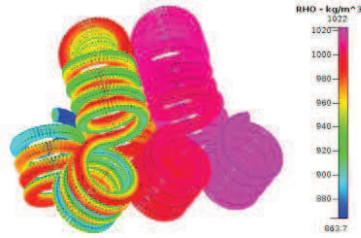
Fig. 19- Variations de la viscosité, de la chute de pression et de la masse volumique le long du CFIR pour deux coefficients de diffusion différents.

La figure 20 démontre l'existence d'une advection chaotique dans le CFIR à l'origine du meilleur contrôle des propriétés du polymère synthétisés qu'autorise ce type de réacteur et cela en dépit du très faible nombre de Reynolds pour les écoulements à viscosité variable et fixe.
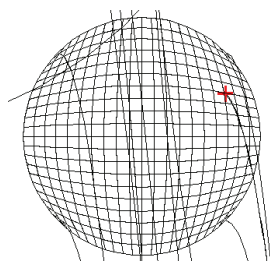
2 particles location — $5 \times 10^{-11}\ m^2/s$, constant
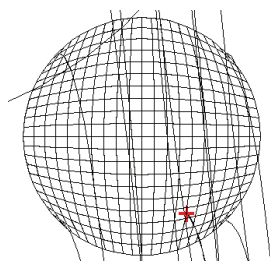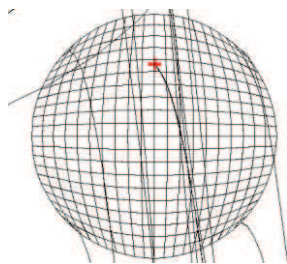
2 particles location — $5 \times 10^{-11}\ m^2/s$, constant
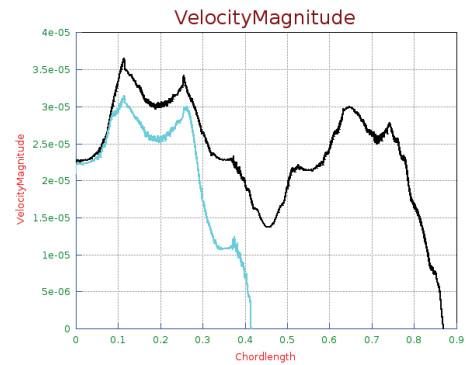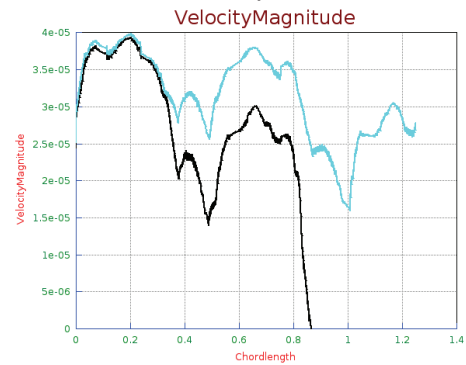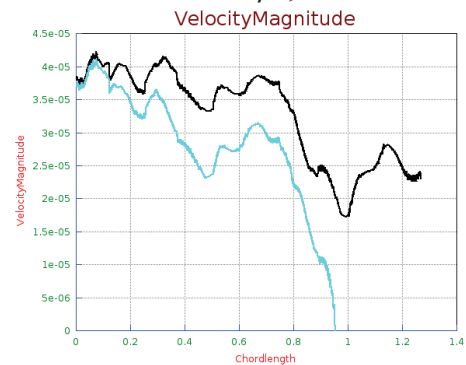
2 particles location — $5 \times 10^{-11}\ m^2/s$, variable

Fig. 20- Résultats démontrant la nature chaotique de la trajectoire de deux particules initialement très proches à l'entrée du CFIR.

11. Conclusion sur la CFD

Ainsi de nettes améliorations dans les simulations CFD ont été obtenues en utilisant la nouvelle transformation. Nous avons aussi démontré l'importance de la modélisation de la variation de la masse volumique et de la viscosité et cela quelles que furent les conditions de mélange en entrée de réacteur. Une simulation pour le cas de la variation du coefficient de diffusion a également été réalisée imitant ainsi le comportement réel de la diffusion des espèces chimiques dans une certaine mesure. Sur l'ensemble des résultats obtenus, le CFIR s'est avéré être un réacteur prometteur pour le contrôle des réactions de polymérisation radicalaires en conditions de microréaction.

12. References

1. Balke, S. T.; Hamielec, A. E., Bulk Polymerization of Methyl Methacrylate. *Journal of Applied Polymer Science* **1973,** *17*, 905-949.

2. Soh, S. K.; Sundberg, D. C., Diffusion-Controlled Vinyl Polymerization .1. The Gel Effect. *J Polym Sci Pol Chem* **1982,** *20* (5), 1299-1313.

3. Zhu, S.; Hamielec, A. E., Gel Formation in Free-Radical Polymerization Via Chain Transfer and Terminal Branching. *J Polym Sci Pol Phys* **1994,** *32* (5), 929-943.

4. Venkateshwaran, G.; Kumar, A., Solution of Free-Radical Polymerization. *Journal of Applied Polymer Science* **1992,** *45* (2), 187-215.

5. Chiu, W. Y.; Carratt, G. M.; Soong, D. S., A Computer-Model for the Gel Effect in Free-Radical Polymerization. *Macromolecules* **1983,** *16* (3), 348-357.

6. Fenouillot, F.; Terrisse, J.; Rimlinger, T., Polymerization of methyl methacrylate at high temperature with 1-butanethiol as chain transfer agent. *Journal of Applied Polymer Science* **1999,** *72* (12), 1589-1599.

7. Achilias, D. S.; Kiparissides, C., Development of a General Mathematical Framework for Modeling Diffusion-Controlled Free-Radical Polymerization Reactions. *Macromolecules* **1992,** *25* (14), 3739-3750.

8. Zhu, S. P., Modeling of molecular weight development in atom transfer radical polymerization. *Macromol Theor Simul* **1999,** *8* (1), 29-37.

9. Serra, C.; Schlatter, G.; Sary, N.; Schonfeld, F.; Hadziioannou, G., Free radical polymerization in multilaminated microreactors: 2D and 3D multiphysics CFD modeling. *Microfluid Nanofluid* **2007,** *3* (4), 451-461.

10. Mandal, M. M.; Serra, C.; Hoarau, Y.; Nigam, K. D. P., Numerical modeling of polystyrene synthesis in coiled flow inverter. *Microfluid Nanofluid* **2011,** *10* (2), 415-423.

Table of Content

List of Tables

Chapter1   Introduction

Introduction

In today's time, when prices are soaring high, environmental concerns are increasing, safety issues are gaining greater and greater prominence, competition is rising among various industrial producers, there is a clear need for higher investment on research and development more than ever. This is required to make the process economical in all possible aspects. With the continual increase of computational power with an equal decrease in its cost, greater availability of several user-friendly software, trained manpower, more efficient numerical methods and techniques compounded with the need to gain greater understanding of the process, modeling and simulation on computers have gained huge interest in the past from both academia and industry. It offers high flexibility in terms of getting results for various conditions which may not be possible to do otherwise in the field.

Modeling and simulation are two different branches of study. Modeling is the mathematical formulation of a given process under certain conditions. It can vary from describing the velocity during free fall at different times to description of protein molecule folding in a given environment to the movement of planets. The extent of modeling may be limited by the knowledge of the actual process or the process may be too complex to be solved even with the existing computation power currently available. So, several simplifications are applied to make a suitable and workable modeling of the process. The suitability of the modeling depends on the desired objectives to be achieved. Thus modeling is the first step towards solving any problem. On the other hand, simulation is the process of solving the mathematical model under the given conditions. It may vary from using simple calculator to make simple calculation of velocity during free fall by hand to using supercomputers to calculate the positions of various atoms in the protein molecule during its folding/unfolding process. So as the modeling becomes complex, the computational power requirement increases and manually monitoring of the progress of calculations become impossible. Many mathematical models could be solved directly in one step but several others could not be solved in one step despite the availability of tools to solve them. This may be due to very high requirement of computational power or machine hardware limitations. A very simple example is to get the determinant of a square matrix. It can easily be solved using Cramer's rule for matrix size till 3x3. But for higher matrix size, it becomes more and more cumbersome to use this technique to solve this problem. So, various other methods/techniques are to be developed such problems. One of the most common used techniques is iterative scheme. In this, the solution is obtained in steps and the value evaluated in each step is feedback to the same set of equations to generate new one. This scheme may be used to reduce error at a given point or to generate results for different points in space and time or both.

There are several issues encountered with successful simulation. One wants the simulation process to be both efficient and effective. A simulation is said to be effective when it is completed with least numerical error. Now, errors are introduced in simulations due to machine hardware limitations, improper numerical methods and techniques, or wrong modeling itself etc. Simulation process is said to be efficient when it is done in least time with lesser computational power. The first requirement for any simulation is to be effective. This issue is defined using the concepts of convergence, consistency and stability for simulations

by various researchers. Convergence is the property to produce the exact solution under the limits of decreasing time-step, grid size to zero. Consistent means that the numerical method produces the set of algebraic equations which approaches the original set of governing equations when the grid spacing limits to zero. Stability is associated with the reduction of numerical errors as the simulations proceeds.

Several techniques like finite difference method, finite volume method and finite element method are being developed. They have been to show to give same results but each method is found to be more efficient than others in certain types of problem. This can greatly reduce the computational power, time and efforts to solve a given problem. Finite volume method is found to be more useful and efficient for the case of study of fluids motion.

Since any modeling is based on certain assumptions, so it is imperative to test the modeling results by comparing them with experimental physical data. This process is called validation and is intended to check the correctness of both modeling and corresponding simulations. Without this, all simulations are just pure speculations despite the results looking great.

Polymerization is one such challenging area which offers scope for improvement in its modeling as well as simulation under flow and batch conditions. This thesis is part of the so-called DIP² project which aims at the intensification of a radical polymerization process for the production of architecture-controlled (co)polymers. The Process Intensification method in this project relies on the use of continuous flow Coiled Flow Inverters (CFIs) as reactors which were recently found to be extremely efficient mixers/heat exchangers. The goal of the DIP² project is to propose a reproducible and intensified process to synthesize architecture-controlled homopolymers and copolymers. One novelty of this project is the intensive use of numerical simulations. This is not a trivial task: in addition to the very huge number of simulations that has to be performed, we will have to propose a numerical modeling of the physical properties of the polymer. The polymerization depends on the kinetics, on the concentrations of reactants, on the flow rate (hydrodynamics), on the temperature and on the flow behavior of the reactive solution. To simulate properly this polymerization, we have to model the chemical reactions (through the mixing theorem or moment method), the flow (through the Navier-Stokes equations), thermal and mass transfers (through convective-diffusion equations) and to solve for the coupled system raised from those equations. Thus one has to know the viscosity, the density, the thermal diffusivity and the scalar diffusivity. These parameters depend on the monomer/polymer concentrations, on the temperature and on the shear rate. We will have to quantify and to model this dependency. Another goal of the numerical study is to be as accurate as possible which means that one might needs to increase the grid resolution up to Batchelor scale.

Thus, Free radical polymerization (FRP) is considered in this thesis for the study. An effort is made to improve its modeling and simulation process so as to gain more insight into the problem. This gained knowledge can then be used to improve the polymer production and its quality control in flow processes by optimizing reactor design. This optimizing process again can be done using computers using various models and mathematical tools.

This thesis is divided into six chapters. The chapter-2 is about the literature survey. In this chapter, the published work by various researchers relevant to this thesis work is discussed. In the beginning, a brief description of type of reactors, type of flow and mixing in the reactors is presented. Then, the effect of curvature on the flow profile is discussed. The coiled flow inverter is discussed in detail about its various characteristics and developments so far. The chaotic advection is discussed in some details. Then, microfluidics is introduced which includes micromixers and microreactors. Then, FRP is discussed. It also includes various effects like gel effect, glass effect and cage effects and their modeling using various relevant models along with a discussion on their limitations.. This chapter presents the various assumptions taken for simulating FRP under flow conditions by various researchers and also discusses the importance of modeling the variation of fluid thermo-physical data based on published data.

Chapter-3 is about the description of actual mathematical models relevant to our work as discussed in chapter-2. It presents all the modeling at one place so that they can easily be referred to by the reader. This includes the mathematical model of FRP based on its kinetic scheme. It then describes two models for simulating gel and glass effect, namely Chiu, Carratt & Soong (CCS) model and Achilias and Kiparissides (AK) model. AK model can also simulate cage effect using variation in diffusion coefficient based on the free volume theory developed by Vrentas and Duda. This model for diffusion coefficient is presented subsequently. Expressions for modeling variation of various fluid thermo-physical properties are also presented. Then the complete physical and kinetic data related to various monomer-polymer systems studied in this work is presented. The numerical techniques to solve the set of equations resulting from the modeling using Matlab for batch reactor are presented. This is then extended to CFD modeling and simulation. A reputed commercial CFD package software CFD-ACE+ is used for this work. The geometries generation in CFD-GEOM, their implementation in CFD-ACE and post-processing in CFD-VIEW are presented. The mesh independency test and its results for various reactor geometries for the conditions studied in this work are also detailed.

Chapter-4 presents the theoretical developments achieved for FRP. An analytical solution (AS) is being obtained under isothermal, homogeneous, solution polymerization batch reactor without gel effect. Its derivation and validation with published experimental data and numerical solutions for various monomers is presented in section-4.1. The implementation of AS is then extended to cover the full range of monomer conversion by implementing the variation in kinetic rate coefficients, i.e. the modeling of gel and glass effects using CCS model, in section-4.2. The results are then validated with published experimental data and numerical solutions. Section-4.3 presents the use of AK model for implementing the variation in initiator efficiency with an improvement in the model of gel and glass effects. Again the results are validated with published experimental data and numerical solutions. Section-4.4 presents the use of AS under non-isothermal condition without and with modeling of gel/glass and cage effects using both CCS and AK model. The results are then validated with published experimental results and numerical solutions.

Chapter-5 presents the CFD aspects of the modeling of FRP under flow condition for three different reactor geometries namely straight tube reactor (STR), coil tube reactor (CTR) and coiled flow inverter reactor (CFIR). Section-5.1 presents a new transformation to improve the modeling of FRP in CFD problem; the results are then compared with published results to highlight the resulting improvements. Section-5.2 deals with the results for unmixed feed condition with constant fluid thermo-physical properties and discrete variation of diffusion coefficients to mimic the effect of viscosity on diffusion, assumed to be same for all the chemical species, for two reactor geometries (ST and CFIR) using the new transformation developed in section-5.1. Variation of fluid thermo-physical properties is also made still keeping the discrete variation of diffusion coefficient and simulations are performed for the same. The results for constant fluid thermo-physical properties are compared with published results confronted with variable fluid thermo-physical properties results. Section-5.3 is an extension to the work presented in previous section. The feed condition at reactor inlet is now considered to be fully mixed. Besides performing the simulations for constant and variable fluid thermo-physical properties with discrete variation of diffusion coefficient, one case of varying diffusion coefficient keeping physical properties constant is also studied. The results are compared with other to gain better understanding of the process.

Finally, chapter-6 presents the general conclusion about the whole work achieved and the significant contributions made in this thesis. Some perspectives are also presented about future areas of improvements.

Chapter2   Literature Review

Introduction

This chapter deals with the literature survey of the work published by various researchers related to this thesis. This includes the study of basic concepts of reactors, different flow types and issues related to them. Then it will discuss the effect of curvature of path on fluid flow and various designs arise out of it. A new design Coiled flow inverter (CFI) is also discussed which can demonstrate chaotic advection. Further, fundamentals of chaotic advection are discussed with its important aspects related to our work. Then microfluidics, micromixers and microreactors are discussed. Free radical polymerization (FRP) is then discussed with various effects like gel, glass and cage effect. Various works modeling these effects are also discussed. Free volume theory is then discussed in brief. In the end, some aspects of CFD are discussed with developments and issues related to proposed work in this work.

2.1 Dimensionless numbers

Before starting, few important dimensionless[1] numbers are defined which will be used in this chapter and the thesis.

1. Reynolds number, (Re): $Re = \frac{d_t u \rho}{\eta} = \frac{d_t u}{\eta_k} = \frac{inertial\ force}{viscous\ force}$ $\qquad$ (2-1)

2. Dean number, (De): $De = Re.\sqrt{\frac{d_t}{D_c}} = Re.\lambda_c^2$ $\qquad$ (2-2)

   where $\lambda_c = \frac{d_t}{D_c}$ is called curvature ratio. $\qquad$ (2-3)

   It represents the intensity of centrifugal forces to create secondary flow in the fluid.

3. Peclet number, (Pe): $Pe = \frac{uL_c}{D} = \frac{advective\ transport\ rate}{diffusive\ transport\ rate}$ $\qquad$ (2-4)

   Radial Peclet number (Pe_r): $Pe_r = \frac{uL_c}{D}.\left(\frac{r_t}{d_t}\right) = \frac{Pe}{2}$ $\qquad$ (2-5)

   Axial Peclet number (Pe_a): $Pe_a = \frac{uL_c}{D}.\left(\frac{L_c}{d_t}\right) = Pe.\left(\frac{L_c}{d_t}\right)$ $\qquad$ (2-6)

   where $\left(\frac{L_c}{d_t}\right)$ is aspect ratio. $\qquad$ (2-7)

4. Nusselt number, (Nu): $Nu = \frac{hL_c}{k} = \frac{convective\ heat\ transfer}{conductive\ heat\ transfer}$ $\qquad$ (2-8)

5. Schmidt number, (Sc): $Sc = \frac{\eta_k}{D} = \frac{viscous\ diffusion\ rate}{molecular\ diffusion\ rate}$ $\qquad$ (2-9)

6. Prandtl number, (Pr): $Pr = \frac{\eta_k}{\alpha} = \frac{viscous\ diffusion\ rate}{thermal\ diffusion\ rate}$ $\qquad$ (2-10)

where
d_t is tube inner diameter, r_t is the radius, $2r_t = d_t$

D_c is coil diameter

L_c is the length characteristic length

u is average cross-sectional velocity of the fluid

ρ is fluid density

η is the dynamic viscosity of the fluid & η_k is kinematic viscosity of the fluid

k is thermal conductivity, α is thermal diffusivity and h is convective heat transfer coefficient

D is molecular diffusivity.

2.2 Type of reactors

To carry out any chemical reaction, chemical reactor is required. There are three categories of chemical reactors based on flow conditions[2]:
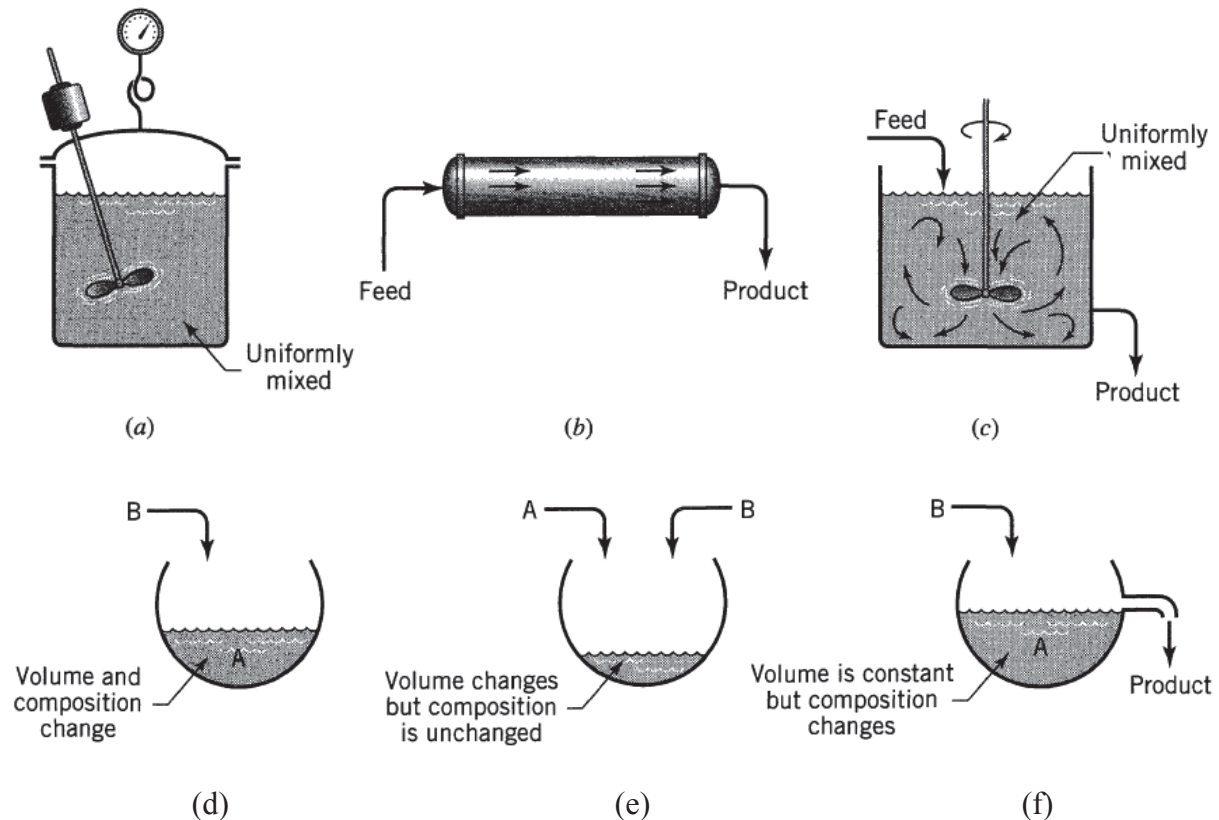
Fig. 2-1- Different types of reactors[2], a) batch, b) continuous-plug flow, c) continuous- mixed flow, d), e) & f) semi-batch reactor.

1. Batch (Fig. 2-1(a)) – In this type, there is no flow. The whole reaction mixture is kept in a vessel whose shape could be anything. All the reaction goes on in the vessel only. There is constant mechanical stirring (if required) for ensuring thorough mixing and thus the concentration of any chemical species is same throughout the reactor under ideal conditions. The composition inside the vessel changes with time. Thus it is transient in nature. Once the reaction is over, the charge is taken out and fresh mixture is added and the process continues. Each batch can have different composition and quality of the product. Hence it is important to maintain these within a range. It is highly flexible and inexpensive. Specially used in industries where specialty products are produced in small quantities and it is required to produce different types of products like pharmaceuticals. Most preferred choice in laboratories.
2. Continuous (Fig. 2-1(b)-(c))- in this there is continuous flow through the reactor, hence continuous production. They are generally operated in steady state and hence unlike batch reactor, parameters like temperature, pressure etc. remains constant with time. It produces consistent quality. It is one of the most preferred choice in industry for bulk production.

3. Semi-batch or semi-continuous (Fig. 2-1(d)-(f)) – they are basically batch reactors containing one of the reactants with addition of other reactant(s) either continuously or intermittently. Now depending on which component is of the main interest to the producer, it is called as semi-continuous (if the main component is being added continuously) or semi-batch (if the main component is added in a batch). It can be used for controlling several reactions where stoichiometric ratios could not be maintained from safety point of view (highly exothermic) or may promote side reactions.

2.3   Type of continuous reactors

There are three types of continuous flow reactors depending on flow conditions

1. Plug flow (Fig. 2-1(b))- in this type, there is complete radial mixing and thus there is no concentration gradient radially. There is no axial mixing i.e. no mixing with next or back element. So there is concentration gradient in axial direction. The velocity profile is flat. Hence the flow basically flows in blocks. It is similar to batch reactor in its analysis as each block can be considered as fully mixed batch reactor at different times. The only difference in the analysis is that the time term is now replaced with distance term. It is one of the main type of industrial flow desired. In practice, this type of flow can be achieved in turbulent conditions during flow.

2. Continuous stirred tank reactor (CSTR) (Fig. 2-1(c)) – In this type there is complete is complete axial and radial mixing. Thus there is no concentration gradient in any point in the reactor. This type of flow is used where no concentration gradient is required. In this complete mixing is achieved by mechanical stirrers or recycling the output back to the reactor alongwith feed. Here also the flow remains in turbulent regime if in tube like flow.

3. Laminar (Fig. 2-2- Velocity profile in (a) Plug flow, (b) laminar flow[2]- in this, the flow remains in laminar regime. The flow is basically segregated flow and there is no axial and radial mixing. There are not much examples of using it industrially as mixing is quite poor in it. The velocity profile is parabolic. Several researchers have worked in this flow regime for the problems of flow profile, heat transfer, mass transfer, chemical reactors, residence time distribution, non-newtonian flow etc.[3-19]
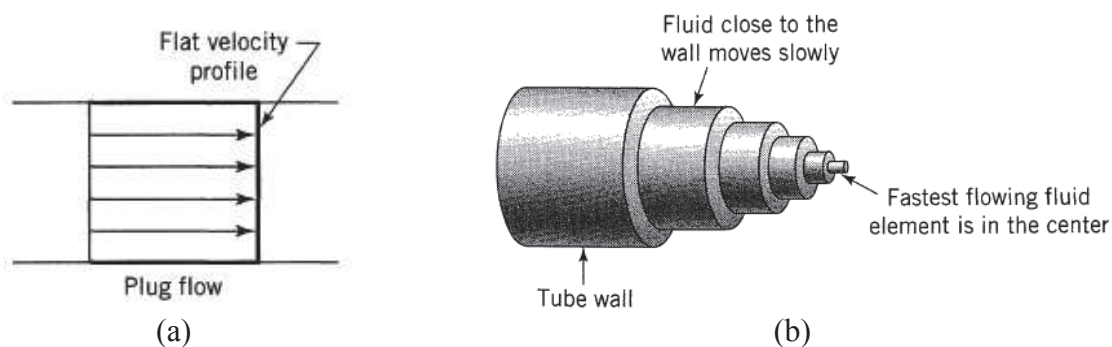
Fig. 2-2- Velocity profile in (a) Plug flow, (b) laminar flow[2]

2.4 Geometry of tubular flow reactors

The normal cross-sectional geometry used in industry is circular because of ease of its construction and use, lower cost of production and no dead pockets because of geometry. So, tubular geometry is most common in industry. There are various shapes of tubular geometry used in industry depending of ease of construction, process requirement, availability etc.

1. Straight tube – This type is one of the most preferred types of geometry because of ease it offers in construction, operation and maintenance.
2. Curved tube – This is also used in industry. It offers several advantages over straight tube like low floor area due to compactness it offers and increased mixing (discussed later)

There are different types of curved tubular geometries

1. Spiral (Fig. 2-3(a))- In this, there is continuous change of curvature with zero pitch i.e. it exists in same plane. It can be spirally inward or spirally outward.
2. Helical (Fig. 2-3(b)) – In this there is constant curvature with finite pitch.
3. Chaotic configurations (Fig. 2-3(c)) – In this there could be several shapes leading to chaotic advection. They are operated in laminar regime of flow to take advantage of chaotic advection. Various chaotic configurations and chaotic advection are discussed later.

(a) Spiral[20]   (b) Coil tube (CT)   (c) Coiled flow inverter (CFI)
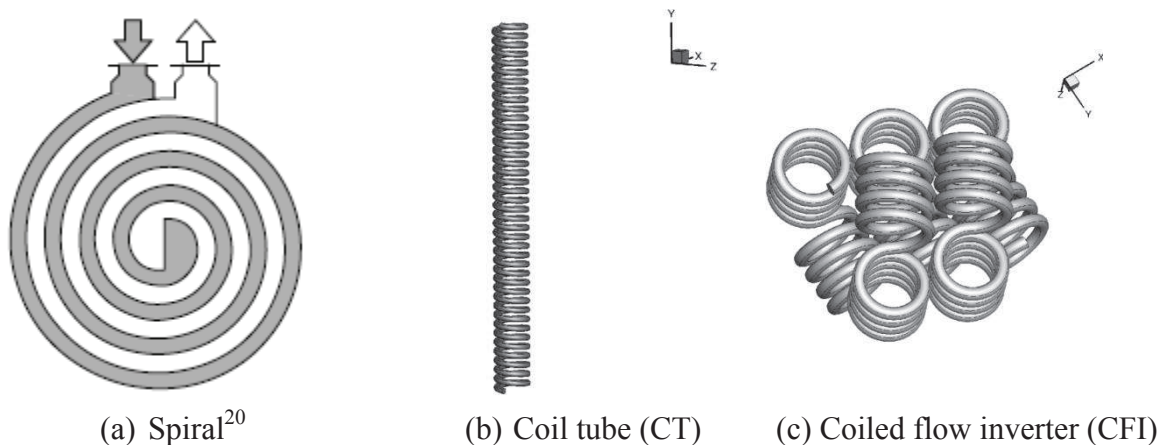
Fig. 2-3- Different types of curved geometry reactor.

2.5 Flow under curved geometry

Secondary flow occurs due to curvature in the path of the flow. This leads to the formation of centrifugal forces which forces the fluid to move towards the wall. The fluid moves along the direction of force and reaches wall. When reached the wall, it pushes the fluid there. The fluid thus moves along the wall on both sides and reaches the plane of direction of force. This completes the loop. Thus, the recirculation flow in the form of two symmetrical loops is set up as shown in Fig. 2-4. This recirculation improves mixing as it pushes the fluid from central zone to outer zone and vice-versa.
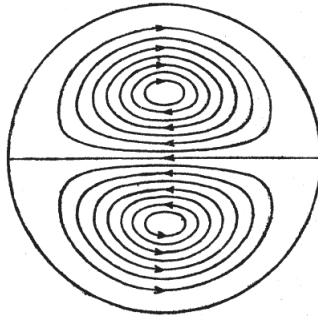
Fig. 2-4- Secondary flow[21]

Secondary flow was first reported by Eustice[22] and its theoretical analysis was first presented by Dean[23]. On his name there is dimensionless number De called as Dean number (eqn.(2)).

The value of De tells the strength of secondary flow developed thus higher mixing. As can be seen in eqn.(2), higher De can be achieved by increasing either Re or curvature ratio, λ_c or both. thus higher mixing can be achieved at low Re by increasing curvature. Reducing Re can reduce pressure drop thus pumping power. There is a limit to which curvature ratio can be increased depending on material of tube strength and operating conditions as curvature induces severe stresses in the tube. There is a lot of work carried out on flow in curved tubes[21,24-27], torsion effect on the flow[28], its effect on heat transfer[29-35], mixing in curved tubes[36,37], two phase flow[38-39], study using power law fluid[40,41], CFD analysis[42], optimization[43], and as a chemical reactor[44]. A good review can be referred for more details in this regard[45,46].

2.6   Coiled Flow Inverter (CFI)

But there arise problem with secondary flow. Although it improves overall mixing but the mixing in the central portion of the recirculation loops is quite poor. Significant concentration and temperature differences were found between central portion and the bulk. This problem can be overcame and mixing can be improved by using a chaotic configuration proposed by Saxena and Nigam[47] as shown in Fig. 2-3(c) called as coiled flow inverter (CFI). In this work, several 90° bends at regular intervals were used which lead to rotation of recirculation cells by 90° at every bend as shown in Fig. 2-5. Thus, low velocity zone is now covered by high velocity and vice-versa. This is what is called as inversion by the authors.
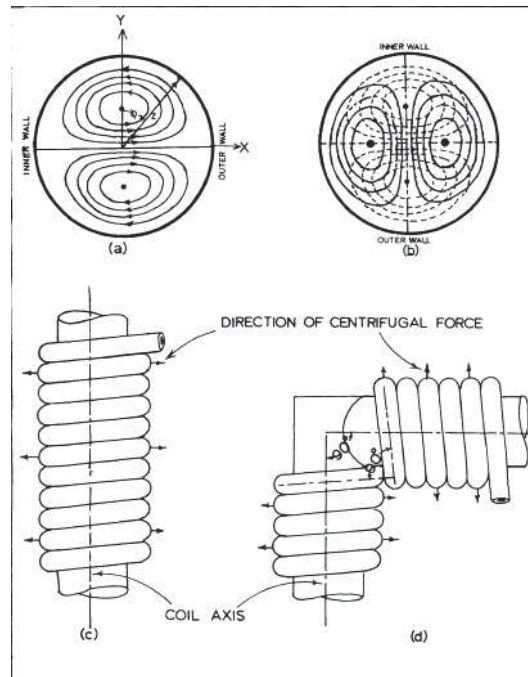
Fig. 2-5- Inversion of flow due to 90° bend in CFI[47]

The authors have shown that in this device, for more than 3 bends, the residence time distribution (RTD) narrows down drastically. This device was shown to have RTD as high as 0.8547 for the significant diffusion (Fig. 2-6) and non-diffusion case (Fig. 2-7) by using 57 bends. Thus, its performance was quite near to the desirable plug flow value of 1.0. The narrowing of RTD could begin in CFI at $De \geq 1.5$ and a unique RTD could be achieved even at low $De > 3$ (Fig. 2-8). The CFI with 57 bends was found to give about 20 times decrease in dispersion number compared to straight helical coiled tube. The dispersion number was also found to be independent of De for CFI. The range of Re used was 10-200 and for De, it was 3-60 in their work. The authors have also found that equidistant bends gave the best results compared non-equidistant ones. They had used 5 turns between two bends. The friction factor was also found to be about 1.7 times compared to the one in straight helicalcoil tube (CT) for 57 bends at a $De = 35$.
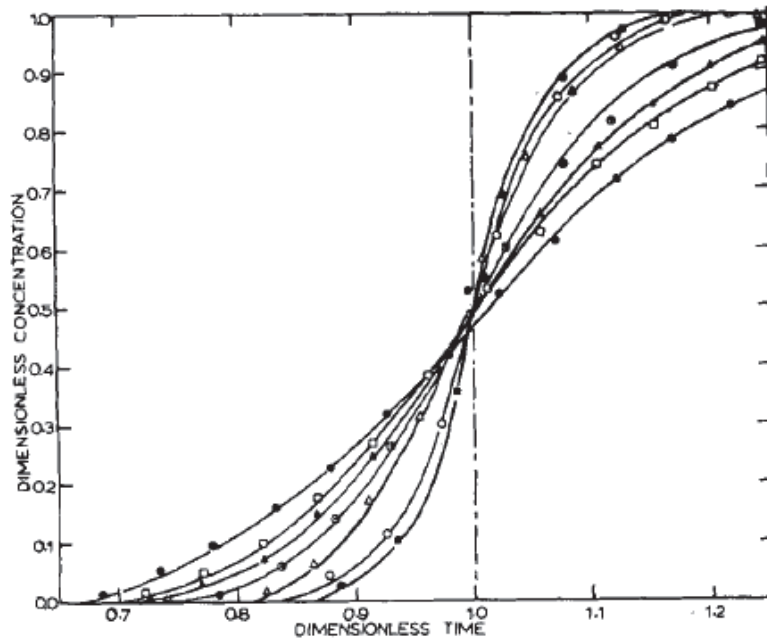
Figure 7. Step response curves with significant molecular diffusion (N_{Re} = 140). R_A - Symbol; 1 - ●, 0.5 - □, 0.33 - ▲, 0.125 - ⊙, 0.0625 - △, 0.0312 - ○, 0.0172 - ■, RTD for plug flow - - - - - -.

Fig. 2-6- RTD results for step response with significant molecular diffusion for CFI done by Saxena and Nigam[47]
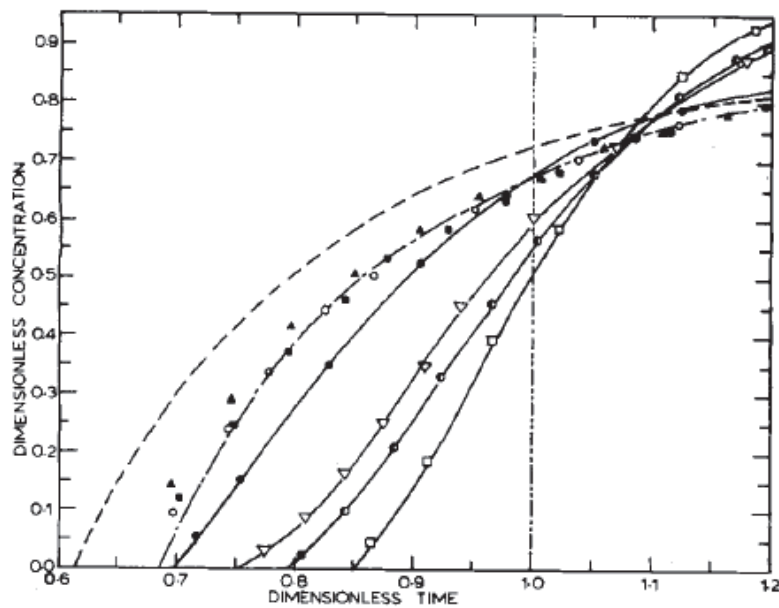
Figure 4. Effect of number of 90-degree equispaced bends on diffusion-free RTD. Number of bends-symbol: 1 - ■, 2 - ▲, 3 - ○, 7 - ●, 15 - ▽, 31 - ◐, 57 - □; theoretical RTD's; straight helix - - - - -, Bent coil having one centrally-located 90-degree bend —· —· —

Fig. 2-7- RTD results for step response with diffusion free case for CFI done by Saxena and Nigam[47]
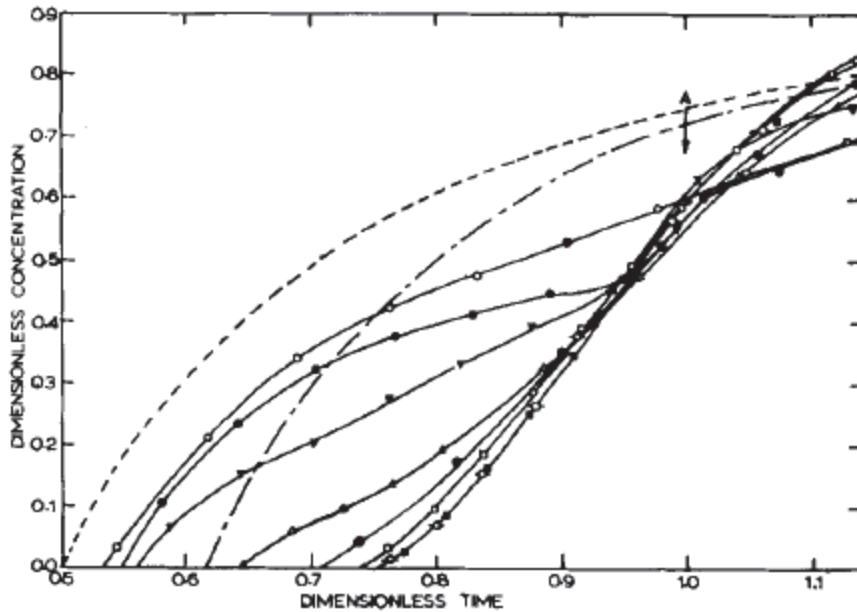
Figure 5. Effect of Dean number on diffusion-free RTD in bent coil having 15 equispaced 90-degree bends. Dean Number: Symbol: 0.1–0, 0.3 - ●, 0.43 - ▼, 0.59 - △; 1.2 - ⊙, 2.35 - □, 3.0 - ■, 4.5 - -○-; Theoretical RTD's for straight tube - - - - - - and for straight helix — — — — —

Fig. 2-8- Effect of *De* on diffusion-free RTD in CFI having 15 bends[47]

Considerable study has been done on CFI since then. CFI has been proved to be an efficient inline mixer[50,49] as shown in Fig. 2-9 and Fig. 2-10. Fig. 2-9 shows that unmixedness coefficient as defined by the authors[49] decreases faster on increasing *De* as well as on increasing bends in CFI compared to CT. CFI with just one bend did not seem to have any advantage over CT. But adding one more bend increased its mixing characteristic better than CT of comparable length and even of greater length. Fig. 2-10 shows the CFD simulation results for the distribution of two miscible liquids modeled as scalars in three different geometries. The geometries considered were straight tube (ST), CT and CFI by the authors[49]. CFI is clearly shown to have good mixing capabilities reaching uniform mixing at 3rd bend itself compared to straight helical coil which could not achieve uniform mixing even at its outlet. Both these results shows that CFI is quite good at mixing compared to CT which is better than ST.
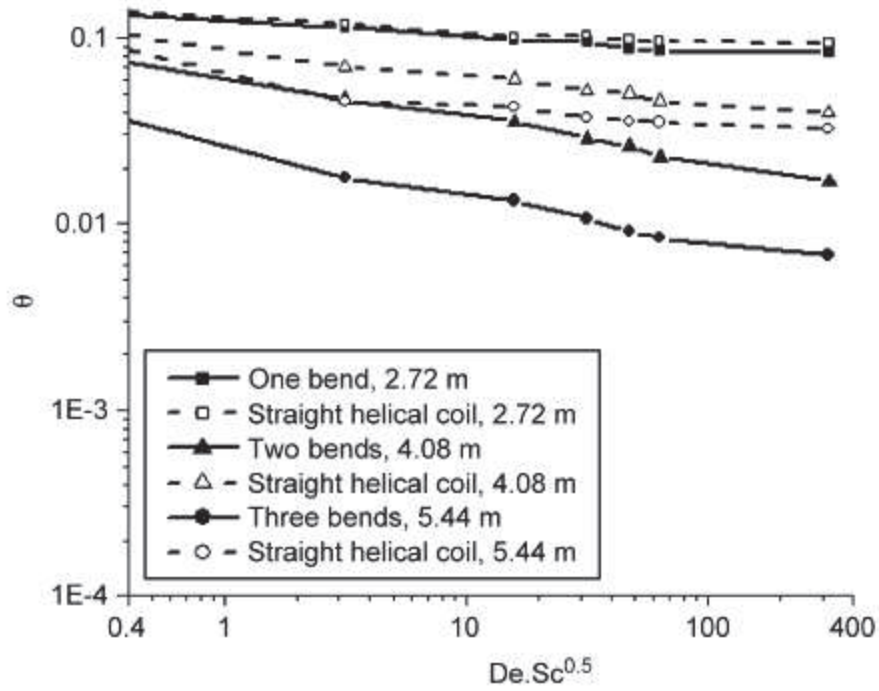
Fig. 2-9- Effect of De on unmixedness coefficient for $d_t = 0.02m$, $\lambda_c = 10$, $Sc = 100$[49].
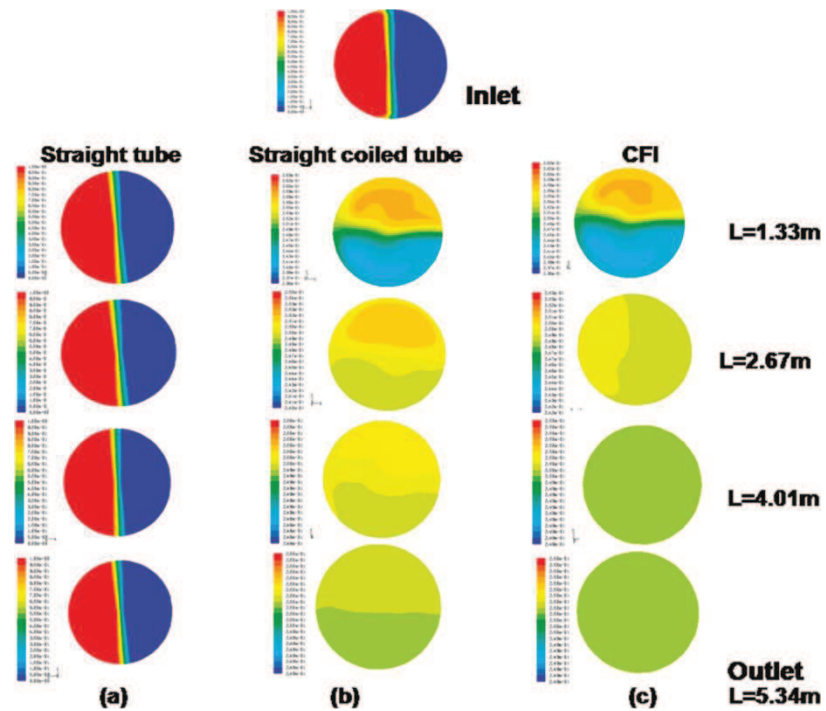
Fig. 2-10- Results for the distribution of scalar concentration of liquids at $u = 2\ m/s$, at $d_t = 0.01m$, ST, CT and CFI[50].

Kumar and Nigam[48] have made CFD analysis of the velocity and temperature contour development in CT and CFI for $Re = 7 - 400$ and Prandtl no. $Pr = 0.74 - 150$ with $\lambda_c = 10$.constant. The fluid thermo-physical properties were assumed constant and fluid taken was Newtonian. The results are shown in Fig. 2-11. Before the first bend, the results for

CT and CFI would be same. The rotation of velocity contours by 90° after each bend can easily be observed. The temperature contour also improved for CT after bends and temperature differences reduced as shown with less contour lines after 2nd bend. Hence CFI was shown to reducing temperature gradients through its variation in flow profile.

Computed velocity contour in CT at different cross sections from 15° to 340°	Computed temperature contour in CT at different cross sections from 15° to 340
Computed velocity contour in CFI after 1st bend at different cross sections from 15° to 340°	Computed temperature contour in CFI after 1st bend at different cross sections from 15° to 340°

| Computed velocity contour in CFI after 2nd bend at different cross sections from 15° to 340° | Computed temperature contour in CFI after 2nd bend at different cross sections from 15° to 340° |

Fig. 2-11- CFD results for velocity and temperature contours at various cross sections in CT and CFI after 1st and 2nd bends[48].

The above mentioned results should promote CFI as good candidate for heat exchange. Indeed, CFI was also shown to be as good heat exchanger[51,52]. Fig. 2-12[51] clearly shows high overall heat transfer rates (a) and higher Nu (b); the fluid taken were water at tube side (CFI) and water and air at shell side. Fig. 2-13 shows its better overall heat transfer coefficient compared to shell and tube heat exchanger (SHE) and plate type heat exchanger (PHE) under similar conditions. Kumar and Nigam[53] have also studied the laminar convective heat transfer in CFI. The authors found that heat transfer increased by min.22% to 37% while increase in pressure drop increased by only 7% for the same range of change of De (Fig. 2-14). All these results clearly show CFI's good heat transfer characteristics.

Several other studies regarding flow profile inside CFI under different conditions like using power law fluids, turbulent forced convection, under two phase flow [54-56], pressure drop for two phase flow[57] and RTD for two phase flow[58] are also done. But despite its good inline mixing and higher heat transfer characteristics, it has been not used as a reactor at industrial or pilot plant scale so far. Recently, there has been some CFD analysis in which it was used as a microreactor for polymerization of styrene[59]. Fig. 2-15 shows the CFD results for simultaneous mixing with polymerization reaction of styrene under unmixed feed condition. The physical properties were taken to be constant and inlet Re was of *order of 0.1*. The reaction related results will be discussed later.
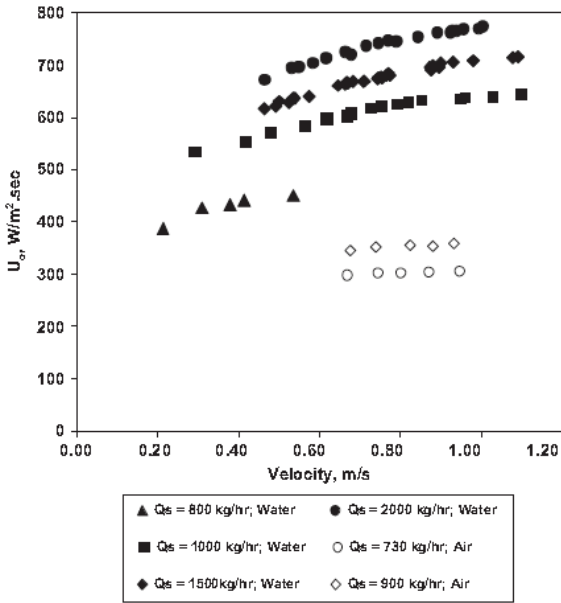
(a)
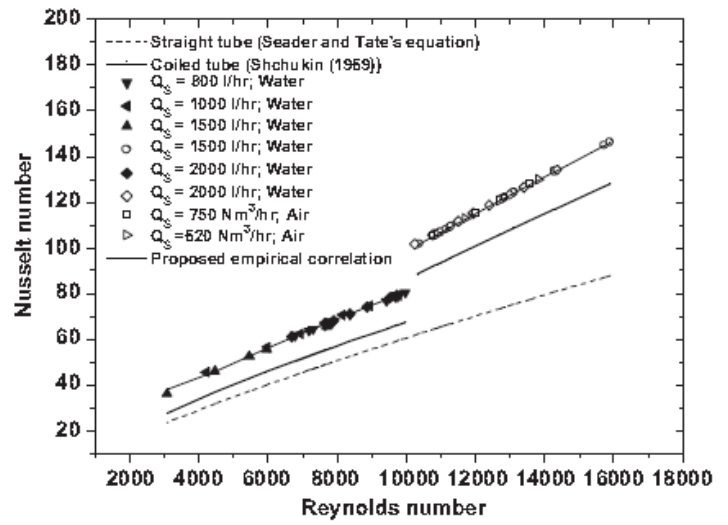
(b)

Fig. 2-12- Results for study of CFI as heat exchanger with CFI as tube side in shell and tube
heat exchanger[51]
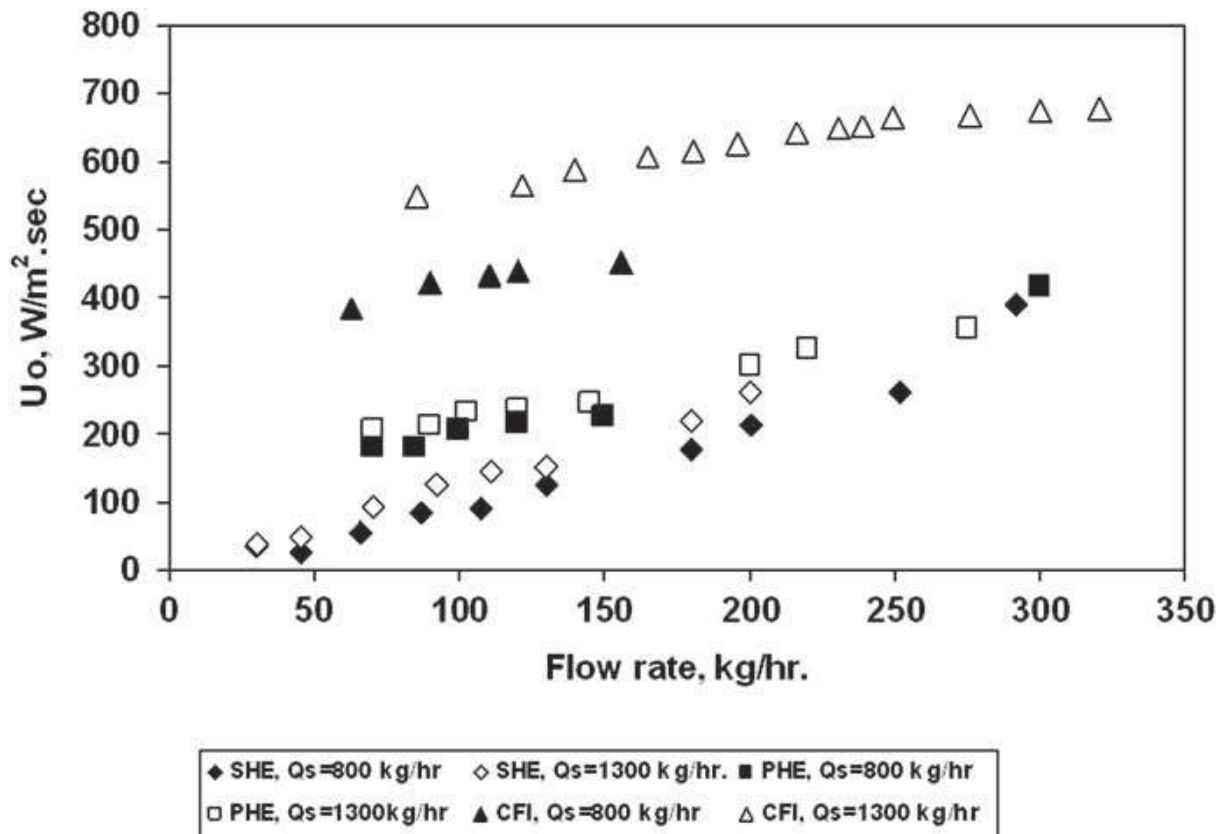
Fig. 2-13- Results for comparison of CFI as heat exchanger with shell and tube heat
exchanger (SHE) and plate heat exchanger (PHE)[52]
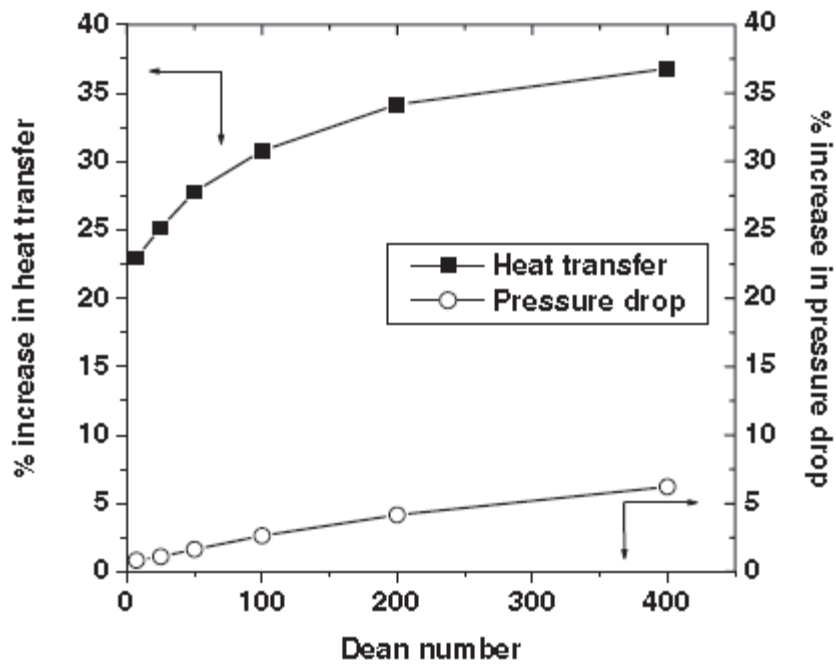
Fig. 2-14- Results of the study of laminar convective heat transfer in CFI[53]
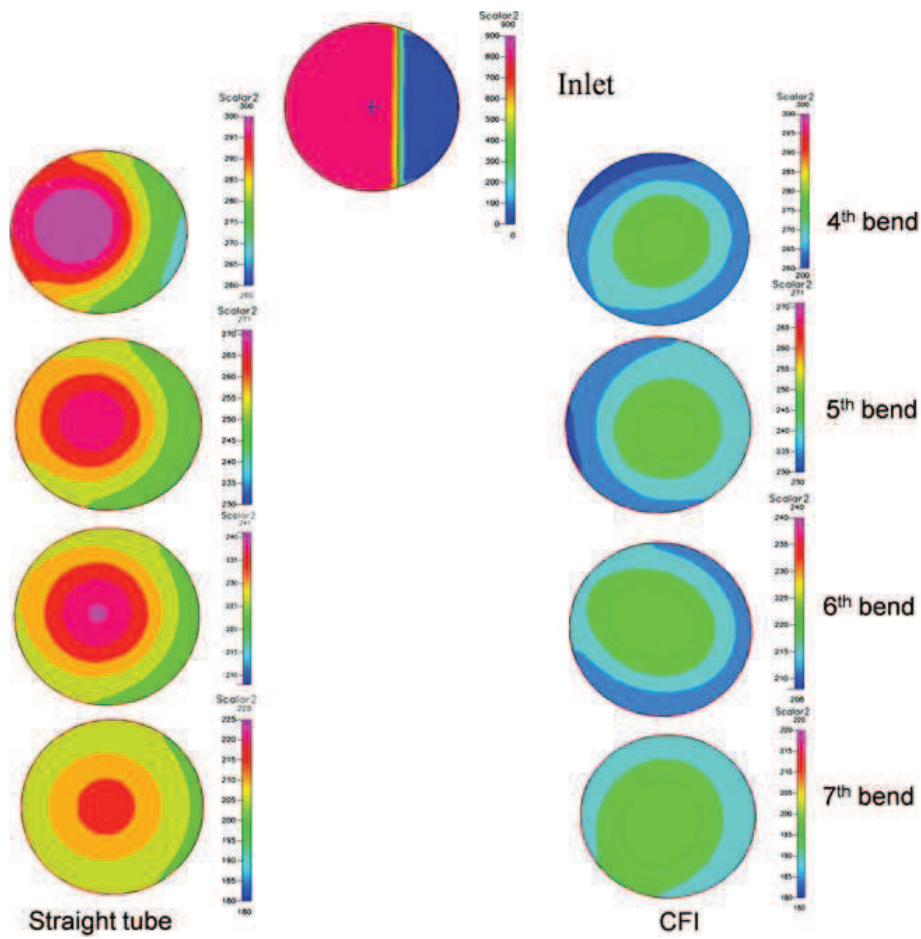
Fig. 2-15- CFD results for mixing and polymerization reaction for styrene under unmixed feed condition. (at inlet, monomer - red, initiator+solvent - blue)[59]

There are other designs also with 90°bend with different orientation as shown in Fig. 2-16. They have been studied for chaotic advection[60-62, 87] and its effect on residence time[63,64] and has been used as heat exchanger[65-69, 87].

<div align="center">(a)[60]   (b)[87]</div>
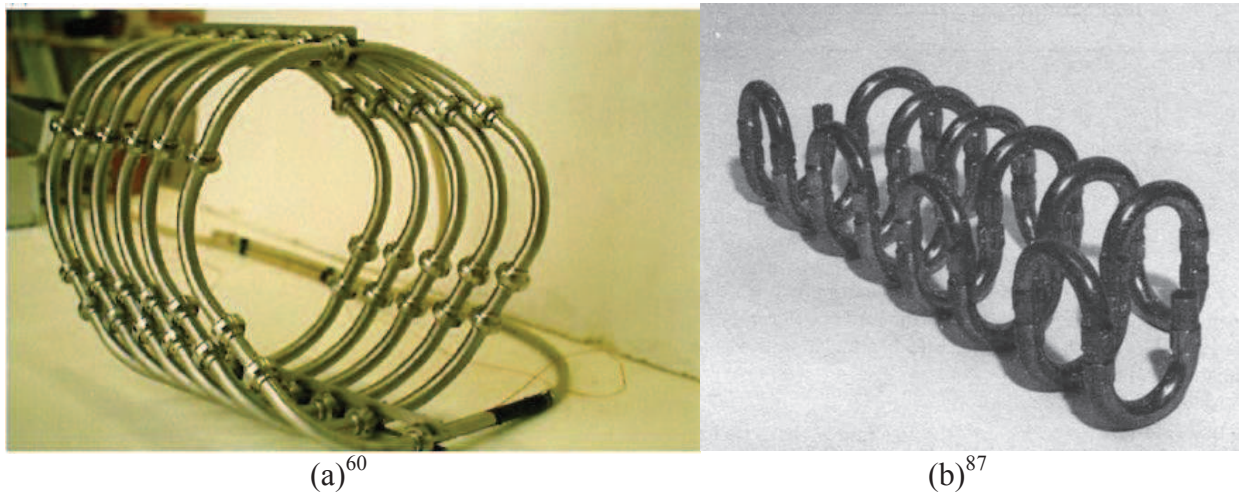
<div align="center">Fig. 2-16- Chaotic configuration</div>

2.7   Chaotic advection

Chaotic advection as mentioned above was first coined by Aref[70]. He explained the case of chaotic advection by a very simple case of two stirrers. These two stirrers can be assumed to be fixed at some positions separated by distance *2b* within a circle of radius *a*. Only one stirrer can rotate with a given vortex strength (Γ) at a time for a given time interval (T). So only one stirrer will operate for one-half of the time interval chosen, and another stirrer will operate for other remaining half of the time interval. So in the beginning, the path of the particle around the stirrer would be circular and thus can be solved analytically. Same thing can applied during second stirrer operation. So sample particle trajectories can be seen as shown in Fig. 2-17. So, the situation can vary from integrability of the trajectory to complete non-integrability of the path of the particle (chaos). So, by varying various factors like speed of rotation (vortex strength), distance between the stirrers, length of time interval, different results (degree of chaos) can be obtained as shown in Fig. 2-18 & Fig. 2-19 showing no chaos to total chaos.
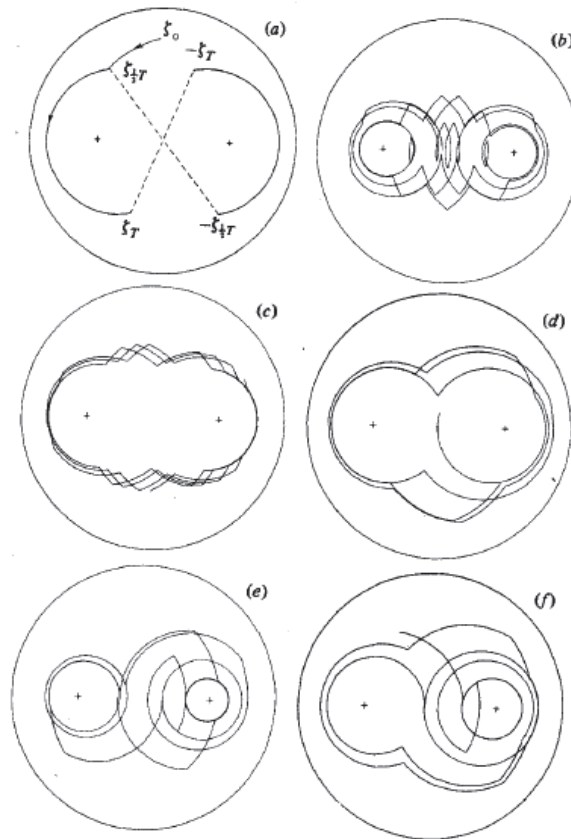
Fig. 2-17-Sample particle trajectories under different conditions[70]
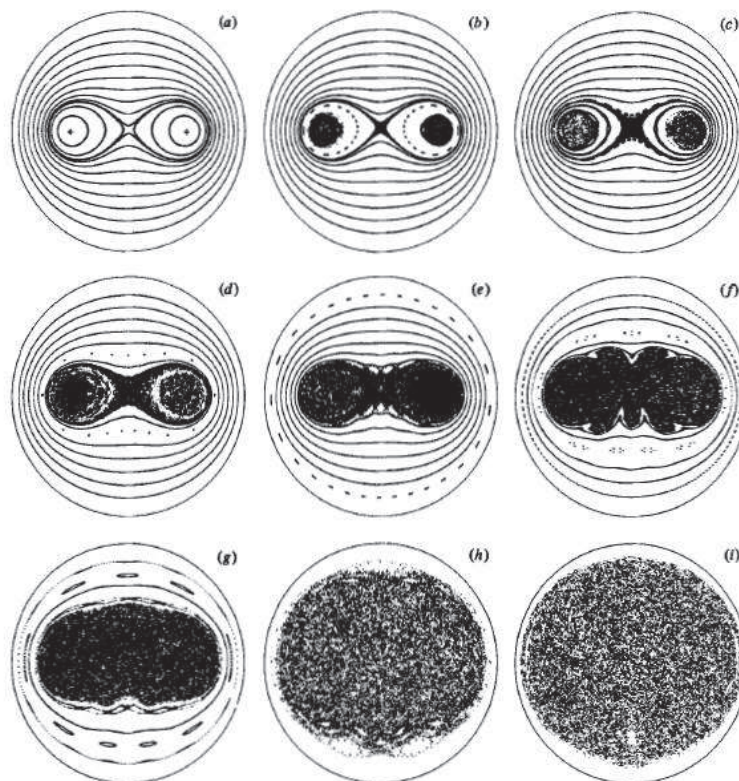
FIGURE 2. Iterated-map results described in §4. Parameters are $\beta = 0.5$ and (a) $\mu = 0.05$; (b) 0.10; (c) 0.125; (d) 0.15; (e) 0.20; (f) 0.35; (g) 0.50; (h) 1.0; (i) 1.5. Crosses indicate agitator positions.

Fig. 2-18- Iterated map results under different conditions from no chaos from top left to full chaos at right bottom[70]
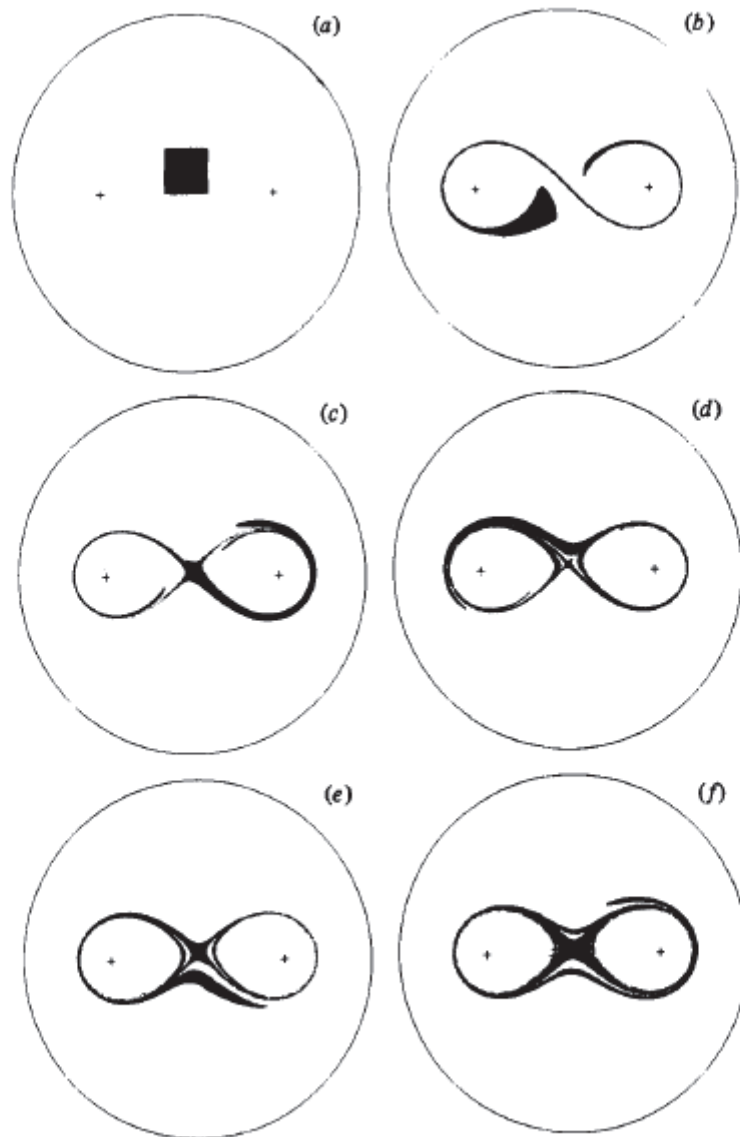
FIGURE 5. Phases in the stirring of an initially square array of particles. Parameters are $\beta = 0.5$, $\mu = 0.1$. Panels shown are at times (a) $t = 0$; (b) 1; (c) 2; (d) 3; (e) 4; (f) 12.

(a)
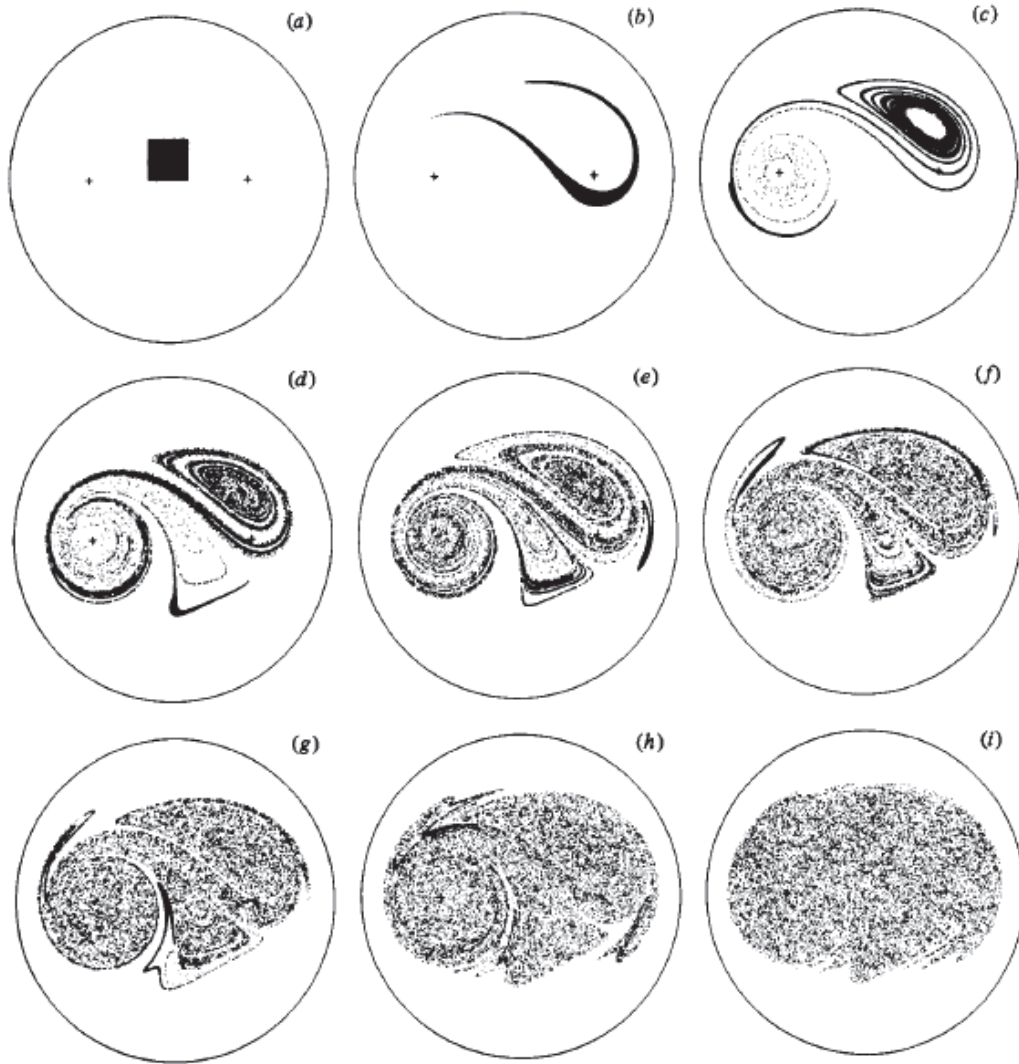
FIGURE 4. Phases in the stirring of an initially square array of particles. Parameters are $\beta = 0.5$, $\mu = 1.0$. Panels shown are at times (a) $t = 0$; (b) 1; (c) 2; (d) 3; (e) 4; (f) 5; (g) 6; (h) 9; (i) 12.

(b)

Fig. 2-19- Different phases of stirring initial square array of particles[70]

The author defined two dimensionless parameters which completely defined stirring. These parameters are

$$\beta_A = \frac{b}{a} \tag{2-11}$$

$$\mu_A = \frac{T\Gamma}{2\pi a^2} \tag{2-12}$$

Where β_A gives dimensionless amplitude for the oscillations of the agitator, μ_A gives a dimensionless period of its motion. For chaos, $0 < \beta_A \leq 0.7$, μ_A should be high as much possible. But there is a limit for increasing μ_A. In curved flow, higher De will increase vortex

61

strength, but that will also increase the center of the dean vortices and hence it will increase β_A. So β_A crossing 0.7 will not give good results in terms of chaos. We can also observe that $\mu_A \propto \frac{1}{a^2}$, so a small decrease in tube diameter will greatly increase μ_A. For details please refer to Aref[70].

This treatment presented by him was general in nature and could be applied to *n* number of stirrers working alternately. So in this light, the two vortices formed during secondary flow in CT with their positions at the center of these vortices could be taken as two stirrers and their vortex strength is dependent on *De*. So, when a bend in CT inclined at some angle is encountered, the positions of these vortices are changed. Thus, as already mentioned above, different conditions will give different degrees of chaos. This also implies that simply by having 90° bend does not necessarily create chaos. So CFI may generate different degree of chaos under different conditions. So 90° bend will definitely produce secondary flow but that is not the guarantee of chaotic flow as generally stated.

Chaotic advection is also called as lagrangian chaos as it can occur even in the flow field at steady state unlike in the case of turbulence which is eulerian chaos. Chaotic advection is a result of flow kinematics[71]. Chaotic advection can be explained in very simple term by example of two very nearly placed particles in a given flow field. In chaotic advection, the two particles' trajectory will differ completely despite having very small differences in their position and the particles could not be traced back to their original position (non-integrability of path) by reversing the flow field. There is a considerable study done on chaotic advection[72-81] and the references mentioned here are just to name a few. It has been found that even laminar flow at very low *Re* can produce chaotic advection under suitable conditions[82]. One of the advantages of chaotic flow is that unlike in turbulence, it enhances mixing without any additional requirement of energy because it is of lagrangian type. For chaotic advection, 2D flow necessarily to be unsteady state but there can be chaos even in steady state 3D flow[72].

Several researches have used the concept of chaotic advection for mixing problem[83-86], heat transfer[87], effect on residence time[88], and chemical reactions[89].

2.8   Microfluidics

Another way to improve mixing is to decrease the dimensions of the reactor so that the gradients are quite small. Now-a-days, there is considerable interest and progress made in the field of microfluidics[90-92]. In it, the characteristic lengths are of the order of microns. It offers several advantages over larger size. Due to reduction in size, quantity of reagents used is small, less heat is generated, higher surface-to-volume ratio gives higher heat transfer rates and less thermal and temperature gradients. All these make them inherently safe and economical and give much better control and yield in the chemical reactions. A lot of progress has been made in this field of micromixers[93-96] (Fig. 2-20) and microreactors[97-106]. Several studies have been done to evaluate micromixers and microreactors[108-112].
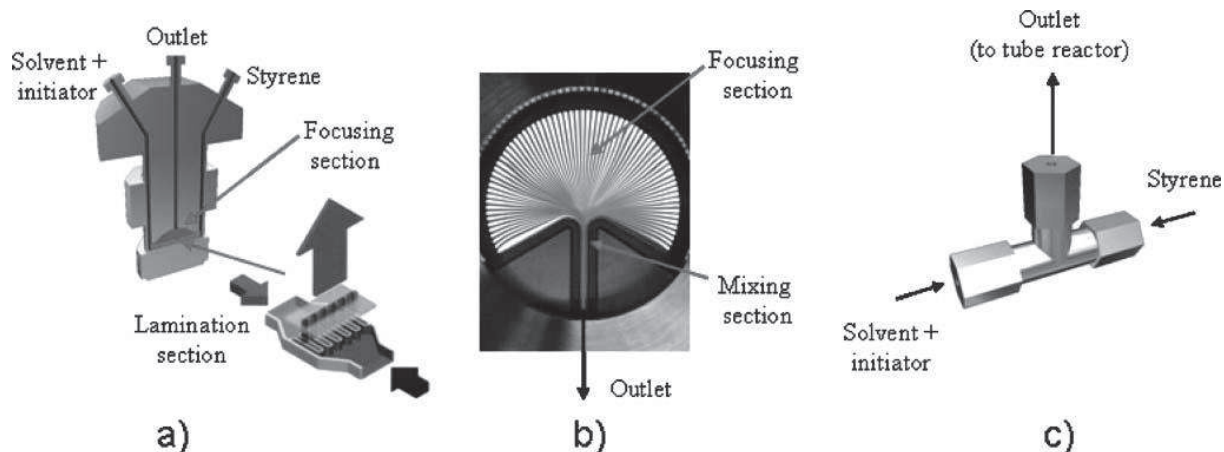
Fig. 2-20- Different types of micromixers, a) High Pressure Interdigital Multilamination Micromixer (HPIMM), b) Superfocus Interdigital Multilamination Micromixer (SFIMM), c) T-junction[107]

Chaotic advection also has been used for designing various micromixers[113-115]. Normally, the reactions are conducted at lab scale and then are scaled up to pilot plant and then industrial level for large scale production. But many advantages at small dimensions like low concentration and temperature gradients are lost as size increases. So another way out to bypass this problem is to scale out. i.e. to keep the small dimensions intact but to use more no. to increase the production. Some successful attempts were already made in this direction[116-117].

Although various chemical processes have been carried out in microreactor but polymerization is special. It is special in terms of extreme variation of viscosity with conversion. This may plug the microreactor. Still, polymerization reaction have also been carried out in microreactor geometries by some researchers[57,112,118].

2.9 Free radical polymerization

Free radical polymerization (FRP)[119] is considered in this study. In FRP, radicals are required to initiate polymerization. This is done by an initiator which dissociates thermally. This radical then react with monomer to generate primary radical. This primary radical then propagate this reaction by reacting with another monomer and thus chain length is increased. This process of propagation is stopped by termination process where the two radicals become dead after reacting and neutralizing each other with or without combining with each other. Besides this several side reactions also take place like transfer processes. In transfer processes, the radical reacts with other molecules (which may be of solvent, monomer, chain transfer agent or polymer), turn that molecule into radical and become dead itself. This can lead to branching of polymers and under certain conditions can lead to gel effect[120-124].

2.9.1 Gel/Glass/Cage effects

Gel effect or Trommsdorff-Norish effect is the sudden rise of reaction rate in polymerization after certain conversion is reached. This is attributed to decrease in termination kinetic rate

coefficient due to decreased diffusivity of polymer radical chains. This effect can occur even during isothermal conditions. It has detrimental effects on the properties of polymers and can also lead to thermal runaway of the reaction[125]. With increase in viscosity due to increased conversion, the mobility of even monomer is severely impaired and the reaction almost freezes. This is called as glass effect. The initiator efficiency is affected by the cage of molecules around the radicals formed due to dissociation of initiator and they need to come out of it before reacting with monomer molecules. It is called cage effect.

2.9.2 CCS model

Chiu, Carratt & Soong (CCS)[126] using the theoretical concept of polymer diffusion, were able to develop a model which simulate gel and glass effect smoothly over the complete conversion range. It did not require any critical point to initiate gel effect in the model. In their theoretical development of the model, they defined a sphere of reaction around polymer chain where reaction needs to take place. The monomer from large distance from the bulk needs to diffuse to this sphere of reaction to accomplish the reaction. Thus they obtained the expression accounting for the diffusion effect affecting kinetic rate coefficient of termination (for gel effect) and propagation (for glass effect). They then separated the diffusion term into two terms in which one was dependent on temperature and molecular weight and other on conversion. Then they obtained the expression for conversion based term by applying Fujita-Doolittle theory[127] based on free volume concept. Whereas expression for the temperature based term was obtained by best fit of experimental data. Although this model was successful in predicting the gel and glass effect quite well but the prediction for weight average molecular weight was poor.

2.9.3 AK model

Achilias and Kiparissides[128] (AK) improved this model by retaining the diffusion and other terms and used Vrentas and Duda model[129,130] for diffusion coefficient based on free volume theory. They further expanded and improved their model by including cage effect in it[125]. AK model was quite successful in predicting weight average molecular weight and polydispersity index (PDI). Several researchers used this model successfully and this model has been improved over the years[131-140].

2.9.4 Modeling and simulation of FRP

Besides carrying out, modeling and simulating reactions in batch reactor, various researchers have carried out the experiments and simulation of FRP in flow reactors using variation in physical properties like density, viscosity, and thermal conductivity, with good success[141-145]. But no analysis is done for microreactor dimensions.

2.9.5 Free volume theory

Free volume theory states that the molecular diffusion rate is dependent on the space available between the molecules called as free volume. It was first used to explain the diffusion process in liquids. Cohen and Turnbul[l146] assumed that the liquid molecules in spherical form can move from through this free space through random thermal fluctuations if the sufficiently

large space is available to them. This transition should occur without any extra expense of thermal energy. Fujita[147] extended it to solvent self-diffusion in rubbery polymer-solvent system. Vrentas and Duda improved this theory[129,130] and over the year this theory was further refined[148-174].

2.10   Computational fluid dynamics (CFD)

Computational fluid dynamics (CFD) has gained much importance now-a-days due to improved computational capability availability at a cheaper rate, easy availability of trained manpower and improved numerical methods and techniques. Researchers now are applying CFD to various problems to gain deeper understanding of the processes. Many times, several simplifications are used, other times complete models are used to eliminate any source of possible error. All this depends on the complexity of the problem, availability of computational power, results desired and resources available at disposal.

2.10.1 CFD Modeling of variation in fluid thermo-physical properties

CFD analysis of polymerization poses special problem as the viscosity varies by about 4-6 orders from inlet to outlet. Several researchers have modeled the variation of viscosity and density and matched their results with experimental data successfully[141-145]. Kumar *et al.*[31] had carried out study of variation in fluid thermo-physical properties like density, viscosity, thermal conductivity and specific heat under both heating and cooling condition. They have CT as the flow geometry with *Re* ranged from 100-400. Two different fluids – water (non-viscous) and diethylene glycol (highly viscous), were used for study. The effect of temperature alongwith the secondary flow induced from the finite curvature and pitch of CT on the thermo-physical properties was studied. The CFD results are shown in Fig. 2-21.

Recently Andrade and Zaparoli[139] have done CFD analysis of variation of water viscosity with temperature in curved tube. So we can observe an important variation in flow profile and hence mixing characteristics due to variation in thermo-physical properties in curved tube. Some researchers have used CFI to model and simulate polymerization of styrene under microreactor condition using constant viscosity and density assumption with discrete variation of diffusion coefficient to mimic the effect of diffusion coefficient[59,112]. The effect of diffusion coefficient is not visible for large sizes[145] but when the dimensions reached to the level of microreactor, it gained importance. The results[59,112] have predicted the increased mixing of components in straight tube reactor despite feeding them in unmixed condition. In absence of any mechanical mixing, only diffusion can do it. The implementation of variation of fluid thermo-physical properties and diffusion coefficient will increase the complexity of code, increase the computational load and time, may require several adjustments like increasing mesh size, adjusting relaxation parameters etc. to make the simulation stable and converge. This can further increase the computational requirement in terms of processing power and time.

Velocity fields variation for temperature dependent in CT at Re=400 for (i) heating, (ii) cooling and (iii) constant conditions at (a) 15°, (b) 30°, (c) 60°and (d) 180°.	Temperature fields variation for temperature dependent in CT at Re=400 for (i) heating, (ii) cooling and (iii) constant conditions at (a) 15°, (b) 30°, (c) 60°and (d) 180°.

Velocity fields for temperature dependent in CT for (i) heating, (ii) cooling and (iii) constant conditions at (a) Re=100, (b) Re=200, (c) Re=300, and (d) Re=400.	Temperature fields for temperature dependent in CT for (i) heating, (ii) cooling and (iii) constant conditions at (a) Re=100, (b) Re=200, (c) Re=300, and (d) Re=400.

Fig. 2-21-Results for variation of thermo-physical properties under various conditions[31]

2.11   This thesis

In this thesis, we will evaluate three different reactor geometries- namely STR, CTR & CFIR. But to evaluate these reactors on proper basis, a good modeling is needed for both kinetic and physical conditions and parameters. Besides this, a benchmark was required, against which the predictions of monomer conversion, polydispersity index (PDI) and molecular

weight distributions could be counterchecked. This is necessary because higher values of monomer conversion and molecular weight distributions and lower value of PDI can be predicted because of wrong choice of numerical schemes or other errors. So this will lead to wrong analysis and understanding of the process. So, a model was needed to be built that can improve the modeling as well as help in counterchecking the results lest we overshoot the theoretical results. So we need to have some sort of analytical solution (AS) for FRP. Once that AS is obtained, it needs to be validated. We then go on to prove its worth for whole range of conversion so that we need not to restrict ourselves for the limitations of the method. We then found out a new transformation that helped in removing a basic problem; using mass form for modeling chemical species Models for varying the fluid thermo-physical properties are available from various sources[141-145]. For modeling variation diffusion coefficient, Vrentas and Duda model based on free volume theory will be used.

2.12 References

1. McCabe, W. L.; Smith, J., C.; Harriott, P., Unit Operations of Chemical Engineering. McGraw-Hill Inc., Singapore, fifth edition, 1993.

2. Levenspiel, O., Chemical Reaction Engineering. *John Wiley & Sons*, New York, third edition, 1999.

3. Nigam, K. D. P.; Agarwal, S.; Srivastava, V. K., Laminar convection of non-Newtonian fluids in the thermal entrance region of coiled circular tubes. *Chem Eng J* **2001,** *84* (3), 223-237.

4. Kleinstreuer, C.; Agarwal, S., Coupled Heat and Mass-Transfer in Laminar-Flow, Tubular Polymerizers. *Int J Heat Mass Tran* **1986,** *29* (7), 979-986.

5. Shah, S. N.; Cox, K. E., Dispersion in Non-Newtonian Laminar-Flow through a Tube. *Chem Eng Sci* **1976,** *31* (3), 241-242.

6. Dang, V. D.; Steinberg, M., Laminar-Flow Mass-Transfer with Axial Diffusion in a Tube with Chemical-Reaction. *Chem Eng Sci* **1977,** *32* (3), 326-328.

7. Nigam, K. D. P.; Vasudeva, K., Diffusion and Reaction in Tubular Reactor with Non-Newtonian Laminar-Flow. *Chem Eng Sci* **1977,** *32* (6), 673-677.

8. Saxena, A. K.; Nigam, K. D. P., Rtd for Laminar-Flow in Helical-Coils. *Chem Eng Sci* **1979,** *34* (3), 425-426.

9. Janssen, L. A. M.; Hoogendoorn, C. J., Laminar Convective Heat-Transfer in Helical Coiled Tubes. *Int J Heat Mass Tran* **1978,** *21* (9), 1197-1206.

10. Mansour, A. R.; Hussein, A. M., An Approximate Analytical Solution for the Nonlinear Inverse Axial-Dispersion Model. *Int Commun Heat Mass* **1990,** *17* (6), 823-830.

11. Mansour, A. R.; Sheboul, M.; Hussein, A. M.; Nusayr, A., An Analytical Solution for Diffusion and Reaction in a Laminar-Flow Tubular Reactor. *Int Commun Heat Mass* **1989,** *16* (4), 603-608.

12. Mansour, A. R., An Analytical Solution of Laminar Heat-Transfer to Power-Law Non-Newtonian Fluids in Circular Ducts Graetz-Nusselt Problem. *Int Commun Heat Mass* **1989,** *16* (2), 199-204.

13. Erdogan, S.; Worner, M., Influence of channel cross-sectional shape on diffusion-free residence time distribution in fully developed laminar Newtonian flow. *Chem Eng J* **2013,** *227*, 158-165.

14. Worner, M., Approximate residence time distribution of fully develop laminar flow in a straight rectangular channel. *Chem Eng Sci* **2010,** *65* (11), 3499-3507.

15. Garcia-Serna, J.; Garcia-Verdugo, E.; Hyde, J. R.; Fraga-Dubreuil, J.; Yan, C.; Poliakoff, M.; Cocero, M. J., Modelling residence time distribution in chemical reactors: A novel generalised n-laminar model - Application to supercritical CO2 and subcritical water tubular reactors. *J Supercrit Fluid* **2007,** *41* (1), 82-91.

16. Kheshgi, H. S., Laminar-Flow in Twisted Ducts. *Phys Fluids a-Fluid* **1993,** *5* (11), 2669-2681.

17. Ranade, V. R.; Ulbrecht, J. J., The Residence Time Distribution for Laminar-Flow of Non-Newtonian Liquids through Helical Tubes. *Chem Eng Commun* **1981,** *8* (1-3), 165-176.

18. Kleinstreuer, C.; Agarwal, S., Coupled Heat and Mass-Transfer in Laminar-Flow, Tubular Polymerizers. *Int J Heat Mass Tran* **1986,** *29* (7), 979-986.

19. Conte, I.; Peng, X. F., Numerical investigations of laminar flow in coiled pipes. *Appl Therm Eng* **2008,** *28* (5-6), 423-432.

20. Sinnott, R. K., Chemical Engineering Design. Coulson & Richardson's Chemical Engineering, Volume 6, Fourth edition, Elsevier Butterworth-Heinemann, Oxford , 2005

21. White, C. M., Streamline Flow through Curved Pipes. *Proc. R. Soc. Lond. A* **1929**, *123*, 645-663.

22. Eustice, J., Flow of Water in Curved Pipes. Proceedings of the Royal Society of London. Series A, Containing Papers of a Mathematical and Physical Character **1910**, 84 (568), 107–118.

23. Dean, W. R., The streamline motion of fluid in a curved pipe. *Philos. Mag.* **1928**, *30*, 673–93.

24. Dean, W. R.; Hurst, J. M., Note on the motion of fluid in a curved pipe. *Mathematika* **1959**, *6*, 77-85.

25. McConalogue, D. J.; Srivastava, R. S., Motion of a fluid in a curved tube. *Proc. Roy. Soc. A* **1968**, *307*, 37-53**.**

26. Cuming, H. G., The secondary flow in curved pipes. *Aeronaut. Res. Counc. Rep.* **1952**, Mem. No. 2880.

27. Goering, D. J.; Humphrey, J. A. C., On the Spatial Stability of Tube Flows Subject to Body Forces. *Phys Fluids a-Fluid* **1993,** *5* (12), 3107-3121.

28. Yamamoto, K.; Yanase, S.; Yoshida, T., Torsion Effect on the Flow in a Helical Pipe. *Fluid Dyn Res* **1994,** *14* (5), 259-273.

29. Zapryanov, Z.; Christov, C.; Toshev, E., Fully-Developed Laminar-Flow and Heat-Transfer in Curved Tubes. *Int J Heat Mass Tran* **1980,** *23* (6), 873-880.

30. Kumar, V.; Saini, S.; Sharma, M.; Nigam, K. D. P., Pressure drop and heat transfer study in tube-in-tube helical heat exchanger. *Chem Eng Sci* **2006,** *61* (13), 4403-4416.

31. Kumar, V.; Gupta, P.; Nigam, K. D. P., Fluid flow and heat transfer in curved tubes with temperature-dependent properties. *Ind Eng Chem Res* **2007,** *46* (10), 3226-3236.

32. Naphon, P.; Wongwises, S., A review of flow and heat transfer characteristics in curved tubes. *Renew Sust Energ Rev* **2006,** *10* (5), 463-490.

33. Wongwises, S.; Naphon, P., Thermal performance of a spirally coiled finned tube heat exchanger under wet-surface conditions. *J Mech Sci Technol* **2006,** *20* (2), 212-226.

34. Wongwises, S.; Naphon, P., Heat transfer characteristics of a spirally coiled, finned-tube heat exchanger under dry-surface conditions. *Heat Transfer Eng* **2006,** *27* (1), 25-34.

35. Ghobadi, M.; Muzychka, Y. S., Effect of entrance region and curvature on heat transfer in mini scale curved tubing at constant wall temperature. *Int J Heat Mass Tran* **2013,** *65*, 357-365.

36. Kumar, V.; Aggarwal, M.; Nigam, K. D. P., Mixing in curved tubes. *Chem Eng Sci* **2006,** *61* (17), 5742-5753.

37. Vanka, S. P.; Luo, G.; Winkler, C. M., Numerical study of scalar mixing in curved channels at low Reynolds numbers. *Aiche J* **2004,** *50* (10), 2359-2368.

38. Jayakumar, J. S.; Mahajani, S. M.; Mandal, J. C.; Iyer, K. N.; Vijayan, P. K., Thermal hydraulic characteristics of air-water two-phase flows in helical pipes. *Chem Eng Res Des* **2010,** *88* (4A), 501-512.

39. Vashisth, S.; Nigam, K. D. P., Prediction of flow profiles and interfacial phenomena for two-phase flow in coiled tubes. *Chem Eng Process* **2009,** *48* (1), 452-463.

40. Agrawal, S.; Jayaraman, G., Numerical-Simulation of Dispersion in the Flow of Power-Law Fluids in Curved Tubes. *Appl Math Model* **1994,** *18* (9), 504-512.

41. Agrawal, S.; Srivastava, V. K.; Jayaraman, G.; Nigam, K. D. P., Power-Law Fluids in a Circular Curved Tube .3. Numerical-Simulation of Laminar-Flow. *Polym-Plast Technol* **1994,** *33* (3), 357-379.

42. Jayakumar, J. S.; Mahajani, S. M.; Mandal, J. C.; Iyer, K. N.; Vijayan, P. K., CFD analysis of single-phase flows inside helically coiled tubes. *Comput Chem Eng* **2010,** *34* (4), 430-446.

43. Chen, J. J.; Chen, C. H.; Shie, S. R., Optimal Designs of Staggered Dean Vortex Micromixers. *Int J Mol Sci* **2011,** *12* (6), 3500-3524.

44. Agrawal, S.; Nigam, K. D. P., Modelling of a coiled tubular chemical reactor. *Chem Eng J* **2001,** *84* (3), 437-444.

45. Berger, S. A.; Talbot, L.; Yao, L. S., Flow in Curved Pipes. *Annu Rev Fluid Mech* **1983,** *15*, 461-512.

46. Vashisth, S.; Kumar, V.; Nigam, K. D. P., A review on the potential applications of curved geometries in process industry. *Ind Eng Chem Res* **2008,** *47* (10), 3291-3337.

47. Saxena, A. K.; Nigam, K. D. P., Coiled Configuration for Flow Inversion and Its Effect on Residence Time Distribution. *Aiche J* **1984,** *30* (3), 363-368.

48. Kumar, V.; Nigam, K. D. P., Numerical simulation of steady flow fields in coiled flow inverter. *Int J Heat Mass Tran* **2005,** *48* (23-24), 4811-4828.

49. Mridha, M.; Nigam, K. D. P., Coiled flow inverter as an inline mixer. *Chem Eng Sci* **2008,** *63* (6), 1724-1732.

50. Mandal, M. M.; Aggarwal, P.; Nigam, K. D. P., Liquid-Liquid Mixing in Coiled Flow Inverter. *Ind Eng Chem Res* **2011,** *50* (23), 13230-13235.

51. Kumar, V.; Mridha, M.; Gupta, A. K.; Nigam, K. D. P., Coiled flow inverter as a heat exchanger. *Chem Eng Sci* **2007,** *62* (9), 2386-2396.

52. Mandal, M. M.; Kumar, V.; Nigam, K. D. P., Augmentation of heat transfer performance in coiled flow inverter vis-a-vis conventional heat exchanger. *Chem Eng Sci* **2010,** *65* (2), 999-1007.

53. Kumar, V.; Nigam, K. D. P., Laminar convective heat transfer in chaotic configuration. *Int J Heat Mass Tran* **2007,** *50* (13-14), 2469-2479.

54. Singh, J.; Verma, V.; Nigam, K. D. P., Flow Characteristics of Power-Law Fluids in Coiled Flow Inverter. *Ind Eng Chem Res* **2013,** *52* (1), 207-221.

55. Mridha, M.; Nigam, K. D. P., Numerical study of turbulent forced convection in coiled flow inverter. *Chem Eng Process* **2008,** *47* (5), 893-905.

56. Vashisth, S.; Nigam, K. D. P., Experimental investigation of void fraction and flow patterns in coiled flow inverter. *Chem Eng Process* **2008,** *47* (8), 1287-1297.

57. Vashisth, S.; Nigam, K. D. P., Experimental investigation of pressure drop during two-phase flow in a coiled flow inverter. *Ind Eng Chem Res* **2007,** *46* (14), 5043-5050.

58. Vashisth, S.; Nigam, K. D. P., Liquid-phase residence time distribution for two-phase flow in coiled flow inverter. *Ind Eng Chem Res* **2008,** *47* (10), 3630-3638.

59. Mandal, M. M.; Serra, C.; Hoarau, Y.; Nigam, K. D. P., Numerical modeling of polystyrene synthesis in coiled flow inverter. *Microfluid Nanofluid* **2011,** *10* (2), 415-423.

60. Castelain, C.; Legentilhomme, P., Residence time distribution of a purely viscous non-Newtonian fluid in helically coiled or spatially chaotic flows. *Chem Eng J* **2006,** *120* (3), 181-191.

61. Castelain, C.; Mokrani, A.; Le Guer, Y.; Peerhossaini, H., Experimental study of chaotic advection regime in a twisted duct flow. *Eur J Mech B-Fluid* **2001,** *20* (2), 205-232.

62. Chagny-Regardin, C.; Castelain, C.; Peerhossaini, H., Numerical simulation of chaotic advection in an alternated Dean flow for complex fluids. *Simulation in Industry'2000* **2000**, 675-681.

63. Castelain, C.; Mokrani, A.; Legentilhomme, P.; Peerhossaini, H., Residence time distribution in twisted pipe flows: Helically coiled system and chaotic system. *Exp Fluids* **1997,** *22* (5), 359-368.

64. Castelain, C.; Berger, D.; Legentilhomme, P.; Mokrani, A.; Peerhossaini, H., Experimental and numerical characterisation of mixing in a steady spatially chaotic flow by means of residence time distribution measurements. *Int J Heat Mass Tran* **2000,** *43* (19), 3687-3700.

65. Lasbet, Y.; Auvity, B.; Castelain, C.; Peerhossaini, H., A chaotic heat-exchanger for PEMFC cooling applications. *J Power Sources* **2006,** *156* (1), 114-118.

66. Chagny, C.; Castelain, C.; Peerhossaini, H., Chaotic heat transfer for heat exchanger design and comparison with a regular regime for a large range of Reynolds numbers. *Appl Therm Eng* **2000,** *20* (17), 1615-1648.

67. Mokrani, A.; Castelain, C.; Peerhossaini, H., Lagrangian chaos and heat transfer. *Heat Transfer 1998, Vol 6* **1998**, 125-130.

68. Mokrani, A.; Castelain, C.; Peerhossaini, H., The effects of chaotic advection on heat transfer. *Int J Heat Mass Tran* **1997,** *40* (13), 3089-3104.

69. Peerhossaini, H.; Castelain, C.; Leguer, Y., Heat-Exchanger Design Based on Chaotic Advection. *Exp Therm Fluid Sci* **1993,** *7* (4), 333-344.

70. Aref, H., Stirring by Chaotic Advection. *J Fluid Mech* **1984,** *143* (Jun), 1-21.

71. Aref, H., Chaotic Advection of Fluid Particles. *Philos T Roy Soc A* **1990,** *333* (1631), 273-288.

72. Aref, H., The development of chaotic advection. *Phys Fluids* **2002,** *14* (4), 1315-1325.

73. Wiggins, S.; Ottino, J. M., Foundations of chaotic mixing. *Philos T Roy Soc A* **2004,** *362* (1818), 937-970.

74. Ottino, J. M.; Wiggins, S., Introduction: mixing in microfluidics. *Philos T Roy Soc A* **2004,** *362* (1818), 923-935.

75. Fountain, G. O.; Khakhar, D. V.; Mezic, I.; Ottino, J. M., Chaotic mixing in a bounded three-dimensional flow. *J Fluid Mech* **2000,** *417*, 265-301.

76. Ottino, J. M.; Souvaliotis, A.; Metcalfe, G., Chaotic Mixing Processes - New Problems and Computational Issues. *Chaos Soliton Fract* **1995,** *6*, 425-438.

77. Ottino, J. M., Mixing and Chemical-Reactions - a Tutorial. *Chem Eng Sci* **1994,** *49* (24A), 4005-4027.

78. Kusch, H. A.; Ottino, J. M., Experiments on Mixing in Continuous Chaotic Flows. *J Fluid Mech* **1992,** *236*, 319-348.

79. Muzzio, F. J.; Swanson, P. D.; Ottino, J. M., Mixing Distributions Produced by Multiplicative Stretching in Chaotic Flows. *Int J Bifurcat Chaos* **1992,** *2* (1), 37-50.

80. Swanson, P. D.; Ottino, J. M., A Comparative Computational and Experimental-Study of Chaotic Mixing of Viscous Fluids. *J Fluid Mech* **1990,** *213*, 227-249.

81. Ottino, J. M., Mixing, Chaotic Advection, and Turbulence. *Annu Rev Fluid Mech* **1990,** *22*, 207-253.

82. Cartwright, J. H. E.; Feingold, M.; Piro, O., An introduction to chaotic advection. *Nato Adv Sci I B-Phy* **1999,** *373*, 307-342.

83. Yamagishi, A.; Inaba, T.; Yamaguchi, Y., Chaotic analysis of mixing enhancement in steady laminar flows through multiple pipe bends. *Int J Heat Mass Tran* **2007,** *50* (7-8), 1238-1247.

84. Jang, B.; Funakoshi, M., Chaotic mixing in a helix-like pipe with periodic variations in curvature and torsion. *Fluid Dyn Res* **2010,** *42* (3).

85. Habchi, C.; Lemenand, T.; Della Valle, D.; Peerhossaini, H., Liquid/liquid dispersion in a chaotic advection flow. *Int J Multiphas Flow* **2009,** *35* (6), 485-497.

86. Amon, C. H.; Guzman, A. M.; Morel, B., Lagrangian chaos, Eulerian chaos, and mixing enhancement in converging-diverging channel flows. *Phys Fluids* **1996,** *8* (5), 1192-1206.

87. Acharya, N.; Sen, M.; Chang, H. C., Heat-Transfer Enhancement in Coiled Tubes by Chaotic Mixing. *Int J Heat Mass Tran* **1992,** *35* (10), 2475-2489.

88. Vikhansky, A., Effect of diffusion on residence time distribution in chaotic channel flow. *Chem Eng Sci* **2008,** *63* (7), 1866-1870.

89. Tang, X. Z.; Boozer, A. H., Design criteria of a chemical reactor based on a chaotic flow. *Chaos* **1999,** *9* (1), 183-194.

90. Verpoorte, E.; De Rooij, N. F., Microfluidics meets MEMS. *P Ieee* **2003,** *91* (6), 930-953.

91. Mark, D.; Haeberle, S.; Roth, G.; von Stetten, F.; Zengerle, R., Microfluidic lab-on-a-chip platforms: requirements, characteristics and applications. *Chem Soc Rev* **2010,** *39* (3), 1153-1182.

92. Squires, T. M.; Quake, S. R., Microfluidics: Fluid physics at the nanoliter scale. *Rev Mod Phys* **2005,** *77* (3), 977-1026.

93. Hessel, V.; Lowe, H.; Schonfeld, F., Micromixers - a review on passive and active mixing principles. *Chem Eng Sci* **2005,** *60* (8-9), 2479-2501.

94. Aubin, J.; Ferrando, M.; Jiricny, V., Current methods for characterising mixing and flow in microchannels. *Chem Eng Sci* **2010,** *65* (6), 2065-2093.

95. Suh, Y. K.; Kang, S., A Review on Mixing in Microfluidics. *Micromachines-Basel* **2010,** *1* (3), 82-111.

96. Kumar, V.; Paraschivoiu, M.; Nigam, K. D. P., Single-phase fluid flow and mixing in microchannels. *Chem Eng Sci* **2011,** *66* (7), 1329-1373.

97. Fletcher, P. D. I.; Haswell, S. J.; Pombo-Villar, E.; Warrington, B. H.; Watts, P.; Wong, S. Y. F.; Zhang, X. L., Micro reactors: principles and applications in organic synthesis. *Tetrahedron* **2002,** *58* (24), 4735-4757.

98. Wiles, C.; Watts, P., Continuous flow reactors, a tool for the modern synthetic chemist. *Eur J Org Chem* **2008,** (10), 1655-1671.

99. Mason, B. P.; Price, K. E.; Steinbacher, J. L.; Bogdan, A. R.; McQuade, D. T., Greener approaches to organic synthesis using microreactor technology. *Chem Rev* **2007,** *107* (6), 2300-2318.

100. Geyer, K.; Codee, J. D. C.; Seeberger, P. H., Microreactors as tools for synthetic chemists - The chemists' round-bottomed flask of the 21st century? *Chem-Eur J* **2006,** *12* (33), 8434-8442.

101. Jensen, K. F., Microreaction engineering - is small better? *Chem Eng Sci* **2001,** *56* (2), 293-303.

102. Hessel, V.; Lowe, H., Microchemical engineering: Components, plant concepts, user acceptance - Part III. *Chem Eng Technol* **2003,** *26* (5), 531-544.

103. Hessel, V.; Lowe, H., Microchemical engineering: Components, plant concepts, user acceptance - Part II. *Chem Eng Technol* **2003,** *26* (4), 391-408.

104. Hessel, V.; Lowe, H., Microchemical engineering: Components, plant concepts user acceptance - Part I. *Chem Eng Technol* **2003,** *26* (1), 13-24.

105. Yoshida, J.; Nagaki, A.; Iwasaki, T.; Suga, S., Enhancement of chemical selectivity by microreactors. *Chem Eng Technol* **2005,** *28* (3), 259-266.

106. Iwasaki, T.; Yoshida, J., Free radical polymerization in microreactors. Significant improvement in molecular weight distribution control. *Macromolecules* **2005,** *38* (4), 1159-1163.

107. Serra, C.; Sary, N.; Schlatter, G.; Hadziioannou, G.; Hessel, V., Numerical simulation of polymerization in interdigital multilamination micromixers. *Lab Chip* **2005,** *5* (9), 966-973.

108. Boskovic, D.; Loebbecke, S., Modelling of the residence time distribution in micromixers. *Chem Eng J* **2008,** *135*, 138-146.

109. Trachsel, F.; Gunther, A.; Khan, S.; Jensen, K. F., Measurement of residence time distribution in microfluidic systems. *Chem Eng Sci* **2005,** *60* (21), 5729-5737.

110. Liu, R. H.; Stremler, M. A.; Sharp, K. V.; Olsen, M. G.; Santiago, J. G.; Adrian, R. J.; Aref, H.; Beebe, D. J., Passive mixing in a three-dimensional serpentine microchannel. *J Microelectromech S* **2000,** *9* (2), 190-197.

111. Kanaris, A. G.; Mouza, A. A., Numerical investigation of the effect of geometrical parameters on the performance of a micro-reactor. *Chem Eng Sci* **2011,** *66* (21), 5366-5373.

112. Serra, C.; Schlatter, G.; Sary, N.; Schonfeld, F.; Hadziioannou, G., Free radical polymerization in multilaminated microreactors: 2D and 3D multiphysics CFD modeling. *Microfluid Nanofluid* **2007,** *3* (4), 451-461.

113. Nguyen, T. N. T.; Kim, M. C.; Park, J. S.; Lee, N. E., An effective passive microfluidic mixer utilizing chaotic advection. *Sensor Actuat B-Chem* **2008,** *132* (1), 172-181.

114. Stroock, A. D.; Dertinger, S. K. W.; Ajdari, A.; Mezic, I.; Stone, H. A.; Whitesides, G. M., Chaotic mixer for microchannels. *Science* **2002,** *295* (5555), 647-651.

115. Stremler, M. A.; Haselton, F. R.; Aref, H., Designing for chaos: applications of chaotic advection at the microscale. *Philos T R Soc A* **2004,** *362* (1818), 1019-1036.

116. Iwasaki, T.; Kawano, N.; Yoshida, J., Radical polymerization using microflow system: Numbering-up of microreactors and continuous operation. *Org Process Res Dev* **2006,** *10* (6), 1126-1131.

117. Mettler, M. S.; Stefanidis, G. D.; Vlachos, D. G., Scale-out of Microreactor Stacks for Portable and Distributed Processing: Coupling of Exothermic and Endothermic Processes for Syngas Production. *Ind Eng Chem Res* **2010,** *49* (21), 10942-10955.

118. Hornung, C. H.; Guerrero-Sanchez, C.; Brasholz, M.; Saubern, S.; Chiefari, J.; Moad, G.; Rizzardo, E.; Thang, S. H., Controlled RAFT Polymerization in a Continuous Flow Microreactor. *Org Process Res Dev* **2011,** *15* (3), 593-601.

119. Handbook of Radical Polymerization. Edited by Matyjaszewski, K.; Davis, T. P., John Wiley and Sons, Hoboken, 2002.

120. Zhu, S.; Hamielec, A. E., Influence of Cross-Link Density Distribution on Network Formation in Free-Radical Copolymerization of Vinyl Divinyl Monomers. *Macromolecules* **1992,** *25* (20), 5457-5464.

121. Zhu, S.; Hamielec, A. E., Modeling of Free-Radical Polymerization with Cross-Linking - Monoradical Assumption and Stationary-State Hypothesis. *Macromolecules* **1993,** *26* (12), 3131-3136.

122. Zhu, S.; Hamielec, A. E., Kinetics of Network Formation Via Free-Radical Mechanisms - Polymerization and Polymer Modification. *Makromol Chem-M Symp* **1993,** *69*, 247-256.

123. Zhu, S.; Hamielec, A. E., Gel Formation in Free-Radical Polymerization Via Chain Transfer and Terminal Branching. *J Polym Sci Pol Phys* **1994,** *32* (5), 929-943.

124. Zhu, S.; Hamielec, A. E.; Pelton, R. H., Modeling of Cross-Linking and Cyclization in Free-Radical Copolymerization of Vinyl Divinyl Monomers. *Makromol Chem-Theor* **1993,** *2* (4), 587-604.

125. Achilias, D. S.; Kiparissides, C., Development of a General Mathematical Framework for Modeling Diffusion-Controlled Free-Radical Polymerization Reactions. *Macromolecules* **1992,** *25* (14), 3739-3750.

126. Chiu, W. Y.; Carratt, G. M.; Soong, D. S., A Computer-Model for the Gel Effect in Free-Radical Polymerization. *Macromolecules* **1983,** *16* (3), 348-357.

127. Fujita, H.; Kishimoto, A.; Matsumoto, K., Concentration and temperature dependence of diffusion coefficients for systems polymethyl acrylate and n-alkyl acetates. *Trans. Faraday Soc.*, **1960**, *56*, 424-437.

128. Achilias, D.; Kiparissides, C., Modeling of Diffusion-Controlled Free-Radical Polymerization Reactions. *Journal of Applied Polymer Science* **1988,** *35* (5), 1303-1323.

129. Vrentas, J. S.; Duda, J. L., Diffusion in Polymer-Solvent Systems .2. Predictive Theory for Dependence of Diffusion-Coefficients on Temperature, Concentration, and Molecular-Weight. *J Polym Sci Pol Phys* **1977,** *15* (3), 417-439.

130. Vrentas, J. S.; Duda, J. L., Diffusion in Polymer - Solvent Systems .1. Re-Examination of Free-Volume Theory. *J Polym Sci Pol Phys* **1977,** *15* (3), 403-416.

131. Verros, G. D.; Achilias, D. S., Modeling Gel Effect in Branched Polymer Systems: Free-Radical Solution Homopolymerization of Vinyl Acetate. *Journal of Applied Polymer Science* **2009,** *111* (5), 2171-2185.

132. Keramopoulos, A.; Kiparissides, C., Development of a comprehensive model for diffusion-controlled free-radical copolymerization reactions. *Macromolecules* **2002,** *35* (10), 4155-4166.

133. Keramopoulos, A.; Kiparissides, C., Mathematical Modeling of diffusion-controlled free-radical terpolymerization reactions. *Journal of Applied Polymer Science* **2003,** *88* (1), 161-176.

134. Wu, J. Y.; Shan, G. R., Kinetic and molecular weight control for methyl methacrylate semi-batch polymerization. I. Modelling. *Journal of Applied Polymer Science* **2006,** *100* (4), 2838-2846.

135. Dar, Y.; Caneba, G., Free-radical retrograde-precipitation polymerization: A mathematical modeling study of polymerization of styrene in diethyl ether. *Chem Eng Commun* **2004,** *191* (12), 1634-1659.

136. Ray, A. B.; Saraf, D. N.; Gupta, S. K., Free-Radical Polymerizations Associated with the Trommsdorff Effect under Semibatch Reactor Conditions .1. Modeling. *Polym Eng Sci* **1995,** *35* (16), 1290-1299.

137. Srinivas, T.; Sivakumar, S.; Gupta, S. K.; Saraf, D. N., Free radical polymerizations associated with the Trommsdorff effect under semibatch reactor conditions .2. Experimental responses to step changes in temperature. *Polym Eng Sci* **1996,** *36* (3), 311-321.

138. Dua, V.; Saraf, D. N.; Gupta, S. K., Free-radical polymerizations associated with the Trommsdorff effect under semibatch reactor conditions .3. Experimental responses to step changes in initiator concentration. *Journal of Applied Polymer Science* **1996,** *59* (4), 749-758.

139. http://www.abcm.org.br/pt/wp-content/anais/encit/2000/arquivos/s11/s11p11.pdf

140. Kotoulas, C.; Krallis, A.; Pladis, P.; Kiparissides, C., A comprehensive kinetic model for the combined chemical and thermal polymerization of styrene up to high conversions. *Macromol Chem Physic* **2003,** *204* (10), 1305-1314.

141. Chen, C. C., A Continuous Bulk-Polymerization Process for Crystal Polystyrene. *Polym-Plast Technol* **1994,** *33* (1), 55-81.

142. Cabral, P. A.; Melo, P. A.; Biscaia, E. C.; Lima, E. L.; Pinto, J. C., Free-radical solution polymerization of styrene in a tubular reactor - Effects of recycling. *Polym Eng Sci* **2003,** *43* (6), 1163-1179.

143. Chen, C. C., A Continuous Bulk-Polymerization Process for Crystal Polystyrene. *Polym-Plast Technol* **1994,** *33* (1), 55-81.

144. Costa, E. F.; Lage, P. L. C.; Biscaia, E. C., On the numerical solution and optimization of styrene polymerization in tubular reactors. *Comput Chem Eng* **2003,** *27* (11), 1591-1604.

145. Baillagou, P. E.; Soong, D. S., Free-Radical Polymerization of Methyl-Methacrylate in Tubular Reactors. *Polym Eng Sci* **1985,** *25* (4), 212-231.

146. Cohen, M. H.; Turnbull, D., Molecular transport in liquids and glasses. *J. Chem. Phys.* **1959**, *31*, 1164-1169.

147. Fujita, H., Diffusion in Polymer-Diluent Systems. *Fortschr. Hochpolym.-Forsch.*, **1961**, *3*, 1-47.

148. Vrentas, J. S.; Chu, C. H., Concentration-Dependence of Solvent Self-Diffusion Coefficients. *Journal of Applied Polymer Science* **1987,** *34* (2), 587-592.

149. Vrentas, J. S.; Chu, C. H., Free-Volume Analysis of Solvent Self-Diffusion in Polymer-Solutions. *J Colloid Interf Sci* **1989,** *130* (1), 293-295.

150. Vrentas, J. S.; Chu, C. H.; Drake, M. C.; Vonmeerwall, E., Predictive Capabilities of a Free-Volume Theory for Solvent Self-Diffusion Coefficients. *J Polym Sci Pol Phys* **1989,** *27* (5), 1179-1184.

151. Vrentas, J. S.; Duda, J. L., Diffusion in Dilute Polystyrene Solutions. *J Polym Sci Pol Phys* **1976,** *14* (1), 101-109.

152. Vrentas, J. S.; Duda, J. L., Solvent and Temperature Effects on Diffusion in Polymer-Solvent Systems. *Journal of Applied Polymer Science* **1977,** *21* (6), 1715-1728.

153. Vrentas, J. S.; Duda, J. L., Molecular-Diffusion in Polymer-Solutions. *Aiche J* **1979,** *25* (1), 1-24.

154. Vrentas, J. S.; Duda, J. L.; Lau, M. K., Solvent Diffusion in Molten Polyethylene. *Journal of Applied Polymer Science* **1982,** *27* (10), 3987-3997.

155. Vrentas, J. S.; Duda, J. L.; Ling, H. C., Self-Diffusion in Polymer-Solvent-Solvent Systems. *J Polym Sci Pol Phys* **1984,** *22* (3), 459-469.

156. Vrentas, J. S.; Duda, J. L.; Ling, H. C., Free-Volume Theories for Self-Diffusion in Polymer Solvent Systems .1. Conceptual Differences in Theories. *J Polym Sci Pol Phys* **1985,** *23* (2), 275-288.

157. Vrentas, J. S.; Duda, J. L.; Ling, H. C.; Hou, A. C., Free-Volume Theories for Self-Diffusion in Polymer Solvent Systems .2. Predictive Capabilities. *J Polym Sci Pol Phys* **1985,** *23* (2), 289-304.

158. Vrentas, J. S.; Liu, H. T.; Duda, J. L., Estimation of Diffusion-Coefficients for Trace Amounts of Solvents in Glassy and Molten Polymers. *Journal of Applied Polymer Science* **1980,** *25* (7), 1297-1310.

159. Vrentas, J. S.; Vrentas, C. M., Influence of Solvent Size on the Diffusion Process for Polymer-Solvent Systems. *J Polym Sci Pol Lett* **1990,** *28* (12), 379-383.

160. Vrentas, J. S.; Vrentas, C. M., Solvent Self-Diffusion in Cross-Linked Polymers. *Journal of Applied Polymer Science* **1991,** *42* (7), 1931-1937.

161. Vrentas, J. S.; Vrentas, C. M., Fickian Diffusion in Glassy Polymer Solvent Systems. *J Polym Sci Pol Phys* **1992,** *30* (9), 1005-1011.

162. Vrentas, J. S.; Vrentas, C. M., Energy Effects for Solvent Self-Diffusion in Polymer Solvent Systems. *Macromolecules* **1993,** *26* (6), 1277-1281.

163. Vrentas, J. S.; Vrentas, C. M., Evaluation of Free-Volume Theories for Solvent Self-Diffusion in Polymer Solvent Systems. *J Polym Sci Pol Phys* **1993,** *31* (1), 69-76.

164. Vrentas, J. S.; Vrentas, C. M., Solvent Self-Diffusion in Glassy Polymer-Solvent Systems. *Macromolecules* **1994,** *27* (20), 5570-5576.

165. Vrentas, J. S.; Vrentas, C. M., Solvent Self-Diffusion in Rubbery Polymer-Solvent Systems. *Macromolecules* **1994,** *27* (17), 4684-4690.

166. Vrentas, J. S.; Vrentas, C. M., Determination of Free-Volume Parameters for Solvent Self-Diffusion in Polymer-Solvent Systems. *Macromolecules* **1995,** *28* (13), 4740-4741.

167. Vrentas, J. S.; Vrentas, C. M., Predictive methods for self-diffusion and mutual diffusion coefficients in polymer-solvent systems. *Eur Polym J* **1998,** *34* (5-6), 797-803.

168. Vrentas, J. S.; Vrentas, C. M., Prediction of mutual diffusion coefficients for polymer-solvent systems. *Journal of Applied Polymer Science* **2000,** *77* (14), 3195-3199.

169. Vrentas, J. S.; Vrentas, C. M., Prediction of the molecular-weight dependence of mutual diffusion coefficients in polymer-solvent systems. *Journal of Applied Polymer Science* **2003,** *89* (10), 2778-2779.

170. Vrentas, J. S.; Vrentas, C. M., Effect of glass transition on the concentration dependence of self-diffusion coefficients. *Journal of Applied Polymer Science* **2003,** *89* (6), 1682-1684.

171. Vrentas, J. S.; Vrentas, C. M., Evaluation of the free-volume theory of diffusion. *J Polym Sci Pol Phys* **2003,** *41* (5), 501-507.

172. Vrentas, J. S.; Vrentas, C. M., Theoretical aspects of ternary diffusion. *Ind Eng Chem Res* **2005,** *44* (5), 1112-1119.

173. Vrentas, J. S.; Vrentas, C. M.; Duda, J. L., Comparison of Free-Volume Theories. *Polym J* **1993,** *25* (1), 99-101.

174. Vrentas, J. S.; Vrentas, C. M.; Faridi, N., Effect of solvent size on solvent self-diffusion in polymer-solvent systems. *Macromolecules* **1996,** *29* (9), 3272-3276.

Chapter3   Modeling

3.1 Preface

In the last chapter, we have discussed about the literature review of the work published relevant to our thesis. In this chapter, we have presented the numerical aspects of the literature review just made. The idea is to put all the numerical things which form the foundation of our work at one place for easy reference. To start with, the kinetic scheme of free radical polymerization (FRP), on which our whole work is based, is presented first. Then the mathematical model for the kinetic reaction rates for various components in the kinetic scheme is presented. That forms the mathematical foundation of all our work. Numerical schemes are presented then with variation in the main mathematical model using Matlab. The discussion about the processing of data in Matlab is also made. Two models modeling effects like gel, glass effect and cage effect are presented with the values of their parameters. The technique to model the variation of diffusion coefficient is also mentioned. Then discussion about the CFD modeling is made. This includes the reactor geometry, meshing for mixed feed and unmixed feed condition. The physical and chemical data for various chemical species are presented. The expressions to model the variation in density and viscosity are also mentioned. Various numerical requirements regarding CFD simulations are presented.

3.2   Modeling

3.2.1   Introduction

This chapter deals with the all those modeling techniques which are used in this thesis. It includes kinetic scheme, mathematical model related to it, models describing gel, glass and cage effects etc. They are presented as follows:

3.2.2   Kinetic Scheme

First of all, the kinetic scheme of free radical polymerization (FRP) is considered. There are several elementary steps that go on in actual polymerization. To use all of them is not practically possible although a limited number of them can be used. Most of the additional reactions are side reactions but main reactions that characterize FRP are dissociation and initiation of initiator to initiate the polymerization, propagation of polymerization and termination of polymerization. Termination process can occur by two ways – termination by combination and termination by disproportionation. There are other processes that may be significant. They are transfer to monomer, transfer to solvent, transfer to chain transfer agent (CTA) and transfer to polymer. Transfer to polymer step is not considered in this study. So following are the elementary kinetic steps that constitute the kinetic scheme used in this thesis work.

Initiator decomposition $\qquad\qquad$ $I \xrightarrow{K_d} 2R_0$ $\qquad\qquad\qquad\qquad$ (a)

Initiation $\qquad\qquad\qquad\qquad$ $R_0 + M \xrightarrow{K_i} R_1$ $\qquad\qquad\qquad\qquad$ (b)

Propagation $\qquad\qquad\qquad\qquad$ $R_n + M \xrightarrow{K_p} R_{n+1}$ $\qquad\qquad\qquad$ (c)

Termination by combination $\qquad$ $R_n + R_m \xrightarrow{K_{tc}} P_{n+m}$ $\qquad\qquad\quad$ (d)

Termination by disproportionation $\quad$ $R_n + R_m \xrightarrow{K_{td}} P_n + P_m$ $\qquad\qquad$ (e)

Transfer to monomer $\qquad\qquad$ $R_n + M \xrightarrow{K_{fm}} R_1 + P_n$ $\qquad\qquad\quad$ (f)

Transfer to solvent $\qquad\qquad\quad$ $R_n + S \xrightarrow{K_{fs}} R_1 + P_n$ $\qquad\qquad\quad$ (g)

Transfer to CTA $\qquad\qquad\qquad$ $R_n + A \xrightarrow{K_{fa}} R_1 + P_n$ $\qquad\qquad\quad$ (h)
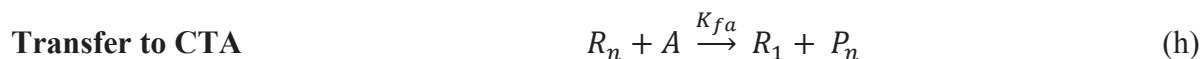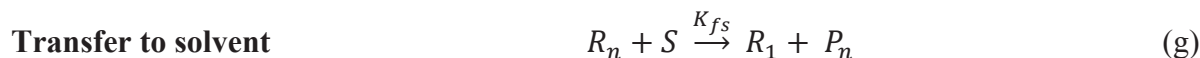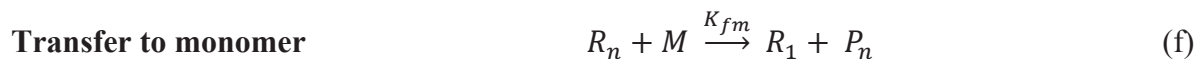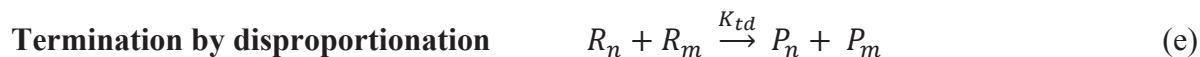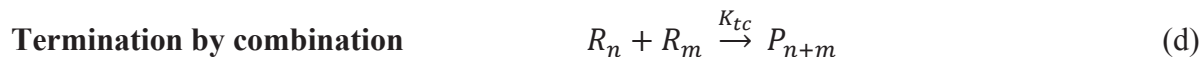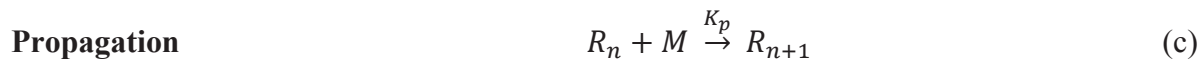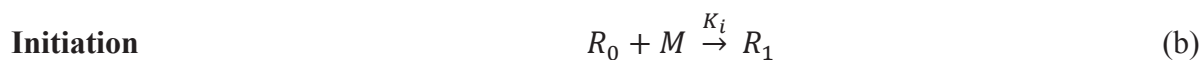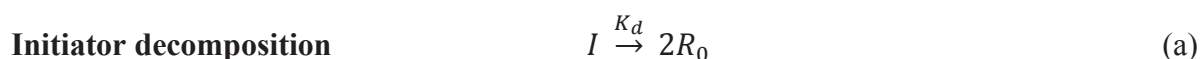
Scheme 1- Kinetic scheme for free radical polymerization used in this work

Here, I is initiator, R_0 is radical formed after dissociation of initiator, M is monomer molecule, R_1 is primary radical or in other words, live radical polymer chain of one monomer molecule, R_n is live radical polymer chain of n monomers, P_n is dead polymer chain of length n monomers, S is solvent molecule and A is chain transfer agent (CTA) molecule. All these terms also present their respective concentrations too. Various Ks' present in the Scheme 1 are kinetic rate coefficient of that elementary step. Since K_i in step (b) is much fast compared to K_d, so K_i effect is considered by taking the factor f called as initiator efficiency factor. This

kinetic scheme was used by Tefera *et al.*[1] This scheme is quite wide encompassing all important reaction steps having practical industrial application.

3.2.3 Mathematical Model

Since the reaction steps presented in Scheme 1 consist of elementary steps so that the reaction rate terms can be derived directly from them. But the problem is that the set of equations would be very large as each polymer chain – dead and live require an individual equation to represent its generation rate term. Although all the equations can be solved together in principle but that would be an enormous task. Thus, the mathematical model for this kinetic scheme is based on the moment method[2,3] which is quite common and also quite successful in predicting the various statistical average properties of polymers. Here we have defined the moments of nth order

$$\lambda_n = \sum_{i=1}^{\infty} i^n . R_i \tag{3-1}$$
$$\mu_n = \sum_{i=1}^{\infty} i^n . P_i \tag{3-2}$$

where λ_n is n^{th} order of moment of live polymer chains length distribution whereas μ_n is n^{th} order of moment of dead polymer chains length distribution.

Physical effect of solvent through its contribution to reaction mixture density, viscosity, specific heat capacity and thermal conductivity and chemical effect of solvent through transfer to solvent elementary reaction step (g) of Scheme 1 is taken into account. The variation in volume with monomer conversion is also modeled. The detailed mathematical model[1] studied in this work is based on the mole balances of the different chemical species in an ideal batch reactor and is given below.

Initiator decomposition (from step (a))

$$-\frac{1}{V_R}\frac{d(I.V_R)}{dt} = K_d I \tag{3-3}$$

Monomer concentration (from step (c) & (f))

$$-\frac{1}{V_R}\frac{d(M.V_R)}{dt} = (K_p + K_{fm})M\lambda_0 = (1 + C_M)K_p M\lambda_0 = K_{pr}M\lambda_0 \tag{3-4}$$

Monomer conversion (from eqn.(3-4),(3-38) & (3-39))

$$\frac{dx_M}{dt} = (K_p + K_{fm})(1 - x_M)\lambda_0 = (1 + C_M)K_p(1 - x_M)\lambda_0 = K_{pr}(1 - x_M)\lambda_0 \tag{3-5}$$

Solvent concentration (from step (g))

$$-\frac{1}{V_R}\frac{d(S.V_R)}{dt} = K_{fs}S\lambda_0 = C_S K_p S\lambda_0 = R_S K_{pr}S\lambda_0 \tag{3-6}$$

Chain transfer agent concentration (from step (h))

$$-\frac{1}{V_R}\frac{d(A.V_R)}{dt} = K_{fa}A\lambda_0 = C_A K_p A\lambda_0 = R_A K_{pr}A\lambda_0 \tag{3-7}$$

Zeroth order moments of live polymer chains length distribution (from step (a),(b),(d) & (e))

$$\frac{1}{V_R}\frac{d(\lambda_0.V_R)}{dt} = 2fK_d I - (K_{tc} + K_{td})\lambda_0^2 = 2fK_d I - K_t\lambda_0^2 \tag{3-8}$$

81

First order moments of live polymer chains length distribution

$$\frac{1}{V_R}\frac{d(\lambda_1.V_R)}{dt} = 2fK_dI + K_pM\lambda_0 + \left(K_{fm}M + K_{fs}S + K_{fa}A\right)(\lambda_0 - \lambda_1) - (K_{tc} + K_{td})\lambda_0\lambda_1$$

$$= 2fK_dI + (M + R_SS + R_AA)K_{pr}\lambda_0 - K_t\lambda_0\lambda_1 - (R_MM + R_SS + R_AA)K_{pr}\lambda_1$$

$$\boldsymbol{= 2fK_dI + (1 + R_{SM} + R_{AM})K_{pr}M\lambda_0 - K_t\lambda_0\lambda_1 - (R_{MM} + R_{SM} + R_{AM})K_{pr}M\lambda_1}$$

$$(3\text{-}9)$$

Second order moments of live polymer chains length distribution

$$\frac{1}{V_R}\frac{d(\lambda_2.V_R)}{dt} = 2fK_dI + K_pM(2\lambda_1 + \lambda_0) + \left(K_{fm}M + K_{fs}S + K_{fa}A\right)(\lambda_0 - \lambda_2) - (K_{tc} + K_{td})\lambda_0\lambda_2$$

$$= 2fK_dI + (M + R_SS + R_AA)K_{pr}\lambda_0 + 2K_pM\lambda_1 - K_t\lambda_0\lambda_2 - (R_MM + R_SS + R_AA)K_{pr}\lambda_2$$

$$\boldsymbol{= 2fK_dI + (1 + R_{SM} + R_{AM})K_{pr}M\lambda_0 + 2K_pM\lambda_1 - K_t\lambda_0\lambda_2 - (R_{MM} + R_{SM} + R_{AM})K_{pr}M\lambda_2}$$

$$(3\text{-}10)$$

Zeroth order moments of dead polymer chain length distribution

$$\frac{1}{V_R}\frac{d(\mu_0.V_R)}{dt} = \left(K_{fm}M + K_{fs}S + K_{fa}A\right)\lambda_0 + \left(K_{td} + \frac{K_{tc}}{2}\right)\lambda_0^2$$

$$= (R_MM + R_SS + R_AA)K_{pr}\lambda_0 + \left(1 - \frac{R_T}{2}\right)K_t\lambda_0^2 \qquad (3\text{-}11)$$

First order moments of dead polymer chain length distribution

$$\frac{1}{V_R}\frac{d(\mu_1.V_R)}{dt} = \left(K_{fm}M + K_{fs}S + K_{fa}A\right)\lambda_1 + (K_{td} + K_{tc})\lambda_0\lambda_1$$

$$= (R_MM + R_SS + R_AA)K_{pr}\lambda_1 + K_t\lambda_0\lambda_1 \qquad (3\text{-}12)$$

Second order moments of dead polymer chain length distribution

$$\frac{1}{V_R}\frac{d(\mu_2.V_R)}{dt} = \left(K_{fm}M + K_{fs}S + K_{fa}A\right)\lambda_2 + (K_{td} + K_{tc})\lambda_0\lambda_2 + K_{tc}\lambda_1^2$$

$$= (R_MM + R_SS + R_AA)K_{pr}\lambda_2 + K_t\lambda_0\lambda_2 + R_TK_t\lambda_1^2 \qquad (3\text{-}13)$$

Energy balance equation

$$\boldsymbol{\rho.Cp.V_R\frac{dT}{dt} = (-\Delta H_P)K_pM\lambda_0V_R - UA(T - T_{bath})} \qquad (3\text{-}14)$$

Volume variation with monomer conversion

$$\frac{dV_R}{dt} = -\varepsilon V_{R0}\frac{dx_M}{dt} \qquad (3\text{-}15)$$

and

Number average molecular weight $\boldsymbol{MW_n = \frac{\lambda_1 + \mu_1}{\lambda_0 + \mu_0}MW_M \approx \frac{\mu_1}{\mu_0}MW_M = DP_n.MW_M}$

$$(3\text{-}16)$$

Weight average molecular weight $\boldsymbol{MW_w = \frac{\lambda_2 + \mu_2}{\lambda_1 + \mu_1}MW_M \approx \frac{\mu_2}{\mu_1}MW_M}$ $\qquad$ (3-17)

Polydispersity Index $PDI = \frac{MW_w}{MW_n} = \frac{(\lambda_2+\mu_2)(\lambda_0+\mu_0)}{(\lambda_1+\mu_1)^2} \approx \frac{(\mu_2.\mu_0)}{(\mu_1)^2}$ (3-18)

where

Net kinetic rate coefficient of termination is

$$K_t = K_{tc} + K_{td} \tag{3-19}$$

Sum of kinetic rate coefficients of propagation and transfer to monomer is

$$K_{pr} = K_p + K_{fm} = (1 + C_M)K_p \tag{3-20}$$

Ratio of kinetic rate coefficient of transfer to monomer to propagation

$$C_M = \frac{K_{fm}}{K_p} \tag{3-21}$$

Ratio of kinetic rate coefficient of transfer to solvent to propagation

$$C_S = \frac{K_{fs}}{K_p} \tag{3-22}$$

Ratio of kinetic rate coefficient of transfer to CTA to propagation

$$C_A = \frac{K_{fa}}{K_p} \tag{3-23}$$

Ratio of kinetic rate coefficient of termination by disproportionation to termination by combination

$$C_T = \frac{K_{td}}{K_{tc}} \tag{3-24}$$

$$R_T = \frac{K_{tc}}{K_{tc}+ K_{td}} = \frac{K_{tc}}{K_t} = \frac{1}{1+C_T} \tag{3-25}$$

$$R_M = R_{MM} = \frac{K_{fm}}{K_p+K_{fm}} = \frac{K_{fm}}{K_{pr}} = \frac{C_M}{1+C_M} \tag{3-26}$$

$$R_S = \frac{C_S}{1+C_M} = \frac{K_{fs}}{K_{pr}} \tag{3-27}$$

$$R_{SM} = \frac{C_S}{1+C_M} \frac{S}{M} = R_S.\frac{S}{M} \tag{3-28}$$

$$R_A = \frac{C_A}{1+C_M} = \frac{K_{fa}}{K_{pr}} \tag{3-29}$$

$$R_{AM} = \frac{C_A}{1+C_M} \frac{A}{M} = R_A.\frac{A}{M} \tag{3-30}$$

Term representing the contribution of all transfer processes considered in this work

$$R_P = R_{MM} + R_{SM} + R_{AM} = R_{MM} + R_{SA} \tag{3-31}$$
$$R_{SA} = R_{SM} + R_{AM} \tag{3-32}$$

Reaction mixture density

$$\rho = \rho_M \Phi_M + \rho_P \Phi_P + \rho_S \Phi_S \tag{3-33}$$

Reaction mixture specific heat

$$Cp = Cp_M \Phi_M + Cp_P \Phi_P + Cp_S \Phi_S \tag{3-34}$$

Volume fraction of monomer

$$\Phi_M = \frac{(1-x_M)}{(1-\varepsilon_0 x_M+\beta)} = \frac{(1-x_M)}{(1+\beta)(1-\varepsilon.x_M)} \tag{3-35}$$

Volume fraction of polymer

$$\Phi_P = \frac{x_M(1-\varepsilon)}{(1-\varepsilon_0 x_M+\beta)} = \frac{x_M(1-\varepsilon(1+\beta))}{(1+\beta)(1-\varepsilon.x_M)} \tag{3-36}$$

Volume fraction of solvent

$$\Phi_S = \frac{\beta}{(1-\varepsilon_0 x_M+\beta)} = \frac{\beta}{(1+\beta)(1-\varepsilon.x_M)} \tag{3-37}$$

Volume of reaction mixture at conversion x_M

$$V_R = V_{R0}(1-\varepsilon.x_M) \tag{3-38}$$

Monomer concentration at monomer conversion x_M

$$M = M_0\frac{(1-x_M)}{(1-\varepsilon.x_M)} \tag{3-39}$$

Volume contraction constant "with solvent"

$$\varepsilon = \frac{\varepsilon_0}{1+\beta} \tag{3-40}$$

Volume contraction constant "without solvent"

$$\varepsilon_0 = \frac{(\rho_P-\rho_M)}{\rho_P} = 1-\frac{\rho_M}{\rho_P} \tag{3-41}$$

Initial volume fraction ratio of solvent to monomer

$$\beta = \frac{f_s}{(1-f_s)} \tag{3-42}$$

where f_s is initial volume fraction of solvent to total reaction mixture volume

Meaning of all these symbols can be found in notation section.

This model has been simplified by several researchers by applying Quasi-Steady State Assumption (QSSA) to zeroth, first and second order moment of live chain length distributions. This means that the change in concentration is slow enough to consider them as constant. Thus the rate of change of concentration can be taken to be zero for all practical purposes. This assumption is quite accurate till the gel effect sets in where reaction rate is suddenly increased due to decrease in termination coefficient.

By applying QSSA on eqn.(3-8), we have

$$\lambda_0 = \sqrt{\frac{2fK_dI}{(K_{tc}+K_{td})}} = \sqrt{\frac{2fK_dI}{K_t}} \tag{3-43}$$

Before going further, we need to define two extra terms to simplify our model. These are as follows:

$$L = \frac{(K_p+K_{fm})M\lambda_0}{2fK_dI} = \frac{K_{pr}M\lambda_0}{2fK_dI} \tag{3-44}$$

$$\bar{L} = \frac{K_pM\lambda_0}{2fK_dI+(K_{fm}M+K_{fs}S+K_{fa}A)\lambda_0} = \frac{(1-R_{MM})K_{pr}M\lambda_0}{2fK_dI+(R_{MM}+R_{SM}+R_{AM})K_{pr}M\lambda_0} = \frac{(1-R_{MM})K_{pr}M\lambda_0}{2fK_dI+R_PK_{pr}M\lambda_0} \tag{3-45}$$

$$\bar{L} = L.\left(\frac{1-R_{MM}}{1+R_P L}\right) = L.\left(\frac{1-R_M}{1+R_P L}\right) \tag{3-46}$$

where L is instantaneous kinetic chain length.

so, now by applying QSSA on eqn.(3-9), and using above defined terms, we have

$$\lambda_1 = \left[\frac{2fK_d I + (1+R_{SM}+R_{AM})K_{pr}M\lambda_0}{K_t\lambda_0 + (R_{MM}+R_{SM}+R_{AM})K_{pr}M}\right] = \lambda_0\left[\frac{1+(1+R_{SA})L}{1+R_P L}\right] = \lambda_0(\bar{L}+1) \tag{3-47}$$

By applying QSSA on eqn.(3-10), and by using above defined new terms, we have

$$\lambda_2 = \left[\frac{2fK_d I + (1+R_{SM}+R_{AM})K_{pr}M\lambda_0 + 2K_p M\lambda_1}{K_t\lambda_0 + (R_{MM}+R_{SM}+R_{AM})K_{pr}M}\right] = \lambda_1(2\bar{L}+1) = \lambda_0(\bar{L}+1)(2\bar{L}+1)$$
$$\tag{3-48}$$

Further simplifications can be obtained by applying the condition

$$\bar{L} \gg 1 \tag{3-49}$$

This leads to

$$\lambda_1 = \lambda_0\bar{L} \tag{3-50}$$
$$\lambda_2 = 2\bar{L}\lambda_1 = 2\bar{L}^2\lambda_0 \tag{3-51}$$

When $R_P = 0$, i.e. all the transfer processes considered under our kinetic scheme here are absent. So chain transfer to monomer (R_{MM}), solvent (R_{SM}) and chain transfer agent (R_{AM}) are zero. Then $L' = L$ obtained from eqn.(3-46). The above simplifications are commonly used by many researchers[4,5].

3.2.4 Methodology adopted

The complete set of eqn.(3-1) to (3-42) is named as FRP_Full model in this study. Thus this model constitutes the set of equations without any further assumptions. The second model FRP_QSSA is obtained by applying QSSA (Quasi-Steady State Assumption) [4,5] to living polymer chain length distributions as already mentioned earlier. Thus FRP_QSSA contains all equations as FRP_Full except for eqn.(3-8) - (3-10) which are now replaced by eqn.(3-43), (3-47) & (3-48) using eqn.(3-44) - (3-46) along. FRP_QSSA is quite suitable and sufficient for many practical situations of conversions below gel effect where assumption of QSSA is well justified.

To solve these sets of ordinary differential equations, a numerical solver was required. Matlab R2008a was used to code FRP_Full and FRP_QSSA and to obtain their numerical solution by using ordinary differential equation (ode) solver inbuilt in it. For isothermal condition and non-gel/glass/cage effect condition, the set of equations in both FRP_Full and FRP_QSSA is not stiff so they can be solved using simple ode solver. So non-stiff solver for ordinary differential equation ode23, an inbuilt solver in Matlab, was used for such conditions. The whole set of equations in either set is quite stiff during gel/glass/cage effect and non-isothermal conditions. So another inbuilt ode solver in Matlab for stiff ordinary differential equations ode15s was used to solve both FRP_Full and FRP_QSSA. The initial conditions used to solve for FRP_Full and FRP_QSSA are as follows:

$$I = I_0, M = M_0; \tag{3-52}$$

$\lambda_0, \lambda_1, \& \lambda_2 = 0$; (For FRP_QSSA, this was not required)   (3-53)

$\mu_0, \mu_1, \& \mu_2 = 0$;   (3-54)

$T = T_0$.   (3-55)

Once the results were obtained, then various plots were generated for the desired variables using Matlab only. In all the plots, results were compared with each other for the given variable so as to analyze and compare the results with each other. Experimental data like monomer conversion, MW_n, MW_w, PDI were taken from published articles. In limited cases only, this data was available in tabular form. In rest of the cases, the data was present in plot form. So to extract the data from the plots, a freeware program called "engauge digitizer[6]" was used. This data was then arranged in tabular form. While plotting the results in Matlab, experimental data in discrete form was also read from the excel files and plotted against the relevant variable to compare the numerical solution with it. Sometimes multiple experimental values for the same given time were found in the literature. So the whole data was plotted without any selection or averaging out.

3.2.5   Physical, chemical and kinetic data

Four monomers were studied under this work. They were styrene (St), methyl methacrylate (MMA), butyl acrylate (BuA) and vinyl acetate (VAc). Physical and chemical kinetic data for these monomers under study was required for modeling and simulation. It was taken from different sources and has been commonly used by several researchers and is thus selected and presented in Table. 3-1 & Table. 3-2. The data for initiators (2,2′-Azobis(2-methylpropionitrile) (AIBN) and Benzoyl peroxide (BPO)) and solvents are presented in Table. 3-3 & Table. 3-4 respectively. To model the variation in physical properties like density, viscosity, specific heat capacity and thermal conductivity, their expressions are presented in Table. 3-1 - Table. 3-4, except for viscosity which is presented separately for MMA and styrene.

Table 3-1-Physical and Chemical kinetic data for MMA and Styrene

	MMA[8]	Styrene[15]
K_p (l/mol/ min)	$2.95 \times 10^7 exp(-4353/RT)$	$6.54 \times 10^8 exp(-7051/RT)$
K_{fm} (l/mol/ min)	$2.797 \times 10^{11} exp(-18233/RT)$	$1.38 \times 10^8 exp(-12670/RT)$
K_t (l/mol/ min)	$5.88 \times 10^9 exp(-701/RT)$	$1.022 \times 10^{11} exp(-2268/RT)$
$\frac{K_{td}}{K_{tc}} = C_T$	$2.5278 \times 10^3 exp(-4090/RT)$	0
$\frac{K_{fm}}{K_p} = C_M$	$9.48 \times 10^3 exp(-13880/RT)$	$1 \times exp(-6379/RT)$[19]
$\frac{K_{fs}}{K_p} = C_S$	$1.01 \times 10^3 exp(-11400/RT)$ - Toluene	$0.0188\ exp(-4361/RT)$– Tol.[19] $56\ exp(-9116/RT)$–Xylene [20]
$\frac{K_{fa}}{K_p} = C_A$	$18.15exp(-2733/RT)$, $CTA - 1 - Butanethiol$ [18]	
MW (g/mol)	100.13	104.14
ρ_M (g/cm^3)	$0.968 - 1.225 \times 10^{-3}(T - 293.15)$	$0.9236 - 0.887 \times 10^{-3}(T - 273.15)$
ρ_P (g/cm^3)	$1.212 - 8.45 \times 10^{-4}(T - 273.15)$	$1.0855 - 6.05 \times 10^{-4}(T - 273.15)$
δ (A°)	6.9	7.4
X_{C0} (dimnles)	100	385

	MMA[8]	Styrene[15]
V_{fM} (Ref. 10)	$0.149 + 2.9 \times 10^{-4}T(^{\circ}C)$	$0.112 + 6.2 \times 10^{-4}T(^{\circ}C)$
V_{fP} (Ref. 10)	$0.0194 + 3.0 \times 10^{-4}(T(^{\circ}C)-105)$, $T(^{\circ}C) \geq 105\ ^{\circ}C$ $0.0194 + 0.13 \times 10^{-4}(T(^{\circ}C)-105)$, $T(^{\circ}C) < 105\ ^{\circ}C$	$0.0245 + 4.5 \times 10^{-4}(T(^{\circ}C)-82)$, $T(^{\circ}C) \geq 82\ ^{\circ}C$ $0.0245 + 1.4 \times 10^{-4}(T(^{\circ}C)-82)$, $T(^{\circ}C) < 82\ ^{\circ}C$
T_{gM} (K)	159.15	185
T_{gP} (K)	378.15	363.15
V_M^* (cm³/g)	0.868	0.846, 0.912
V_P^* (cm³/g)	0.788	0.850 (Ref. 7), 0.835
r_e (A°)	17.0	16.9
M_{jP}	187.81	163.6[7]
D_{M0} (dm²/min)	8.27×10^{-9}	1.97×10^{-8}
$\log_{10}(\eta)$ (cP)	$453.25 \times \left[\dfrac{1}{T} - \dfrac{1}{254.92}\right]$	$528.64 \times \left[\dfrac{1}{T} - \dfrac{1}{276.71}\right]$
σ (A°)	6.9	7.4
γ_P	0.968	0.78
γ_M	0.968	0.6
$[\eta]$ (dl/g) (Ref.16)	$6.63 \times 10^{-5}\bar{M}_w^{0.73}$, 50° C, $5 - 41 \times 10^4\ \bar{M}_w$, PMMA-Tol	$17 \times 10^{-5}\bar{M}_w^{0.69}$, 25°C, $0.3 - 165 \times 10^4\ \bar{M}_w$, PS-Tol
ε/D_{i0} (s/cm²) (with AIBN)	372.38	50.0
C_{pM} (cal/g/° C)	$114.12 + 6.83T$ (J/Kg/K) $(225.6 - 350K)$ [21]	$1.334 \times 10^5 + 2.9020 \times 10^2 T - 6.05 \times 10^{-1}T^2 + 1.3567 \times 10^{-3}T^3$, (J/Kmol/K) $(242.54 - 418.3K)$ [24]
C_{pP} (cal/g/° C)	$1.90245 \times 10^4 T^{-2} + 0.404624T + 16.1182$, (J/mol/K) $(150 - 370 - 378K)$ [22] $0.2374T + 112.95$ (J/mol/K) $(378 - 550K)$ [22]	$7.7551 \times 10^5 T^{-2} + 0.53447T - 41.58$, (J/mol/K) $(200 - 360 - 373K)$ [23] $0.2653T + 95.12$, (J/mol/K) $(373 - 606K)$ [23]
ΔH, (Kcal.mol⁻¹)	-13.808	-16.67
k_m, (Wm⁻¹K⁻¹)	$\dfrac{418.6 \times 47.61}{(T(^{\circ}C)+273.15)} \times \left[\dfrac{0.9665-0.0011T(^{\circ}C)}{100.12}\right]^{\frac{4}{3}}$ (26)	$4.187 \times 10^{-2}[2.72 - 2.8 \times 10^{-3}(T(K) - 423) + 1.6 \times 10^{-5}(T(K) - 423)^2]$ [27]
k_p, (Wm⁻¹K⁻¹)	$418.6 \times 4.5 \times 10^{-4}$ (25)	$4.187 \times 10^{-2}[2.93 - 5.17 \times 10^{-3}(T(K) - 353)]$ [27]

Table 3-2-Physical and Chemical kinetic data for BuA and VAc

	BuA[8]	VAc[8]
K_p ($l/mol/min$)	$1.08 \times 10^9 exp(-4156/RT)$	$4.2 \times 10^9 exp(-6300/RT)$
K_{fm} ($l/mol/min$)	$1.74 \times 10^7 exp(-7786/RT)$	$1.0206 \times 10^6 exp(-6300/RT)$
K_t ($l/mol/min$)	$2.6 \times 10^{12} exp(-4885/RT)$	$1.62 \times 10^{12} exp(-2800/RT)$
$\dfrac{K_{td}}{K_{tc}} = C_T$	0	0
$\dfrac{K_{fm}}{K_p} = C_M$	0	0
$\dfrac{K_{fs}}{K_p} = C_S$	$96\ exp(-8824/RT)$–Xylene [20]	-
MW (g/mol)	128.17	86.09
ρ_M (g/cm^3)	$0.9255 - 1.075 \times 10^{-3}(T - 273.15)$	$0.9584 - 1.3276 \times 10^{-3}(T - 293.15)$
ρ_P (g/cm^3)	$1.085 - 6.05 \times 10^{-4}(T - 273.15)$	$1.211 - 8.496 \times 10^{-4}(T - 273.15)$
δ (A°)	6.9	6.9
X_{C0} (*dimnles*)	200	256
V_{fM} (Ref.10)	$0.025 + 1.19 \times 10^{-3}(T - T_{gM})$	$0.154 + 5.1 \times 10^{-4}T(^\circ C)$
V_{fP} (Ref. 10)	$0.025 + 4.8 \times 10^{-4}(T - T_{gP})$	$0.0218 + 5.0 \times 10^{-4}(T(^\circ C) - 26.5),\ T(^\circ C) \geq 26.5\ ^\circ C$ $0.0218 + 2.7 \times 10^{-4}(T(^\circ C) - 26.5),\ T(^\circ C) < 26.5\ ^\circ C$
T_{gM} (K)	185.15	109.0
T_{gP} (K)	218	305.15
V_M^* (cm^3/g)	0.904	0.840
V_P^* (cm^3/g)	0.842	0.748
r_e (A°)	15.4	16.0
M_{jP}	106.5 calc (Ref 11)	134.2
D_{M0} (dm^2/min)	6.4×10^{10}	2×10^{-8}
$\log_{10}(\eta)$ (cP)	$610.73 \times \left[\dfrac{1}{T} - \dfrac{1}{287.20}\right]$	$457.89 \times \left[\dfrac{1}{T} - \dfrac{1}{235.35}\right]$
σ (A°)	6.2 (Ref.12)	6.9
γ_P	0.6	0.783
γ_M	0.3	0.6
$[\eta]$ (dl/g) (Ref.16)	$11.8 \times 10^{-5}\bar{M}_w^{0.71}$,30°C, $7 - 20 \times 10^4\ \bar{M}_w$, PBuA-Tol	$156 \times 10^{-5}\bar{M}_w^{0.49}$; 67°C, $4 - 15 \times 10^4\ \bar{M}_w$, PVAc-Tol
ε/D_{i0} (s/cm^2) (with AIBN)	10.08	54.24

Table 3-3-Physical and Chemical kinetic data for AIBN and BPO initiators

	AIBN (Ref.7)	BPO (Ref. 17)
K_d (1/min)	$6.32 \times 10^{16} exp(-30660/RT)$	$1.69 \times 10^{14} exp(-25383/RT)$
MW (g/mol)	164.21	242
a_{seg}	0.28	0.28
f_0	0.58	1
M_{jI}	68	77
V_I^* (cm^3/g)	0.913	0.825
γ_I	1.0	1.0

Table 3-4-Physical and Chemical kinetic data for Toluene and Benzene solvents

	Toluene (Ref.11)	Benzene (Ref. 17)
MW (g/mol)	92.13	78.11
ρ_S (g/cm^3)	$0.883 - 9 \times 10^{-4}T(^\circ C)$ (Ref.14)	$0.84418 - 1.07165 \times 10^{-3}T(^\circ C)$
M_{jS}	92.13	78.11
V_S^* (cm^3/g)	0.917	0.901
T_{gS} (K)	117	171.15
V_{fS}	$0.025 + 1 \times 10^{-3}(T - T_{gs})$ (Ref. 9)	$0.025 + 0.39 \times 10^{-3}(T - T_{gs})$
C_{pS} (cal/g/°C)	$154.73 + 0.0981(T(^\circ K) - 273.15) + 0.001949(T(^\circ K) - 273.15)^2$ (J/mol/K)[28]	
k_s, ($Wm^{-1}K^{-1}$) (Ref. 26)	$\frac{418.6 \times 66.70}{(T(^\circ C)+273.15)} \cdot \left[\frac{0.8838 - 0.00087T(^\circ C)}{92.14}\right]^{\frac{4}{3}}$	

3.2.5.1 Viscosity relationship for styrene

Viscosity relationship for styrene[27] is divided into two parts- one for low monomer conversion, and other is for higher conversion. The relationship used mass fraction of polymer as variable to calculate viscosity of the mixture. The unit of viscosity is Pa.s.

For polymer mass fraction varying from $\omega_p = 0.0\ to\ < 40\%$, the relationship is taken from Harkness 1942,(Ref.29).

$$\eta = exp\left[-13.04 + \frac{2013}{T(K)} + \overline{MW}_w^{0.18}\left(3.915\omega_p - 5.437\omega_p^2 + \left(0.623 + \frac{1387}{T(K)}\right)\omega_p^3\right)\right]$$
(3-56)

For polymer mass fraction from $\omega_p = 40\%$ to 100%, the relationship is taken from Mendelson 1979 (Ref. 30). The temperature range in which this relationship is valid is $60 - 225°C$.

$$E_a = 2300\ exp(2.4\omega_p), cal/mol \tag{3-57}$$
$$\eta = 3.31 \times 10^{-15}.\omega_p^{10.7}\overline{MW}_w^{3.4}\ exp\left[\left(\frac{E_a}{R}\right)\left(\frac{1}{T(K)} - \frac{1}{473}\right)\right] \tag{3-58}$$
$$\omega_p\ (mass\ fraction\ of\ polymer) = \frac{x_M}{1+s'} \tag{3-59}$$
$$s' = \beta\frac{\rho_s}{\rho_m} \tag{3-60}$$
$$\beta = \frac{f_s}{1-f_s} \tag{3-61}$$
$$\overline{MW}_w = \frac{\mu_2}{\mu_1}.MW_M \tag{3-62}$$

3.2.5.2 Viscosity relationship for MMA

For MMA, the viscosity relationship was taken from Baillagou et al.[26]. Here instead of mass fraction of polymer, volume fraction is taken. The relationship is valid for complete range of conversion. The unit of viscosity here is centipoise.

$$c_p = 1.2\Phi_p \tag{3-63}$$
$$f_v = [0.025 + 10^{-3}(T(°\ C) + 106)]\Phi_m + [0.025 + 10^{-3}(T(°\ C) + 180)]\Phi_s + [0.025 + 0.48 \times 10^{-3}(T(°\ C) - 114)]\Phi_p \tag{3-64}$$
$$\eta_m = exp\left[2.303\left(\frac{0.115}{0.025 + 10^{-3}(T(°\ C) + 106)} - 1\right)\right] \tag{3-65}$$
$$\eta = \eta_m + 0.6c_p^{1.4}exp\left(\frac{0.8}{f_v}\right)\ for\ c_p < 0.13g/cm^3 \tag{3-66}$$
$$\eta = \eta_m + 200c_p^{4.2}exp\left(\frac{0.8}{f_v}\right)\ for\ c_p > 0.13g/cm^3 \tag{3-67}$$

where Φ_m, Φ_p, Φ_s are volume fraction of monomer, polymer and solvent respectively calculated using eqn.(3-33)-(3-35) and .η is viscosity in centipoise. f_v is fractional free volume, c_p is polymer concentration in g/cm^3 and η_m is a parameter.

3.2.6 CCS model

Chiu, Carratt & Soong (CCS) [31] model models gel and glass effect which takes into account the diffusion effect on the kinetic rate coefficient of termination (gel effect) and propagation (glass effect). The theoretical part of the model is explained in literature review. The

constitutive equations of the CCS model for gel and glass effect are presented below. The values of parameters namely $\Theta_t, \Theta_p,$ $A1, B1$ vary from monomer to monomer and also depend on type of data fitting method used for the available data.

$$\frac{1}{K_t} = \frac{1}{K_t^0} + \frac{r_m^2 C_b}{3D_{eff}} = \frac{1}{K_t^0} + \frac{r_m^2 C_b}{3D_0 C1} = \frac{1}{K_t^0} + \Theta_t \frac{\lambda_0}{C1} \tag{3-68}$$

$$\frac{1}{K_p} = \frac{1}{K_p^0} + \frac{r_m^2 C_b}{3D_{eff}} = \frac{1}{K_p^0} + \frac{r_m^2 C_b}{3D_0 C1} = \frac{1}{K_p^0} + \Theta_p \frac{\lambda_0}{C1} \tag{3-69}$$

$$C1 = exp\left[2.303\frac{\Phi_M}{(A1+B1.\Phi_M)}\right] \tag{3-70}$$

For MMA, the data was taken from Baillagau et al.[14] . The initiator used for this case is AIBN. This model does not take into account the transfer to chain transfer agent. For that, another data values were taken presented after this.

$$\Theta_t = \frac{1}{8.8083\times10^{22}[I]} exp\left(\frac{3.46\times10^4}{R.T(K)}\right), (s) \tag{3-71}$$

$$\Theta_p = \frac{1}{2.5292\times10^{15}} exp\left(\frac{2.8\times10^4}{R.T(K)}\right), (s) \tag{3-72}$$

$$A1 = 0.168 - 8.21\times10^{-6}\left(T(K) - T_{gp}\right)^2 \tag{3-73}$$

$$B1 = 0.03 \tag{3-74}$$

For MMA with CTA – This data was taken from Fenouillot et al.[18]. Although the form of the equation is similar to eqn.(3-68), it was specifically suited for transfer to chain transfer agent process. The initiator used in this case was di-*tert*-butyl peroxide (DTBP) and CTA is 1-butanethiol (BSH).

$$\frac{1}{K_t} = \frac{1}{K_t^0} + \frac{1}{K_t^0 exp[\beta_c(X_c-X)]} \tag{3-75}$$

$$\beta_c = -17.85 + 0.5756T - 0.002519T^2 \tag{3-76}$$

$$X_c = 4.289 - 0.05799T + 0.00020422T^2 + 0.11Ln(1000A_0 + 3) \tag{3-77}$$

For styrene, the data was taken from Lima et al.[32]. The initiator used here was AIBN.

$$ln\left[\frac{1}{\Theta_t}\right] = 172.98 - 1.057ln\left[\frac{1}{I_0}\right] - \frac{59447}{T(K)}, (s) \tag{3-78}$$

$$ln\left[\frac{1}{\Theta_p}\right] = 204.35 - \frac{71710}{T(K)}, (s) \tag{3-79}$$

$$A1 = 0.4688 - 4.608\times10^{-4}\left(T(K) - T_{gp}\right)^2 \tag{3-80}$$

$$B1 = 0.02 \tag{3-81}$$

3.2.7 AK model

Achilias & Kiparssides (AK) [7] model is an improvement of CCS model using Vrentas and Duda[34,35] model for diffusion coefficient using free volume theory[36,37]. The theoretical details of this model are presented in literature review. Here we are presenting only the constitutive equations of cage, glass and gel effect. For details of the AK model, please refer elsewhere[7,8,33].

3.2.7.1 Cage effect

It models the variation in initiator efficiency with monomer conversion. The equations are as follows:

$$\frac{1}{f} = \frac{1}{f_0} + \frac{r_2^3}{3r_1} \frac{K_{i0}}{f_0} \frac{[M]}{D_I} \tag{3-82}$$

$$K_{i0} = \epsilon_i K_{p0} \tag{3-83}$$

$$r_1 = \left[\frac{6V_m}{\pi N_A}\right]^{\frac{1}{3}} \tag{3-84}$$

$$D_I \approx D_M \tag{3-85}$$

$$r_2 = 2R_H \tag{3-86}$$

$$R_H = \left(\frac{3}{10\pi N_A}[\eta]MW_w\right)^{\frac{1}{3}} \tag{3-87}$$

$$[\eta] = K_{MH}.MW_w^{a_{MH}} \tag{3-88}$$

$$D_I = D_{I0}exp\left(-\frac{\gamma_I \xi_{IP}}{V_f}\left(\frac{\omega_M V_M^*}{\xi_{MP}} + \frac{\omega_P V_P^*}{\xi_{PP}} + \frac{\omega_S V_S^*}{\xi_{SP}} + \frac{\omega_I V_I^*}{\xi_{IP}}\right)\right) \tag{3-89}$$

$\omega_I \ll 1$ and $\xi_{PP} = 1$, therefore

$$D_I = D_{I0}exp\left[-\frac{\gamma_I \xi_{IP}}{V_f}\left(\frac{\omega_M V_M^*}{\xi_{MP}} + \omega_P V_P^* + \frac{\omega_S V_S^*}{\xi_{SP}}\right)\right] \tag{3-90}$$

$$V_f = \omega_M V_M^* V_{fM} + \omega_P V_P^* V_{fP} + \omega_S V_S^* V_{fS} \tag{3-91}$$

$$\xi_{kP} = \frac{M_{jk}V_k^*}{M_{jP}V_P^*} \tag{3-92}$$

where $k = M, S, P, I$

3.2.7.2 Glass effect

It models the variation in kinetic rate coefficient for propagation with monomer conversion. The equations are as follows:

$$\frac{1}{K_p} = \frac{1}{K_p^0} + \frac{1}{4\pi r_m D_M N_A} \tag{3-93}$$

$$D_M = D_{M0}exp\left[-\frac{\gamma_M \xi_{MP}}{V_f}\left(\frac{\omega_M V_M^*}{\xi_{MP}} + \omega_P V_P^* + \frac{\omega_S V_S^*}{\xi_{SP}}\right)\right] \tag{3-94}$$

$$r_m = r_t \tag{3-95}$$

$$r_t = \frac{\left[ln\left[\frac{1000\tau^3}{N_A\lambda_0\pi^{\frac{3}{2}}}\right]\right]^{\frac{1}{2}}}{\tau} \tag{3-96}$$

$$\tau = \left(\frac{3}{2j_c\delta^2}\right)^{\frac{1}{2}} \tag{3-97}$$

$$\frac{1}{j_c} = \frac{1}{j_{c0}} + \frac{2\Phi_p}{X_{c0}} \tag{3-98}$$

3.2.7.3 Gel effect

This models the variation of kinetic rate coefficient of termination with monomer conversion. The equations are as follows:

$$K_{te} = K_t + K_{t,res} \tag{3-99}$$

$$\frac{1}{K_t} = \frac{1}{K_t^0} + \frac{1}{4\pi r_t D_{Pe} N_A} \tag{3-100}$$

$$D_{Pe} = F_{seg} D_P \tag{3-101}$$

$$D_P = \frac{D_{P0}}{\left(\frac{MW_M^2}{MW_M}\right)} \cdot exp\left[-\frac{\gamma_P}{V_f}\left(\frac{\omega_M V_M^*}{\xi_{MP}} + \omega_P V_P^* + \frac{\omega_S V_S^*}{\xi_{SP}}\right) + \frac{\gamma_P}{\xi_{MP} V_{fM}}\right] \tag{3-102}$$

where

$$D_{P0} = \frac{k_B T}{6\pi \eta_M (R_H)_0} \tag{3-103}$$

$$(R_H)_0 = \left(\frac{3}{10\pi N_A}[\eta]_0 MW_M\right)^{\frac{1}{3}} \tag{3-104}$$

$$[\eta]_0 = K_{MH} \cdot MW_M^{a_{MH}} \tag{3-105}$$

$$F_{seg} = \frac{r_e^3}{16\pi r_B^4}\left[\pi r_e + 6\sqrt{2} \cdot \alpha_{seg} r_B\right] \tag{3-106}$$

$$K_{t,res} = A_{s,avg} K_p M \tag{3-107}$$

Lower value of

$$A_{s,L} = \frac{4\pi\sigma\delta^2 N_A}{3 \times 1000} \tag{3-108}$$

Upper value of A_s

$$A_{s,U} = 8\pi\sigma\delta^3 j_c^{1/2} N_A/(3 \times 1000) \tag{3-109}$$

$$A_{s,avg} = \frac{A_{s,L} + A_{s,U}}{2} \tag{3-110}$$

3.2.8 Constitutive equations to calculate diffusion coefficient

Diffusion coefficient can also be calculated independently by using the method developed by Vrentas and Duda[34,35] based on the free volume theory[36,37]. Free volume theory states that molecular mobility is based on the free space available between the molecules called as free volume. The molecules or a segment of it (if it is too large as in case of polymer) can jump in this free space if it is of sufficient size by random thermal fluctuation. It assumes that no extra energy is required for molecule or a segment of it to move into it. During modeling the variation of diffusion coefficient in the simulations, the value of diffusion coefficient of monomer was used for initiator diffusion coefficient also as their mass and sizes are comparable. Whereas, same value of the diffusion coefficient for polymer was used for μ_0, μ_1 & μ_2 as they represent polymer chains. The expression for diffusion coefficient for monomer and polymer is given below. Note that molecular weight effect is taken into account for evaluating diffusion coefficient of polymer.

$$D_M = D_{M0}exp\left[-\frac{\gamma_M \xi_{MP}}{V_f}\left(\frac{\omega_M V_M^*}{\xi_{MP}} + \omega_P V_P^* + \frac{\omega_S V_S^*}{\xi_{SP}}\right)\right]$$ (3-111)

$$D_P = \frac{D_{P0}}{\left(\frac{MW_M^2}{MW_M}\right)} \cdot exp\left[-\frac{\gamma_P}{V_f}\left(\frac{\omega_M V_M^*}{\xi_{MP}} + \omega_P V_P^* + \frac{\omega_S V_S^*}{\xi_{SP}}\right) + \frac{\gamma_P}{\xi_{MP}V_{fM}}\right]$$ (3-112)

where

$$D_{P0} = \frac{k_B T}{6\pi \eta_M (R_H)_0}$$ (3-113)

$$(R_H)_0 = \left(\frac{3}{10\pi N_A}[\eta]_0 MW_M\right)^{\frac{1}{3}}$$ (3-114)

$$[\eta]_0 = K_{MH} \cdot MW_M^{a_{MH}}$$ (3-115)

$$V_f V_f = \omega_M V_M^* V_{fM} + \omega_P V_P^* V_{fP} + \omega_S V_S^* V_{fS}$$ (3-116)

$$\xi_{kP} = \frac{M_{jk}V_k^*}{M_{jP}V_P^*}$$ (3-117)

3.2.9 Model for CFD

CFD was used to simulate flow in a given reactor geometry. Finite volume method was used. CFD-ACE+, a reputed proven commercial CFD package was used[38]. Flow, scalar and heat module were used for the simulations. Following conservation equations are used for CFD modeling:

1. **The conservation of Mass** (incompressible fluid)

$$\nabla u = 0$$ (3-118)

The conservation of Momentum of Navier-Stokes equation is used.

$$\rho\frac{\partial u}{\partial t} + \rho(u\nabla)u = -\nabla p + \nabla(\eta[\nabla u + (\nabla u)^T])$$ (3-119)

The conservation of Energy with heat generation Q

$$\rho C_P\frac{\partial T}{\partial t} + \nabla(-K\nabla T) = Q - \rho C_P u\nabla T$$ (3-120)

where $Q = -\Delta H_p K_p \lambda_0 M$ (3-121)

The conservation of Chemical Species: Transfer to solvent and CTA are not modeled in CFD modeling and simulation. The method presented here is generalized in nature and thus can be extended to above mentioned steps as and when required. The reaction chemical species are modeled as passive scalars. The modeled species are initiator concentration, monomer concentration, $\mu_0, \mu_1 \& \mu_2$. If there is uniform mixing all the time thus no concentration gradient and if there is no flow, then second (diffusion) and third term (convective) of eqn.(3-122) will vanish and what remains will be the equation for batch reactor. Thus the generation rate term R_i (eq. 3-122) is derived from the polymerization model based on moment method for batch reactor. This can also be used to validate the formulation of CFD problem for flow reactor by simulating it as batch reactor and compare the results with analytical solution for the batch reactor under similar conditions.

$$\frac{\partial C_i}{\partial t} + \nabla(-D_i\nabla C_i + C_i u) = R_i$$ (3-122)

where R_i are defined by eqn.(3-3), (4), (11) to (13) for initiator concentration, monomer concentration, $\mu_0, \mu_1 \& \mu_2$ respectively. Scalar1 represented initiator concentration through

eqn.(3-3), scalar2 represented monomer concentration through eqn.(3-4), scalar3 represented μ_0 through eqn.(3-11), Scalar4 represented μ_1 through eqn.(3-12), and scalar5 represented μ_2 through eqn.(3-13).

3.2.10 Reactor geometry and mesh

Three tubular reactor geometries were used for study in this thesis. They are straight tube (ST), coil tube (CT) and coiled flow inverter (CFI) as shown in Fig. 3-1& Fig. 3-2. Two type of inlet conditions were studied: unmixed and mixed feed. Different grids were used for different conditions. For unmixed condition, the grid used by Mandal *et al.*[39] were used. They consisted of ST and CFI geometry only. The mesh used was unstructured and 30% cut was present at inlet to simulate unmixed feed condition. The detailed meshing for unstructured grid is shown in Fig. 3-1.

(a)   (c)   (d)

(b)   (e)
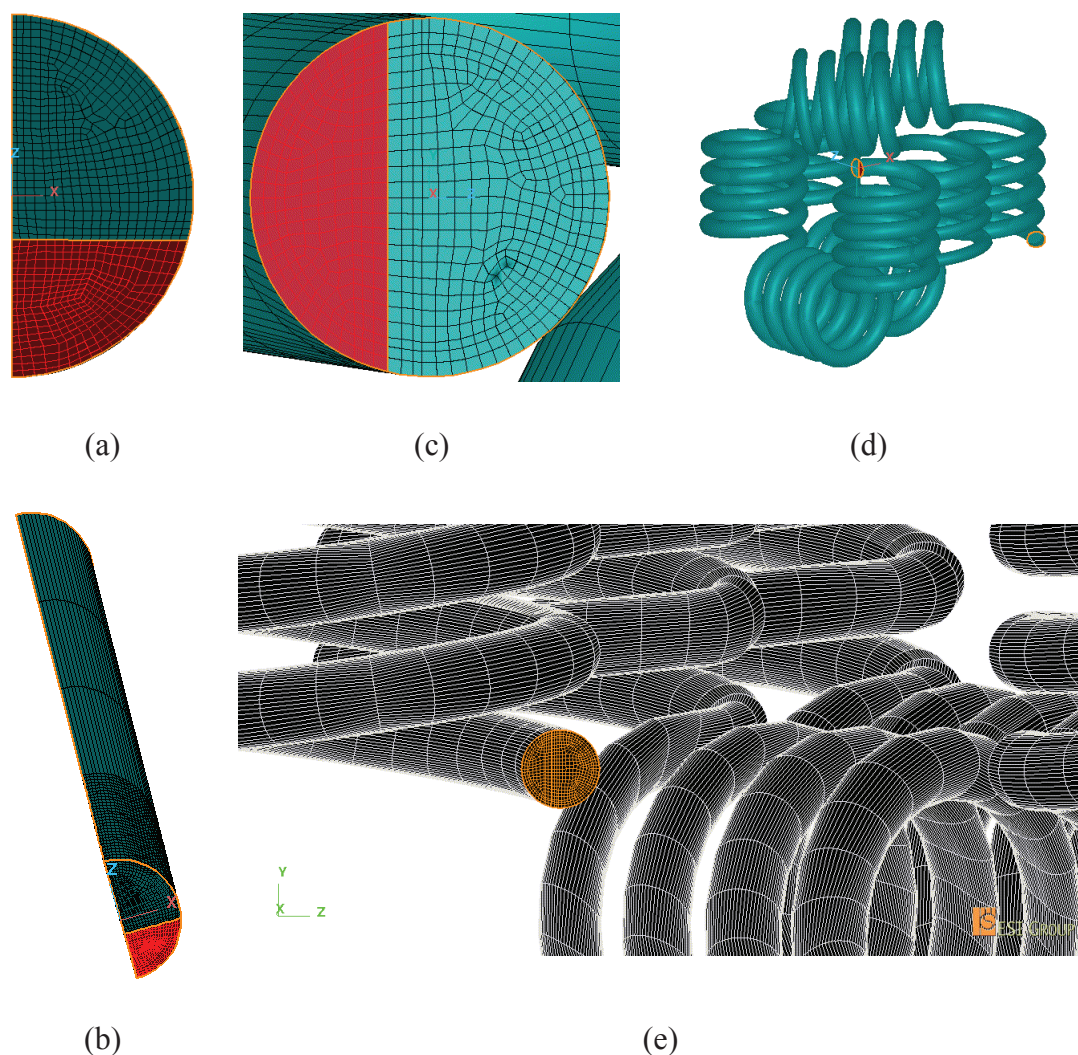
Fig. 3-1- Unstructured grid used for unmixed flow condition, a) ST inlet with 30% cut, b) volume grid for ST, c) CFI inlet with 30% cut, d) general view of CFI, e) detailed mesh for CFI

For mixed feed condition, all the three reactor geometries were used. Structured grid with square cross-sectional meshing was used for all of them. They are shown in Fig. 3-2.

| | | | |
| (a) | (c) | (d) | (e) |

| | | |
| (b) | (f) | (g) |
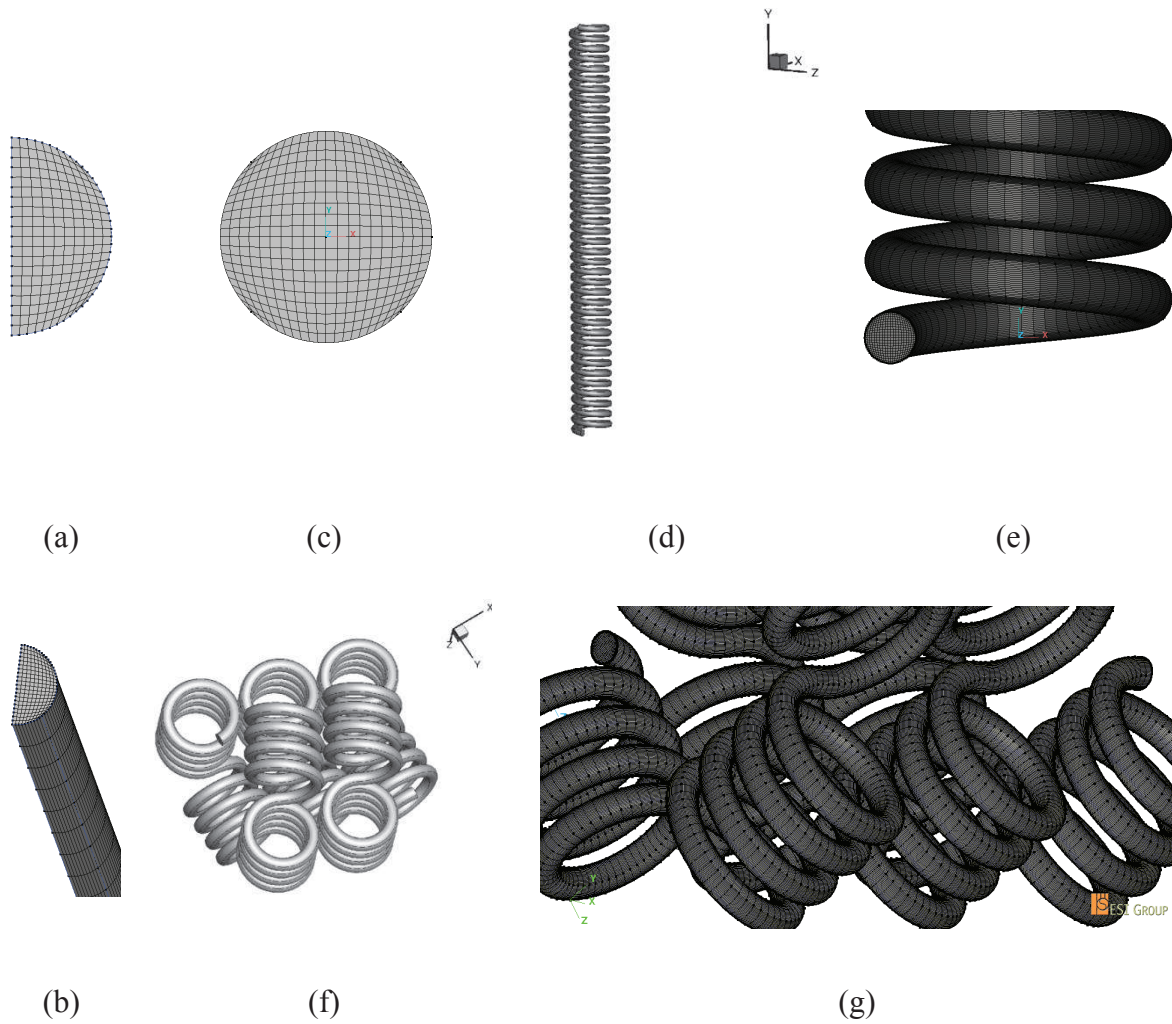
Fig. 3-2- a) Cross-section meshing of STR inlet, b) STR volume grid, c) cross-section meshing of CTR and CFI inlet, d) CTR general view, e) CTR volume grid, f) CFI general view, g) CFI volume grid.

All these geometries were created using CFD-GEOM, part of a well know commercial CFD package CFD-ACE+. For CTR and CFI, a program was written to generate directly the required geometry for any desired parameters like pitch, curvature ratio, no. of turns, no. of points in axial direction etc. Only cross-sectional 2D geometry for inlet was required to generate the whole geometry. Any type of structured mesh like butterfly grid, O grid or square grid could be used to generate the geometry. The geometries generated using it are shown in Fig. 3-2 & Fig. 3-3. Square mesh was used here for cross-section as can be seen on Fig. 3-2 a), b) and d).

(a)   (b)
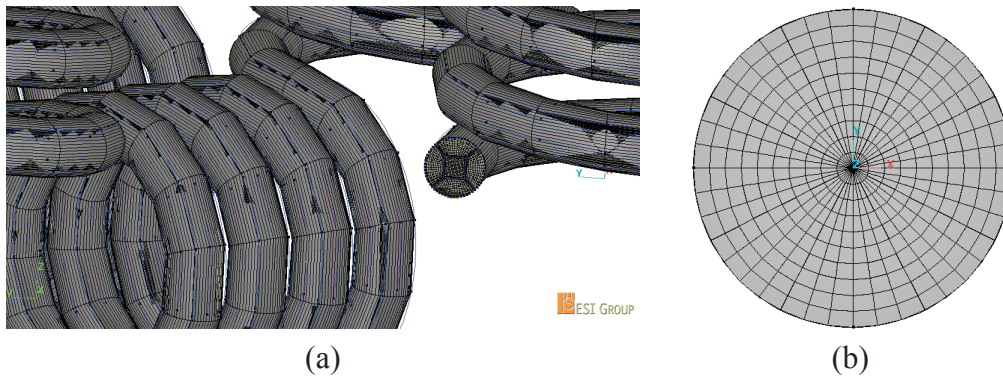
Fig. 3-3- CFI generated using the program for butterfly mesh (a), (b), O-grid.

Operating conditions and reactor data used for simulations are given in Table. 3-5 & Table. 3-6 respectively. For constant fluid thermo-physical property case, the physical property data for water was used.

Table 3-5- Operating conditions for the reactor

	Operating Conditions
Wall temp. (K)	343.15
Chemical Species Diff. Coeff. (m²/s)	$1 \times 10^{-12} \ to \ 1 \times 10^{-8}$
Fluid density (kg/m³)	1×10^3
Fluid viscosity (Pa.s)	1×10^{-3}
Average fluid velocity at inlet (m/s)	2.9×10^{-5}
Specific heat (J/K/Kg)	4182
Thermal conductivity (W/m/K)	0.6
Inlet feed temp (K)	343.15
Peclet no.	$\sim 3.5 \times 10^3 - 3.5 \times 10^8$

Table 3-6- Reactor data

Reactor Type	Length (m)	Curvature ratio	No. of turns	No. of bends	Pitch (m)	Residence Time (s)	Excess length (%)
STR	1.252	-	-	0	-	43200	0
CTR	1.262	5	40	0	0.003	43546	+0.8
CFI	1.285	5	40	9	0.003	44340	+2.6

3.2.11 Mesh independency test

Extensive mesh independency analysis was done for a given reactor geometry for fully mixed feed condition. For each reactor geometry, three different diffusivity coefficients ($D = 1 \times 10^{-12}, 1 \times 10^{-10}, 1 \times 10^{-8} \ m^2/s$) were used to cover the complete range of variation of diffusivity coefficient under study. Mesh was made to vary in both radical and axial directions and then it was checked for convergence. The results are shown in Table. 3-7.

97

Table 3-7- Mesh independency result for x_M for fully mixed inlet to STR.

Conversion, x_M	Axial, Z=10	Z=50	Z=100	Z=200	Z=500
20x20 (cross-section)	0.7621	0.7681	0.7682	0.7683	0.7683
30x30	0.7621	0.7681	0.7682	0.7683	0.7683
50x50	0.7621	0.7681	0.7683	0.7683	0.7683
100x100	0.7621	0.7681	0.7683	0.7683	0.7683

Only four most suitable cases for meshing were selected for further evaluation where all the variables satisfactorily become mesh independent. These four cases arise from the combination of change in axial direction point and cross-sectional cell density.

All the variables were made to become independent of mesh for the mesh to be selected. Only one such variable, monomer conversion x_M analysis data is shown in For fully mixed inlet condition, for a given reactor geometry, after mesh independency test, a common mesh was found to be suitable for whole range of variation of values of diffusivity coefficient taken under study. In this problem, the mesh independency was found to be more dependent upon no. of grid points in flow direction rather than on cross-sectional meshing for the mixed inlet case. This was found to be true for all the three reactor geometries. This helps in selecting coarse cross-sectional mesh to reduce the total no. of mesh point but still getting the same results. The final mesh selected for a given geometry for mix inlet condition is given in Table. 3-8.

Table 3-8- selected grids for various reactor geometries for the simulation.

Reactor Geometry	Mix Inlet	
	Cross section	*Flow direction*
STR	20x20	100
CTR	20x20	55*
CFI	20x20	55*

* For CTR and CFI, this is the no. of points in flow direction in one complete turn. So total no. of points = 55 x (no. of turns)

The relaxation technique (inbuilt in CFD-ACE+) was used which put constraint on the variation of dependent or auxiliary variables from one iteration to another. This helps in convergence of the simulation. Relaxation parameters values enable us to do so. The first requirement for any CFD problem is to make it converging by tuning relaxation parameters for various variables. The values of relaxation parameters were then found to have quite big impact on the rate of convergence as well as on the level of convergence during our study. After choosing proper values, the simulations were made to converge in 150-3000 iterations depending on the case. But once the simulation was converged (based on residual ratio value criteria already mentioned), the values of variables in converged solution was found to be

independent of relaxation parameters values. The values of relaxation parameters were found to be affected by the values of diffusivity coefficient.

Flow average values of all variables were evaluated at reactor outlet which is given by:

$$\overline{scalar_i} = \frac{\sum_j scalar_{ij}.VelMag_j.Area_j}{\sum_j VelMag_j.Area_j}$$ (3-123)

where $\overline{scalar_i}$ is flow average value, of $scalar_i$, $scalar_{ij}$ is the value of $scalar_i$ in j^{th} cell of the outlet, $VelMag_i$ & $Area_j$ are velocity magnitude at and area of cell j of outlet.

3.2.12 References

1. Tefera, N.; Weickert, G.; Westerterp, K. R., Modeling of free radical polymerization up to high conversion .1. A method for the selection of models by simultaneous parameter estimation. *Journal of Applied Polymer Science* **1997,** *63* (12), 1649-1661.
2. Bamford, C. H. and Tompa, H., On the calculation of molecular weight distributions from kinetic schemes. *J. Polym. Sci.* **1953**, *10*, 345–350.
3. Bamford, C. H. and Tompa, H. The calculation of molecular weight distributions from kinetic schemes, *Trans. Faraday Soc.* **1954**, *50*, 1097-1115.
4. Serra, C.; Schlatter, G.; Sary, N.; Schonfeld, F.; Hadziioannou, G., Free radical polymerization in multilaminated microreactors: 2D and 3D multiphysics CFD modeling. *Microfluid Nanofluid* **2007,** *3* (4), 451-461.
5. Mandal, M. M.; Serra, C.; Hoarau, Y.; Nigam, K. D. P., Numerical modeling of polystyrene synthesis in coiled flow inverter. *Microfluid Nanofluid* **2011,** *10* (2), 415-423.
6. http://digitizer.sourceforge.net/
7. Achilias, D. S.; Kiparissides, C., Development of a General Mathematical Framework for Modeling Diffusion-Controlled Free-Radical Polymerization Reactions. *Macromolecules* **1992,** *25* (14), 3739-3750.
8. Keramopoulos, A.; Kiparissides, C., Mathematical Modeling of diffusion-controlled free-radical terpolymerization reactions. *Journal of Applied Polymer Science* **2003,** *88* (1), 161-176.
9. Soh, S. K.; Sundberg, D. C., Diffusion-Controlled Vinyl Polymerization .3. Free-Volume Parameters and Diffusion-Controlled Propagation. *J Polym Sci Pol Chem* **1982,** *20* (5), 1331-1344.
10. Soh, S. K.; Sundberg, D. C., Diffusion-Controlled Vinyl Polymerization .4. Comparison of Theory and Experiment. *J Polym Sci Pol Chem* **1982,** *20* (5), 1345-1371.
11. Zielinski, J. M.; Duda, J. L., Predicting Polymer Solvent Diffusion-Coefficients Using Free-Volume Theory. *Aiche J* **1992,** *38* (3), 405-415.
12. Russell, G. T.; Napper, D. H.; Gilbert, R. G., Termination in Free-Radical Polymerizing Systems at High Conversion. *Macromolecules* **1988,** *21* (7), 2133-2140.
13. J.E.Mark (editor), Physical properties of polymer Handbook, American Institute of Physics, NewYork, 1996

14. Baillagou, P. E.; Soong, D. S., Major Factors Contributing to the Nonlinear Kinetics of Free-Radical Polymerization. *Chem Eng Sci* **1985,** *40* (1), 75-86.

15. Keramopoulos, A.; Kiparissides, C., Development of a comprehensive model for diffusion-controlled free-radical copolymerization reactions. *Macromolecules* **2002,** *35* (10), 4155-4166.

16. Polymer handbook, Brandrup, J.; Immergut, E. H.- Ed., *Interscience Publishers*, New York, 1966.

17. Wu, J. Y.; Shan, G. R., Kinetic and molecular weight control for methyl methacrylate semi-batch polymerization. I. Modelling. *Journal of Applied Polymer Science* **2006,** *100* (4), 2838-2846.

18. Fenouillot, F.; Terrisse, J.; Rimlinger, T., Polymerization of methyl methacrylate at high temperature with 1-butanethiol as chain transfer agent. *Journal of Applied Polymer Science* **1999,** *72* (12), 1589-1599.

19. Marten, F. L.; Hamielec, A. E., High-Conversion Diffusion-Controlled Polymerization of Styrene .1. *Journal of Applied Polymer Science* **1982,** *27* (2), 489-505.

20. Wang, W.; Hutchinson, R. A., A Comprehensive Kinetic Model for High-Temperature Free Radical Production of Styrene/Methacrylate/Acrylate Resins. *Aiche J* **2011,** *57* (1), 227-238.

21. Karabaev, M.; Abduzhaminov, T. P.; Saidov, A. A.; Igamberdyev, Kh. T., Thermophysical properties of liquid methacrylic acid and its simple esters, *Izv. Akad. Nauk Uzb. SSR,Ser. Fiz.-Mat. Nauk* **1985**, *4*, 71-74.

22. Gaur, U.; Lau, S. F.; Wunderlich, B. B.; Wunderlich, B., Heat-Capacity and Other Thermodynamic Properties of Linear Macromolecules .6. Acrylic Polymers. *J Phys Chem Ref Data* **1982,** *11* (4), 1065-1089.

23. Gaur, U.; Wunderlich, B., Heat-Capacity and Other Thermodynamic Properties of Linear Macromolecules .5. Polystyrene. *J Phys Chem Ref Data* **1982,** *11* (2), 313-325.

24. Perry's Chemical Engineers' Handbook. — 7th ed. editor, Don W. Green, 1997.

25. Shoulberg, R.H. & Shetter, J.A., The thermal conductivity of poly(methyl methacrylate), *Journal of Applied Polymer Science* **1962**, *6*(23), 32-33.

26. Baillagou, P. E.; Soong, D. S., Free-Radical Polymerization of Methyl-Methacrylate in Tubular Reactors. *Polym Eng Sci* **1985,** *25* (4), 212-231.

27. Chen, C. C., A Continuous Bulk-Polymerization Process for Crystal Polystyrene. *Polym-Plast Technol* **1994,** *33* (1), 55-81.

28. Pedersen, M. J.; Kay, W. B.; Hershey, H. C., Excess Enthalpies, Heat-Capacities, and Excess Heat-Capacities as a Function of Temperature in Liquid-Mixtures of Ethanol + Toluene, Ethanol + Hexamethyldisiloxane, and Hexamethyldisiloxane + Toluene. *J Chem Thermodyn* **1975,** *7* (12), 1107-1118.

29. Harkness, M. R., A computer simulation of the bulk polymerization of polystyrene, in tubular reactor. MS thesis, Rensselaer Polytechnic Institute, Tr'oy, New York, 1982.

30. Mendelson, R. A., Concentrated-Solution Viscosity Behavior at Elevated-Temperatures - Polystyrene in Ethylbenzene. *J Rheol* **1980,** *24* (6), 765-781.

31. Chiu, W. Y.; Carratt, G. M.; Soong, D. S., A Computer-Model for the Gel Effect in Free-Radical Polymerization. *Macromolecules* **1983,** *16* (3), 348-357.

32. Lima, E. V.; Guerra, E. S., Digital Simulation of Bulk and Suspension Polymerization of Styrene, Using Non-linear Regression for Curve Fitting the Kinetic Parameters. *Journal of Reinforced Plastics and Composites* **1993,** *12* (7), 800-812.

33. Achilias, D.; Kiparissides, C., Modeling of Diffusion-Controlled Free-Radical Polymerization Reactions. *Journal of Applied Polymer Science* **1988,** *35* (5), 1303-1323.

34. Vrentas, J. S.; Duda, J. L., Diffusion in Polymer - Solvent Systems .1. Re-Examination of Free-Volume Theory. *J Polym Sci Pol Phys* **1977,** *15* (3), 403-416.

35. Vrentas, J. S.; Duda, J. L., Diffusion in Polymer-Solvent Systems .2. Predictive Theory for Dependence of Diffusion-Coefficients on Temperature, Concentration, and Molecular-Weight. *J Polym Sci Pol Phys* **1977,** *15* (3), 417-439.

36. Cohen, M. H.; Turnbull, D., Molecular transport in liquids and glasses. *J. Chem. Phys.* **1959**, *31*, 1164-1169.

37. Fujita, H., Diffusion in Polymer-Diluent Systems. *Fortschr. Hochpolym.-Forsch.* **1961**, *3*, 1-47.

38. CFD-ACE documentation, https://www.esi-group.com/software-services/virtual-environment/cfd-multiphysics/ace-suite/cfd-ace.

39. Mandal, M. M.; Serra, C.; Hoarau, Y.; Nigam, K. D. P., Numerical modeling of polystyrene synthesis in coiled flow inverter. *Microfluid Nanofluid* **2011,** *10* (2), 415-423.

Chapter4   Analytical Solution of Free Radical Polymerization: Derivation, Validation and Applications

Preface

This chapter deals about the theoretical aspects of the kinetic scheme of free radical polymerization (FRP). The kinetic scheme-1 as shown in chapter-3 contains the elementary reaction steps of dissociation and initiation, propagation, termination by combination and disproportionation, transfer to monomer, solvent and chain transfer agent (CTA). A mathematical model based on moment method is used for this kinetic scheme. This method is widely used method among researchers for determining statistically averaged values like conversion, MW_w, MW_n and PDI.

An analytical solution (AS) for this mathematical model is being derived using simple assumptions. This is presented in sec.4.1. The assumptions include isothermal, homogeneous, solution, homopolymerization batch reactor with variation in volume with reaction. AS is validated against experimental results obtained under different conditions. There were also 2 sets of numerical solutions (NS) against which analytical solution is rigorously tested and validated. The first one, FRP_FULL as explained in chapter-3, contains all the ordinary differential equations (ODEs) of the model without any further assumptions and consists of 11 ODEs including energy balance equation for temperature. The second one, FRP_QSSA as explained in chapter-3, contains the set of ODEs from which the analytical solution has been derived. The only difference between FRP_Full and FRP_QSSA lies in the assumption of QSSA for the macroradicals concentration. Thus FRP_QSSA consists of 8 ODEs including one for energy balance equation. AS has been used along with energy balance equation, thus requiring only one ODE to be solved in non-isothermal condition. Otherwise, no ODE is to be solved for isothermal condition compare to 10 and 7 ODEs for FRP_Full and FRP_QSSA respectively.

AS needs to be tested for 3 conditions so as to prove it correctness compare to NS and experimental results whenever available over the complete range of conversion. These conditions are as follows:

1. To model variation in kinetic rate coefficients to simulate gel and glass effect (sec.4.2),

2. To model variation in initiator efficiency to simulate cage effect along with gel and glass effect (sec.4.3),

3. To model temperature variations due to heat of reaction and heat transfer rate variations to simulate non-isothermal conditions (sec.4.4).

This chapter is composed of the four following articles corresponding to the four aforementioned sections

*(1) Garg D.K., C.A. Serra, Y. Hoarau, D. Parida, M. Bouquey, R. Muller, Analytical Solution of Free Radical Polymerization: Derivation and Validation. Macromolecules **2014,** to be submitted.*

(2) Garg D.K., C.A. Serra, Y. Hoarau, D. Parida, M. Bouquey, R. Muller, Analytical Solution of Free Radical Polymerization: Applications- Implementing Gel effect using CCS method. Macromolecules **2014**, *to be submitted.*

(3) Garg D.K., C.A. Serra, Y. Hoarau, D. Parida, M. Bouquey, R. Muller, Analytical Solution of Free Radical Polymerization: Applications- Implementing Gel effect using AK Model. Macromolecules **2014**, *to be submitted.*

(4) Garg D.K., C.A. Serra, Y. Hoarau, D. Parida, M. Bouquey, R. Muller, Analytical Solution of Free Radical Polymerization: Applications- Implementing Non-isothermal Effect. Macromolecules **2014**, *to be submitted.*

4.1 Analytical Solution of Free Radical Polymerization: Derivation and Validation

4.1.1 Abstract

An elegant, simple and exact analytical solution was obtained for the widest possible range of elementary steps with practical importance in free radial polymerization. The analytical solution matches excellently with the numerical solution for the four cases of monomer-polymer systems studied ranging from the slowest to the fastest. It works equally well for different initiators, different initiator and monomer concentrations, presence or absence of solvent, various solvent volume fractions and different temperatures. It matches also quite perfectly with experimental data reported in the literature. This analytical solution is not only in-line with previous published solutions but also extends their applicability in a natural way. Overall, the conceptual correctness as well as predictive capabilities of the derived analytical solution is established beyond doubt. This analytical solution has the potential to be used in various practical applications like model based process control, CFD simulations etc.

Key Words – Analytical solution, free radical polymerization, styrene, methyl methacrylate, butyl acrylate, vinyl acetate.

4.1.2 Introduction

An explicit analytical solution is always desirable for a given set of mathematical equations. It is especially valuable for mathematical models. It not only reduces the effort by generating final accurate solution in one step but also gives a significant insight of the problem. It is also helpful in the validation of the formulation of numerical problem by comparing the numerical solution with analytical solution. Free radical polymerization (FRP) is one such problem which was widely simulated[1-7] and an analytical solution of its mathematical model will always be helpful.

To obtain any meaningful result from the simulation of any problem, it is necessary that the problem should be modeled properly. Theoretically, the best modeling of any problem is the one which encompasses all the aspects of the problem. But this ideal condition is often not so practical. Indeed, not all aspects of the problems are properly understood to formulate them mathematically. On the other hand, it may be too computationally exhaustive to include all effects, both minor and major. Thus it might not be economically feasible in terms of time and resources to obtain any meaningful results. So, several assumptions are made to simplify the problem. Too much simplification also has the adverse effect of losing all the vital aspects of the problem thus rendering the solution useless. An adequate simplification of the problem is the one which reduces the unnecessary and insignificant aspects of the problem under the given conditions while still retaining the essence of the problem. The extent of simplification and thus the assumptions can vary with the conditions under which solution is desired or the level of insight required in the problem.

There are several elementary reaction steps that characterize a real FRP scheme but any model of FRP includes minimum four steps shown in scheme.1, namely (a) Initiator decomposition, (b) initiation, (c) propagation, (d) termination. Step (a) and (b) are generally

clubbed together with an initiator efficiency factor *f*, for simplifying modeling. There is one parallel reaction each to step (c) and step (d) namely transfer to monomer (step (f)) and termination by disproportionation (step (e)) respectively. There are several other competitive reactions to propagation step e.g. transfer to solvent (g), transfer to chain transfer agent (CTA) (h) etc. Many researchers use various combinations of the above mentioned steps for modeling and matching experimental results with different success[1-7]. Effect of solvent is also considered to different extent in the modeling either by considering the reaction steps involving solvent or its dilution effects on species concentration and temperature or both. The kinetic model of FRP considered in this paper is also used by many researchers[7,8] and is fairly good and sufficient enough for many practical situations. Not all steps could practically be considered due to the excessively increased level of complexity for deriving analytical solution.

One of the most sought solution for any chemical reaction is the one for ideal batch reactor form. However, plug flow reactor in continuous flow process is equivalent to batch reactor. So any solution obtained for batch reactor is directly applicable to plug flow reactors and hence to continuous flow reactors. Thus, it is this benchmark against which the efficiency and effectiveness of all other reactors and reactor conditions are tested. To obtain any solution including analytical solution for ideal batch reactor, it has to be formulated for those conditions. For this, several assumptions have to be made. The mathematical formulation of FRP in its entirety is quite non-linear. Various chemical and physical variables e.g. kinetic rate coefficients, initiator efficiency, density of various chemical species, etc. are function of temperature, pressure, species concentration, solution density and viscosity. But to keep the problem manageable, one generally makes certain assumptions and extent of accuracy of these assumptions depends on the conditions in which they are applied. So, various assumptions are taken to make the problem linear and then arrive at any solution including analytical solution.

Several researchers have given empirical, semi-empirical or semi-analytical solution for FRP and can be found out in a complete review[10]. Zhu *et al.*[21] have given the analytical solution for initiator and monomer conversion only. Another attempt was made in the past for giving an analytical solution for FRP by. Venkateshwaran *et al.*[9] However, there are several notable and significant differences between their work and the one presented here. Authors worked on reaction steps which included only initiation, propagation, termination by combination and disproportionation as well as transfer to CTA. Their main assumptions are isothermal, homogeneous, constant volume homopolymerization with time invariant kinetic rate coefficients. They did not consider the quasi-steady state assumption (QSSA) for the moments of live polymer chains length distribution of various orders including zeroth (λ_0) – the most important one. Using aforementioned assumptions, they had derived the analytical solution for λ_0. The solution is in terms of infinite series of Bessel equations. Then, they went on to derive the analytical solution for other variables like monomer concentration, second and third order moments of the living polymer chain lengths distribution and zeroth, first and second order moment of the dead polymer chain lengths distribution. Their analytical solution obtained is too complicated and lengthy. The solution seems to be very impractical in its

application. Besides this, the analytical solution matches quite poorly with numerical solution even for isothermal, non-gel/glassy situation for which it was originally derived. Furthermore, they have used several assumptions to express the monomer concentration and came up with a final form. The latter being similar to the one shown by Zhu *et al.*[21], although that work was based on QSSA for the live polymer chain lengths distribution. Venkateshwaran *et al.* had also integrated the energy equation for temperature using the same assumption of constant kinetic rate coefficients. This assumption will further be discussed and commented in the Discussion section.

Compared to their work, we have extended the set of reactions to transfer to monomer and transfer to solvent, similar to the one used by Tefera *et al.*[5]. The reaction scheme now includes seven major steps, namely, initiator dissociation and initiation, chain propagation, chain transfer to monomer, chain transfer to solvent, chain transfer to CTA, chain termination by combination and chain termination by disproportionation. It is derived directly from theoretical kinetics, so it is neither empirical nor semi-empirical nor semi-analytical. An explicit analytical solution is obtained for isothermal, variable volume, homogeneous batch reactor condition for bulk/solution free radical homopolymerization. No gel effect, glass effect and cage effect is modeled. Four monomer-polymer systems are considered in this work based on their rate of reaction which varies from slow for one monomer to extremely fast for another. These monomers are styrene (St), methyl methacrylate (MMA), butyl acrylate (BuA) and vinyl acetate (VAc). The solution is also validated with solvent (solution polymerization) and without solvent (bulk polymerization) conditions. Two different initiators, namely 2,2′-Azobis(2-methylpropionitrile) (AIBN) and benzoyl peroxide (BPO) with different concentrations are also used for simulation. Isothermal condition is considered with constant temperature varying from 60°C to 100°C. The results are compared with numerical solution as well as with published experimental data.

4.1.3 Model of FRP for this work
The detail kinetic scheme used in this work is given in section 3.2.2. The details of the mathematical model used are given in section 3.2.3.

4.1.4 Derivation
To derive analytical solution, following assumptions were applied to eqn.(3-3)-(3-13)
1. Only one monomer-polymer system is considered at a time (homopolymerization),
2. Constant temperature (isothermal condition), so that kinetic rate coefficients and density of monomer and polymer remain constant with respect to temperature,
3. Uniform mixing (so no spatial variation of concentration thus no effect of diffusion and convection is to be considered),
4. Constant initiator efficiency f, throughout reaction (no cage effect),
5. Kinetic rate coefficients are considered to be function of only temperature (thus no gel and glass effect) and thus constant during derivation,
6. Quasi-Steady State Assumption (QSSA) applied to radical polymer chains number instead of concentration in eqn.(3-8)-(3-10). This is important as it enables to bypass the problem of non-linearity introduced by the variation of volume only.
7. Long chain hypothesis for the monomer consumption

After applying the above mentioned assumptions, we will take one equation at a time and solve it appropriately. We will be taking limits from time step t_{n-1} to t_n and all other variables values will be evaluated accordingly for the integration. This approach will lead to final derived equations that might be useful for semi-batch conditions where conditions can be changed at a given time or for a given time step. This form will also be useful for process control purposes as the equations can be rearranged for $t_n - t_{n-1} = \Delta t$ form. For more general form, i.e. calculating any variable at a given time t, equations can be evaluated using the limits $t_0 = 0$ and $t_n = t$. The equations can also be used for constant volume conditions.

4.1.4.1 Initiator concentration (eqn.3-3)

$$\frac{1}{V_R}\frac{d(I.V_R)}{dt} = -K_d I \tag{3-3}$$

Rearranging and integrating leads to

$$I.V_R = e^{-K_d.t} \tag{4-1}$$

Applying limits from time step t_{n-1} to t_n, gives

$$\frac{[I.V_R]_n}{[I.V_R]_{n-1}} = e^{-K_d.(t_n-t_{n-1})} \tag{4-2}$$

Rearranging

$$[I]_n = [I]_{n-1}.\frac{[V_R]_{n-1}}{[V_R]_n}.e^{-K_d.(t_n-t_{n-1})} \tag{4-3}$$

We will now introduce a new term so-called corrected volume ratio, V_{corr}, to account for volume variation; which is defined as

$$V_{corr} = \frac{[V_R]_{n-1}}{[V_R]_n} \tag{4-4}$$

For constant volume condition, $V_{corr} = 1$. $\tag{4-5}$

Let $y_n = e^{\frac{-K_d.t_n}{2}}$ $\tag{4-6}$

and $\frac{y_n}{y_{n-1}} = e^{\frac{-K_d.(t_n-t_{n-1})}{2}} = e^{\frac{-K_d.\Delta t}{2}} = \Delta y$, where $\Delta t = (t_n - t_{n-1})$ $\tag{4-7}$

Therefore

$$[I]_n = [I]_{n-1}.\frac{[V_R]_{n-1}}{[V_R]_n}.e^{-K_d.(t_n-t_{n-1})} = [I]_{n-1}.V_{corr}.[\Delta y]^2 \tag{4-8}$$

Applying limits of $t_{n-1} = t_0 = 0$ to $t_n = t$, we have

$$I = I_0.\frac{V_{R0}}{V_R}.e^{-K_d.t} = I_0.\frac{V_{R0}}{V_R}.y^2 \tag{4-9}$$

where:

$$y = e^{\frac{-K_d.t}{2}}$$

(4-10)

4.1.4.2 Monomer conversion (eqn. 3-5)

Applying QSSA to eqn.(3-8) (cf. eqn.(4-36)) and using above obtained result (eqn.(4-9) in eqn.(3-5)) leads to:

$$\frac{dx_M}{dt} = K_{pr}(1 - x_M)\lambda_0 = K_{pr}(1 - x_M)\sqrt{\frac{2fK_dI}{K_t}} = K_{pr}(1 - x_M)\sqrt{\frac{2fK_dI_0}{K_t} \cdot \frac{V_{R0}}{V_R}} \cdot e^{\frac{-K_d.t}{2}}$$

(4-11)

Rearranging,

$$\int \frac{dx_M}{(1 - x_M)} = K_{pr}\sqrt{\frac{2fK_dI_0}{K_t} \cdot \frac{V_{R0}}{V_R}} \int e^{\frac{-K_d.t}{2}} dt$$

(4-12)

Integration gives

$$ln(1 - x_M) = \tilde{B}.e^{\frac{-K_d.t}{2}}$$

(4-13)

$$(1 - x_M) = exp\left[\tilde{B}.e^{\frac{-K_d.t}{2}}\right]$$

(4-14)

where:

$$\tilde{B} = K_{pr}\frac{2}{K_d}\sqrt{\frac{2fK_dI_0}{K_t} \cdot \frac{V_{R0}}{V_R}}$$

(4-15)

Applying limits from time step t_{n-1} to t_n, we obtain:

$$\frac{[1-x_M]_n}{[1-x_M]_{n-1}} = exp\left[K_{pr}\frac{2}{K_d}\sqrt{\frac{2fK_dI_0}{K_t} \cdot \frac{V_{R0}}{V_R}} \cdot \left(e^{\frac{-K_d.t_n}{2}} - e^{\frac{-K_d.t_{n-1}}{2}}\right)\right] = exp\left[K_{pr}\sqrt{\frac{2fK_dI_0}{K_t} \cdot \frac{V_{R0}}{V_R}} \cdot (y_n - y_{n-1})\right] = exp\left[-B_{n-1} \cdot \left(1 - \frac{y_n}{y_{n-1}}\right)\right]$$

(4-16)

where:

$$B_{n-1} = \sqrt{\frac{8f[K_{pr}]^2 I_{n-1}}{K_d K_t}},$$

(4-17)

Now recalling eqn.(4-7) and rearranging leads to:

$$[x_M]_n = 1 - [1 - x_M]_{n-1}.exp[-B_{n-1}.(1 - \Delta y)]$$

(4-18)

Applying limits of $t_{n-1} = t_0 = 0$ to $t_n = t$, we have $\Delta t = t$ & $\Delta y = y$

(4-19)

$$x_M = 1 - exp[-B_0.(1 - y)]$$

(4-20)

where:

$$B_0 = \sqrt{\frac{8f[K_{pr}]^2 I_0}{K_d K_t}}$$ (4-21)

From eqn.(3-39) for monomer concentration and above eqn.(4-18), we can derive relationship between monomer concentrations at two different time intervals

$$[M]_n = [M]_{n-1}.\frac{[1-x_M]_n}{[1-x_M]_{n-1}}.\frac{[V_R]_{n-1}}{[V_R]_n} = [M]_{n-1}.\frac{[1-x_M]_n}{[1-x_M]_{n-1}}.V_{corr} = [M]_{n-1}.exp[-B_{n-1}.(1-\Delta y)].V_{corr}$$ (4-22)

By integrating eqn.(3-4) directly for monomer concentration, we will still get the same equation as above.

Applying limits of $t_{n-1} = t_0 = 0$ to $t_n = t$, we have:

$$M = M_0.\frac{exp[B_0.(y-1)]}{(1-\varepsilon.x_M)} = M_0.\frac{exp[-B_0.(1-y)]}{(1-\varepsilon.x_M)} = \frac{M_0.[V_R]_0}{V_R}.exp[-B_0.(1-y)]$$ (4-23)

4.1.4.3 Transfer to solvent (eqn.3-6)

$$-\frac{1}{V_R}\frac{d(S.V_R)}{dt} = K_{fs}S\lambda_0 = C_S K_p S\lambda_0 = R_S K_{pr}S\lambda_0$$ (3-6)

Integrating similarly as for x_M, we have

$$(S.V_R) = exp\left[R_S.B.e^{\frac{-K_d.t}{2}}\right]$$ (4-24)

Applying limits from time step t_{n-1} to t_n, we obtain after rearranging:

$$[S]_n = [S]_{n-1}.exp[-R_S.B_{n-1}.(1-\Delta y)].\frac{[V_R]_{n-1}}{[V_R]_n} = [S]_{n-1}.exp[-R_S.B_{n-1}.(1-\Delta y)].V_{corr}$$ (4-25)

Applying limits of $t_{n-1} = t_0 = 0$ to $t_n = t$, we have

$$S = S_0.\frac{exp[-R_S.B_0.(1-y)]}{(1-\varepsilon.x_M)} = \frac{S_0 V_{R0}}{V_R}.exp[-R_S.B_0.(1-y)]$$ (4-26)

So dividing above equation with M (eqn.4-23), we have

$$\frac{S}{M} = \frac{S_0}{M_0}.\frac{exp[-R_S.B_0.(1-y)]}{exp[-B_0.(1-y)]} = \frac{S_0}{M_0}.exp[(1-R_S).B_0.(1-y)]$$ (4-27)

4.1.4.4 Transfer to CTA (eqn.3-7)
Similarly for CTA

$$-\frac{1}{V_R}\frac{d(A.V_R)}{dt} = K_{fa}A\lambda_0 = C_A K_p A\lambda_0 = R_A K_{pr}A\lambda_0$$ (3-7)

Applying limits from time step t_{n-1} to t_n, we have after rearranging

$$[A]_n = [A]_{n-1}.exp[-R_A.B_{n-1}.(1-\Delta y)].\frac{[V_R]_{n-1}}{[V_R]_n} = [A]_{n-1}.exp[-R_A.B_{n-1}.(1-\Delta y)].V_{corr}$$

(4-28)

Applying limits of $t_{n-1} = t_0 = 0$ to $t_n = t$, we have

$$A = A_0.\frac{exp[-R_A.B_0.(1-y)]}{(1-\varepsilon.x_M)} = \frac{A_0.V_{R0}}{V_R}.exp[-R_A.B_0.(1-y)]$$

(4-29)

So dividing previous equation with M (eqn.4-23), we have

$$\frac{A}{M} = \frac{A_0}{M_0}.\frac{exp[-R_A.B_0.(1-y)]}{exp[-B_0.(1-y)]} = \frac{A_0}{M_0}.exp[(1-R_A).B_0.(1-y)]$$

(4-30)

Now let

$$L = \frac{(K_p+K_{fm})M\lambda_0}{2fK_dI} = \frac{K_{pr}M\lambda_0}{2fK_dI}$$

(4-31)

At the beginning of nth time step

$$[L]_n = \frac{K_{pr}[M]_n[\lambda_0]_n}{2fK_d[I]_n}$$

(4-32)

$$\bar{L} = \frac{K_pM\lambda_0}{2fK_dI + (K_{fm}M+K_{fs}S+K_{fa}A)\lambda_0} = \frac{(1-R_{MM})K_{pr}M\lambda_0}{2fK_dI + (R_{MM}+R_{SM}+R_{AM})K_{pr}M\lambda_0} = \frac{(1-R_{MM})K_{pr}M\lambda_0}{2fK_dI + R_PK_{pr}M\lambda_0}$$

(4-33)

$$\bar{L} = L.\left(\frac{1-R_{MM}}{1+R_PL}\right) = L.\left(\frac{1-R_M}{1+R_PL}\right)$$

(4-34)

At the beginning of nth time step

$$[\bar{L}]_n = [L]_n.\left(\frac{1-R_M}{1+R_P[L]_n}\right)$$

(4-35)

4.1.4.5 λ_0, Zeroth order moment of live polymer chain length distribution (eqn.3-8)
By applying QSSA on eqn.(3-8), we have

$$\lambda_0 = \sqrt{\frac{2fK_dI}{(K_{tc}+K_{td})}} = \sqrt{\frac{2fK_dI}{K_t}}$$

(4-36)

At the beginning of nth time step

$$[\lambda_0]_n = \sqrt{\frac{2fK_d[I]_n}{K_t}}$$

(4-37)

4.1.4.6 λ_1, First order moment of live polymer chain length distribution (eqn.3-9)

By applying QSSA on eqn.(3-9), we have

$$\lambda_1 = \left[\frac{2fK_dI + (1+R_{SM}+R_{AM})K_{pr}M\lambda_0}{K_t\lambda_0 + (R_{MM}+R_{SM}+R_{AM})K_{pr}M} \right] = \lambda_0 \left[\frac{1+(1+R_{SA})L}{1+R_PL} \right] = \lambda_0(\bar{L}+1) \tag{4-38}$$

At the beginning of nth time step

$$[\lambda_1]_n = [\lambda_0]_n([\bar{L}]_n + 1) \tag{4-39}$$

4.1.4.7 λ_2, Second order moment of live polymer chain length distribution (eqn.3-10)

By applying QSSA on eqn.(3-10), we have

$$\lambda_2 = \left[\frac{2fK_dI + (1+R_{SM}+R_{AM})K_{pr}M\lambda_0 + 2K_pM\lambda_1}{K_t\lambda_0 + (R_{MM}+R_{SM}+R_{AM})K_{pr}M} \right] = \lambda_1(2\bar{L}+1) = \lambda_0(\bar{L}+1)(2\bar{L}+1)$$
$$\tag{4-40}$$

At the beginning of nth time step

$$[\lambda_2]_n = [\lambda_1]_n(2[\bar{L}]_n + 1) = [\lambda_0]_n([\bar{L}]_n + 1)(2[\bar{L}]_n + 1) \tag{4-41}$$

When $\bar{L} \gg 1$ $\tag{4-42}$

$$\lambda_1 = \lambda_0\bar{L} \tag{4-43}$$

$$\lambda_2 = 2\bar{L}\lambda_1 = 2\bar{L}^2\lambda_0 \tag{4-44}$$

and when $R_P = 0$, i.e. chain transfer to monomer (R_{MM}), solvent (R_{SM}) and chain transfer agent (CTA) (R_{AM}) are negligible then $L' = L$ obtained from eqn.(4-34). The above simplifications are commonly used by many researchers but we have not used them for the derivation to keep all the complexity to the possible extent.

Before proceeding any further, some useful relationships are presented below. They are required for simplifying set of equations presented later. This will help in solving them in a better way.

$$K_t\lambda_0^2 = 2fK_dI = 2f\left(-\frac{1}{V_R}\frac{d(I.V_R)}{dt} \right) \tag{4-45}$$

$$K_t\lambda_0^2L = 2fK_dI.\left[\frac{K_{pr}M\lambda_0}{2fK_dI} \right] = K_{pr}M\lambda_0 = -\frac{1}{V_R}\frac{d(M.V_R)}{dt} \tag{4-46}$$

$$K_t\lambda_0^2L^2 = 2fK_dI.\left[\frac{K_{pr}M\lambda_0}{2fK_dI} \right]^2 = \frac{(K_{pr}M)^2}{K_t} = \frac{(K_{pr}M_0.V_{R0})^2}{K_t}.\frac{(1-x_M)^2}{V_R^2} \tag{4-47}$$

4.1.4.8 μ_0, Zeroth order moment of dead polymer chains chain length distribution (eqn.3-11)

$$\frac{1}{V_R}\frac{d(\mu_0.V_R)}{dt} = (K_{fm}M + K_{fs}S + K_{fa}A)\lambda_0 + \left(K_{td} + \frac{K_{tc}}{2}\right)\lambda_0^2 =$$

$$(R_M M + R_S S + R_A A)K_{pr}\lambda_0 + \left(1 - \frac{R_T}{2}\right)K_t\lambda_0^2 \qquad (3\text{-}11)$$

using eqn.(4-45), we have

$$\frac{1}{V_R}\frac{d(\mu_0.V_R)}{dt} = R_M K_{pr}M\lambda_0 + R_S K_{pr}S\lambda_0 + R_A K_{pr}A\lambda_0 + \left(1 - \frac{R_T}{2}\right).2fK_dI \qquad (4\text{-}48)$$

using eqn.(3-3), (3-4), (3-6) & (3-7) we have

$$\frac{1}{V_R}\frac{d(\mu_0.V_R)}{dt} =$$

$$R_M\left[-\frac{1}{V_R}\frac{d(M.V_R)}{dt}\right] + \left[-\frac{1}{V_R}\frac{d(S.V_R)}{dt}\right] + \left[-\frac{1}{V_R}\frac{d(A.V_R)}{dt}\right] + \left(1 - \frac{R_T}{2}\right).2f\left[-\frac{1}{V_R}\frac{d(I.V_R)}{dt}\right]$$

$$(4\text{-}49)$$

Multiplying this equation by V_R and integrating further, we have

$$\mu_0.V_R = -R_M.M.V_R - S.V_R - A.V_R - \left(1 - \frac{R_T}{2}\right).2f.I.V_R \qquad (4\text{-}50)$$

Applying limits from time step t_{n-1} to t_n, we have

$$\{[\mu_0.V_R]_n - [\mu_0.V_R]_{n-1}\} = -R_M.\{[M.V_R]_n - [M.V_R]_{n-1}\} - \{[S.V_R]_n - [S.V_R]_{n-1}\} -$$

$$\{[A.V_R]_n - [A.V_R]_{n-1}\} - \left(1 - \frac{R_T}{2}\right).2f.\{[I.V_R]_n - [I.V_R]_{n-1}\} \qquad (4\text{-}51)$$

rearranging, we have

$$[\mu_0]_n = [\mu_0]_{n-1}.\frac{[V_R]_{n-1}}{[V_R]_n} - R_M.\left\{[M]_n - [M]_{n-1}.\frac{[V_R]_{n-1}}{[V_R]_n}\right\} - \left\{[S]_n - [S]_{n-1}.\frac{[V_R]_{n-1}}{[V_R]_n}\right\} -$$

$$\left\{[A]_n - [A]_{n-1}.\frac{[V_R]_{n-1}}{[V_R]_n}\right\} - \left(1 - \frac{R_T}{2}\right).2f.\left\{[I]_n - [I]_{n-1}.\frac{[V_R]_{n-1}}{[V_R]_n}\right\} \qquad (4\text{-}52)$$

Modifying we have

$$[\mu_0]_n =$$

$$[\mu_0]_{n-1}.V_{corr} + R_M.\{[M]_{n-1}.V_{corr} - [M]_n\} + \{[S]_{n-1}.V_{corr} - [S]_n\} + \{[A]_{n-1}.V_{corr} -$$

$$[A]_n\} + \left(1 - \frac{R_T}{2}\right).2f.\{[I]_{n-1}.V_{corr} - [I]_n\} \qquad (4\text{-}53)$$

Applying limits of $t_{n-1} = t_0 = 0$ to $t_n = t$, we have

$$\mu_0 = R_M.\left\{\frac{M_0.V_R}{V_R} - M\right\} + \left\{\frac{S_0.V_{R0}}{V_R} - S\right\} + \left\{\frac{A_0.V_{R0}}{V_R} - A\right\} + \left(1 - \frac{R_T}{2}\right).2f.\left\{\frac{I_0.V_{R0}}{V_R} - I\right\}$$

$$(4\text{-}54)$$

4.1.4.9 μ_1, First order moment of dead polymer chains chain length distribution (eqn.3-12)

$$\frac{1}{V_R}\frac{d(\mu_1.V_R)}{dt} = \left(K_{fm}M + K_{fs}S + K_{fa}A\right)\lambda_1 + (K_{td} + K_{tc})\lambda_0\lambda_1 = (R_M M + R_S S + R_A A)K_{pr}\lambda_1 + K_t\lambda_0\lambda_1 \tag{3-12}$$

Using eqn.(4-38) we have

$$\frac{1}{V_R}\frac{d(\mu_1.V_R)}{dt} = (R_{MM} + R_{SM} + R_{AM})K_{pr}M\lambda_0\left[\frac{1+(1+R_{SA})L}{1+R_PL}\right] + K_t\lambda_0^2\left[\frac{1+(1+R_{SA})L}{1+R_PL}\right] \tag{4-55}$$

Using eqn.(3-31), (3-32) & eqn.(4-46) we have

$$\frac{1}{V_R}\frac{d(\mu_1.V_R)}{dt} = R_PL.K_t\lambda_0^2\left[\frac{1+(1+R_{SA})L}{1+R_PL}\right] + K_t\lambda_0^2\left[\frac{1+(1+R_{SA})L}{1+R_PL}\right] = K_t\lambda_0^2[(1+R_{SA})L+1] \tag{4-56}$$

$$\frac{1}{V_R}\frac{d(\mu_1.V_R)}{dt} = (1 + R_{SM} + R_{AM})K_t\lambda_0^2 L + K_t\lambda_0^2 = (1 + R_{SM} + R_{AM})K_{pr}M\lambda_0 + K_t\lambda_0^2 \tag{4-57}$$

Expanding we have

$$\frac{1}{V_R}\frac{d(\mu_1.V_R)}{dt} = K_{pr}M\lambda_0 + R_{SM}K_{pr}M\lambda_0 + R_{AM}K_{pr}M\lambda_0 + K_t\lambda_0^2 \tag{4-58}$$

Using eqn.(4-45) we have

$$\frac{1}{V_R}\frac{d(\mu_1.V_R)}{dt} = K_{pr}M\lambda_0 + R_S K_{pr}S\lambda_0 + R_A K_{pr}A\lambda_0 + 2fK_d I \tag{4-59}$$

Using eqn.(3-3), (3-4), (3-6) & (3-7), we have

$$\frac{1}{V_R}\frac{d(\mu_1.V_R)}{dt} = \left[-\frac{1}{V_R}\frac{d(M.V_R)}{dt}\right] + \left[-\frac{1}{V_R}\frac{d(S.V_R)}{dt}\right] + \left[-\frac{1}{V_R}\frac{d(A.V_R)}{dt}\right] + 2f\left[-\frac{1}{V_R}\frac{d(I.V_R)}{dt}\right] \tag{4-60}$$

Multiplying this equation by V_R, and integrating further, we have

$$\mu_1.V_R = -M.V_R - S.V_R - A.V_R - 2f.I.V_R \tag{4-61}$$

Applying limits from time step t_{n-1} to t_n, we have

$$\{[\mu_1.V_R]_n - [\mu_1.V_R]_{n-1}\} = -\{[M.V_R]_n - [M.V_R]_{n-1}\} - \{[S.V_R]_n - [S.V_R]_{n-1}\} - \{[A.V_R]_n - [A.V_R]_{n-1}\} - 2f.\{[I.V_R]_n - [I.V_R]_{n-1}\} \tag{4-62}$$

after rearranging, we have

$$[\mu_1]_n = [\mu_1]_{n-1}.\frac{[V_R]_{n-1}}{[V_R]_n} - \left\{[M]_n - [M]_{n-1}.\frac{[V_R]_{n-1}}{[V_R]_n}\right\} - \left\{[S]_n - [S]_{n-1}.\frac{[V_R]_{n-1}}{[V_R]_n}\right\} - \left\{[A]_n - [A]_{n-1}.\frac{[V_R]_{n-1}}{[V_R]_n}\right\} - 2f.\left\{[I]_n - [I]_{n-1}.\frac{[V_R]_{n-1}}{[V_R]_n}\right\} \tag{4-63}$$

Modifying we have

$$[\mu_1]_n = [\mu_1]_{n-1}.V_{corr} + \{[M]_{n-1}.V_{corr} - [M]_n\} + \{[S]_{n-1}.V_{corr} - [S]_n\} + \{[A]_{n-1}.V_{corr} - [A]_n\} + 2f.\{[I]_{n-1}.V_{corr} - [I]_n\} \tag{4-64}$$

Applying limits of $t_{n-1} = t_0 = 0$ to $t_n = t$, we have

$$\mu_1 = \left\{\frac{M_0.V_{R0}}{V_R} - M\right\} + \left\{\frac{S_0.V_{R0}}{V_R} - S\right\} + \left\{\frac{A_0.V_{R0}}{V_R} - A\right\} + 2f.\left\{\frac{I_0.V_{R0}}{V_R} - I\right\} \tag{4-65}$$

4.1.4.10 μ_2, Second order moment of dead polymer chains chain length distribution (eqn.3-13)

$$\frac{1}{V_R}\frac{d(\mu_2.V_R)}{dt} = (K_{fm}M + K_{fs}S + K_{fa}A)\lambda_2 + (K_{td} + K_{tc})\lambda_0\lambda_2 + K_{tc}\lambda_1^2$$

$$= (R_M M + R_S S + R_A A)K_{pr}\lambda_2 + K_t\lambda_0\lambda_2 + R_T K_t\lambda_1^2 \tag{3-13}$$

using eqn.(4-31), (4-34), (4-38) & (4-40) for $L, \overline{L}, \lambda_1\ and\ \lambda_2$ respectively and with little mathematics, rearrangement and manipulations, we have

$$\frac{1}{V_R}\frac{d(\mu_2.V_R)}{dt} = K_t\lambda_0^2\left\{((1 + R_{SA})L + 1)^2\left[\frac{2}{(R_PL+1)} + \frac{R_T}{(R_PL+1)^2}\right] - ((1 + R_{SA})L + 1)\right\} \tag{4-66}$$

Let $R_L = R_PL$ \hfill (4-67)

and $P = \frac{2}{(R_PL+1)} + \frac{R_T}{(R_PL+1)^2}$ \hfill (4-68)

where R_L and P are two new parameters. So we have

$$\frac{1}{V_R}\frac{d(\mu_2.V_R)}{dt} = K_t\lambda_0^2\left\{P((1 + R_{SA})L + 1)^2 - ((1 + R_{SA})L + 1)\right\} \tag{4-69}$$

$$\frac{1}{V_R}\frac{d(\mu_2.V_R)}{dt} = K_t\lambda_0^2\{P(1 + R_{SA})^2L^2 + (2P - 1)(1 + R_{SA})L + (P - 1)\} \tag{4-70}$$

Here we have assumed that R_P is a constant. As seen from the eqn.(3-31) R_P consists of R_{MM}, R_{SM} and R_{AM} where they are defined by eqn.(3-26) – (3-30) respectively.

We have assumed that $\frac{S}{M} = \frac{S_0}{M_0}$ and $\frac{A}{M} = \frac{A_0}{M_0}$ for the case when integration is done from 0 to t. Whereas, it can also be assumed constant as $\frac{S}{M} \approx \frac{S_{n-1}}{M_{n-1}}$ and $\frac{A}{M} \approx \frac{A_{n-1}}{M_{n-1}}$ for integration from t_{n-1} to t_n. That means, we will be calculating the value of these ratios based on their values at the beginning of the time interval and will keep it constant for the whole time interval. We have used this assumption of taking a fixed constant value of R_P for all individual time intervals for obtaining this integration. As we will see this does not introduce much error. If we use the strategy of evaluating the value of variables at $t = t_{n-1}$ rather than at $t = 0$, then this form of equations becomes more useful. Such form can easily be used for the semi-batch operation as well as for control purposes. This assumption does not introduce any serious error as can be seen during the validation process.

In line with above observations, three cases arise to obtain analytical solution from eqn.(4-70)

Case 1

$$R_L \ll 1 \Rightarrow R_L < 0.1 \Rightarrow R_L + 1 \rightarrow 1 \qquad (4\text{-}71)$$

Testing condition for computer code $R_L < 0.1$

This case thus represents the physical situation where transfer processes like chain transfer to monomer, solvent and CTA can be neglected completely. So the termination by combination step represented by R_T becomes the deciding factor.

After applying above condition, to eqn.(4-67) and (--4-68), we have

$$P \approx 2 + R_T \qquad (4\text{-}72)$$

$$\Rightarrow (2P - 1) = (3 + 2R_T) \qquad (4\text{-}73)$$

$$\Rightarrow (P - 1) = (1 + R_T) \qquad (4\text{-}74)$$

Replacing this in eqn.(4-70), we have

$$\frac{1}{V_R}\frac{d(\mu_2.V_R)}{dt} = K_t\lambda_0{}^2\{P(1 + R_{SA})^2L^2 + (2P - 1)(1 + R_{SA})L + (P - 1)\} \qquad (4\text{-}75)$$

Multiplying by V_R, and opening the brackets we have

$$\frac{d(\mu_2.V_R)}{dt} = P(1 + R_{SA})^2K_t\lambda_0{}^2L^2.V_R + (2P - 1)(1 + R_{SA})K_t\lambda_0{}^2L.V_R + (P - 1)K_t\lambda_0{}^2.V_R \qquad (4\text{-}76)$$

Let's evaluate the first integral on right hand side as we already know the integration of rest two integrals.

$$K_t\lambda_0^2. \ L^2.V_R = 2fK_dI \left(\frac{K_{pr}M\lambda_0}{2fK_dI}\right)^2.V_R = \frac{(K_{pr}M_0.V_{R0})^2}{K_t}\left[\frac{1-x_M}{V_R}\right]^2.V_R \qquad (4\text{-}77)$$

$$K_t\lambda_0^2. \ L^2.V_R = \frac{(K_{pr}M_0.V_{R0})^2}{K_t.V_R} \ exp\left[-B_0\left(1 - e^{\frac{-K_d.t}{2}}\right)\right]^2 \qquad (4\text{-}78)$$

$$K_t\lambda_0^2. \ L^2.V_R = \frac{(K_{pr}M_0.V_{R0})^2}{K_t.V_R} \ exp\left[-2B_0\left(1 - e^{\frac{-K_d.t}{2}}\right)\right] \qquad (4\text{-}79)$$

$$K_t\lambda_0^2. \ L^2.V_R = \frac{(K_{pr}M_0.V_{R0})^2}{K_t.V_R} \ exp(-2B_0) \ exp\left(2B_0e^{\frac{-K_d.t}{2}}\right) \qquad (4\text{-}80)$$

Applying transformation of variable $y = e^{\frac{-K_d.t}{2}} \Rightarrow \frac{-2}{K_d}\frac{dy}{y} = dt \qquad (4\text{-}81)$

And let $C_0 = 2B_0 \qquad (4\text{-}82)$

We have

118

$$\int exp\left(2B_0 e^{\frac{-K_d.t}{2}}\right) dt = -\int e^{C_0 y} \frac{2}{K_d} \frac{dy}{y} = \frac{2}{K_d} \int e^{C_0 y} \frac{dy}{y} \tag{4-83}$$

This could easily be integrated in many ways and will lead to infinite series solution. So we have adopted the way one which leads to converging series solution which could easily be implemented mathematically. This is done as follows. We expanded $e^{C_0 y}$ in infinite series form and then divided it by y. Then just integrated it point by point and wrote it down in terms of infinite series solution. This is as follows after applying the limits.

$$\frac{2}{K_d}\int_{y_n}^{y_{n-1}} e^{C_0 y} \frac{dy}{y} = \frac{2}{K_d}\left[\sum_{m=1}^{\infty}\left(\frac{(C_0 y_{n-1})^m}{m.m!} - \frac{(C_0 y_n)^m}{m.m!}\right) - ln\left(\frac{y_n}{y_{n-1}}\right)\right] \tag{4-84}$$

Now

$$C_0 y_{n-1} = 2B_0 = 2y_{n-1}\sqrt{\frac{8f[K_{pr}]^2 I_0}{K_d K_t}} = 2\sqrt{\frac{8f[K_{pr}]^2 [I]_{n-1}}{K_d K_t}}.\frac{[V_R]_{n-1}}{V_{R0}} = 2B_{n-1}.\sqrt{\frac{[V_R]_{n-1}}{V_{R0}}} = C_{n-1} \tag{4-85}$$

Similarly $C_0 y_n = C_0 y_{n-1}.\frac{y_n}{y_{n-1}} = C_{n-1}.\Delta y$ \hfill (4-86)

So we have

$$\int_{t_{n-1}}^{t_n} K_t \lambda_0^2 L^2.V_R dt = \frac{(K_{pr}M_0.V_{R0})^2}{K_t.[V_R]_{n-1}}e^{-C_0}\frac{2}{K_d}\left[\sum_{m=1}^{\infty}\left(\frac{(C_{n-1})^m}{m.m!} - \frac{(C_{n-1}.\Delta y)^m}{m.m!}\right) - ln(\Delta y)\right] \tag{4-87}$$

After multiplying and dividing the above equation by $[1 - x_M]_{n-1}^2.[V_R]_{n-1}$, and then rearranging after little manipulation, we have

$$\int_{t_{n-1}}^{t_n} K_t \lambda_0^2 L^2.V_R dt = \frac{2(K_{pr}[M]_{n-1})^2}{K_t K_d}e^{-C_{n-1}}.[V_R]_{n-1}\left[\sum_{m=1}^{\infty}\left[\left(\frac{(C_{n-1})^m}{m.m!} - \frac{(C_{n-1}.\Delta y)^m}{m.m!}\right)\right] - ln(\Delta y)\right] \tag{4-88}$$

$$\int_{t_{n-1}}^{t_n} K_t \lambda_0^2 L^2.V_R dt = D_{n-1}.[V_R]_{n-1}\left[\sum_{m=1}^{\infty}\left[\left(\frac{(C_{n-1})^m}{m.m!} - \frac{(C_{n-1}.\Delta y)^m}{m.m!}\right)\right] - ln(\Delta y)\right] \tag{4-89}$$

where:

$$D_{n-1} = \frac{2(K_{pr}[M]_{n-1})^2}{K_t K_d}e^{-C_{n-1}} \tag{4-90}$$

So complete integral of μ_2 after applying limits from time step t_{n-1} to t_n, is

$$\int_{[\mu_2.V_R]_{n-1}}^{[\mu_2.V_R]_n} d(\mu_2.V_R) =$$
$$\int_{t_{n-1}}^{t_n} P(1 + R_{SA})^2 K_t \lambda_0^2 L^2.V_R dt + \int_{t_{n-1}}^{t_n} (2P - 1)(1 + R_{SA})K_t \lambda_0^2 L.V_R dt + \int_{t_{n-1}}^{t_n} (P - 1)K_t \lambda_0^2.V_R dt \tag{4-91}$$

Substituting from the equations above we obtain

$$\{[\mu_2.V_R]_n - [\mu_2.V_R]_{n-1}\} =$$
$$P.(1 + R_{SA})^2.D_{n-1}.[V_R]_{n-1}\left[\sum_{m=1}^{\infty}\left[\left(\frac{(C_{n-1})^m}{m.m!} - \frac{(C_{n-1}.\Delta y)^m}{m.m!}\right)\right] - ln(\Delta y)\right] - (2P - 1).(1 + R_{SA}).\{[M.V_R]_n - [M.V_R]_{n-1}\} - (P - 1).2f.\{[I.V_R]_n - [I.V_R]_{n-1}\} \qquad (4\text{-}92)$$

after rearranging, we have

$$[\mu_2]_n = [\mu_2]_{n-1}.\frac{[V_R]_{n-1}}{[V_R]_n} + P.(1 + R_{SA})^2.D_{n-1}.\left[\sum_{m=1}^{\infty}\left[\left(\frac{(C_{n-1})^m}{m.m!} - \frac{(C_{n-1}.\Delta y)^m}{m.m!}\right)\right] - ln(\Delta y)\right].\frac{[V_R]_{n-1}}{[V_R]_n} - (2P - 1).(1 + R_{SA}).\left\{[M]_n - [M]_{n-1}.\frac{[V_R]_{n-1}}{[V_R]_n}\right\} - (P - 1).2f.\left\{[I]_n - [I]_{n-1}.\frac{[V_R]_{n-1}}{[V_R]_n}\right\} \qquad (4\text{-}93)$$

$$[\mu_2]_n = [\mu_2]_{n-1}.V_{corr} + P.(1 + R_{SA})^2.D_{n-1}.\left[\sum_{m=1}^{\infty}\left[\left(\frac{(C_{n-1})^m}{m.m!} - \frac{(C_{n-1}.\Delta y)^m}{m.m!}\right)\right] - ln(\Delta y)\right].V_{corr} + (2P - 1).(1 + R_{SA}).\{[M]_{n-1}.V_{corr} - [M]_n\} + (P - 1).2f.\{[I]_{n-1}.V_{corr} - [I]_n\} \qquad (4\text{-}94)$$

Applying limits of $t_{n-1} = t_0$ to $t_n = t$, we have,

$$\mu_2 = P.(1 + R_{SA})^2.D_0.\left[\sum_{m=1}^{\infty}\left(\frac{(C_0)^m}{m.m!} - \frac{(C_0 y)^m}{m.m!}\right) - ln(y)\right].\frac{V_{R0}}{V_R} + (2P - 1).(1 + R_{SA}).\left\{\frac{M_0.V_{R0}}{V_R} - M\right\} + (P - 1).2f.\left\{\frac{I_0.V_{R0}}{V_R} - I\right\} \qquad (4\text{-}95)$$

where

$$D_0 = \frac{2(K_{pr}M_0)^2}{K_t K_d}e^{-C_0} \qquad (4\text{-}96)$$

Case 2
$$R_L \approx O(1) \Rightarrow 10 > R_L \geq 0.1 \Rightarrow R_L + 1 = constant \qquad (4\text{-}97)$$

Test condition $10 > R_L \geq 0.1$

This is a situation where the effects of transfer processes like chain transfer to monomer, solvent and CTA is intermediate in nature and could no longer be neglected. It was found and will be shown in result section also that in this range, the variation in R_L is quite low. Thus, it can be assumed to be constant without introducing significant error. So, instead of replacing R_L with a fixed numerical value, R_L is retained as variable constant. Its value is evaluated at the beginning of each time interval and will remain constant for that time interval. So one can write

$$P = \frac{2}{(R_L + 1)} + \frac{R_T}{(R_L + 1)^2} \qquad (4\text{-}98)$$

where P is assumed to be constant. As can be seen, both chain transfer to monomer and termination by combination steps seem to play role in affecting the value of μ_2. So eqn.(4-70) would be

$$\frac{1}{V_R}\frac{d(\mu_2.V_R)}{dt} = K_t\lambda_0^2\{P(1 + R_{SA})^2L^2 + (2P - 1)(1 + R_{SA})L + (P - 1)\} \tag{4-99}$$

$$\frac{1}{V_R}\frac{d(\mu_2.V_R)}{dt} = P(1 + R_{SA})^2K_t\lambda_0^2L^2 + (2P - 1)(1 + R_{SA})K_t\lambda_0^2L + (P - 1)K_t\lambda_0^2 \tag{4-100}$$

This form of equation is similar to that of case1, where $P = 2 + R_T$, so its solution would also be similar to the one already obtained in case1 except that the coefficients would be different. So the integration is as follows.

$$[\mu_2]_n =$$

$$[\mu_2]_{n-1}.V_{corr} + P.(1 + R_{SA})^2.D_{n-1}.\left[\sum_{m=1}^{\infty}\left[(y_{n-1})^m\left(\frac{(C_{n-1})^m}{m.m!} - \frac{\left(C_{n-1}\cdot\frac{y_n}{y_{n-1}}\right)^m}{m.m!}\right)\right] - \right.$$

$$\left. ln\left(\frac{y_n}{y_{n-1}}\right)\right].V_{corr} + (2P - 1).(1 + R_{SA}).\{[M]_{n-1}.V_{corr} - [M]_n\} +$$

$$(P - 1).2f.\{[I]_{n-1}.V_{corr} - [I]_n\} \tag{4-101}$$

Applying limits of $t_{n-1} = t_0$ to $t_n = t$, we have

$$\mu_2 = P.(1 + R_{SA})^2.D_0.\left[\sum_{m=1}^{\infty}\left(\frac{(c)^m}{m.m!} - \frac{(cy)^m}{m.m!}\right) - ln(y)\right].\frac{V_{R0}}{V_R} + (2P - 1).(1 +$$

$$R_{SA}).\left\{\frac{M_0.V_{R0}}{V_R} - M\right\} + (P - 1).2f.\left\{\frac{I_0.V_{R0}}{V_R} - I\right\} \tag{4-102}$$

Case3.

$$R_L \gg 1 \Rightarrow R_L \geq 10 \Rightarrow R_L + 1 \rightarrow R_L \tag{4-103}$$

Test condition $R_L \geq 10$

The physical significance of this situation is that the transfer processes like transfers to monomer, solvent and CTA, are quite significant. Similar to case2, here also both termination and transfer steps play an important role in influencing μ_2. So it comes

$$P = \frac{2}{(R_L)} + \frac{R_T}{(R_L)^2} = \frac{2}{(R_PL)} + \frac{R_T}{(R_PL)^2} \tag{4-104}$$

Substituting this in the eqn.(4-70), we have

$$\frac{1}{V_R}\frac{d(\mu_2.V_R)}{dt} = K_t\lambda_0^2\{(1 + R_{SA})^2PL^2 + (1 + R_{SA})(2P - 1)L + (P - 1)\} \tag{4-105}$$

solving and rearranging in terms of decreasing power of L, we have

$$\frac{1}{V_R}\frac{d(\mu_2.V_R)}{dt} = \left(\frac{2}{R_P}(1+R_{SA})^2 - (1+R_{SA})\right)K_t\lambda_0{}^2 L + \left(\frac{R_T}{R_P^2}(1+R_{SA})^2 + \frac{4}{R_P}(1+R_{SA}) - \right.$$

$$1\Big)K_t\lambda_0{}^2 + \frac{2}{R_P}\left(\frac{R_T}{R_P}(1+R_{SA}) + 1\right)\frac{K_t\lambda_0{}^2}{L} + \frac{R_T}{R_P^2}\frac{K_t\lambda_0{}^2}{L^2} \tag{4-106}$$

We already know the integration of first two terms on right hand side. The third and fourth terms have negligible contribution to the overall solution as L is in denominator, which increases with time. So as the power of L increases, the contribution of that term decreases further. We have found with our solution and evaluation of these terms' integrals that their contribution to the overall solution is always negligible and can safely be neglected. Besides this, as we will see, their inclusion increases only the complexity of the solution without giving any benefit in improving the accuracy of the solution to any extent. So the integration of third and fourth term is given here for the sake of completion of analytical solution but does not have any practical use. Let's take the third and fourth term one by one for ease of finding solution.

$$\frac{2}{R_P}\left(\frac{R_T}{R_P}(1+R_{SA}) + 1\right)\frac{K_t\lambda_0{}^2}{L}.V_R = \frac{2}{R_P}\left(\frac{R_T}{R_P}(1+R_{SA}) + 1\right)\sqrt{K_t}\left[\frac{(2fK_dl)^{\frac{3}{2}}.V_R}{K_{pr}M_0.V_{R0}(1-x_M)}\right].V_R$$

$$= \frac{2}{R_P}\left(\frac{R_T}{R_P}(1+R_{SA}) + 1\right)\sqrt{K_t}\left[\frac{(2fK_dI_0)^{\frac{3}{2}}}{K_{pr}M_0e^{-B_0}}\right]\left[\frac{e^{\frac{-3K_d.t}{2}}}{exp\left(B_0e^{\frac{-K_d.t}{2}}\right)}\right].V_{R0}^{\frac{1}{2}}.V_R^{\frac{1}{2}}$$

$$= \frac{2}{R_P}\left(\frac{R_T}{R_P}(1+R_{SA}) + 1\right).V_R^2\sqrt{K_t}\left[\frac{(2fK_dI_0)^{\frac{3}{2}}}{K_{pr}M_0e^{-B_0}}\right]e^{\frac{-3K_dt}{2}}.exp\left(-B_0e^{\frac{-K_d.t}{2}}\right) \tag{4-107}$$

Let's use the same transformation of variable $y = e^{\frac{-K_d.t}{2}} \Rightarrow \frac{-2}{K_d}\frac{dy}{y} = dt$

So finally, we have

$$\frac{2}{R_P}\left(\frac{R_T}{R_P}(1+R_{SA}) + 1\right)\int_{t_{n-1}}^{t_n}\frac{K_t\lambda_0{}^2}{L}.V_R\,dt =$$

$$-\frac{4}{R_P}\left(\frac{R_T}{R_P}(1+R_{SA}) + 1\right).V_{R0}^{\frac{1}{2}}.[V_R]_{n-1}^{\frac{1}{2}}\left[\frac{\sqrt{K_t}}{K_d}\frac{(2fK_dI_0)^{\frac{3}{2}}}{K_{pr}M_0e^{-B_0}}\right]\int_{y_{n-1}}^{y_n}y^2e^{-B_0y}dy \tag{4-108}$$

Integrating it by parts we have

$$\frac{2}{R_P}\left(\frac{R_T}{R_P}(1+R_{SA}) + 1\right)\int_{t_{n-1}}^{t_n}\frac{K_t\lambda_0{}^2}{L}.V_R\,dt =$$

$$\frac{4}{R_P}\left(\frac{R_T}{R_P}(1+R_{SA}) + 1\right)\left[\frac{\sqrt{K_t}}{K_d}\frac{(2fK_dI_0)^{\frac{3}{2}}}{K_{pr}M_0e^{-B_0}}\right].V_{R0}^{\frac{1}{2}}.[V_R]_{n-1}^{\frac{1}{2}}\left[\sum_{m=1}^{3}\left(\frac{2![y_n]^{3-m}}{(3-m)!\,[B_0]^m}\right)e^{-B_0y_n} - \right.$$

$$\left.\sum_{m=1}^{3}\left(\frac{2![y_{n-1}]^{3-m}}{(3-m)!\,[B_0]^m}\right)e^{-B_0y_{n-1}}\right] \tag{4-109}$$

Multiplying and dividing above equation by $[1-x_M]_{n-1}.[y_{n-1}]^3.V_{R0}.[V_R]_{n-1}^{\frac{3}{2}}$, after rearranging and little manipulation, we have

$$\frac{2}{R_P}\left(\frac{R_T}{R_P}(1+R_{SA})+1\right)\int_{t_{n-1}}^{t_n}\frac{K_t\lambda_0{}^2}{L}.V_R\,dt =$$

$$J_{n-1}.[V_R]_{n-1}\left[\sum_{m=1}^{3}\left(\frac{2![y_{n-1}]^{-m}}{(3-m)!\,[B_0]^m}\right)\left(\left[\frac{y_n}{y_{n-1}}\right]^{3-m}.e^{-B_0y_{n-1}.\left(\frac{y_n}{y_{n-1}}-1\right)}-1\right)\right] \qquad (4\text{-}110)$$

$$\frac{2}{R_P}\left(\frac{R_T}{R_P}(1+R_{SA})+1\right)\int_{t_{n-1}}^{t_n}\frac{K_t\lambda_0{}^2}{L}.V_R\,dt =$$

$$J_{n-1}.[V_R]_{n-1}\left[\sum_{m=1}^{3}\left(\frac{2![y_{n-1}]^{-m}}{(3-m)!\,[B_0]^m}\right)\left([\Delta y]^{3-m}.e^{-B_{n-1}.(\Delta y-1)}-1\right)\right] \qquad (4\text{-}111)$$

where:

$$J_{n-1}=\frac{4}{R_P}\left(\frac{R_T}{R_P}(1+R_{SA})+1\right).\frac{\sqrt{K_t}}{K_d}\left[\frac{(2fK_d[I]_{n-1})^{\frac{3}{2}}}{K_{pr}[M]_{n-1}}\right] \qquad (4\text{-}112)$$

Similarly for the fourth part in eqn.(4-62) we have

$$\frac{R_T}{R_P^2}\frac{K_t\lambda_0{}^2}{L^2}.V_R = \frac{R_T}{R_P^2}\frac{K_t(2fK_dI)^2.[V_R]^2}{[K_{pr}M_0.V_{R0}(1-x_M)]^2}.V_R$$

$$=\frac{R_T}{R_P^2}\left[\frac{K_t(2fK_dI_0)^2}{(K_{pr}M_0)^2e^{-C_0}}\right]\frac{e^{-2K_d.t}}{exp\left(C_0e^{\frac{-K_d.t}{2}}\right)}.V_R = \frac{R_T}{R_P^2}\left[\frac{K_t(2fK_dI_0)^2}{(K_{pr}M_0)^2e^{-C_0}}\right]e^{-2K_d t}.exp\left(C_0e^{\frac{-K_d.t}{2}}\right).V_R$$

$$(4\text{-}113)$$

Let's use the same transformation of variable $y = e^{\frac{-K_d.t}{2}} \Rightarrow \frac{-2}{K_d}\frac{dy}{y} = dt$

So we have

$$\frac{R_T}{R_P^2}\int_{t_{n-1}}^{t_n}\frac{K_t\lambda_0{}^2}{L^2}.V_R\,dt = -\frac{2R_T}{R_P^2}\left[\frac{K_t(2fK_dI_0)^2}{K_d(K_{pr}M_0)^2}\right].[V_R]_{n-1}\int_{y_{n-1}}^{y_n}y^3e^{-C_0y}dy \qquad (4\text{-}114)$$

Integrating part by part we have

$$\frac{R_T}{R_P^2}\int_{t_{n-1}}^{t_n}\frac{K_t\lambda_0{}^2}{L^2}.V_R\,dt =$$

$$\frac{2R_T}{R_P^2}\left[\frac{K_t(2fK_dI_0)^2}{K_d(K_{pr}M_0)^2}\right].[V_R]_{n-1}\left[\sum_{m=1}^{4}\left(\frac{3![y_n]^{4-m}}{(4-n)!\,[C_0]^m}\right)e^{-C_0y_n}-\sum_{m=1}^{4}\left(\frac{3![y_{n-1}]^{4-m}}{(4-m)!\,[C_0]^m}\right)e^{-C_0y_{n-1}}\right]$$

$$(4\text{-}115)$$

Multiplying and dividing the equation by $[1-x_M]^2_{n-1}.[y_{n-1}]^4.[V_{R0}]^2.[V_R]^2_{n-1}$, after rearranging and little manipulation, we have

$$\frac{R_T}{R_P^2}\int_{t_{n-1}}^{t_n}\frac{K_t\lambda_0{}^2}{L^2}.V_R\,dt = Q_{n-1}.[V_R]_{n-1}\left[\sum_{m=1}^{4}\left(\frac{3![y_{n-1}]^{-m}}{(4-m)!\,[C_0]^m}\right)\left(\left[\frac{y_n}{y_{n-1}}\right]^{4-m}e^{-C_0y_{n-1}.\left(\frac{y_n}{y_{n-1}}-1\right)}-1\right)\right]$$

$$(4\text{-}116)$$

$$\frac{R_T}{R_P^2}\int_{t_{n-1}}^{t_n}\frac{K_t\lambda_0{}^2}{L^2}.V_R\,dt = Q_{n-1}.[V_R]_{n-1}\left[\sum_{m=1}^{4}\left(\frac{3![y_{n-1}]^{-m}}{(4-m)!\,[C_0]^m}\right)\left([\Delta y]^{4-m}e^{-C_{n-1}.(\Delta y-1)}-1\right)\right]$$

$$(4\text{-}117)$$

where:

$$Q_{n-1} = \frac{2R_T}{R_P^2} \cdot \frac{K_t}{K_d} \left[\frac{(2fK_dI_0)^2}{(K_{pr}[M]_n)^2} \right] \tag{4-118}$$

So finally we have complete solution of eqn.(4-70) in expanded form

$$\int_{[\mu_2.V_R]_{n-1}}^{[\mu_2.V_R]_n} d(\mu_2.V_R) = \int_{t_{n-1}}^{t_n} \left(\frac{2}{R_P}(1+R_{SA})^2 - (1+R_{SA}) \right) K_t\lambda_0{}^2 L.V_R dt \int_{t_{n-1}}^{t_n} \left(\frac{R_T}{R_P^2}(1+ R_{SA})^2 + \frac{4}{R_P}(1+R_{SA}) - 1 \right) K_t\lambda_0{}^2 . V_R dt + + \int_{t_{n-1}}^{t_n} \frac{2}{R_P} \left(\frac{R_T}{R_P}(1+R_{SA}) + 1 \right) \frac{K_t\lambda_0{}^2}{L} . V_R dt +$$

$$\int_{t_{n-1}}^{t_n} \frac{R_T}{R_P^2} \frac{K_t\lambda_0{}^2}{L^2} . V_R dt \tag{4-119}$$

Substituting from the equations above we obtain

$$\{[\mu_2.V_R]_n - [\mu_2.V_R]_{n-1}\} = - \left(\frac{2}{R_P}(1+R_{SA})^2 - (1+R_{SA}) \right) . \{[M.V_R]_n - [M.V_R]_{n-1}\} -$$

$$\left(\frac{R_T}{R_P^2}(1+R_{SA})^2 + \frac{4}{R_P}(1+R_{SA}) - 1 \right) . 2f . \{[I.V_R]_n - [I.V_R]_{n-1}\} +$$

$$J_{n-1} . [V_R]_{n-1} \left[\sum_{m=1}^3 \left(\frac{2![y_{n-1}]^{-m}}{(3-m)! [B_0]^m} \right) \left([\Delta y]^{3-m} . e^{-B_{n-1}.(\Delta y-1)} - 1 \right) \right] +$$

$$Q_{n-1} . [V_R]_{n-1} \left[\sum_{m=1}^4 \left(\frac{3![y_{n-1}]^{-m}}{(4-m)! [C_0]^m} \right) \left([\Delta y]^{4-m} e^{-C_{n-1}.(\Delta y-1)} - 1 \right) \right] \tag{4-120}$$

$$[\mu_2]_n = [\mu_2]_{n-1} . \frac{[V_R]_{n-1}}{[V_R]_n} - \left(\frac{2}{R_P}(1+R_{SA})^2 - (1+R_{SA}) \right) . \left\{ [M]_n - [M]_{n-1} . \frac{[V_R]_{n-1}}{[V_R]_n} \right\} -$$

$$\left(\frac{R_T}{R_P^2}(1+R_{SA})^2 + \frac{4}{R_P}(1+R_{SA}) - 1 \right) . 2f . \left\{ [I]_n - [I]_{n-1} . \frac{[V_R]_{n-1}}{[V_R]_n} \right\} +$$

$$J_{n-1} . \frac{[V_R]_{n-1}}{[V_R]_n} \left[\sum_{m=1}^3 \left(\frac{2![y_{n-1}]^{-m}}{(3-m)! [B_0]^m} \right) \left([\Delta y]^{3-m} . e^{-B_{n-1}.(\Delta y-1)} - 1 \right) \right] +$$

$$Q_{n-1} . \frac{[V_R]_{n-1}}{[V_R]_n} \left[\sum_{m=1}^4 \left(\frac{3![y_{n-1}]^{-m}}{(4-m)! [C_0]^m} \right) \left([\Delta y]^{4-m} e^{-C_{n-1}(\Delta y-1)} - 1 \right) \right] \tag{4-121}$$

$$[\mu_2]_n = [\mu_2]_{n-1} . V_{corr} + \left(\frac{2}{R_P}(1+R_{SA})^2 - (1+R_{SA}) \right) . \{[M]_{n-1} . V_{corr} - [M]_n\} +$$

$$\left(\frac{R_T}{R_P^2}(1+R_{SA})^2 + \frac{4}{R_P}(1+R_{SA}) - 1 \right) . 2f . \{[I]_{n-1} . V_{corr} - [I]_n\} +$$

$$J_{n-1} . V_{corr} \left[\sum_{m=1}^3 \left(\frac{2![y_{n-1}]^{-m}}{(3-m)! [B_0]^m} \right) \left([\Delta y]^{3-m} . e^{-B_{n-1}.(\Delta y-1)} - 1 \right) \right] +$$

$$Q_{n-1} . V_{corr} \left[\sum_{m=1}^4 \left(\frac{3![y_{n-1}]^{-m}}{(4-m)! [C_0]^m} \right) \left([\Delta y]^{4-m} e^{-C_{n-1}(\Delta y-1)} - 1 \right) \right] \tag{4-122}$$

Neglecting last two parts for the aforementioned reasons, we get

$$[\mu_2]_n = [\mu_2]_{n-1} . V_{corr} + \left(\frac{2}{R_P}(1+R_{SA})^2 - (1+R_{SA}) \right) . \{[M]_{n-1} . V_{corr} - [M]_n\} +$$

$$\left(\frac{R_T}{R_P^2}(1+R_{SA})^2 + \frac{4}{R_P}(1+R_{SA}) - 1 \right) . 2f . \{[I]_{n-1} . V_{corr} - [I]_n\} \tag{4-123}$$

Applying limits of $t_{n-1} = t_0$ to $t_n = t$, we have

$$\mu_2 = \left(\frac{2}{R_P}(1 + R_{SA})^2 - (1 + R_{SA})\right).\left\{\frac{M_0.V_{R0}}{V_R} - M\right\} + \left(\frac{R_T}{R_P^2}(1 + R_{SA})^2 + \frac{4}{R_P}(1 + R_{SA}) - 1\right).2f.\left\{\frac{I_0.V_{R0}}{V_R} - I\right\} \tag{4-124}$$

This clearly shows that the μ_2 depends only on initiator and monomer concentration when $R_L \gg 1$, i.e. when chain transfer processes are quite significant.

4.1.4.11 T, Energy balance (eqn.3-14)

$$\rho.Cp.V_R\frac{dT}{dt} = (-\Delta H_P)K_pM\lambda_0V_R - UA_H(T - T_{bath}) \tag{3-14}$$

We have assumed Cp to be constant here which is quite practical assumption in most cases. Rearranging this equation for T, we have

$$\rho.Cp.V_R\frac{dT}{dt} - UA_H(T - T_{bath}) = (-\Delta H_P)K_pM\lambda_0V_R \tag{4-125}$$

Dividing it by $\rho.Cp.V_R$, we have

$$\frac{dT}{dt} - \frac{UA_H}{\rho.Cp.V_R}(T - T_{bath}) = \frac{(-\Delta H_P)}{\rho.Cp.V_R}K_pM\lambda_0V_R \tag{4-126}$$

here $\rho.V_R = M_{mix}$ will remain constant by conservation of mass.

$$\text{Let } K1 = \frac{UA_H}{\rho.Cp.V_R}, \tag{4-127}$$

$$K2 = \frac{(-\Delta H_P)}{\rho.Cp.V_R}, \tag{4-128}$$

and applying the transformation of variable $T' = T - T_{bath}$, $\qquad$ (4-129)

we have

$$\frac{dT'}{dt} - K1.T' = K2.K_pM\lambda_0V_R = K2.(1 - R_M)K_{pr}M\lambda_0V_R \tag{4-130}$$

This is a linear differential equation in terms of T', provided that right hand side variables are no strong function of temperature. So we have

$$\frac{d}{dt}\left(e^{(-K1.t)}\,T'\right) = e^{(-K1.t)}K2.(1 - R_M)K_{pr}M\lambda_0V_R \tag{4-131}$$

Integrating we have

$$\int d\left(e^{(-K1.t)}\,T'\right) = \int e^{(-K1.t)}K2.(1 - R_M)K_{pr}M\lambda_0V_R.dt \tag{4-132}$$

$$T' = e^{(K1.t)}\int e^{(-K1.t)}K2.(1 - R_M)K_{pr}M\lambda_0V_R.dt \tag{4-133}$$

The right hand equation seems to be integrable. In fact, Venkateshwaran et al.[9] have integrated it in their paper and publish the results without much success. From our point of

view, this should not be integrable. One of the main reasons is that to integrate right hand side, one has to assume that the explicit and implicit kinetic rate coefficients are constant with respect to change in temperature. And the problem is that it is the temperature only that we are integrating on left hand side. So which temperature the kinetic rate coefficient will correspond to during integration? To keep this effect of temperature on kinetic rate coefficients, one needs to keep time step low so that kinetic rate coefficients can be assumed nearly constant for the temperature change. This will make the problem stiff and thus we can say that temperature equation is the source of stiffness for the above mentioned reason in this system. The detail of the cause of this stiffness is discussed in Discussion section.

4.1.5 Summary for time step format
Initiator consumption

$$[I]_n = [I]_{n-1} \cdot \frac{[V_R]_{n-1}}{[V_R]_n} \cdot e^{-K_d \cdot (t_n - t_{n-1})} = [I]_{n-1} \cdot V_{corr} \cdot [\Delta y]^2 \tag{4-8}$$

Let $y_n = e^{\frac{-K_d \cdot t_n}{2}}$ $\tag{4-10}$

and $\frac{y_n}{y_{n-1}} = e^{\frac{-K_d \cdot (t_n - t_{n-1})}{2}} = e^{\frac{-K_d \cdot \Delta t}{2}} = \Delta y$, where $\Delta t = (t_n - t_{n-1})$ $\tag{4-7}$

$$V_{corr} = \frac{[V_R]_{n-1}}{[V_R]_n} \tag{4-4}$$

Monomer conversion

$$[x_M]_n = 1 - [1 - x_M]_{n-1} \cdot exp[-B_{n-1} \cdot (1 - \Delta y)] \tag{4-18}$$

where $B_{n-1} = \sqrt{\frac{8f[K_{pr}]^2 I_{n-1}}{K_d K_t}}$, $\tag{4-17}$

Monomer consumption

$$[M]_n = [M]_{n-1} \cdot \frac{[1 - x_M]_n}{[1 - x_M]_{n-1}} \cdot V_{corr} = [M]_{n-1} \cdot exp[-B_{n-1} \cdot (1 - \Delta y)] \cdot V_{corr} \tag{4-22}$$

Transfer to Solvent

$$[S]_n = [S]_{n-1} \cdot exp[-R_S \cdot B_{n-1} \cdot (1 - \Delta y)] \cdot V_{corr} \tag{4-25}$$

Transfer to CTA

$$[A]_n = [A]_{n-1} \cdot exp[-R_A \cdot B_{n-1} \cdot (1 - \Delta y)] \cdot V_{corr} \tag{4-28}$$

Zeroth order moment of live polymer chains (QSSA)

$$[\lambda_0]_n = \sqrt{\frac{2fK_d[I]_n}{K_t}} \tag{4-37}$$

First order moment of live polymer chains (QSSA)

$$[\lambda_1]_n = [\lambda_0]_n([\bar{L}]_n + 1) \tag{4-39}$$

Second order moment of live polymer chains (QSSA)

$$[\lambda_2]_n = [\lambda_1]_n(2[\bar{L}]_n + 1) = [\lambda_0]_n([\bar{L}]_n + 1)(2[\bar{L}]_n + 1) \tag{4-41}$$

Zeroth order moment of dead polymer chains

$$[\mu_0]_n = [\mu_0]_{n-1}.V_{corr} + R_M.\{[M]_{n-1}.V_{corr}-[M]_n\} + \{[S]_{n-1}.V_{corr} - [S]_n\} + \{[A]_{n-1}.V_{corr} - [A]_n\} + \left(1 - \frac{R_T}{2}\right).2f.\{[I]_{n-1}.V_{corr}-[I]_n\} \tag{4-53}$$

First order moment of dead polymer chains

$$[\mu_1]_n = [\mu_1]_{n-1}.V_{corr} + \{[M]_{n-1}.V_{corr}-[M]_n\} + \{[S]_{n-1}.V_{corr} - [S]_n\} + \{[A]_{n-1}.V_{corr} - [A]_n\} + 2f.\{[I]_{n-1}.V_{corr}-[I]_n\} \tag{4-64}$$

Second order moment of dead polymer chains

Case1

$$R_L \ll 1 \Rightarrow R_L < 0.1 \Rightarrow \ R_L + 1 \ \rightarrow 1 \tag{4-71}$$

$$P \approx 2 + R_T \tag{4-72}$$

$$[\mu_2]_n = [\mu_2]_{n-1}.V_{corr} + P.(1 + R_{SA})^2.D_{n-1}.\left[\sum_{m=1}^{\infty}\left[\left(\frac{(C_{n-1})^m}{m.m!} - \frac{(C_{n-1}.\Delta y)^m}{m.m!}\right)\right] - ln(\Delta y)\right].V_{corr} + (2P - 1).(1 + R_{SA}).\{[M]_{n-1}.V_{corr}-[M]_n\} + (P - 1).2f.\{[I]_{n-1}.V_{corr}-[I]_n\} \tag{4-94}$$

$$\text{where } D_{n-1} = \frac{2\left(K_{pr}[M]_{n-1}\right)^2}{K_t K_d}e^{-C_{n-1}} \tag{4-90}$$

$$C_{n-1} = 2B_{n-1}.\sqrt{\frac{.[V_R]_{n-1}}{.[V_R]_0}} \tag{4-85}$$

Case2

$$R_L \approx O(1) \Rightarrow 10 > R_L \geq 0.1 \Rightarrow \ R_L + 1 = constant, \tag{4-97}$$

$$P = \frac{2}{(R_L+1)} + \frac{R_T}{(R_L+1)^2} \tag{4-98}$$

$$[\mu_2]_n = [\mu_2]_{n-1}.V_{corr} + P.(1 + R_{SA})^2.D_{n-1}.\left[\sum_{m=1}^{\infty}\left[\left(\frac{(C_{n-1})^m}{m.m!} - \frac{(C_{n-1}.\Delta y)^m}{m.m!}\right)\right] - ln(\Delta y)\right].V_{corr} + (2P - 1).(1 + R_{SA}).\{[M]_{n-1}.V_{corr}-[M]_n\} + (P - 1).2f.\{[I]_{n-1}.V_{corr}-[I]_n\} \tag{4-101}$$

Case3

$$R_L \gg 1 \Rightarrow R_L \geq 10 \Rightarrow \ R_L + 1 \rightarrow R_L \tag{4-103}$$

$$[\mu_2]_n = [\mu_2]_{n-1}.V_{corr} + \left(\frac{2}{R_P}(1 + R_{SA})^2 - (1 + R_{SA})\right).\{[M]_{n-1}.V_{corr}-[M]_n\} + \left(\frac{R_T}{R_P^2}(1 + R_{SA})^2 + \frac{4}{R_P}(1 + R_{SA}) - 1\right).2f.\{[I]_{n-1}.V_{corr}-[I]_n\} \tag{4-123}$$

$$[L]_n = \frac{K_{pr}[M]_n[\lambda_0]_n}{2fK_d[I]_n} \tag{4-32}$$

$$[\bar{L}]_n = [L]_n \cdot \left(\frac{1-R_M}{1+R_P[L]_n}\right) \tag{4-35}$$

$$R_L = R_P L \tag{4-67}$$

whereas all the remaining relevant equations can be found in section 3.2.3.

4.1.6 Summary for constant volume condition

$$I = I_0 e^{-K_d.t} = Iy^2 \tag{4-134}$$

$$x_I = \left(1 - \frac{I}{I_0}\right) = 1 - e^{-K_d.t} = 1 - y^2 \tag{4-135}$$

$$M = M_0\, exp\left[-B_0\left(1 - e^{\frac{-K_d.t}{2}}\right)\right] = M\, exp[-B_0(1 - y)] \tag{4-136}$$

$$x_M = \left(1 - \frac{M}{M_0}\right) = 1 - exp\left[-B_0\left(1 - e^{\frac{-K_d.t}{2}}\right)\right] = 1 - exp[-B_0(1 - y)] \tag{4-137}$$

$$S = S_0.\,exp[-R_S.B_0.(1 - y)] \tag{4-138}$$

$$A = A_0.\,exp[-R_A.B_0.(1 - y)] \tag{4-139}$$

$$\lambda_0 = \sqrt{\frac{2fK_dI_0}{(K_{tc} + K_{td})}} = \sqrt{\frac{2fK_dI_0}{K_t}} \tag{4-140}$$

$$\lambda_1 = \lambda_0(\bar{L} + 1) = \lambda_0\left[\frac{1 + L}{1 + R_PL}\right] \tag{4-141}$$

$$\lambda_2 = \lambda_1(2\bar{L} + 1) = \lambda_0(\bar{L} + 1)(2\bar{L} + 1) = \lambda_0\left\{\frac{1 + (3 - R_P)\,L + (2 - R_P)L^2}{[1 + R_PL]^2}\right\} \tag{4-142}$$

$$\mu_0 = R_M.\{M_0 - M\} + \{S_0 - S\} + \{A_0 - A\} + \left(1 - \frac{R_T}{2}\right).2f.\{I_0 - I\} \tag{4-143}$$

$$\mu_1 = \{M_0 - M\} + \{S_0 - S\} + \{A_0 - A\} + 2f.\{I_0 - I\} \tag{4-144}$$

Case1 - For $R_L < 0.1$, $P \approx 2 + R_T$

$$\mu_2 = P.(1 + R_{SA})^2.D_0.\left[\sum_{m=1}^{\infty}\left(\frac{(C_0)^m}{m.m!} - \frac{(C_0y)^m}{m.m!}\right) - ln(y)\right] + (2P - 1).(1 + R_{SA}).\{M_0 - M\} + (P - 1).2f.\{I_0 - I\} \tag{4-145}$$

Case2 - For $10 > R_L \geq 0.1$, $P = \frac{2}{(R_L + 1)} + \frac{R_T}{(R_L + 1)^2}$

$$\mu_2 = P.(1 + R_{SA})^2.D_0.\left[\sum_{m=1}^{\infty}\left(\frac{(C_0)^m}{m.m!} - \frac{(C_0y)^m}{m.m!}\right) - ln(y)\right] + (2P - 1).(1 + R_{SA}).\{M_0 - M\} + (P - 1).2f.\{I_0 - I\} \tag{4-146}$$

Case3 - For $R_L \geq 10$

$$\mu_2 = \left(\frac{2}{R_P}(1 + R_{SA})^2 - (1 + R_{SA})\right).\{M_0 - M\} + \left(\frac{R_T}{R_P^2}(1 + R_{SA})^2 + \frac{4}{R_P}(1 + R_{SA}) - 1\right).2f.\{I_0 - I\} \tag{4-147}$$

4.1.7 Methodology adopted

The details of mathematical sets FRP_Full and FRP_QSSA chosen in this study are given in section 3.2.4.

The analytical solution was obtained from FRP_QSSA for very simplistic and ideal case i.e. fully mixed, isothermal batch reactor. This removes a lot of complexities and non-linearity in this mathematical model which helped in obtaining the analytical solution. The solution is strictly valid till the gel effect sets-in, after which the assumptions for obtaining analytical solution are not valid. Third mathematical set called as Analytical constitutes equations as given in section 4.1.5.

All the variables were calculated at the beginning of each time step. Each variable calculated was stored in array form with length of array equal to number of time steps. For initiator and monomer, the values obtained in each time step were stored as such in the array. Whereas, for μ_0 & μ_1, the values obtained in each time step were added to the cumulative value of μ_0 & μ_1 obtained till the previous time-step. Thus the value of μ_0 & μ_1 stored at the end of each time step was cumulative value till that time step. For μ_2 also, the value calculated at the end of each time step was cumulative value till that time step. But to calculate the value of μ_2 in each time step, there was slightly different strategy because of the presence of three cases. μ_2 was evaluated simultaneously for all the three cases (as given by eqn.(4-71), eqn.(4-97), eqn.(4-103)) in each time step and was being added individually as if each one was the only case. Depending on the value of R_L, calculated at the end of each time step, μ_2 value belonging to appropriate case in that time step was chosen. It was then added to previous time step value as per eqn.(4-71), eqn.(4-97) or eqn.(4-103) to get the final value of μ_2. Thus the final value of μ_2 may differ from individual cases depending on the value of R_L, whose value may vary from one case to another during simulation. All the three cases of μ_2 along with final value of μ_2 are shown in separate figure in the result section to make this point more clear. Using this way, MW_n, MW_w and PDI as calculated from eqn.(3-16) to (3-18) respectively, thus represented cumulative values instead of instantaneous values till that time instead of value *in* that time-step.

This solution was validated under similar conditions against numerical solution of the FRP_Full and FRP_QSSA. Matlab R2008a was used for numerical integration and solving analytical solution and post-processing of the results. Since only isothermal condition is simulated, temperature equation was not required to be solved. As mentioned earlier and will also be presented in detail in Discussion section, the source of stiffness in this model without gel effect comes from temperature equation. So, only non-stiff solver was required for isothermal conditions. Therefore, inbuilt solver of Matlab R2008a - ode23 was used for both FRP_Full and FRP_QSSA.

The simulation results from all the three models, namely FRP_QSSA, FRP_Full and Analytical were simultaneously plotted on each graph. FRP_QSSA was represented by green line, FRP_Full by blue line and Analytical by red line. The experimental data was also plotted in the relevant graphs whenever available and were represented by round circles to signify

their discrete nature. Sometimes multiple experimental values for the same given time were found in the literature. So the whole data was plotted without any selection or averaging.

The analytical solution was validated first for isothermal, bulk polymerization with no transfer process case. The theoretical validation by predicting PDI for two different cases of C_T ratio was also done. Then the case of solution polymerization was taken up. After this, the three cases for μ_2 were taken up and had shown how good the analytical solution matches with numerical solution under those conditions. The kinetic and physical data used to simulate above conditions are related to MMA. But the variation in C_T and other parameters like solvent fraction and various transfer kinetic rate coefficients are varied in general manner. This helped to draw general results rather than specific to some monomer. This analytical solution was then finally validated by comparing the results for four monomer-polymer systems namely St/PS, MMA/PMMA, BuA/PBuA and VAc/PVAc. Two initiators AIBN and BPO with varying concentrations were also taken. Toluene was also used as solvent in relevant cases. The data for their various kinetic rate coefficients, physical properties etc. were taken from published literature[3,15-19] and is presented in Table 3-1 to Table 3.4. The other experimental data on MW_n, MW_w and PDI was also used whenever available.

4.1.8 Results

In Fig. 4.1-1, AS is confronted with numerical solution for the simplest case of negligible transfer process in bulk isothermal polymerization. As can be seen the AS matches excellently with numerical solution for all the variables.
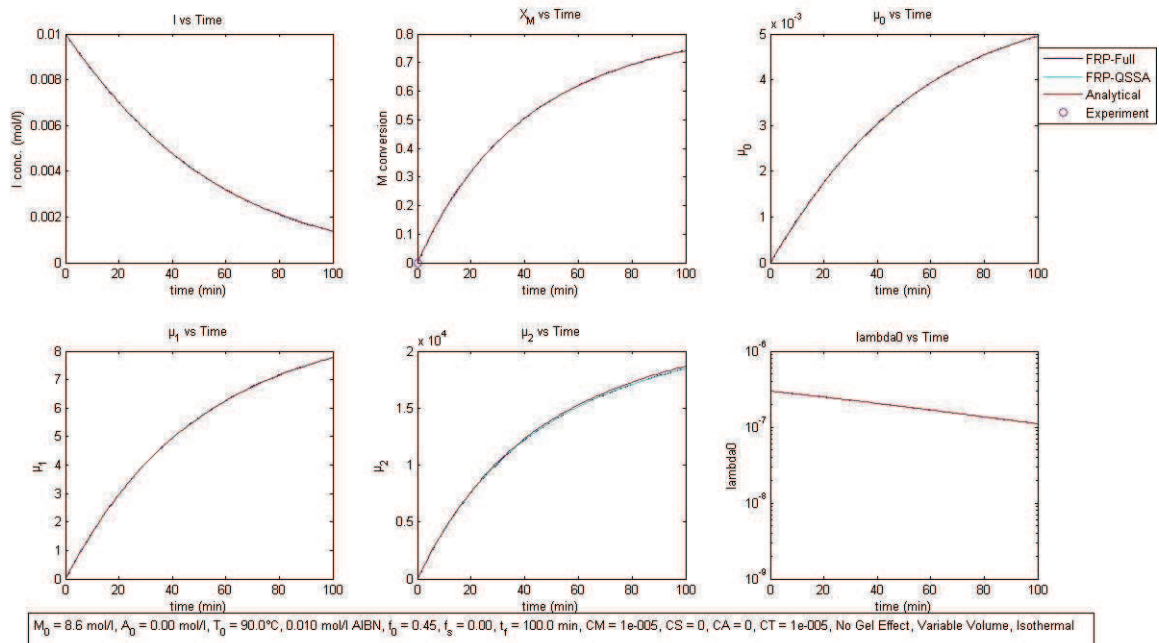
Fig. 4.1-1- Comparison between AS and numerical solution for general case of isothermal bulk polymerization and negligible transfer processes

The AS must also predict the theoretical results well to prove its validity. When $C_T \ll 1$ i.e. when K_{td} is much smaller than K_{tc}, the PDI should be 1.5. When the condition is reverse, then PDI should be 2. So C_T is taken to be equal to either 10^{-5} or 10^5 for simulating these two situations repectively. As can be seen in Fig. 4.1-2, the PDI is calculated as 1.5 for $C_T = 10^{-5}$. For $C_T = 10^5$, PDI is calculated to be 2 as shown in Fig. 4.1-3 which is same as predicted for the conditions mentioned above. Besides this, despite having similar conversion, decrease in MW_n and MW_w for later case compared to former can easily be observed. This is as per theoretical prediction.
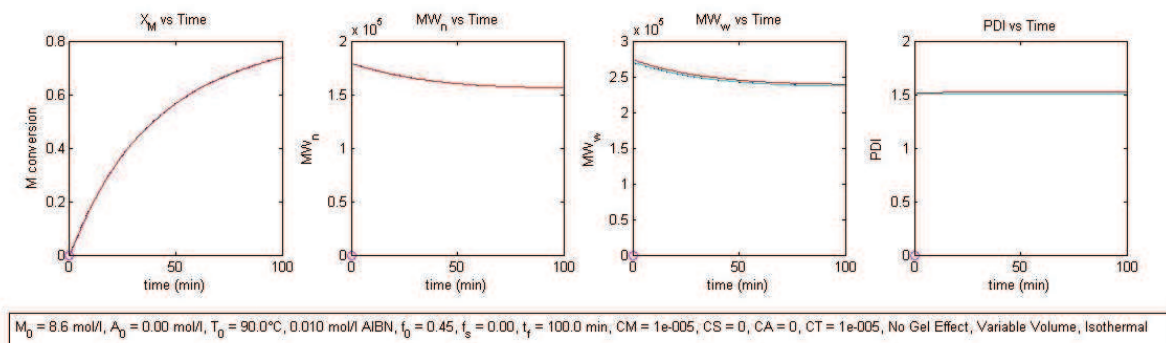
Fig. 4.1-2- PDI prediction for $C_T = 10^{-5}$ for general case of isothermal bulk polymerisation with negligible transfer processes.
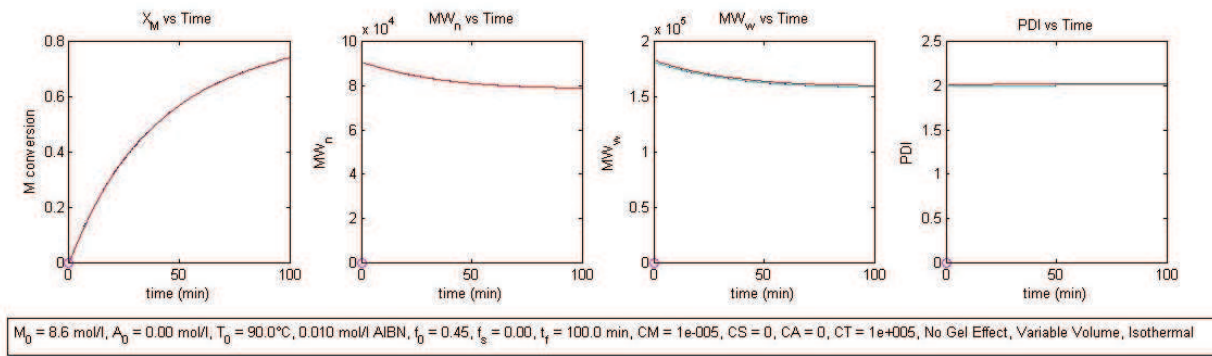
Fig. 4.1-3- *PDI* prediction for $C_T = 10^5$ for general case of isothermal bulk polymerisation with negligible transfer processes.
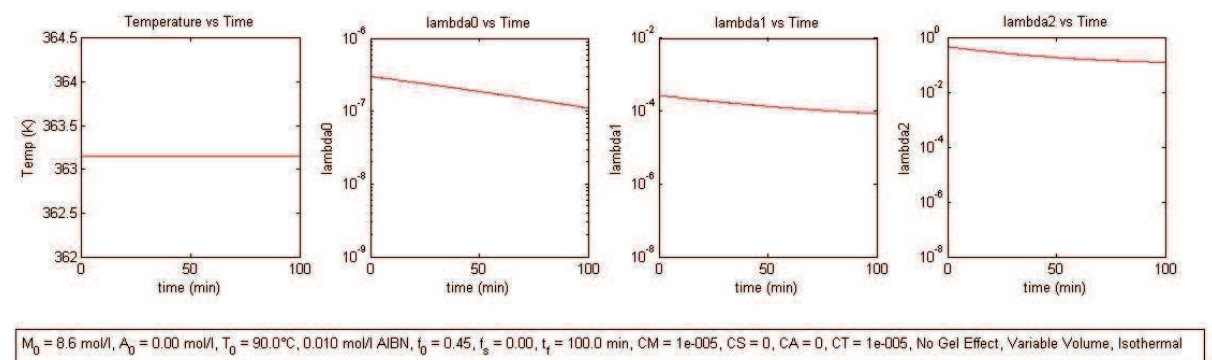
Fig. 4.1-4- Comparison of $\lambda_0, \lambda_1 and \lambda_2$ as calculated by FRP_Full, FRP_QSSA and AS

As can be seen in Fig. 4.1-4, the graphs for $\lambda_0, \lambda_1 and \lambda_2$ as calculated by FRP_Full, FRP_QSSA and AS matches exactly proving the assumption of QSSA under the given situation.

Now Fig. 4.1-5 shows the validation of AS against numerical solution for 30% solvent polymerization with negligible transfer processes. This validates the AS for solution polymerization condition. Again the matching is excellent with numerical solution.
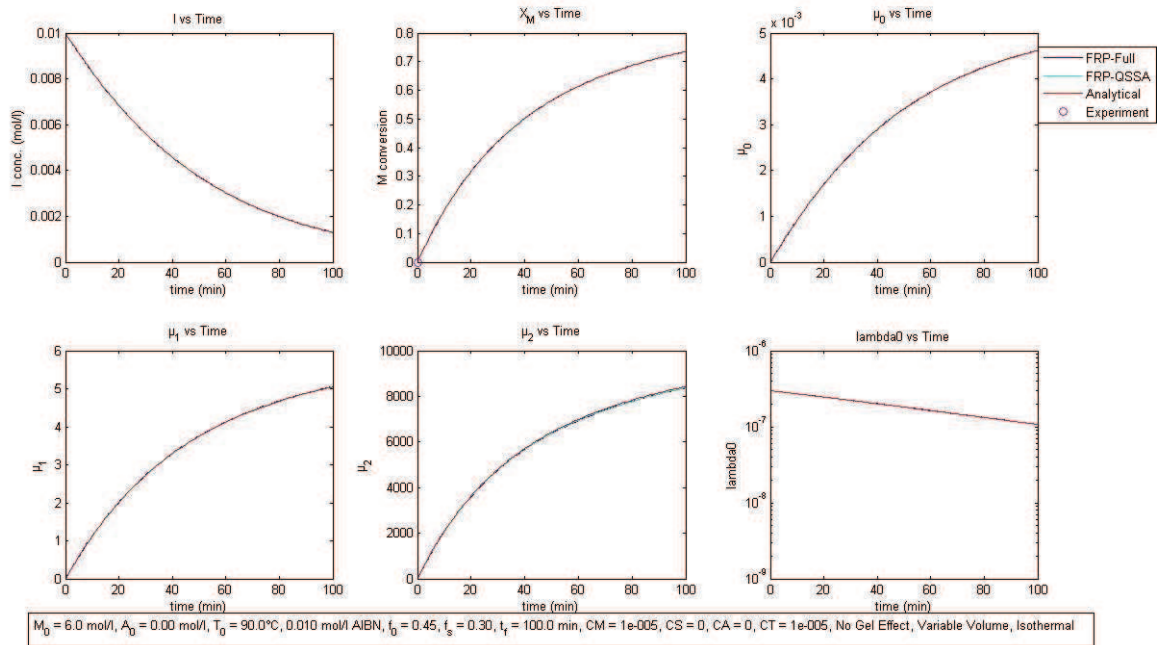
Fig. 4.1-5- AS is compared for general case of isothermal solution polymerization with negligible transfer processes.

Now, the 3 cases for μ_2 as obtained in AS, are shown in Fig. 4.1-6 to Fig. 4.1-8. Individual cases of AS are evaluated only for transfer to monomer. The results of individual cases are compared with numerical solution for more clarity. As can be seen, individual cases differ significantly from the numerical solution depending upon the value of R_L. Only the one which lies in the range of the R_L value used matches with the numerical solution and is selected for further calculation of MW_w and PDI. This clearly proves the importance of AS from practical point of view. This proves also why it is so difficult to design empirical or semi-theoretical formulation for predicting MW_w under various conditions since R_L can have very different values depending on operating conditions (e.g. polymerization time) and monomer-polymer system.

As can be seen for case2, the value of R_L is varying throughout the time of reaction but the variation is not much. This justifies the assumption of taking RL constant for this case. Besides this, for time step manner, R_L can be evaluated for each time step for increasing the accuracy of solution instead of choosing the fixed value obtained at $t = 0$.

It is also found that R_L increases by increasing C_M. As a result, μ_2 decreases when shifting from case1 to case2 and then to case3. It is noteworthy that PDI increases and tends to 2 despite C_T being quite less when transfer processes are significant. The latter may include just transfer to monomer as shown in Fig. 4.1-6 to Fig. 4.1-8 or may also include transfer to solvent (C_S) and transfer to chain transfer agent (CTA) (C_A) as shown in Fig. 4.1-9.

135
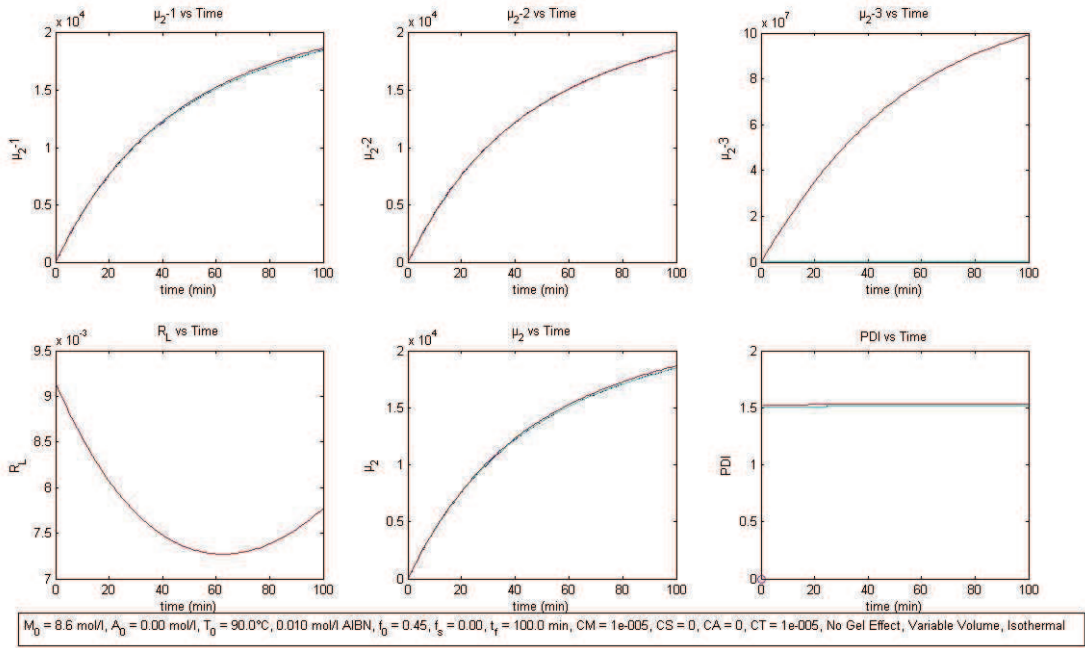
Fig. 4.1-6- Case1: $R_L < 0.1$, for general case of isothermal bulk polymerization with only transfer to monomer
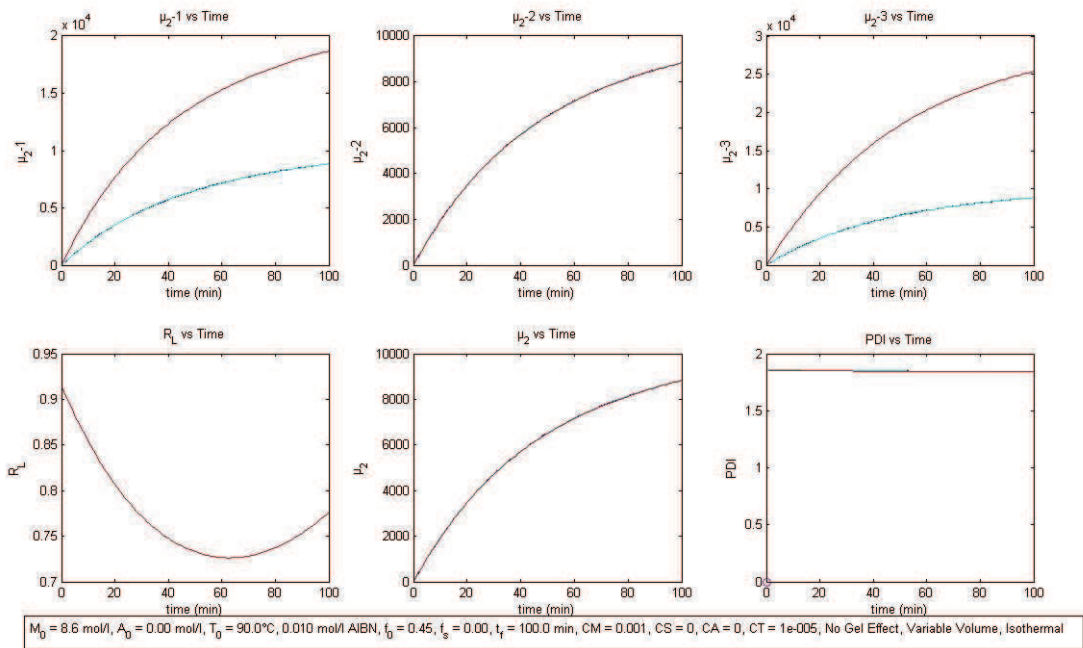
Fig. 4.1-7- Case2: $0.1 \leq R_L < 10$, for general case of isothermal bulk polymerization with only transfer to monomer
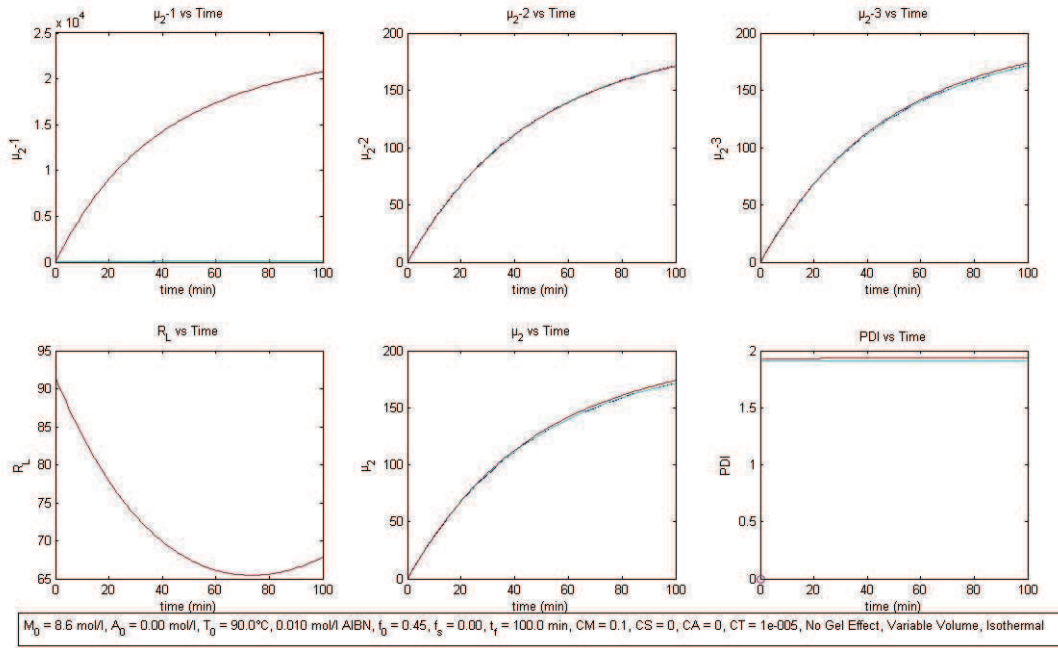
Fig. 4.1-8- Case3: $R_L \geq 10$, for general case of isothermal bulk polymerization with only transfer to monomer
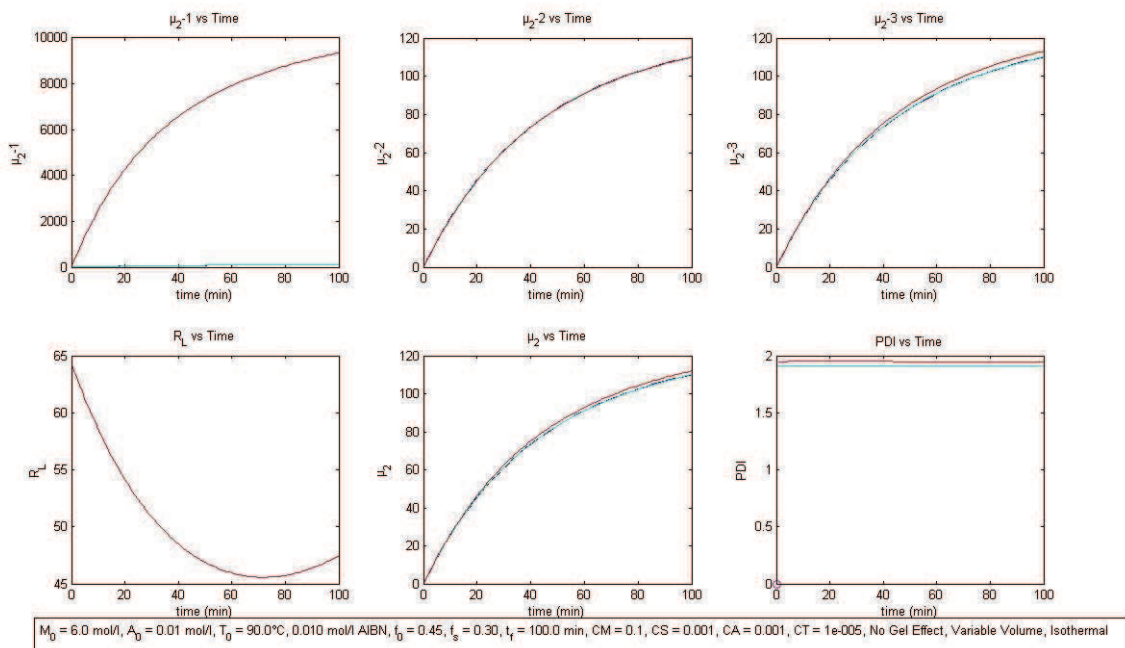
Fig. 4.1-9- Case3: $R_L \geq 10$, for general case of isothermal bulk polymerization with all transfer processes considered for the model i.e. C_M, C_S & C_A.

One can also observe the discrepancy between the results for μ_2 selected in Fig. 4.1-9. It shows the case2 matches well with numerical solution instead of case3 which was selected accordingly to our aforementioned criteria (eqn.(4-71, 4-97, 4-103)). This is due to the value of R_L. It was found in our study that case2 and case3 overlaps from $R_L = 10 \ to \ 50$ and case1 and case2 overlaps from $R_L = 0.1 \ to \ 0.05$. So we can only say that the ranges selected for R_L is good for general condition. But it can be chosen selectively for individual cases for

increasing the quality of results of predictions using AS. Besides, this discrepancy between the AS and numerical solution for case3 in Fig. 4.1-9 is also due to assumption taken for obtaining solution for case3. This also proves that the assumption is quite good and thus justifies itself. To improve the calculations for time step manner, just like R_L, R_{SA} can also be calculated at the beginning of each time step instead of taking constant value calculated at $t = 0$.

Now AS is to be confronted with experimental data. For this, 4 monomers (St, MMA, BuA and VAc) are considered. The validation is compared under various conditions of different temperatures, initiators, solvent fractions. Data compared are conversion with time but also MW_n, MW_w and PDI wherever data was available.
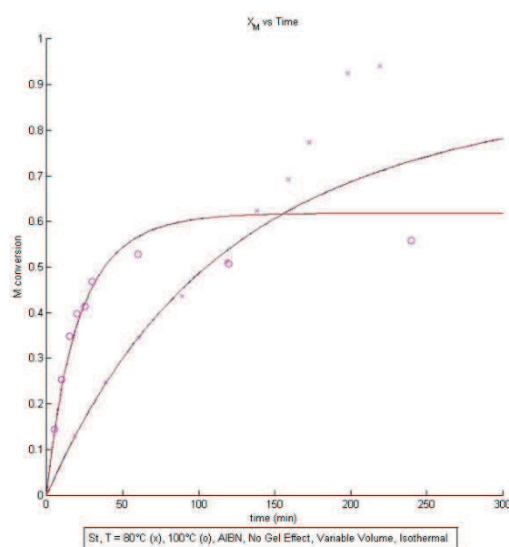
Fig. 4.1-10- Styrene[16], $T = 80°C, 0.5$ mol/l AIBN (x), $T = 100°C, 0.0337$ mol/l AIBN (o), $f_s = 0.0, f_0 = 0.45$

As can be seen in Fig. 4.1-10 and following, AS along with numerical solution matches quite well with experimental data for the condition before gel effect. In Fig. 4.1-10, for $T = 80°C$, it matches well till gel effect sets in but for $T = 100°C$, it matches throughout the range of conversion. This proves also the observation that with increase in temperature, gel effect shift to higher conversion and can be absent for higher temperature.
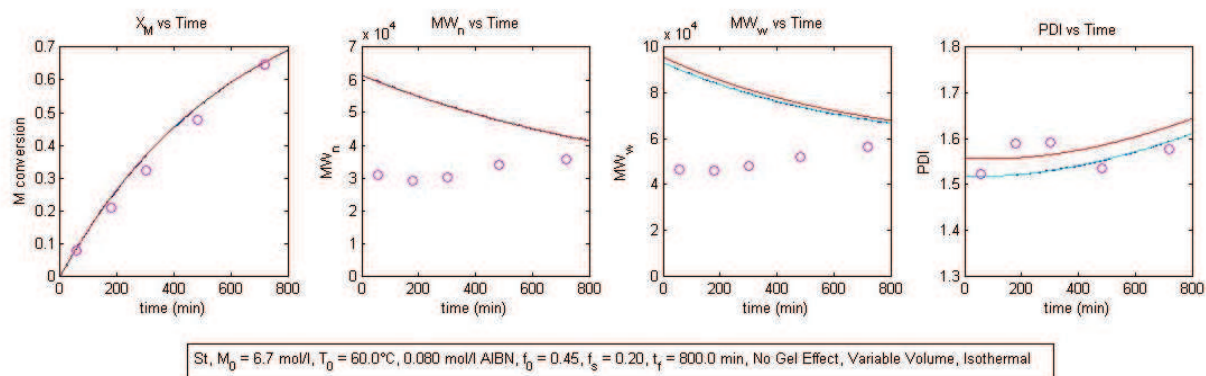
Fig. 4.1-11- St[16] data for solution polymerization at $T = 60°C$, $f_s = 0.20$

138
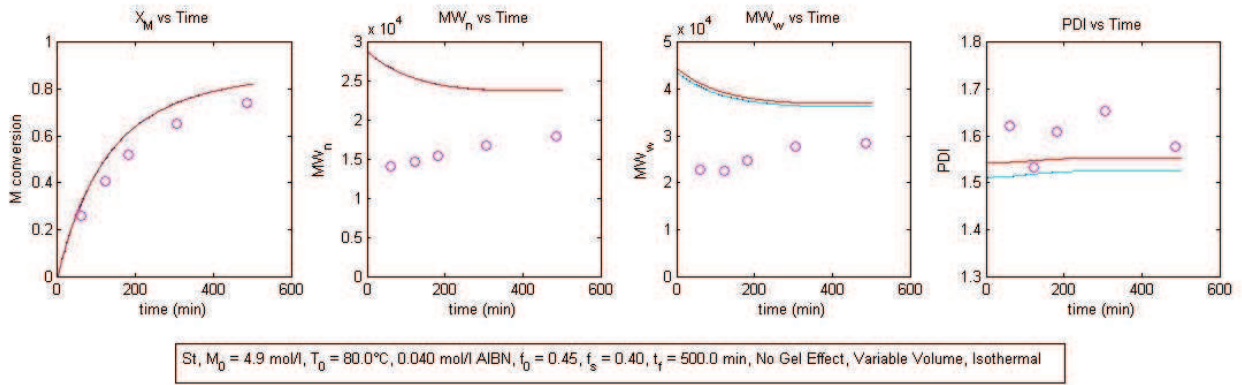
Fig. 4.1-12- St[16] data for solution polymerization at $T = 80°C, f_s = 0.40$

Fig. 4.1-11 and Fig. 4.1-12 shows the validation of AS with experimental data for solution polymerization for two different temperatures as well as two different solvent fractions. As can be seen, the results match well with conversion and PDI but exhibit some discrepancies when MW_n and MW_w are compared with experimental data. However, this is also the same for the numerical solution as well and it still matches well with AS. The discrepancy observed for PDI results is probably due to small numerical error which occurs at the beginning of the reaction as the values of μ_0, μ_1 & μ_2 are quite small. Even small changes in these values in denominator of PDI expression (eqn.(3-18)) can lead to large discrepancies. But this numerical error gets stabilized with conversion, however the offset still remains.

Similar results and conclusions can be observed for MMA in Fig. 4.1-13 - Fig. 4.1-15, where temperature varies from $T = 50°C$ $(a), 70°C$ (b) and $90°C$ (c). Again the match is good till the gel effect sets in. Here the match with MW_n, MW_w and PDI is better compared to the case of styrene. One can also observe that the conversion at which gel effect occurs shifts to higher value with temperature as mentioned above.
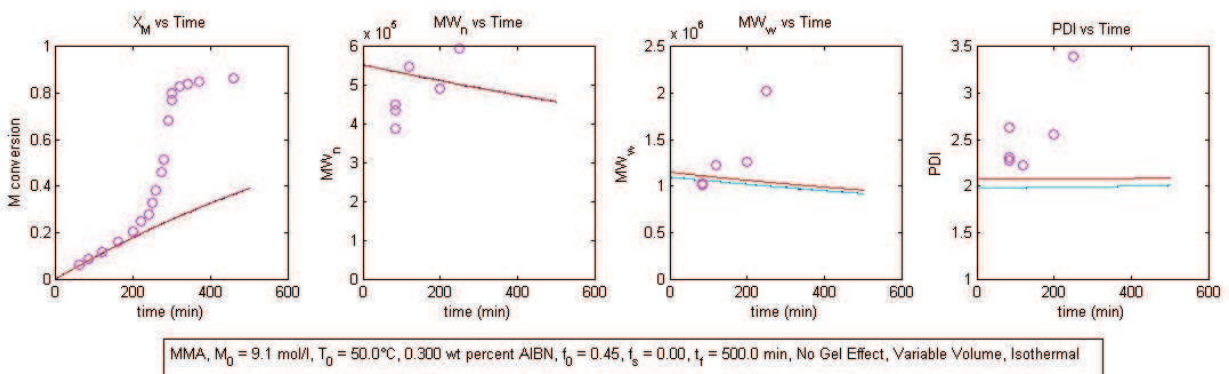
Fig. 4.1-13- MMA[17] for isothermal bulk polymerization at $T = 50°C$
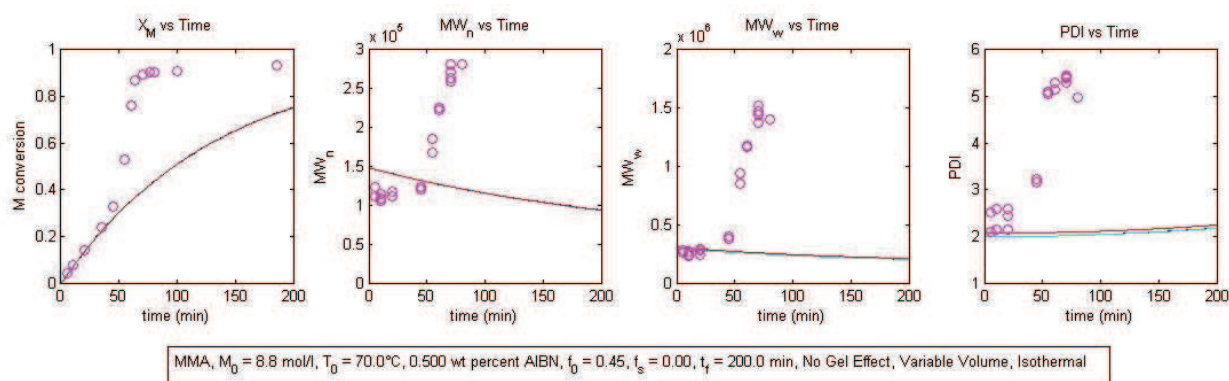
Fig. 4.1-14- MMA[17] for isothermal bulk polymerization at $T = 70°C$
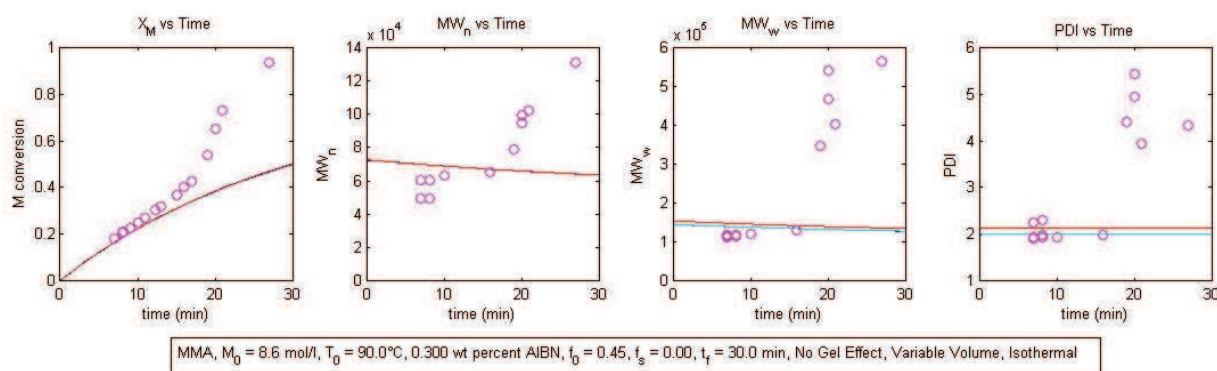
Fig. 4.1-15- MMA[17] for isothermal bulk polymerization at $T = 90°C$

Now we study the cases of BuA and VAc for which the reaction is much faster. Experimental data are available for solution polymerization with different solvent volume fractions. Fig. 4.1-16 & Fig. 4.1-17 consider two different temperatures with two different solvent fractions and common initiator AIBN; while Fig. 4.1-18 addresses effect of another initiator (BPO) to demonstrate the versatility and generality of AS.

One can also observe that initiator efficiency exhibits quite low values and is a strong function of the solvent fraction. Similar observation has been reported by Verros and Achilias[29]. This could possibly due to large cage effect experienced by initiator at such a large solvent presence. This can change its efficiency even by small variation in solvent fraction. So, constant initiator efficiency could not be taken for all simulations as against the previous cases of St/PS and MMA/PMMA and should be adapted to each operating conditions. Therefore, the value of initiator efficiency is taken by matching the simulation results with experimental conversion data. The results match quite well for PDI although the prediction for MW_n is quite poor. The reason for this anomaly is unknown yet to us.
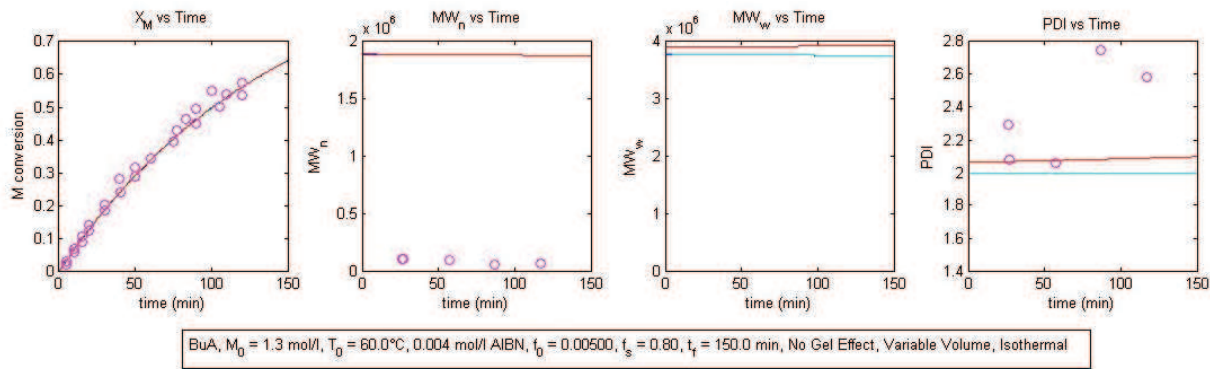
Fig. 4.1-16- BuA[18] for isothermal solution polymerization at $T = 60°C$, AIBN
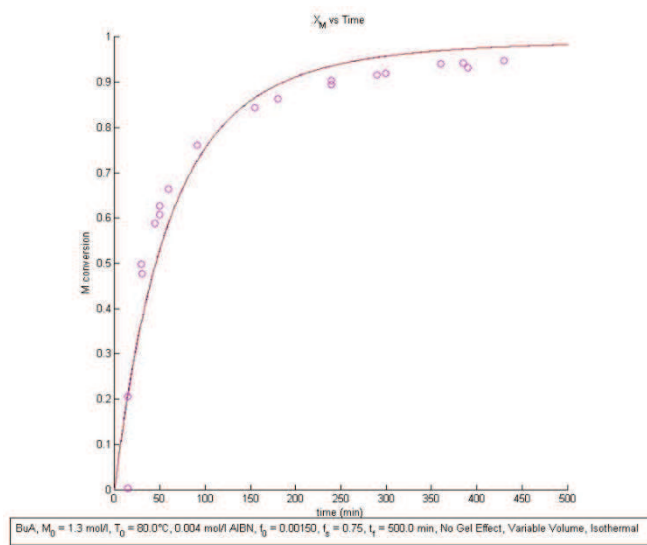
Fig. 4.1-17- BuA[18] for isothermal solution polymerization at $T = 80°C$, AIBN
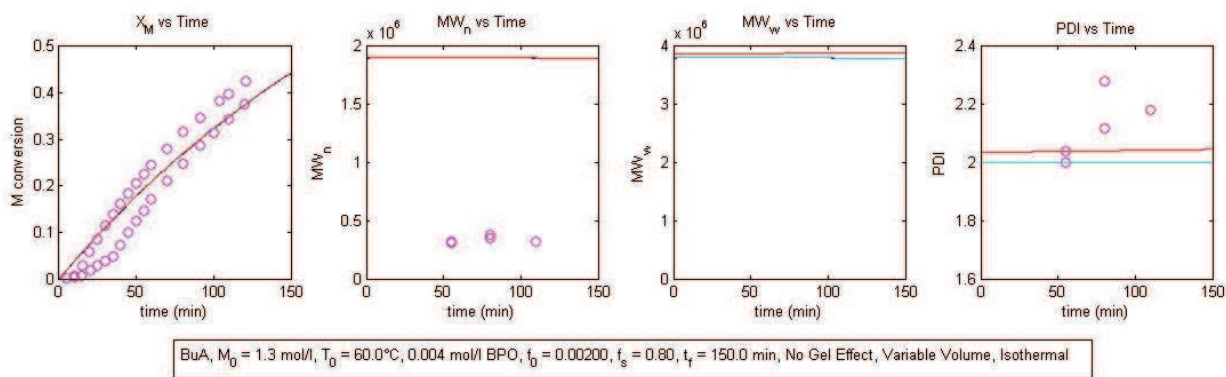
Fig. 4.1-18- BuA[18] for isothermal solution polymerization at $T = 60°C$, BPO
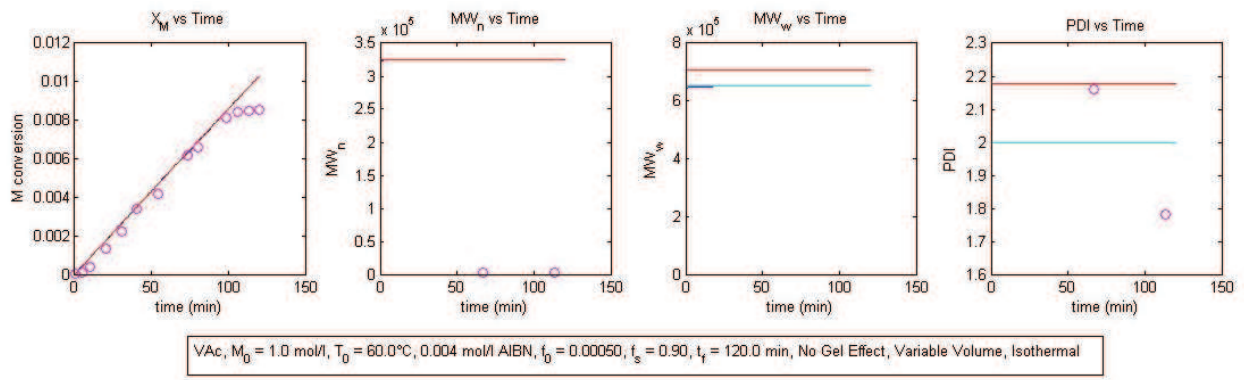
Fig. 4.1-19- VAc[19] for isothermal solution polymerization at $T = 60°C$, AIBN
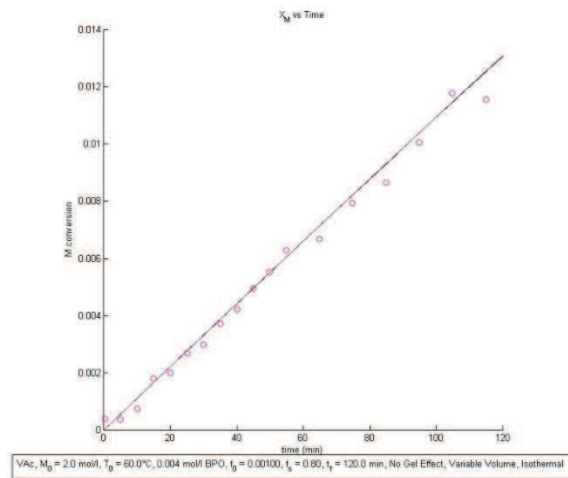
Fig. 4.1-20- VAc[19] for isothermal solution polymerization at $T = 60°C$, BPO

Similar results are visible for VAc through Fig. 4.1-19 & Fig. 4.1-20 and same conclusions can be drawn. The authors[19] have stated the very strong influence of solvent (toluene) on polymerization rate of reaction as main reason for low conversion for VAc.

4.1.9 Discussion

From the above validation against numerical solution and confrontation with experimental data, many important comments can be made for the developed analytical solution.

μ_2 is found to be function of both R_L and R_T. No single solution exists, but rather three cases arise based on value of R_L. Recalling eqn.(4-67)

$R_L = R_P L$, where R_P is given by eqn.(3-31)

$$R_P = R_{MM} + R_{SM} + R_{AM} = \frac{C_M}{1+C_M} + \frac{C_S}{1+C_M}\frac{S}{M} + \frac{C_A}{1+C_M}\frac{A}{M} = \frac{1}{1+C_M}\left[C_M + C_S\frac{S}{M} + C_A\frac{A}{M}\right]$$

and L by eqn.(4-31)

$$L = \frac{(K_p + K_{fm})M\lambda_0}{2fK_dI} = \frac{K_{pr}M\lambda_0}{2fK_dI}$$

Soh et al.[25] have presented the four phases of vinyl polymerization of monomer soluble in its own polymer. The first phase represented the conventional kinetics, i.e. the area of this work. Second phase represented the gel effect. The third phase was characterized by the slowing down of gel effect and finally the fourth phase was identified by glass effect if the reaction temperature is less than the glass temperature of the polymer. Depending on the type of monomer used and/or the reaction conditions, one or more phases can be absent. The first phase according to the authors comes under conventional kinetics where gel effect has not set in yet. It is same phase for which the analytical solution was derived. They have characterized the last three phases by two important parameters (β_s & γ_s) and have obtained the results for the case of transfer to monomer and transfer to CTA. Comparing with the developed analytical solution, we found that these two parameters also appear in our solution as a function of R_P and L . They are as follows

$$\frac{x_c}{\gamma_s\sqrt{Z_s}} = \frac{(1-R_M)K_{pr}M\lambda_0}{2fK_dI} = (1-R_M)L \tag{4-148}$$

$$\frac{\beta_s}{x_c} = \left[C_M + C_A\frac{A}{M}\right] = (1+C_M)R_P \tag{4-149}$$

Recalling that both R_P & L define R_L through eqn.(4-67) and that this last parameter describes the phase1 covered by our analytical solution, it seems that Soh et al.[25] parameters not only account for phase2-4 of vinyl polymerization but should also characterize phase1. Thus the developed analytical solution extends their result to the whole range of phases.

Zhu and Hamielec[24] have defined the conditions under which gel formation can take place for isothermal homogeneous batch homopolymerization. The steps considered were initiation, propagation, chain transfer to polymer, termination by combination and disproportionation and chain transfer to monomer. The assumptions used for their work were 1) monoradical assumption, 2) stationary state hypothesis and 3) random chain transfer to polymer. They found that gel formation in free radical polymerization can occur only through 1) transfer to polymer + termination by combination, 2) transfer to polymer + termination by disproportionation and 3) transfer to monomer + termination by recombination.

They have shown that three factors $(\frac{K_{fm}M_0}{K_t\lambda_0}, \frac{K_{tc}}{K_t}, \frac{K_{p*}}{K_p})$ are of importance when the transfer to monomer leads to gel effect. It is noteworthy that for presence of chain transfer to monomer $(C_M \neq 0)$ and absence of chain transfer to solvent $(C_S = 0)$ and CTA $(C_A = 0)$, our R_L parameter is reduced to $\frac{K_{fm}M}{K_t\lambda_0}$, which is the first Zhu and Hamielec[24] parameter but at $t \neq 0$, i.e. at the beginning of the reaction. The second parameter is simply R_T and third is absent in our analytical solution since we have not modeled K_{p*}, the reaction rate coefficient for propagation for chain-end double bond. Authors[24] have shown that there is a combination of values between $\frac{K_{fm}M_0}{K_t\lambda_0}$ and $\frac{K_{tc}}{K_t}$ (i.e. between R_L & R_T) below which gel effect cannot take place and that high value of $\frac{K_{fm}M_0}{K_t\lambda_0}$ does not always mean early gel point. This is quite apparent for the cases of BuA and VAc as shown in Fig. 4.1-21 and Fig. 4.1-22. R_L value is definitely high but there is no sign of gel effect as shown in their experimental conversion presented in Fig. 4.1-18 and Fig. 4.1-20. In our case, R_L is being evaluated at the beginning of each time step. This is particularly a good strategy as R_L can move from one case to another case as the reaction proceeds. So a monomer which may not be capable of moving into gel phase based on the conditions at the beginning of any time step may become capable of gel formation at a higher conversion and vice-versa.

Although we have not taken gel effect into account for the analytical solution, it is worthy to note that a relation has emerged naturally between R_L and R_T in the analytical solution. Indeed we came up with three different cases for μ_2, which seems to be in accordance with the observation made by Zhu & Hamielec[24] for predicting the capability for gel effect. This definitely establishes beyond any doubts that the analytical solution is being evolved in a proper direction.
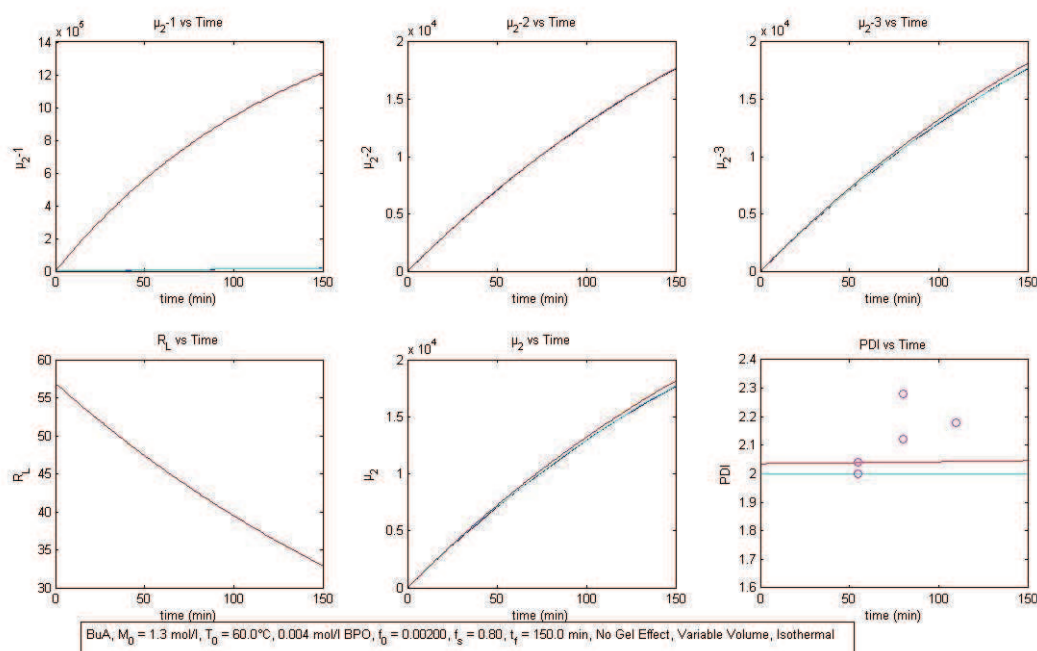
Fig. 4.1-21- BuA[18], result for R_L
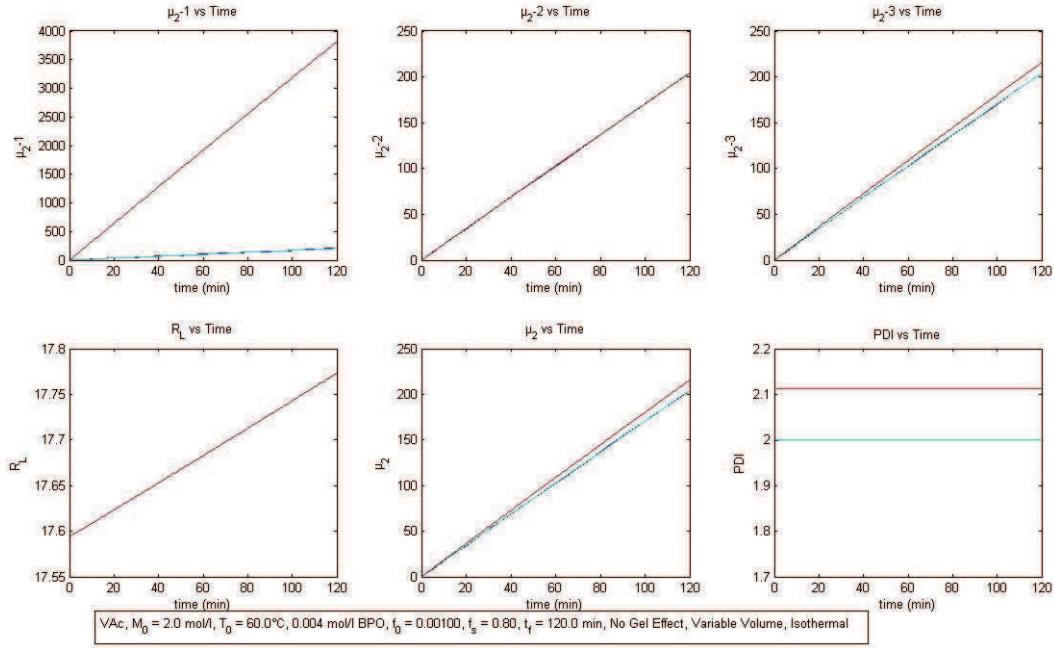
Fig. 4.1-22- VAc, result for R_L

On the other hand, R_L parameter has a physical meaning. It can easily be observed that it represents the ratio of primary radicals produced by consumption of live polymer chain radicals by chain transfer to monomer step to primary radicals' production by initiator. It can also be viewed as the primary radicals' production by chain transfer to monomer step compared to primary radicals produced by original initiator. So its value represents how strong is the chain transfer to monomer process with respect to initiation process in terms of primary radicals' formation as well as termination of polymer chain radicals other than by termination steps. So its high value means that prolongation of polymer chain will be prevented earlier and the resulting chains will mostly be of small lengths.

Our AS also matches with the expression of monomer concentration obtained by Venkateshwaran *et al.*[9] under constant volume condition. Indeed, their solution is as follows

$$M = M_0 e^{-m_v(Z_{0v} - Z_v)} \tag{4-150}$$

Where:

$$Z_v = 2\sqrt{\frac{2fk_t I_0 e^{(-k_d \cdot t)}}{k_d}} \tag{4-151}$$

$$Z_{0v} = 2\sqrt{\frac{2fk_t I_0}{k_d}} \ \& \ m_v = \frac{k_p}{k_t} \tag{4-152}$$

so

$$m_v Z_v = 2\sqrt{\frac{2fk_p I_0 e^{(-k_d \cdot t)}}{k_d k_t}} = B_0 y \tag{4-153}$$

It is noteworthy that this last expression is same as the one shown in eqn.(4-10) & eqn.(4-21). This means that using this expression, one will end up with the same solution for monomer

concentration as obtained in eqn.(4-23). So the solution obtained by the authors without using QSSA and ours using QSSA is same. Except that we have obtained this solution in a much simpler way conversely to the authors who had applied several mathematical manipulations to reach this simple result. In a broad way, it can be concluded that the results obtained by following the model in its complexity of not applying QSSA is still the same when applying QSSA. So this justifies the simplification obtained by this simple QSSA assumption.

Special attention is now directed towards the source of stiffness in FRP model. To get an idea of the time step size during which temperature change is so small that kinetic rate coefficients can be assumed to be constant, let's use the analytical solution for M & λ_0 obtained so far. Recalling eqn.(4-23), (4-36) and eqn.(4-133) we have

$$T' = e^{(K1t)} \int e^{(-K1t)} K2. (1 - R_M) K_{pr} M_0. [V_R]_0. exp[-B_0. (1 - y)] \sqrt{\frac{2fK_dI}{K_t}}. dt \quad (4\text{-}154)$$

Using eqn.(4-9) and eqn.(4-10) for initiator concentration and y respectively, we obtain

$$T' = e^{(K1t)} \int e^{(-K1t)} K2. (1 - R_M) K_{pr} M_0. [V_R]_0. exp[-B_0. (1 - y)] \sqrt{\frac{2fK_dI_0.[V_R]_0}{K_t[V_R]}} e^{-K_d.\frac{t}{2}}. dt$$
$$(4\text{-}155)$$

As one can see, there are many expressions which contain exponential terms explicitly and others, like kinetic rate coefficients, for with these exponential terms are implicit. It will make the expression quite cumbersome if we put all the implicit exponential terms it contains. So let's just take the monomer term's exponential part and evaluate the temperature dependence.

$$exp[-B_0. (1 - y)] = exp(-B_0). exp(B_0 y) = exp(-B_0). exp\left(B_0 e^{-\frac{K_d t}{2}}\right) \quad (4\text{-}156)$$

$$exp(-B_0). exp\left(B_0 e^{-\frac{K_d t}{2}}\right) = exp(-B_0). exp\left(B_0 exp\left[-\frac{K_{d0}.exp\left[-\frac{E_{d0}}{R.T}\right]t}{2}\right]\right) \quad (4\text{-}157)$$

$$= exp(-B_0). exp\left(B_0 exp\left[-K_{d0}.\frac{t}{2}. exp\left[-\frac{E_{d0}}{R.T}\right]\right]\right) \quad (4\text{-}158)$$

So we can easily see that with respect to temperature, the expression is thrice exponential. So even a small change in temperature will lead to large change in monomer conversion and heat generation, which ultimately can induce a thermal run away. This is what happens in poorly controlled polymerization reactors. Thus to keep the temperature change small enough, the time-step during which it is evaluated, should be very small. Depending on initial conditions, heat transfer coefficient (U), heat of reaction and thus time-step value may vary.

We can also observe that the expression is also dependent on time with twice exponential. As time can only increase and will lead to decrease of exponential function, thus heat generation can be delayed by increasing time of reaction, i.e. by slowing down the reaction initially by keeping the temperature low and later speed up the reaction by increasing temperature. This seems to be practical too. So instead of keeping an isothermal condition with one fixed temperature only for the whole conversion, the temperature can be increased after some suitable conversion to speed up the reaction rate. This could be done in steps or continuously. This is just a possibility we are suggesting based on our analysis and results. This may require

separate study and/or reference to exiting work[27,28] as to how to calculate the "suitable conversion" and what should be best temperature profile.

We can observe from the analytical solution and all presented graphs that there is no stiffness in this set of differential equations for the case of no gel effect, i.e. eqn.(3-3) to (3-13). So from this, we can conclude that the only source of stiffness in this system of equations arises from temperature equation as previously discussed. So in the absence of this source, i.e. for isothermal condition, this model for FRP can easily be integrated using non-stiff solvers.

4.1.10 Conclusion

An analytical solution for FRP for variable volume, isothermal, homogeneous bulk/solution homopolymerization conditions is obtained. The solution for initiator and monomer already exists for constant volume case. For monomer, same solution was obtained by Zhu *et al.*[21]. Venkateshwaran *et al.*[9] have also obtained an analytical solution but their solution does not account for transfer to monomer and transfer to solvent. Besides this, the major disadvantage of their solution is that it is too cumbersome and complex, hence almost impractical to choose for any purpose. Moreover, their analytical solution matches poorly with numerical solution.

The solution we have obtained is quite elegant, simple and non-cumbersome. Its match with numerical solution as well as experimental data under various conditions of different monomers, initiators, temperatures, solvent fractions is shown to be excellent. It can be easily implemented on any spreadsheet or programmable software. So, the novelty of this work is to get an analytical solution which is applicable not only for variable volume condition but also accommodates the widest possible range of elementary reaction steps that have practical usage in industry and lab alike.

The relationship of λ_0, λ_1, and λ_2 as shown by eqn.(4-38)-(4-41) is also in accordance with the physical and theoretical reality which states that process of chain transfer like transfer to monomer, solvent and CTA should reduce the live or dead polymer chain length.

μ_0, μ_1 and μ_2 are shown to be dependent on both I_0 and M_0. μ_0 & μ_1 are found to be simple function of final and initial concentration of initiator, monomer, solvent and CTA. They are also independent of R_L.

It can be seen that the results of analytical solution match quite well with numerical integration results for $I, M, \mu_0,$ and μ_1 for all the cases. It matches quite well for μ_2 depending on the value of R_L to select the suitable case between 3 different possible cases. It is also observed that the results are quite sensitive towards the value of C_P rather than C_T. This implies that the side reaction of transfer processes like chain transfer to monomer has more impact on μ_2 and hence on PDI than the type of termination of reaction. It also signifies the importance of inclusion of the chain transfer to monomer for good modeling of FRP. Also assuming R_L constant for the case2 can be seen to be valid to a good extent as the variation in the value of R_L is generally quite small in that case. The procedure aiming at varying C_M value to match the analytical solution of μ_2 with that of experimental data, can be used to calculate the actual value of C_M at a given temperature. So one could estimate how much

significant is the transfer to monomer process under operating conditions and derive some methods to reduce its importance in order to improve or control *PDI*.

It can also be seen that the results match quite well with the experimental data till the gel effect sets in. It is quite understandable as the assumptions of constant reaction rate coefficients no longer remain valid. It can also be observed that model based on QSSA, i.e. FRP_QSSA, matches quite well with full model, i.e. FRP_Full. This is understandable as the condition of QSSA is violated only during the gel effect but not modeled here. Hence the simplest model can be used in CFD for instance to model FRP in a given batch reactor or flow reactor geometry before gel effect.

It could also be used for model based process control in the batch reactor during the production of polymer by FRP up to the conversion before gel effect (Sampath *et al.*[22]).

Finally, this analytical solution can be used to validate the numerical formulation in CFD or can be used in CFD simulations as an initial condition instead of constant initial conditions as generally used. This can greatly reduce the simulation time required as the initial solution will be close to the final solution from the very beginning convergence procedure. For polymerization, using CFD, AS can also be used to evaluate the extent of mixing within the reactor with more precision without resorting to correlation technique as used[26].

The accuracy of prediction of analytical solution is obviously limited by the accuracy of data, especially the kinetic data used for the temperature studied. So the range of applicability of data for that temperature must be verified before use.

In this section we have developed an analytical solution of the FRP which matches well with numerical solutions and experimental data up to the point where gel effect sets in. In nature, this analytical solution does not take into account variation of the kinetic rate coefficients to accommodate the gel and glass effects. In following section, the analytical solution will be extended through the whole range of monomer conversion by implementing the so-called CCS model which allows simulating the gel and glass effect.

4.1.11 References

1. Tulig, T. J.; Tirrell, M., Toward a Molecular Theory of the Trommsdorff Effect. *Macromolecules* **1981,** *14* (5), 1501-1511.

2. Chiu, W. Y.; Carratt, G. M.; Soong, D. S., A Computer-Model for the Gel Effect in Free-Radical Polymerization. *Macromolecules* **1983,** *16* (3), 348-357.

3. Baillagou, P. E.; Soong, D. S., Major Factors Contributing to the Nonlinear Kinetics of Free-Radical Polymerization. *Chem Eng Sci* **1985,** *40* (1), 75-86.

4. Louie, B. M.; Carratt, G. M.; Soong, D. S., Modeling the Free-Radical Solution and Bulk-Polymerization of Methyl-Methacrylate. *Journal of Applied Polymer Science* **1985,** *30* (10), 3985-4012.

5. Tefera, N.; Weickert, G.; Westerterp, K. R., Modeling of free radical polymerization up to high conversion .1. A method for the selection of models by simultaneous parameter estimation. *Journal of Applied Polymer Science* **1997,** *63* (12), 1649-1661.

6. Tefera, N.; Weickert, G.; Westerterp, K. R., Modeling of free radical polymerization up to high conversion .2. Development of a mathematical model. *Journal of Applied Polymer Science* **1997,** *63* (12), 1663-1680.

7. Frounchi, M.; Farhadi, F.; Mohammadi, R. P., Simulation of Styrene Radical Polymerisation in Batch Reactor- A Modified Kinetic Model for High Conversion. *Scientia Iranica* **2002,** *9* (1), 86-92.

8. Achilias, D.; Kiparissides, C., Modeling of Diffusion-Controlled Free-Radical Polymerization Reactions. *Journal of Applied Polymer Science* **1988,** *35* (5), 1303-1323.

9. Venkateshwaran, G.; Kumar, A., Solution of Free-Radical Polymerization. *Journal of Applied Polymer Science* **1992,** *45* (2), 187-215.

10. Achilias, D. S., A review of modeling of diffusion controlled polymerization reactions. *Macromol Theor Simul* **2007,** *16* (4), 319-347.

11. Achilias, D. S.; Kiparissides, C., Development of a General Mathematical Framework for Modeling Diffusion-Controlled Free-Radical Polymerization Reactions. *Macromolecules* **1992,** *25* (14), 3739-3750.

12. Keramopoulos, A.; Kiparissides, C., Development of a comprehensive model for diffusion-controlled free-radical copolymerization reactions. *Macromolecules* **2002,** *35* (10), 4155-4166.

13. Keramopoulos, A.; Kiparissides, C., Mathematical Modeling of diffusion-controlled free-radical terpolymerization reactions. *Journal of Applied Polymer Science* **2003,** *88* (1), 161-176.

14. Verros, G. D.; Achilias, D. S., Modeling Gel Effect in Branched Polymer Systems: Free-Radical Solution Homopolymerization of Vinyl Acetate. *Journal of Applied Polymer Science* **2009,** *111* (5), 2171-2185.

15. Wu, J. Y.; Shan, G. R., Kinetic and molecular weight control for methyl methacrylate semi-batch polymerization. I. Modelling. *Journal of Applied Polymer Science* **2006,** *100* (4), 2838-2846.

16. Marten, F. L.; Hamielec, A. E., High-Conversion Diffusion-Controlled Polymerization of Styrene .1. *Journal of Applied Polymer Science* **1982,** *27* (2), 489-505.

17. Balke, S. T.; Hamielec, A. E., Bulk Polymerization of Methyl Methacrylate. *Journal of Applied Polymer Science* **1973,** *17*, 905-949.

18. McKenna, T. F.; Villanueva, A.; Santos, A. M., Effect of solvent on the rate constants in solution polymerization. Part I. Butyl acrylate. *J Polym Sci Pol Chem* **1999,** *37* (5), 571-588.

19. McKenna, T. F.; Villanueva, A., Effect of solvent on the rate constants in solution polymerization. Part II. Vinyl acetate. *J Polym Sci Pol Chem* **1999,** *37* (5), 589-601.

20. Baillagou, P. E.; Soong, D. S., Molecular-Weight Distribution of Products of Free-Radical Non-Isothermal Polymerization with Gel Effect - Simulation for Polymerization of Poly(Methyl Methacrylate). *Chem Eng Sci* **1985,** *40* (1), 87-104.

21. Zhu, S.; Hamielec, A. E., "Polymerization Kinetic Modeling and Macromolecular Reaction Engineering" in *Polymer Science: A Comprehensive Reference.* Eds: Matyjaszewski, K.; Möller, M., Elsevier B.V. Amsterdam, **2012,** *4*, 779–831.

22. Sampath, V.; Palanki, S.; Cockburn, J. C., Robust nonlinear control of polymethylmethacrylate production in a batch reactor. *Comput Chem Eng* **1998,** *22*, S451-S457.

23. Zhu, S.; Hamielec, A. E., Modeling of Free-Radical Polymerization with Cross-Linking - Monoradical Assumption and Stationary-State Hypothesis. *Macromolecules* **1993,** *26* (12), 3131-3136.

24. Zhu, S.; Hamielec, A. E., Gel Formation in Free-Radical Polymerization Via Chain Transfer and Terminal Branching. *J Polym Sci Pol Phys* **1994,** *32* (5), 929-943.

25. Soh, S. K.; Sundberg, D. C., Diffusion-Controlled Vinyl Polymerization .1. The Gel Effect. *J Polym Sci Pol Chem* **1982,** *20* (5), 1299-1313.

26. Bockhorn, H.; Mewes, D.; Peukert, W.; Warnecke, H.-J., *Micro and Macro Mixing : Analysis, Simulation and Numerical Calculation*. Springer-Verlag Berlin Heidelberg: Berlin, Heidelberg, 2010.

27. Ray, A. B.; Saraf, D. N.; Gupta, S. K., Free-Radical Polymerizations Associated with the Trommsdorff Effect under Semibatch Reactor Conditions .1. Modeling. *Polym Eng Sci* **1995,** *35* (16), 1290-1299.

28. Srinivas, T.; Sivakumar, S.; Gupta, S. K.; Saraf, D. N., Free radical polymerizations associated with the Trommsdorff effect under semibatch reactor conditions .2. Experimental responses to step changes in temperature. *Polym Eng Sci* **1996,** *36* (3), 311-321.

29. Verros, G. D.; Achilias, D. S., Modeling Gel Effect in Branched Polymer Systems: Free-Radical Solution Homopolymerization of Vinyl Acetate. *Journal of Applied Polymer Science* **2009,** *111* (5), 2171-2185.

4.2 Analytical Solution of Free Radical Polymerization: Applications- Implementing Gel effect using CCS model

4.2.1 Abstract

This article presents the integration of the CCS gel/glass model in an analytical solution derived for the free radical polymerization under isothermal condition. This integration allows the analytical solution to be applicable for the whole range of conversion thus making it more useful for practical application. The results were compared with numerical solution as well as with experimental data for two different monomers: styrene and methyl methacrylate (MMA). MMA with chain transfer agent was also used for this purpose. The results were found to be in good agreement with both numerical solution and experimental data. The numerical results with and without quasi-steady state assumption were also found to be in good agreement with each other for the entire range of conversion. As constant time step was used, the effect of stiffness on analytical solution during gel effect was visible at low temperature compared to higher temperature.

Keywords- Analytical solution, free radical polymerization, styrene, methyl methacrylate, CCS model, gel effect, glass effect

4.2.2 Introduction

During any chemical reaction, certain physical phenomena always draw attention and diffusion is one of them. In bulk or concentrated solution polymerization, diffusion plays a very significant role especially at high conversions. Therefore, significant reaction steps like termination, propagation and initiation could become diffusion controlled as the reaction proceeds. As the conversion increases, the viscosity of the reaction mixture increases. This increase of viscosity decreases the translational diffusion of macroradicals. Thus, the termination of radical chains decreases as one radical need to approach another radical for terminating by combination or by disproportionation. Once in the proximity, the alignment of the radical segments is characterized by segmental diffusion. The overall decrease in termination of macroradicals leads to the so-called Trommsdorff effect or gel effect[1] which is accompanied by an increase in the reaction rate. It may happen even in isothermal conditions. This has highly detrimental effects on the product quality, reactor safety and reactor operability.

As the reaction continues, the viscosity increases still further almost exponentially. This decreases even further the species diffusivity so that even monomer is now almost restricted to its place. If the reactor is operating below the glass temperature of the polymer and going for higher conversion, the reaction mixture glassifies. Thus, the reaction freezes at the conversion below completion. This effect is called glass effect[1]. This leads to incomplete usage of monomer and initiator and they remain in the product. They, thus, can act as impurities to cause adverse reactions when the polymer produced is used as final product without further processing. In the tubular flow reactor, the residence time is infinite near the walls. Thus glass type product formation can takes place on the inner walls of the tubular reactor when the reactor operating temperature is less than the glass temperature of the polymer. This decreases the area for flow and hence increases the pressure drop across the

reactor. It can lead to blockage of the tube reactor under severe condition thus making it inoperable. So it becomes necessary either to operate at temperatures higher than the glass temperature of the polymer or diluting the reaction mixture using the inert solvent so as to keep the glass temperature of the mixture below the operating temperature.

When radicals are formed upon initiator decomposition, they need to reach monomer molecules to form the primary radicals. But due to several mechanisms, induced by impurities and chemical species like solvent present in the reaction mixture, many radicals are destroyed or consumed before reacting with monomer. Only a fraction of radicals formed are able to reach monomer molecules and react with them to form these primary radicals. The probability of an initiator radical to reach monomer decreases with increasing viscosity. So, the effect which lowers the initiator efficiency to reach and react with monomer to form primary radicals due to cage formation around initiator radical is called cage effect[1]. It increases with conversion, use of solvent, solvent fraction and presence of impurities.

In this work, we will be limited to gel and glass effects only. Many people have worked on this problem of modeling gel and glass effect and have developed various approaches with different degrees of success. Many researchers have used the critical point or critical conversion to invoke gel effect and glass effect in their model[2]. That means, after a certain conversion, the termination rate will change abruptly and gel effect will be simulated. After another critical point is reached, glass effect will be simulated. This approach is simple but has the disadvantages of being non-generalized and non-predictive. Tulig and Tirrell[3] tried to model these phenomena as continuous process rather than discrete process by taking into account the polymer diffusion theory. This theory was further improved successfully by Chiu, Carratt and Soong[4] (CCS) for gel and glass effect. This theory requires some parameters that have to be determined by best fit of experimental data. Hence many different parameters values can be found in the literature for the same monomer.

This paper is in continuation of our previous work[5] on free radical polymerization (FRP). We had obtained an analytical solution (AS) for isothermal, homogeneous, bulk/solution homopolymerization and volume variation with monomer conversion. The kinetic rate coefficients were taken as function of temperature only. Due to isothermal condition, the kinetic rate coefficients remain constant for the whole derivation. In that work, we had demonstrated the excellent match between AS and the numerical solution. We had validated it further through its comparison with experimental data for four monomers namely- styrene (St), methyl methacrylate (MMA), butyl acrylate (BuA) and vinyl acetate (VAc). The experimental data taken for validation varied in temperature, type of initiators, different initiator concentrations, with and without solvent and different solvent fractions. The data considered were monomer conversion, number-average molecular weight MW_n, weight-average molecular weight MW_w and polydispersity index (PDI). The match was quite good before the gel effect in both the bulk and solution polymerization cases thus establishing its correctness and usefulness.

To this extent, our work is superior to the previous work of Venkateshwaran et al.[6] in terms of the simplicity of the solution, in encompassing additional steps of transfer to monomer and

transfer to chain transfer agent (CTA), variable volume condition and in exhibiting an excellent match with the numerical solution. But their work also included the extension of their AS to the non-isothermal condition, gel effect and their combinations also. Including gel/glass effect means that the kinetic rate coefficients will no longer remain solely a function of the temperature. It also means that they will vary even during isothermal condition depending on the conversion. This variation in kinetic rate coefficients makes the differential equations highly non-linear. Thus standard simplifications or assumptions cannot be considered anymore. This acts as a limitation on the analytical solution in terms of its applicability for the whole range of conversion. Therefore it is inducing a serious limitation in terms of the practical application of analytical solution.

They bypassed this problem by solving the analytical solution in time-step manner. All the variables including temperature and various kinetic rate coefficients were calculated at the beginning of each time step. The time step was kept small enough so that the variables could be considered constant to make the analytical solution applicable. They had used the CCS model for implementing gel/glass effect. The kinetic rate coefficients were evaluated using CCS model before being used to evaluate conversion and other variables. But the match of their analytical solution with the numerical solution was not good in gel effect both during isothermal and non-isothermal conditions.

We have adopted the same strategy of using small time steps and evaluating all the variables at the beginning of each time step. The strategy of evaluating kinetic rate coefficients using CCS model before using them for evaluating the variable is also kept same. For more details, reader can refer to Venkateshwaran et al.[6] The purpose of this work is to demonstrate that the CCS gel/glass model can be incorporated in our analytical solution seamlessly without sacrificing the good match between numerical solution and experimental data. By this, the utility of our analytical solution can be extended to the whole range of monomer conversion for isothermal conditions. To further make it credible, we have used the data for two monomers- St and MMA. We have also used the data for MMA with CTA to display the versatility of our analytical solution with various practical conditions.

4.2.3   Theory

4.2.3.1   Reaction mechanism and kinetic equations
The detailed kinetic scheme used in this work is given in section 3.2.2. The related mathematical model is presented in section 3.2.3.

4.2.3.2   Analytical solution
The summary of analytical solution in time step format is given in section 4.1.5.

4.2.3.3   CCS model
The constitutive equations and the model are presented in section 3.2.6 for MMA with and without chain transfer agent and for styrene.

4.2.3.4 Physical and chemical data

The physical and chemical data used in this are given in the Table 3-1, Table 3-3 and Table 3-4.

4.2.4 Methodology

The details about mathematical sets FRP_Full and FRP_QSSA are given in section 3.2.4. The equations in section 4.1.5 constitute the third mathematical set called as Analytical. Details about it are given in section 4.1.7. For Analytical, constant time step was used, which was taken to be about $1/100^{th}$ of the total reaction time chosen for the simulation.

All the variables were calculated at the beginning of each time step as in section 4.1.7. Before evaluating the various concentration variables, kinetic rate coefficients were evaluated using CCS model for gel/glass effect. K_t^0 in the CCS gel model was function of temperature only and remained constant throughout simulation under isothermal condition. An error correction loop was used for correcting the value of K_t and K_p. In this, the new value of λ_0 based on new values of K_t and K_p was fed back to the CCS model n number of times to further improve the values of K_t and K_p. No other parameter of K_t and K_p was changed or manipulated during this correction loop. The requirement of this loop was to match the model prediction with experimental data. Once, it was repeated n times to match any experimental data, it was found that it remained constant for almost all experimental data-set for that monomer. The value of n varied from monomer to monomer. It depends also upon the model used for the experimental data which varies from one researcher to another for the same monomer. This correction loop was required for all three mathematical sets under study. The number of cycles in each mathematical set was chosen in such a way that the results of each set matched with the experimental data as well as with each other. Number of cycles for correction loop might differ from each other among the three set, maximum by 1.This correction loop was used for both styrene and MMA. No such correction loop was required for MMA with CTA.

The graphs of various variables obtained from all the three mathematical sets were checked with each other as well as with experimental data[7-9] whenever available. The data are presented in various groups of related variables so as to make them more comprehensible.

Slight modifications were made on the values of two literature reported CCS parameters to fit the experimental data with the sets prediction for large range. For MMA, it is 8.8083×10^{22} $instead$ of 8.8083×10^{23} for Θ_t as given by Baillagou et $al.$[10], and for styrene, $T_{gp}$is chosen to be 88.2°C instead of 90°C used by Lima et $al.$[11]

4.2.5   Results
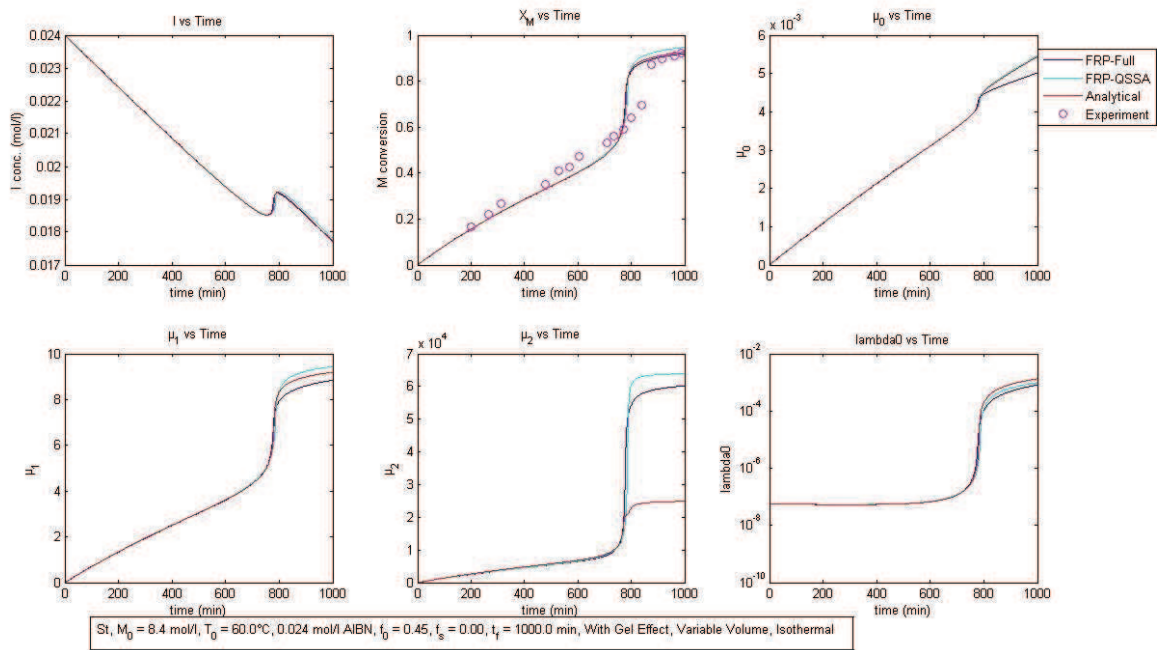
Fig. 4.2-1-CCS model results for Styrene[7]- $I, x_m, \mu_0, \mu_1, \mu_2$ & λ_0

The results for styrene are shown in Fig. 4.2-1 to Fig. 4.2-5. It is clearly visible that our analytical solution (AS) works extremely well with CCS model for gel effect. The graphs of both FRP_Full and FRP_QSSA numerical models not only match very well with each other but also with AS for $I, x_m, \mu_0, \mu_1, \mu_2$ & λ_0 as shown in Fig. 4.2-1. The deviations in other variables among the three sets are minor and occur only after the gel effect and during glass effect. The major deviation occurring for μ_2 which is explained in discussion section. The initiator concentration is also having anomalous behaviors during the gel effect. But it is found to be same for the numerical solution too. This is because of volume variation accounted in the model. This is explained in details in discussion section. For constant volume condition, the concentration would have fallen monotonically.
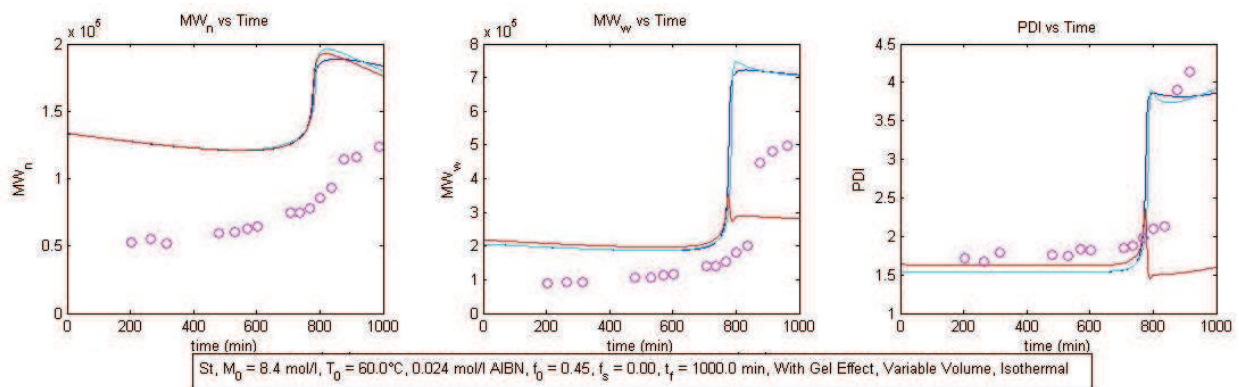
Fig. 4.2-2- CCS model results for Styrene[7]- MW_n, MW_w & PDI

Fig. 4.2-2 shows the match with the experimental data of MW_n, MW_w & PDI. Here again the results of AS matches well with numerical solution for MW_n whereas for MW_w it is good till

155

initial phase of gel effect only. This discrepancy is explained in discussion section. The result match with experimental data is just fair. It can be seen that PDI prediction is quite good and similar by both numerical sets- FRP_Full and FRP_QSSA. This is despite the fact that the match with MW_n and MW_w is not that good. For AS, the match for PDI is good till initial phase of gel effect with both experimental data and numerical solution. The reason for poor match for PDI arises from the poor prediction of MW_w which in turn is affected by the poor prediction of μ_2 as shown in Fig. 4.2-1 and Fig. 4.2-3. One of the possible reasons for this could be the stiffness of the problem which can be seen with sharp spike of R_L value in Fig. 4.2-3 which requires very small time-step during that. Whereas, we had taken constant time-step for AS for the whole duration of simulation
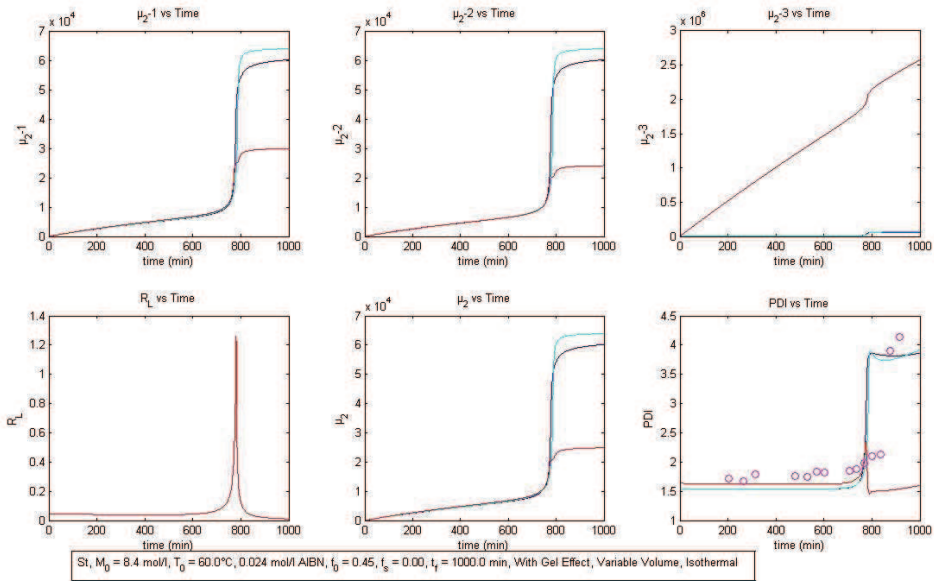
Fig. 4.2-3- CCS model results for Styrene[7]- calculation of three different cases of AS for μ_2 and its selection based on the value of R_L and thus PDI calculation
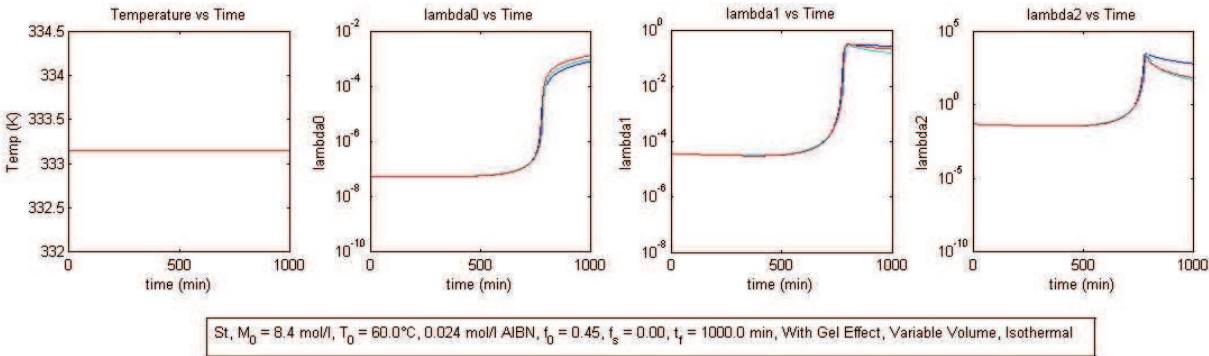
Fig. 4.2-4- CCS model results for Styrene- $\lambda_0, \lambda_1, \& \lambda_2$

In Fig. 4.2-4, it can be seen that the graphs for $\lambda_0, \lambda_1, \& \lambda_2$ match quite well with each other for all the three sets despite the fact that QSSA is not valid during gel effect. This is because of the error correction loop used and fine tuning achieved by adjusting the number of cycles.

These results can be used to encourage the use of simpler model of FRP_QSSA over FRP_Full in CFD simulations.
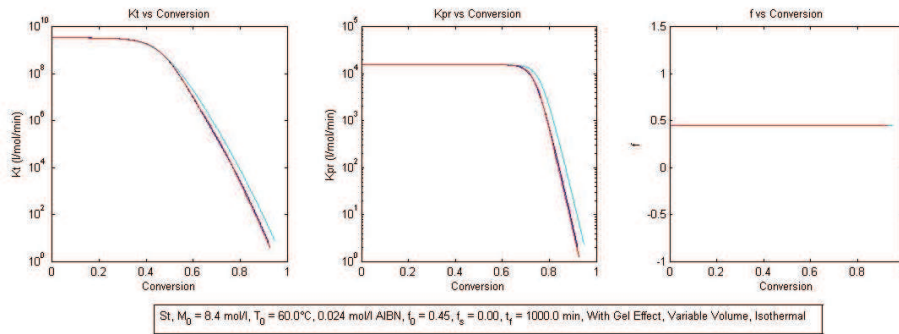
Fig. 4.2-5- CCS model results for Styrene- K_t, K_{pr} & f.

Fig. 4.2-5 depicts the smooth and logarithmic decrease of K_t & K_{pr} with conversion which is in-line with the model given by CCS[4]. Due to increased conversion, volume fraction of monomer decreases. This affects the available free volume and calculated through factor **C1** (eqn. 3-70) which empirically accounts the effect of variation of viscosity with conversion. The effect of change of λ_0 is accounted through correction loop as mentioned in methodology. The temperature dependent factor Θ_t and Θ_p remains constant with respect to temperature under isothermal conditions. Θ_t, being function of I_0 (eqn.(3-78) for styrene), affects K_t more than K_p. One can also observe that K_{pr} starts falling at a later conversion leading to glass effect compare to K_t which starts falling at lower conversion leading to gel effect. Besides this, the rate of fall of K_{pr} is higher than K_t. This is an important result and observation as we will see later. Initiator efficiency f is assumed constant and no cage effect is modeled here. Its effect on the results is also discussed there in discussion section.

Going through Fig. 4.2-1 to Fig. 4.2-5, it is not surprising to find that both the numerical sets (FRP_Full and FRP_QSSA) predicted similar results despite varying on assumption of QSSA. This result is similar to the one obtained by CCS[4]. All this is explained in discussion section in detail.
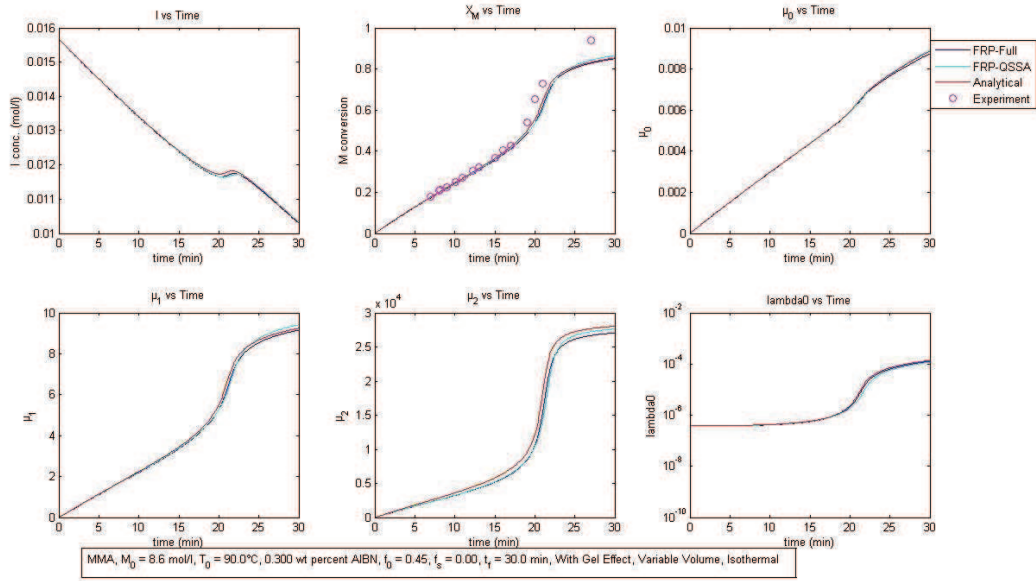
Fig. 4.2-6- CCS model results for MMA[8]- $I, x_m, \mu_0, \mu_1, \mu_2$ & λ_0

With MMA, the results are even better as the simulations are done at higher temperature. All the results as shown in Fig. 4.2-6 to Fig. 4.2-10 are similar to that for styrene qualitatively.
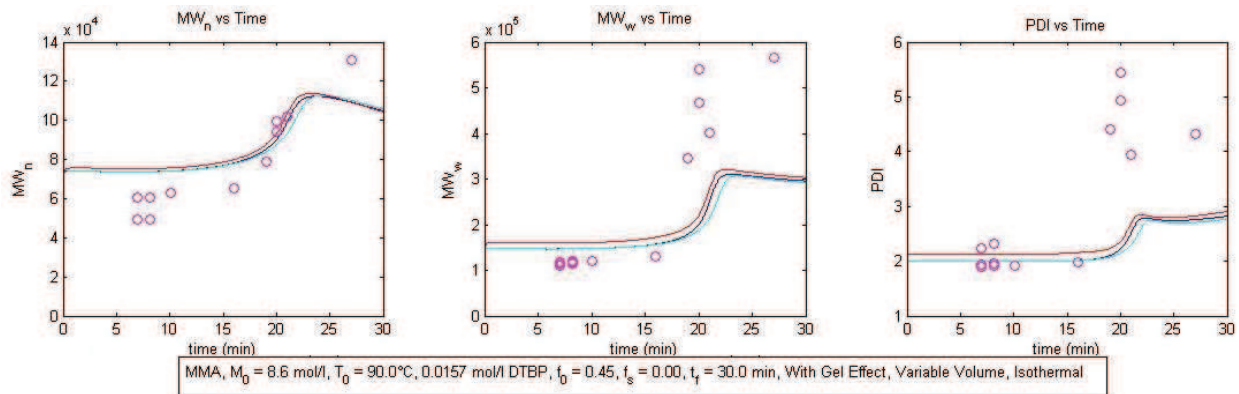
Fig. 4.2-7- CCS model results for MMA[8]- $MW_n, MW_w,$ & PDI

As we can see in Fig. 4.2-7, the prediction of MW_w and hence PDI is better for AS and is matching well with numerical solution. This is because of the better prediction of μ_2. This is probably due to lower stiffness of the problem at higher temperature as seen by R_L value in Fig. 4.2-8. The reason for decrease of stiffness at higher temperature is due to increase in conversion at higher temperature at which gel effect becomes prominent. This leads to less severe gel effect due to lesser concentration of monomer available for gel effect which is not the case at lower temperature. One can easily observe the success of predicting and selecting correct μ_2 depending on the value of R_L in Fig. 4.2-8. Here the value of R_L starts varying from case1 to enter in the range of case2 and thus the composite match of μ_2 value is in excellent match with the numerical solution.

Fig. 4.2-9 and Fig. 4.2-10 show the results for MMA similar to the case of St.
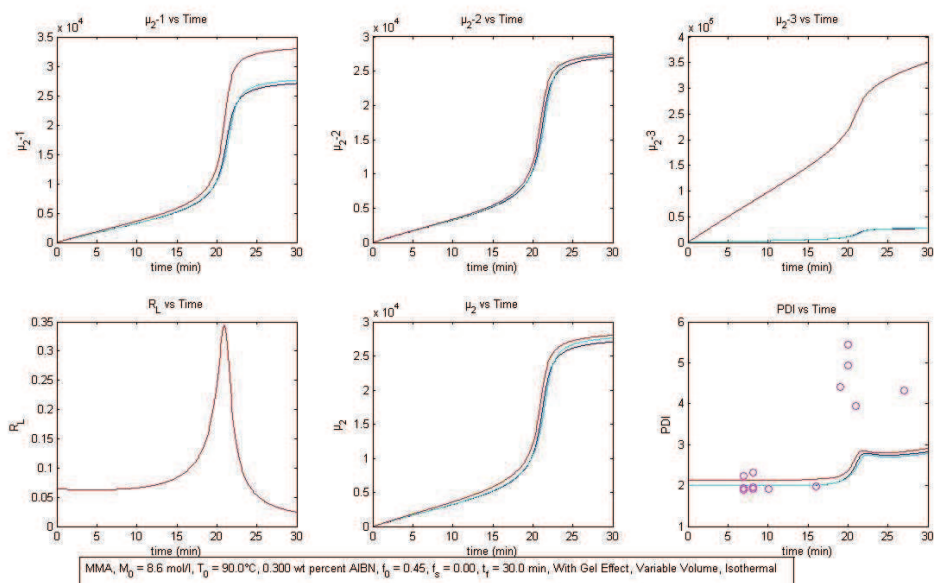
Fig. 4.2-8- CCS model results for MMA[8]- calculation of three different cases of AS for μ_2 and its selection based on the value of R_L and thus *PDI* calculation
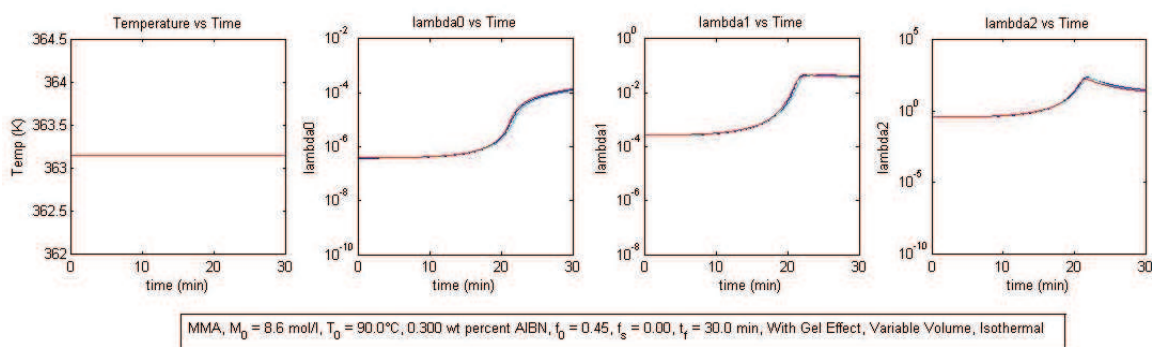
Fig. 4.2-9 - CCS model results for MMA- $\lambda_0, \lambda_1, \& \lambda_2$
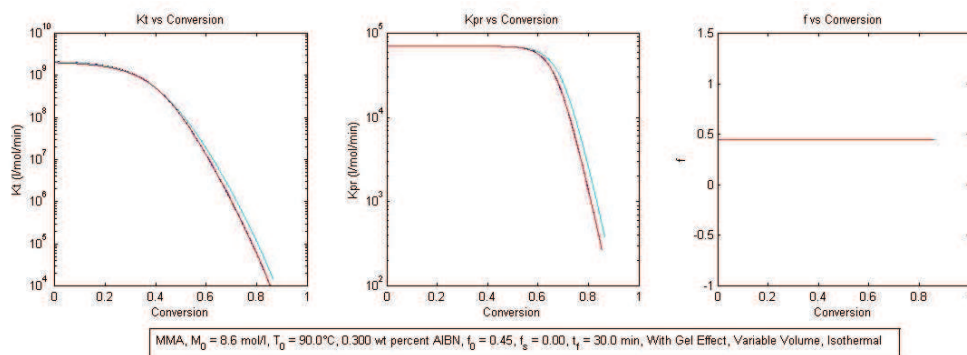
Fig. 4.2-10- CCS model results for MMA- K_t , K_{pr} & f.

(a)	(b)
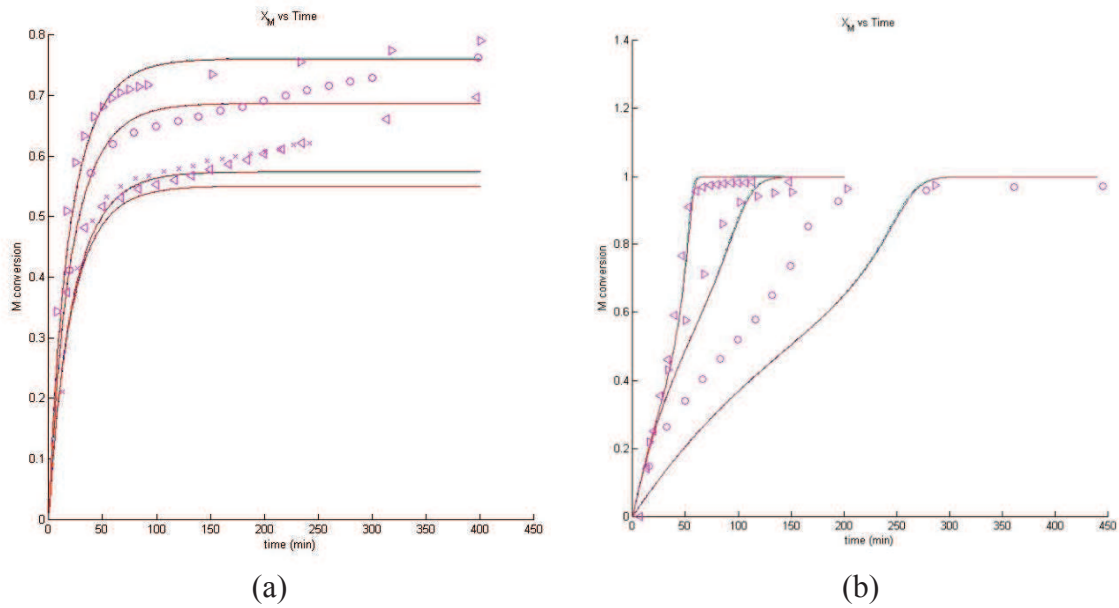
Fig. 4.2-11- Results for MMA[9] with CTA (a) – T_0 = 132°C, I_0= 7x10^{-4}mol/l, A_0= 2.05x10^{-2} mol/l, f_0= 1.0, (circle), T_0 = 150°C, I_0= 7x10^{-4}mol/l, A_0= 2.05x10^{-2} mol/l, f_0= 1.0, (left faced triangle), T_0 = 132°C, I_0= 7x10^{-4}mol/l, A_0= 1.0x10^{-3} mol/l, f_0= 1.0, (right faced triangle);

(b) - T_0 = 168°C, I_0= 7x10^{-4}mol/l, A_0= 2.05x10^{-2} mol/l, f_0= 0.8, (circle), T_0 = 168°C, I_0= 4x10^{-4}mol/l, A_0= 8.90x10^{-3} mol/l, f_0= 0.8, (cross), T_0 = 168°C, I_0= 4x10^{-4}mol/l, A_0= 3.21x10^{-2} mol/l, f_0= 0.8, (right faced triangle), T_0 = 168°C, I_0= 1x10^{-3}mol/l, A_0= 3.21x10^{-2} mol/l, f_0= 0.8, (left faced triangle).

Fig. 4.2-11 shows the results obtained for MMA with CTA. The results are shown at different temperatures, initiator and CTA concentrations. The results are quite good in terms of matching with experimental data as well as with each other for numerical and analytical solution. We have taken a sample case out of them to show the results in Fig. 4.2-12 to Fig. 4.2-14 which are qualitatively similar to results already mentioned for styrene and MMA so far. The effect of algorithm to select the value of μ_2 based on R_L in each time step can be observed in Fig. 4.2-13. In this, the final graph of μ_2 lies between case2 and 3 based on values of R_L. Although the case2 matches well with the numerical solution but still it is not selected because of the values of the limits of R_L to move from one case to another. Match can be improved by changing the limits of different cases, as they are based on assumptions only.
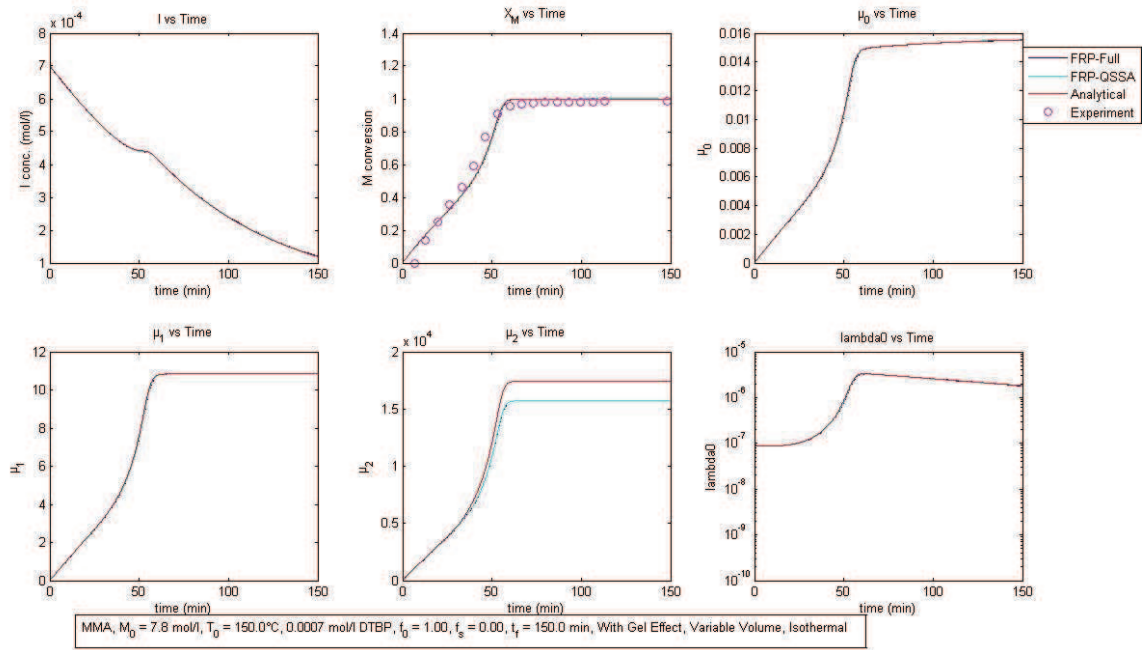
Fig. 4.2-12- CCS model results for MMA[9] with CTA- $I, x_m, \mu_0, \mu_1, \mu_2$ & λ_0
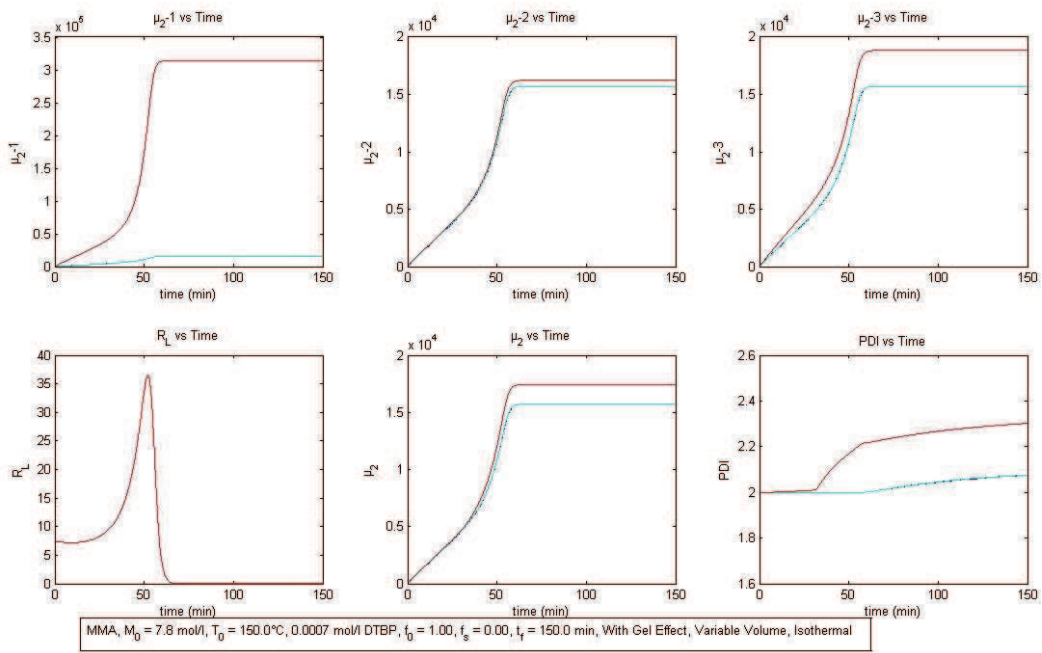
Fig. 4.2-13- CCS model results for MMA with CTA- calculation of three different cases of Analytical for μ_2 and its selection based on the value of R_L and thus PDI calculation
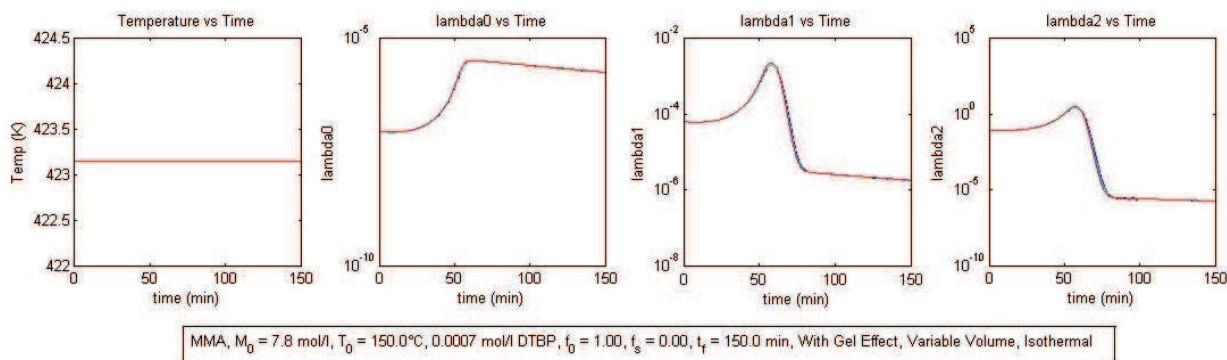
Fig. 4.2-14- CCS model results for MMA with CTA- $\lambda_0, \lambda_1, \& \lambda_2$

4.2.6 Discussion

Besides proposing this model in their work, CCS[4] had also investigated the error introduced by using QSSA as against the case of not using it. They found that for both these cases, the radical concentration λ_0 were identical to each other before the gel effect. Beyond that, they differ significantly. But despite that, the conversion predictions were similar in both the cases through the gel effect till the glass effect. They reasoned that this was because the difference between radical concentrations occurred in the region where polymerization reaction was not governed by radical concentration but by diffusion limitation i.e. mass transfer limitation. The effect on MW_w and MW_n were noticeable in the gel and glass effect regions but final MW_w was similar to one predicted using QSSA. Whereas MW_n was predicted lower using QSSA at end conversion with respect to the one not using QSSA.

This observation that using QSSA still gives similar results compare to one not using it, was also observed by Achilias et al.[12]. They had made this observation for copolymerization reaction. They found that despite the fact that QSSA was not valid at higher conversions, it did not affect the evaluation of conversion and MW_w but with a slight overestimation of MW_n. This was contrary to CCS where the observation regarding MW_w and MW_n were reverse. This could probably due to difference in type of reaction i.e. homopolymerization vs copolymerization, where for the latter, QSSA was required not just for total radical concentration but also for individual monomer radical concentrations.

From CCS model, λ_0 was found to be increased monotonically as shown in Fig. 4.2-4, Fig. 4.2-9 & Fig. 4.2-14. This is a significant deviation from the actual λ_0 profile during the conversion passing from gel effect to glass effect region. Soh and Sundberg[13] had described the whole vinyl polymerization in four phases. The first phase consisted of conventional kinetics where QSSA was applicable. Second phase characterized the gel effect where QSSA failed due to increase in radical concentration. The third phase described the slowing down of gel effect and the fourth phase defined the glass effect. Zhu et al.[14] confirmed the same prediction experimentally by obtaining the radical concentration profile through all these four phases. They clearly showed that during the third phase, the radical concentration decreased instead of increasing and during the fourth phase, it started rising again. The probable reason for the monotonic increasing behavior of λ_0 by CCS model is because the initiator efficiency

162

is assumed constant throughout the conversion. The initiator efficiency actually decreases due to diffusion limitation at higher conversion as shown by Russell et al.[15]. Zhu et al.[14] had also found the similar results. They also found that the initiator efficiency fell almost simultaneously with the fall in propagation rate constant. This decrease of initiator efficiency prevents the monotonic increase of radical concentration. Absence of this 'cage effect' limits the CCS model prediction capability to some extent.

There is another discrepancy with regard to the profile of K_t fall with respect to conversion. Soh and Sundberg[16] in their work of theoretical development for phase-III of vinyl polymerization, introduced residual termination rate coefficient, K_{tp}. They showed that this K_{tp} limited the gel effect by preventing K_t from falling limitlessly. Its presence led to plateau formation for K_t during phase-III. Buback[17] extended this theory further in his work. He had defined two categories of monomers 'A' & 'B' which differ from each other in terms of order of propagation rate coefficient and in segmental mobility. Type 'A' monomers had these value about 2-3 orders higher compared to type 'B'. All others characteristics were similar between these two types of monomers. There were four phases where K_t value was affected by various diffusion processes with conversion. The first phase was controlled by segmental diffusion, second by translational diffusion, third by reaction diffusion and fourth by diffusion controlled propagation[18]. This prevented the uniform fall of K_t through all these phases. In Type 'B' monomer, all these four phases were present whereas in type 'A', first phase was absent. MMA was categorized as type 'B' monomer. But in CCS model, we have observed that there is uniform fall. This affected the capability of CCS model to predict higher order molecular weight distributions.

Soh and Sundberg[13,19] also clearly explained that because there was relationship between reaction propagation rate and L with MW_n, and so dependence of kinetic rate coefficients on chain length did not come into picture. So any model that is not accounting for chain length dependence and is based on time-conversion data to obtain its adjustable parameters would naturally be able to fit the data well for MW_n, but would fail to do so for MW_w. In CCS model, the chain length dependence is accounted implicitly by term $C1$ expressed by eqn.55. Since the rest of the adjustable parameters of CCS model are obtained by best fit with the experimental data and the chain length dependence does not seemed to be properly accounted by $C1$, the poor prediction of CCS model for MW_w, seemed inevitable.

It can also be observed that the R_L spiked during gel effect as shown in Fig. 4.2-3, Fig. 4.2-8 & Fig. 4.2-13. This behavior is similar to parameter called as Gel effect index (GI) presented in the work by Achilias et al.[1] This spike behavior can be explained with the similar reasoning presented by them except with slight modification due to difference in the model. For explaining the behavior of R_L, we need to consider the graphs of conversion, R_L, K_t and K_{pr} at different times. During the phase for the conversion before the gel effect, R_L remains almost constant as K_t, K_{pr} remains constant- characteristics of conventional kinetics- first phase described by Soh and Sundberg[13]. Phase-II during which gel effect sets in, is characterized by the decrease in K_t, R_L starts increasing. This continues till the conversion where K_{pr} began to fall. Besides, the fall of K_{pr} is faster than K_t, so it leads to decrease in R_L.

This constitutes the third phase described by Soh and Sundberg[13]. This fall continues till glass effect sets in where K_t becomes much lower than K_{pr} and thus R_L flattens out. The authors[1] had also considered the effect of decrease of initiator efficiency during this phase due to diffusion limitation. But since it was not modeled here, it could not be taken into consideration.

It can be observed that in all the results presented in this work except for the μ_2 and thus for MW_w, and PDI, the AS matched quite well with numerical solutions. In addition to this, numerical solutions also matched with each other excellently. The match with experimental data for conversion and MW_n, was found to be good. Poor matching of numerical solution with the experimental data of MW_w is already discussed above and is due to the limitation of the gel model. The large difference in MW_w & PDI calculated by AS in Fig. 4.2-2 is mainly because of the problem in evaluation of μ_2 as shown in Fig. 4.2-3. The reasons being two fold – one, the numerical algorithm to evaluate the infinite series solution used in AS (eqn.(4-94) & (4-101)), and the second is the constant time step used throughout the simulation. We tried to modify the numerical algorithm to improve the calculation of infinite series but it paid till certain level only. With regard to constant time step, we did not implement any algorithm so that we could vary the time step especially during the gel effect so as to capture it properly. The variation during gel effect can be seen in Fig. 4.2-3 by the graph of parameter R_L. This is also the indication of the stiffness introduced by the variation of kinetic rate coefficients during gel effect. This justifies the use of stiff solver for solving ordinary differential equations of FRP_Full and FRP_QSSA. This discrepancy is found to reduce with increase in temperature as the gel effect is less severe then as shown for MMA in Fig. 4.2- 8.

The initiator concentration as shown in Fig. 4.2-1 & Fig. 4.2-6 seems to be little puzzling at first glance. The initiator concentration increased during the gel effect instead of decreasing and then decreased again. This can be explained quite easily in terms of volume variation effect. The moles of initiator would decrease monotonically with the conversion. But the reaction mixture volume would also be decreasing. Normally, the rate of polymerization is relatively slow so that the concentration of initiator continued to decrease. But during gel effect, the rate of polymerization increases quite a lot. This leads to significant variation of volume in small time and it can exceed the rate of moles consumption of initiator. This leads to increase of initiator concentration. This effect is more dominant at lower temperatures and is decreased with increase of temperature as can be seen from Fig. 4.2-6. This is because the gel effect shifts to higher conversion with increasing temperature for a given initiator. Besides this, the change in volume is also low at higher conversion as it is already near to final value.

4.2.7 Conclusion

AS has been shown to be successfully integrated with CCS model for gel/glass effect. It was found to work well for different monomers, with variations in temperature, initiator & its concentration and chain transfer agent. The results match quite well with numerical solution of both FRP_Full and FRP_QSSA and experimental data. Besides this, FRP_Full and FRP_QSSA have been shown to have similar results during gel/glass effect despite the fact that QSSA breaks down during gel effect. This result can be used to choose simpler model FRP_QSSA thus reducing the number of variables to be solved through differential equations.

The stiffness of equations arises by change in kinetic rate coefficients during gel effect. The analytical solution seems to work well to face this stiffness easily at least at higher temperatures by using constant time step.

In this section, the CCS model was implemented in our analytical solution to take into account the gel and glass effects. However, this model aggregates all the parameters responsible for the variations of the diffusion coefficient in one single temperature dependent parameter that has to be determined by best fitting with experimental data. Furthermore, this model does not take into account the effect of polymer chain length resulting in a poor match of MW_w and hence PDI. Therefore in the following section, another model (Achilias & Kiparissides, AK model) will be considered to simulate not only the gel/glass effect but also the cage effect which can be significant especially at high solvent volume fractions or at high monomer conversion. This model has an edge over the CSS model in the sense that it does not require any best fitting with experimental data. It relies on the Free Volume Theory to calculate the diffusion coefficients of all the species.

4.2.8 References

1. Achilias, D. S.; Kiparissides, C., Development of a General Mathematical Framework for Modeling Diffusion-Controlled Free-Radical Polymerization Reactions. *Macromolecules* **1992,** *25* (14), 3739-3750.

2. Qin, J. G.; Guo, W. P.; Zhang, Z., Modeling of the bulk free radical polymerization up to high conversion - three stage polymerization model I. Model examination and apparent reaction rate constants. *Polymer* **2002,** *43* (4), 1163-1170.

3. Tulig, T. J.; Tirrell, M., Toward a Molecular Theory of the Trommsdorff Effect. *Macromolecules* **1981,** *14* (5), 1501-1511.

4. Chiu, W. Y.; Carratt, G. M.; Soong, D. S., A Computer-Model for the Gel Effect in Free-Radical Polymerization. *Macromolecules* **1983,** *16* (3), 348-357.

5. Garg, D. K.; Serra, C. A.; Hoarau, Y.; Parida, D.; Bouquey, M.; Muller, R., Analytical Solution of Free Radical Polymerization: Derivation and Validation, *to be published*.

6. Venkateshwaran, G.; Kumar, A., Solution of Free-Radical Polymerization. *Journal of Applied Polymer Science* **1992,** *45* (2), 187-215.

7. Marten, F. L.; Hamielec, A. E., High-Conversion Diffusion-Controlled Polymerization of Styrene .1. *Journal of Applied Polymer Science* **1982,** *27* (2), 489-505.

8. Balke, S. T.; Hamielec, A. E., Bulk Polymerization of Methyl Methacrylate. *Journal of Applied Polymer Science* **1973,** *17*, 905-949.

9. Fenouillot, F.; Terrisse, J.; Rimlinger, T., Polymerization of methyl methacrylate at high temperature with 1-butanethiol as chain transfer agent. *Journal of Applied Polymer Science* **1999,** *72* (12), 1589-1599.

10. Baillagou, P. E.; Soong, D. S., Major Factors Contributing to the Nonlinear Kinetics of Free-Radical Polymerization. *Chem Eng Sci* **1985,** *40* (1), 75-86.

11. Lima, E. V.; Guerra, E. S., Digital Simulation of Bulk and Suspension Polymerization of Styrene, Using Non-linear Regression for Curve Fitting the Kinetic Parameters. *Journal of Reinforced Plastics and Composites* **1993,** *12* (7), 800-812.

12. Achilias, D. S.; Kiparissides, C., On the Validity of the Steady-State Approximations in High Conversion Diffusion-Controlled Free-Radical Copolymerization Reactions. *Polymer* **1994,** *35* (8), 1714-1721.

13. Soh, S. K.; Sundberg, D. C., Diffusion-Controlled Vinyl Polymerization .1. The Gel Effect. *J Polym Sci Pol Chem* **1982,** *20* (5), 1299-1313.

14. Zhu, S.; Tian, Y.; Hamielec, A. E.; Eaton, D. R., Radical Concentrations in Free-Radical Copolymerization of Mma/Egdma. *Polymer* **1990,** *31* (1), 154-159.

15. Russell, G. T.; Napper, D. H.; Gilbert, R. G., Initiator Efficiencies in High-Conversion Bulk Polymerizations. *Macromolecules* **1988,** *21* (7), 2141-2148.

16. Soh, S. K.; Sundberg, D. C., Diffusion-Controlled Vinyl Polymerization .3. Free-Volume Parameters and Diffusion-Controlled Propagation. *J Polym Sci Pol Chem* **1982,** *20* (5), 1331-1344.

17. Buback, M., Free-Radical Polymerization up to High Conversion - a General Kinetic Treatment. *Makromol Chem* **1990,** *191* (7), 1575-1587.

18. Achilias, D. S., A review of modeling of diffusion controlled polymerization reactions. *Macromol Theor Simul* **2007,** *16* (4), 319-347.

19. Soh, S. K.; Sundberg, D. C., Diffusion-Controlled Vinyl Polymerization .4. Comparison of Theory and Experiment. *J Polym Sci Pol Chem* **1982,** *20* (5), 1345-1371.

4.3 Analytical Solution of Free Radical Polymerization: Applications- Implementing Gel effect using AK Model

4.3.1 Abstract

In this work, gel/glass/cage effects using AK model has been incorporated in the analytical solution (AS) obtained in previous work. AK model is based on CCS model and free volume theory. The results of AS matched quite well with the numerical solutions as well as with the experimental data for methyl methacrylate (MMA). Various variables like termination kinetic coefficient, initiator efficiency, macroradicals concentration profile matched with the established published results. The work clearly demonstrates that AS is sufficiently flexible to accommodate gel/glass/cage effects explicitly although it was not primarily derived for these conditions. This extends the practical usage of AS for the whole range of conversion under isothermal conditions.

Keywords- Analytical solution, free radical polymerization, styrene, methyl methacrylate, AK model, gel effect, glass effect, cage effect, free volume theory

4.3.2 Introduction

Diffusion is one physical phenomenon which affects the polymerization reaction very significantly. As conversion increases, the viscosity of the reaction mixture also increases almost exponentially. This significant increase in viscosity affects severely diffusion of various chemical species like monomer, initiator, polymer radicals, in the reaction mixture. This leads to various significant effects during polymerization depending on the chemical species whose diffusion has decreased. Decrease in polymer translational and segmental diffusion leads to gel effect or Trommsdorff effect, decrease in monomer diffusion leads to glass effect and decrease in initiator diffusion leads to cage effect[1]. Another important thing about these effects is that they don't appear randomly but in a particular sequence only. Gel effect appears first as the polymer bigger in size, are naturally influenced by increasing viscosity earlier than other species which are comparatively much lighter. With further increase in viscosity with conversion appears the cage effect as initiator finds it more difficult to reach monomer before getting consumed. If the reaction is occurring below the glass temperature of the polymer, then with further increase in viscosity due to higher conversion leads to the third effect- glass effect. In this, the viscosity becomes so high and the diffusion is so low that even the monomer is not able to move from its position and the reaction almost freezes.

Due to detrimental effects of gel, glass effect, cage effect, it becomes necessary to take care of them during the reaction. A good mathematical model can help in determining conditions for preventing them or reducing their effect without actually conducting any costly experiment. As from the above description, it may seem that these effects occur after certain conversion level only. Indeed many researchers have modeled these effects with critical conversion values after which relevant effect is modeled. But this approach does not help much in different conditions and is not generalized in nature. In reality, the initiation of any effect is not sudden but gradual. Chiu, Carratt & Soong (CCS)[2] had attempted this problem and successfully worked out a model addressing it.

168

The current work is extension of our previous work[3] on the implementation of gel/ glass effect using CCS model[2] in the analytical solution (AS) obtained in our earlier work[4]. The purpose of such work was to demonstrate the flexibility and applicability of AS even to those conditions for which it was not derived for. This includes the variation in various kinetic rate coefficients, initiator efficiency and temperature. This requires a smart strategy/ algorithm so as to enable AS to be applicable under those conditions. This strategy in simple terms includes the use of time-steps small enough so that the various variables mentioned above can be assumed to be constant and the evaluation of all the variables at the beginning of each time-step. For details, previous work can be consulted[3,4]. Using this strategy, the variation in the kinetic rate coefficients was incorporated successfully in previous work. The current work includes the incorporation of variation in initiator efficiency (cage effect) with further improvement of the diffusion model for which free volume theory[5,6] is used. There is a good review on free volume theory by Ramesh *et al.*[7] The incorporation of variation of temperature in AS will be presented in our future work.

In our previous work, the integration of the CCS model of gel/glass effect with the analytical solution was smooth. Its validation with numerical solution (NS) as well as experimental data was also done. The match of AS with NS was excellent for all variables except for μ_2, under all conditions. This difference was observed at low temperature and was due to numerical stiffness of the system arising out of gel effect. To remove this stiffness, smaller time-step were required in the region of gel effect. But this was not the case for AS where only constant time-steps were taken. At higher temperature, this problem was not observed due to reduction in stiffness. The match with the experimental data was good for monomer conversion and MW_n but the match with MW_w was poor. The reason for this was the inherent limitations of CCS model. This includes not accounting for the cage effect as well as not accounting the proper effect of chain length on kinetic rate coefficients. To overcome these limitations, a better theoretical model accounting for these effects was required.

Achilias and Kiparissides (AK) presented a new model that extends the CCS model[8]. Unlike CCS model for which all the parameters responsible for the variations of the diffusion coefficient were aggregated in one single temperature dependent parameter that had to be determined by best fitting with experimental data, diffusion terms were retained. Each effect required different species diffusion coefficient mentioned earlier. These diffusion coefficients were evaluated using free volume theory in their model and thus successfully incorporated the effect of chain length on kinetic rate coefficients. But the K_t profile obtained for MMA was still similar to the one obtained by CCS model which was different from the profile for type 'B' monomer categorized by Buback[9]. AK later refined their model and also incorporated cage effect in it[1]. This time, they obtained the correct K_t profile as well as matched radical concentration model prediction with experimental data by Zhu *et al.*[10] One of the important benefits of this model was the absence of adjustable parameters except for one. All the variables used in this model were physical constants. We have used this AK model with some improvements introduced by Keramopoulos *et al.*[11]

4.3.3 Theory

4.3.3.1 Reaction mechanism and kinetic equations
The detailed kinetic scheme used in this thesis is given in section 3.2.2. The relevant mathematical model is presented in section 3.2.3.

4.3.3.2 Analytical solution
The summary of analytical solution in time-step format is given in section 4.1.5.

4.3.3.3 AK model
The AK model and its constitutive equations are given in section 3.2.7.

4.3.3.4 Physical and chemical data
The physical and chemical data for MMA are given in Table 3-1, for AIBN in Table 3-3 and for toluene in Table 3-4.

4.3.4 Methodology
The details of mathematical models FRP_Full and FRP_QSSA are given in section 3.2.4. For Analytical, details are given in section 4.1.7. The methodology adopted here was similar to the one adopted section 4.2.4. Constant time step was used for Analytical, which was taken to be 0.1 s.

4.3.5 Results
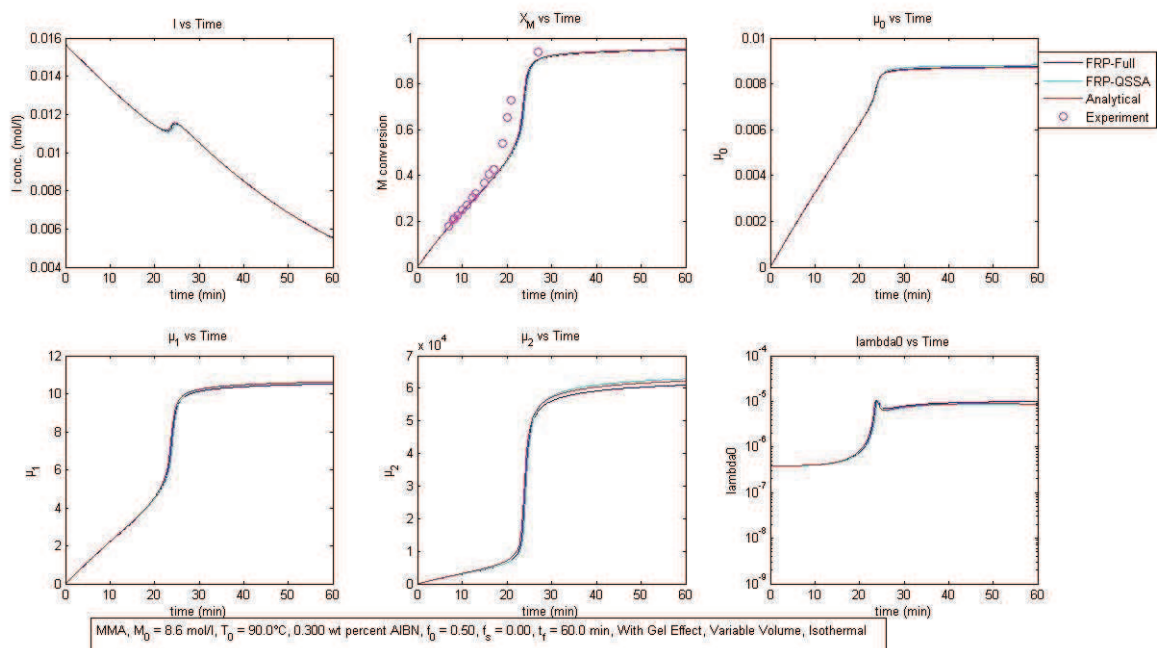
Fig. 4.3-1-AK model results for MMA[13]- $I, x_m, \mu_0, \mu_1, \mu_2$ & λ_0 [13]

As can be seen in Fig. 4.3-1, The results are in excellent matching not only with each other but also for the conversion also. The graph of μ_2 for AS is also in good agreement with the NS. The result obtained by FRP_Full and FRP_QSSA match with each other as explained in

170

discussion section. The reason for increase in initiator concentration during gel effect is also discussed there.
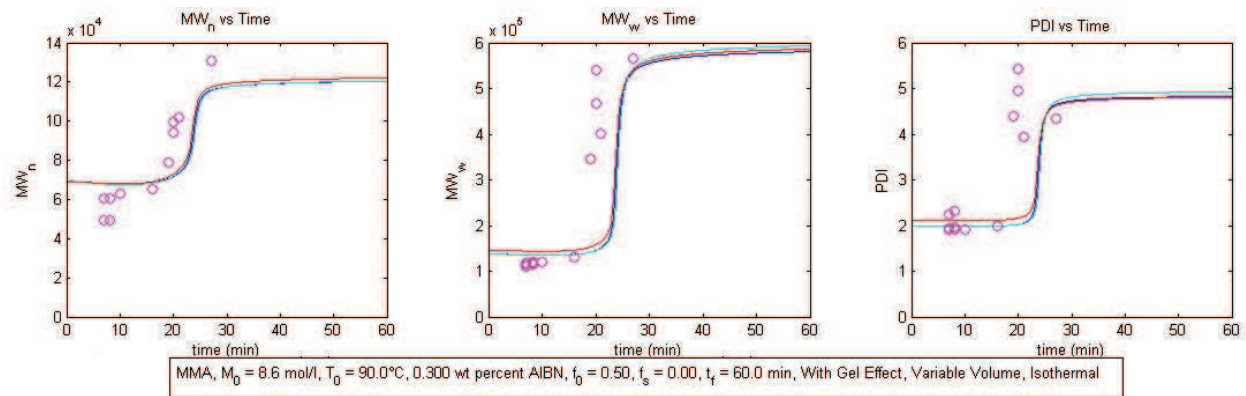
Fig. 4.3-2- AK model results for MMA[13]- $MW_n, MW_w, \& PDI$[13]

Fig. 4.3-2 shows the excellent match of the experimental data with AS as well as with NS. Again, numerical solutions match quite well with each other and also with AS. This is the important improvement against the previous model used.
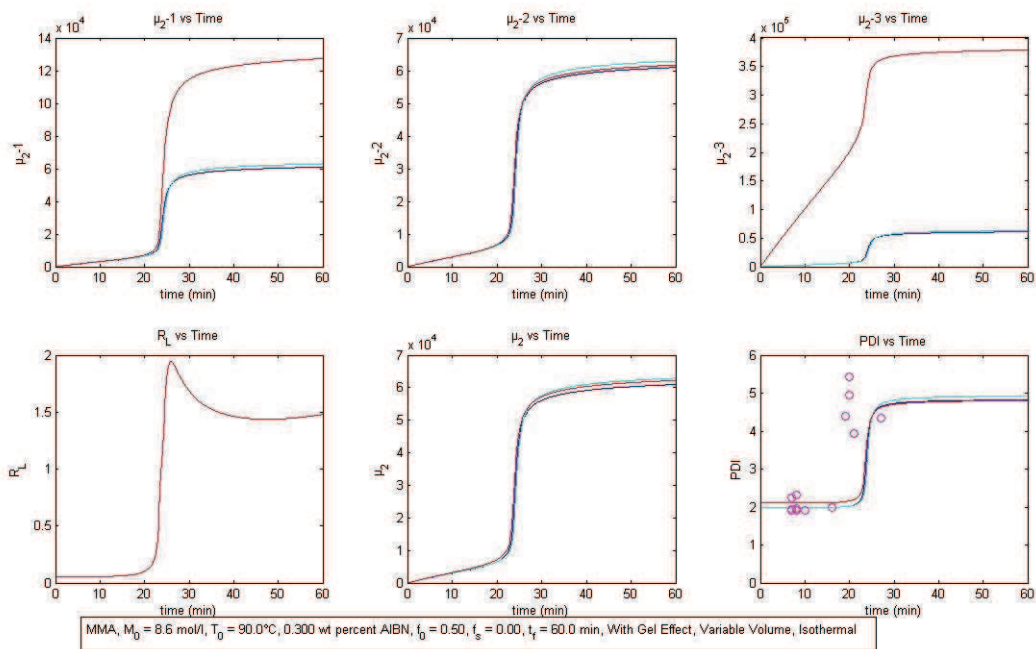
Fig. 4.3-3- AK model results for MMA[13]- calculation of three different cases of AS for μ_2 and its selection based on the value of R_L and thus PDI calculation[13]

The algorithm for selecting correct value of μ_2 from the three cases based on the value of R_L.had also worked well as shown in Fig. 4.3-3. This resulted in correct prediction of MW_w and thus better prediction of PDI as shown in Fig. 4.3-2. The difference between AS and NS is also not significant for μ_2.
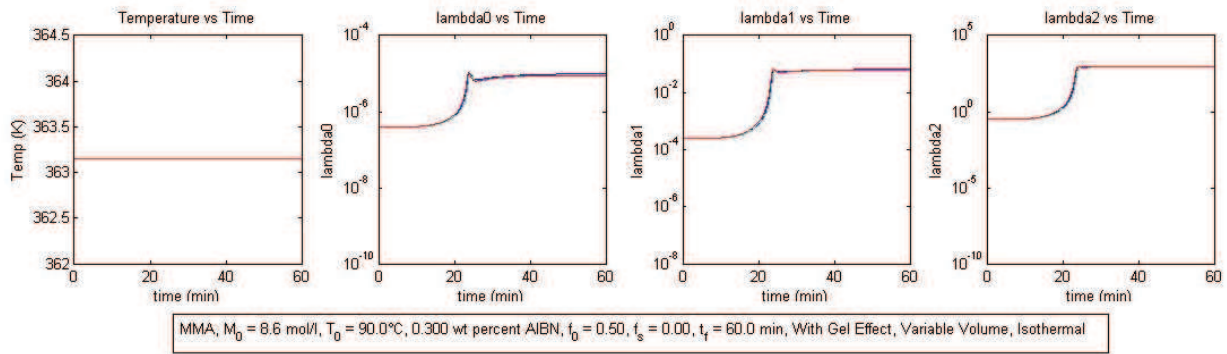
Fig. 4.3-4- AK model results for MMA- $\lambda_0, \lambda_1, \& \lambda_2$

Fig. 4.3-4 shows the excellent match between AS and NS. It shows clearly that AS has been able to capture all the variations in $\lambda_0, \lambda_1, \& \lambda_2$ successfully.
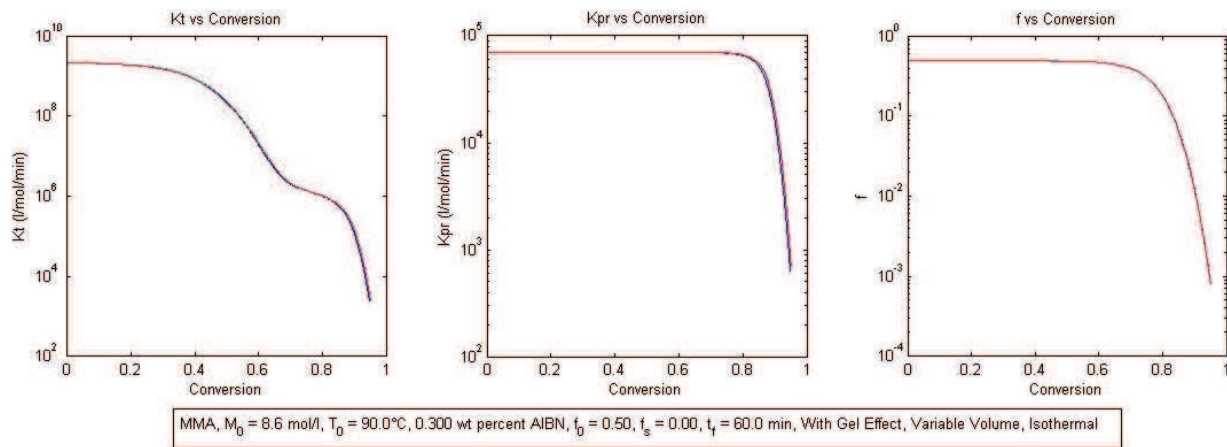
Fig. 4.3-5- AK model results for MMA- $K_t, K_{pr} \& f$.

Fig. 4.3-5 shows the graphs of $K_t, K_{pr} \& f$. The results of AS and NS match excellently with each other as well as experimental data[13] in all the result shown in Fig. 4.3-1 to Fig. 4.3-5.

4.3.6 Discussion

CCS[2] found that despite the significant difference between radical concentrations during gel effect, the conversion predictions were similar in both the cases with and without QSSA, up to the glass effect. They reasoned that this was due to diffusion limitation i.e. mass transfer limitation in the region where the difference between radical concentrations occurred. In that region, polymerization reaction was no longer governed by radical concentration. Similar observation was made by Achilias *et al.*[14]. They had made this observation for copolymerization reaction.

λ_0 as shown in Fig. 4.3-4, is also representing the correct trend for all the four phases defined by Soh and Sundberg[15]. In the phase-I before the gel effect, it remains nearly constant following QSSA. Then during phase-II, gel effect sets in and QSSA breaks down and it starts rising. Then during the phase-III, it starts falling and then in phase-IV, on the onset of glass effect, it starts rising again. This is also in agreement with experimental data by Zhu *et al.*[10]

172

unlike the previous model (CCS) where it continued to increase monotonically reaching a plateau without decreasing anywhere.

The initiator efficiency f as shown in Fig. 4.3-5, decreases due to diffusion limitation at higher conversion. This same was shown experimentally by Russell *et al.*[16]. Zhu *et al.*[10] had also found the similar results. Besides this, they also found that f fell almost simultaneously with the fall in K_{pr} and the same can be observed in Fig. 4.3-5. This adds to the credibility of the model as well as the results obtained using AS.

The graph of K_{pr} is exactly as per theory given by Buback[9]. He described MMA as type 'B' monomer characterized by four phases. In these four phases, K_t was affected by various diffusion processes. This prevented K_t from falling uniformly through all these phases. AK model also included residual termination rate coefficient K_{res} given by Soh and Sundberg[17] which is also important to model this behavior of K_t

R_L, as shown in Fig. 4.3-3, is also representing the correct trend explained by AK[1] for Gel effect Index (GI). In the phase-I before the gel effect, it remains nearly constant. Then during gel effect, it starts rising due to decrease in K_t. Then during the phase-III, it starts falling due to higher decrease in K_{pr} and then on the onset of glass effect (Phase-IV), it starts rising again due to more decrease.in K_t compared to K_{pr}.

The increase in initiator concentration during gel effect as shown in Fig. 4.3-1, is already explained in our previous work[3] in detail. It is due to faster decrease in reaction mixture volume compared to decrease in initiator moles during the gel effect.

4.3.7 Conclusion

AK model has been successfully implemented in AS. By using free volume theory in AK model, gel, glass and cage effects have been modeled with good success. By taking into account the effect of polymer chain lengths on macromolecules diffusion coefficient, this model has been successful in predicting the correct profile and variation of chain lengths distribution based on number and weight. Thus, it has been able to predict the more important characteristics of polymerization like monomer conversion, MW_n, MW_w, and PDI. The added advantage over CCS model was the absence of any parameter requiring best fit with experimental data. The only parameters required to apply AK model are the physical and chemical data of chemical species that are readily available in literature. The AS matched quite well with experimental data as well as with NS. FRP_Full and FRP_QSSA also matched with each other in-line with the observations made by other researchers.

In this section the AK model was successfully implemented in our analytical solution of FRP for isothermal condition. However, in many situations, isothermal condition gets easily breakdown due to various reasons like poor heat transfer, cooling failure etc. So any good model should also work equally well for non-isothermal conditions to make it useful under all conditions of operation. In the following section, thermal effect will be considered by the adjunction of an additional equation reflecting the energy balance of the reactor getting inputs from AS.

4.3.8 References

1. Achilias, D. S.; Kiparissides, C., Development of a General Mathematical Framework for Modeling Diffusion-Controlled Free-Radical Polymerization Reactions. *Macromolecules* **1992,** *25* (14), 3739-3750.

2. Chiu, W. Y.; Carratt, G. M.; Soong, D. S., A Computer-Model for the Gel Effect in Free-Radical Polymerization. *Macromolecules* **1983,** *16* (3), 348-357.

3. Garg, D. K.; Serra, C. A.; Hoarau, Y.; Parida, D.; Bouquey, M.; Muller, R., Analytical Solution of Free Radical Polymerization, I-Implementing Gel Effect using CCS Method. *to be published*.

4. Garg, D. K.; Serra, C. A.; Hoarau, Y.; Parida, D.; Bouquey, M.; Muller, R., Analytical Solution of Free Radical Polymerization: Derivation and Validation. *to be published*.

5. Vrentas, J. S.; Duda, J. L., Diffusion in Polymer - Solvent Systems .1. Re-Examination of Free-Volume Theory. *J Polym Sci Pol Phys* **1977,** *15* (3), 403-416.

6. Vrentas, J. S.; Duda, J. L., Diffusion in Polymer-Solvent Systems .2. Predictive Theory for Dependence of Diffusion-Coefficients on Temperature, Concentration, and Molecular-Weight. *J Polym Sci Pol Phys* **1977,** *15* (3), 417-439.

7. Ramesh, N.; Davis, P. K.; Zielinski, J. M.; Danner, R. P.; Duda, J. L., Application of Free-Volume Theory to Self Diffusion of Solvents in Polymers Below the Glass Transition Temperature: A Review. *J Polym Sci Pol Phys* **2011,** *49* (23), 1629-1644.

8. Achilias, D.; Kiparissides, C., Modeling of Diffusion-Controlled Free-Radical Polymerization Reactions. *Journal of Applied Polymer Science* **1988,** *35* (5), 1303-1323.

9. Buback, M., Free-Radical Polymerization up to High Conversion - a General Kinetic Treatment. *Makromol Chem* **1990,** *191* (7), 1575-1587.

10. Zhu, S.; Tian, Y.; Hamielec, A. E.; Eaton, D. R., Radical Concentrations in Free-Radical Copolymerization of Mma/Egdma. *Polymer* **1990,** *31* (1), 154-159.

11. Keramopoulos, A.; Kiparissides, C., Development of a comprehensive model for diffusion-controlled free-radical copolymerization reactions. *Macromolecules* **2002,** *35* (10), 4155-4166.

12. Zielinski, J. M.; Duda, J. L., Predicting Polymer Solvent Diffusion-Coefficients Using Free-Volume Theory. *Aiche J* **1992,** *38* (3), 405-415.

13. Balke, S. T.; Hamielec, A. E., Bulk Polymerization of Methyl Methacrylate. *Journal of Applied Polymer Science* **1973,** *17*, 905-949.

14. Achilias, D. S.; Kiparissides, C., On the Validity of the Steady-State Approximations in High Conversion Diffusion-Controlled Free-Radical Copolymerization Reactions. *Polymer* **1994,** *35* (8), 1714-1721.

15. Soh, S. K.; Sundberg, D. C., Diffusion-Controlled Vinyl Polymerization .1. The Gel Effect. *J Polym Sci Pol Chem* **1982,** *20* (5), 1299-1313.

16. Russell, G. T.; Napper, D. H.; Gilbert, R. G., Initiator Efficiencies in High-Conversion Bulk Polymerizations. *Macromolecules* **1988,** *21* (7), 2141-2148.

17. Soh, S. K.; Sundberg, D. C., Diffusion-Controlled Vinyl Polymerization .3. Free-Volume Parameters and Diffusion-Controlled Propagation. *J Polym Sci Pol Chem* **1982,** *20* (5), 1331-1344.

4.4 Analytical Solution of Free Radical Polymerization: Applications-Implementing Non-isothermal Effect

4.4.1 Abstract

Analytical solution (AS), as derived in our previous work for free radical polymerization (FRP), has been used under non-isothermal conditions in this work. Only one differential equation, i.e. energy balance equation, was required to calculate temperature profile by stiff solver using AS as input values. The results were compared against the numerical solution (NS) of the complete set of ordinary differential equations (ODE) of FRP, 11 ODE for full set of equations (FRP_Full), and 8 ODE for quasi-steady state approximation (FRP_QSSA). Two different models namely Chiu, Carratt & Soong (CCS) and Achilias & Kiparissides (AK), for implementing gel/glass/cage effect, were also considered. The results were validated against published results and were found to be in excellent agreement with NS for all conditions taken. This work proved the versatility, flexibility and adaptablity of AS under all conditions (except for low temperatures) and with various models to simulate gel/glass/cage effect along with non-isothermal conditions.

Keywords

4.4.2 Introduction

One of the key requirements to control exo and endothermic reactions is the strict management of temperature. Indeed, in first place temperature affects kinetic rate coefficients of different reaction paths through their activation energy. Higher temperature usually increases rates of exothermic reactions and thus decreases reaction time to reach a given conversion. The beneficial consequence is an increase in productivity or space time yield for continuous-flow reactors. But depending on the reaction type, this increase in temperature may trigger unwanted side reactions, change phases equilibrium, affect reactants and products solubility and so on. This can limit the temperature range of operation. Temperature rise may also be required to reduce the viscosity of the reaction mixture to reduce pumping power especially in case of polymers. In many exothermic reactions, loss of temperature control may lead to thermal runaways in the absence of an appropriate heat sink capacity. This is quite detrimental to the safety, maintenance and plant operation. Temperature variations may also lead to the formation of wide range of side products thus decreasing the overall quality of the desired product.

Polymerization reactions are one such type of reactions where temperature and its control play a very vital role in controlling the quality of the product. Unlike other reaction types, conversion is not the most important parameter. One of the important characteristics of the polymerization reaction is to produce product with having number average molecular weight (MW_n), polydispersity index (PDI), branching etc. in a narrow specified range. Otherwise product may be useless for the desired application.

The various properties of polymers are strong function of temperature. So in some cases, even small temperature changes may lead to large variation in the product quality. These temperature variations may occur due to improper mixing, poor cooling/heating arrangement etc. combined with exothermic nature of polymerization reactions. There are various phenomena interrelated with temperature in case of polymerization. Polymer reaction mixture viscosity increases almost exponentially with conversion, so to handle and properly mix such a highly viscous fluid, large mechanical power is required which in turn may contribute to increase the temperature by viscous dissipation. To reduce this power, higher temperature is desirable so as to reduce the viscosity. Another way of reducing viscosity could be the addition of some solvent to the reaction mixture. But this option may be limited by the product quality requirement as well as the downstream solvent separation and recovery processes. Inefficient solvent separation process may deteriorate the quality of the product and inefficient solvent recovery processes may make the operation costly. By increasing temperature, one can increase the polymerization rate but it also increases the decomposition of initiator especially in case of free radical polymerization (FRP) initiated by thermal activation of initiator. This may lead to the situation of incomplete conversion due to the rapid initiator decomposition[1]. This problem can be overcome by adding more initiator but it significantly decreases the molecular weight.

It would always be helpful if there is some study which can help in predicting such undesirable conditions beforehand. The same study could also be used to search for optimum temperature and other parameters value that would optimize the product quality and production rate. Most of the experimental data and numerical solution available is about isothermal conditions[2-7]. Very less research has been done in the field of non-isothermal behavior of polymerization reactions. Baillagou & Soong[1,8] have done such study. But there study is numerical. They have used Chiu, Carratt & Soong[9] (CCS) method for implementing gel/glass effect. They have been able to show various practical aspects of temperature variation under various conditions like different heat sink temperature, initiator concentration, overall heat transfer coefficient, solvent fraction. They have studied the molecular weight distribution, conversion and temperature variation in all such combinations of situations.

Ray *et al.*[10] and Srinivas *et al.*[11] have studied experimentally the stepwise variation in temperature. They have also developed a mathematical model using CCS model with free volume theory. But this model was semi-theoretical in nature as they had used best fit correlations to match the experimental data. They performed the step-increase and step-decrease of temperature at two different times each. They validated their modeling results with experimental data. Sangwai *et al.*[12] have also performed similar work but with an empirical mathematical model with best fit correlations.

Venkateshwaran *et al.*[13] done such non-isothermal study too, using the AS they have derived and tried to compare the results of AS and numerical solution (NS) for isothermal and non-isothermal condition with and without gel conditions. They have used CCS model for implementing gel/glass effect. All this was done for constant volume condition. There match of AS with NS was not that good and the AS they derived was quite complicated, cumbersome and lengthy.

We have derived an analytical solution of the free radical polymerization in our previous work[14] for isothermal, homogeneous, bulk/solution, without gel effect, variable volume batch reactor. We later extended our work[15] to implement gel and glass effect using CCS model. We then further improved our AS[16] by replacing it with Achilias & Kiparissides[17] (AK) model which incorporates CCS model with free volume theory for diffusion coefficients for monomer, polymer and initiator. All these previous works were done at constant temperature. The key objective of this work is to present the implementation of non-isothermal effects in the analytical solution (AS) we have obtained in our previous work. This current work demonstrates the complete versatility of AS with respect to changes in temperature, kinetic rate coefficients and initiator efficiency. The results are obtained for 1) no gel/glass/cage effect, 2) with gel/glass effect with CCS model, and 3) with gel/glass/cage effect using AK model. AS results are then compared with respective numerical solutions. They are also validated against published numerical results[1,8].

4.4.3   Theory

4.4.3.1   Reaction mechanism and kinetic equations
The detailed kinetic scheme used here is given in section 3.2.2. The relevant mathematical model is given in section 3.2.3.

4.4.3.2   Analytical solution
The summary of the analytical solution in time-step format is given in section 4.1.5.

4.4.3.3   CCS model
The CCS model and its constitutive equations are given in section 3.2.6

4.4.3.4   AK model
The AK model and its constitutive equations are given in section 3.2.7.

4.4.3.5   Physical and chemical data
The physical and chemical property data for MMA are given in Table 3-1, for AIBN in Table 3-3 and for toluene in Table 3-4.

4.4.4   Methodology
The details of mathematical models FRP_Full and FRP_QSSA are given in section 3.2.4. For Analytical, details are given in section 4.1.7. The methodology adopted here was similar to the one adopted section 4.2.4 and section 4.3.4. Constant time step was used for Analytical, which was taken to be 0.1 s.

The results are obtained for the polymerization of methyl methacrylate (MMA). Two types of heat transfer cases are considered: one with fixed heat transfer rate and the other one where heat transfer is neglected, i.e. adiabatic condition. The latter case represents the worst condition from thermal point of view as the heat release by the polymerization remains inside

the reactor and leads to a temperature increase. Overall heat transfer coefficient U is taken along with heat transfer area A_H i to make the analysis independent of individual variation of U and A_H. Initial reaction temperature was taken to be $90°C$ in all cases for the sake of simplicity. Heat sink temperature T_{bath} was taken to be same as initial reaction temperature to simulate isothermal condition.

4.4.5 Results

Fig. 4.4-1 to Fig. 4.4-3 show the results for the condition without any gel/glass/cage effect with different heat transfer rates from $UA = 1000 \, cal/min/K$ (Fig. 4.4-1) to adiabatic condition for which $UA = 0 \, cal/min/K$ (Fig. 4.4-3). They clearly showed that temperature profile predicted by AS matched excellently with NS in all cases. The match with other variables predicted is also good.

MMA, M_0 = 8.6 mol/l, T_0 = 90.0°C, 0.300 wt percent AIBN, f_0 = 0.50, f_s = 0.00, t_f = 50.0 min, UA = 1000.0, No Gel Effect, Variable Volume, Non-Isothermal
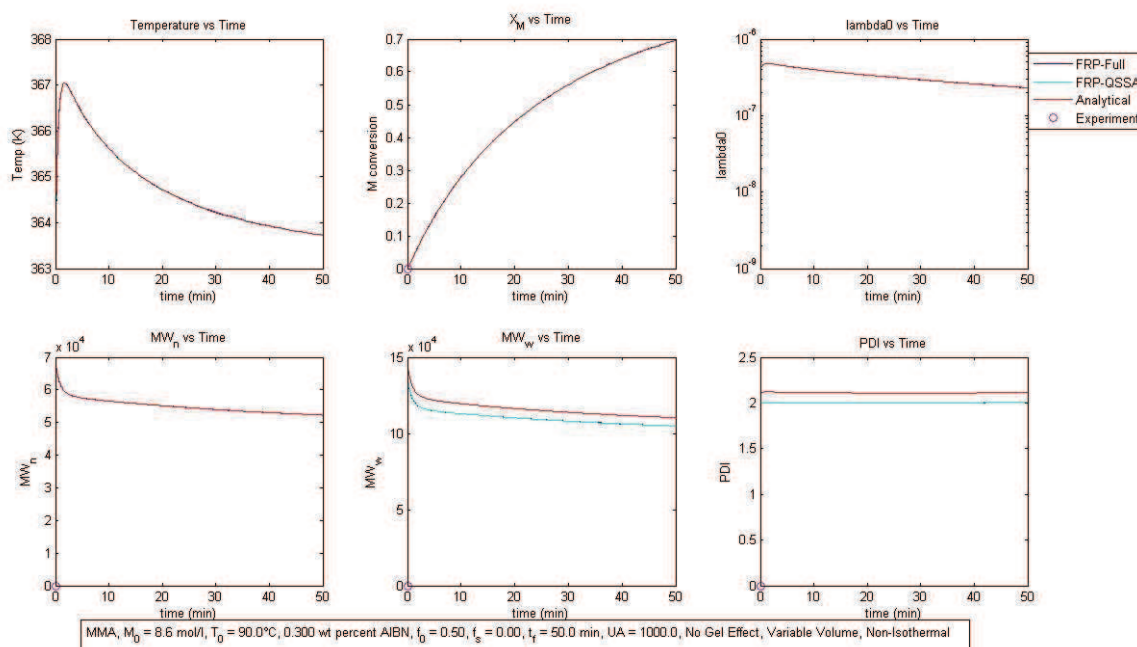
Fig. 4.4-1-MMA- Results obtained for temperature variation with $UA = 1000 \, cal/min/K$ for no gel/glass/cage effect

MMA, M_0 = 8.6 mol/l, T_0 = 90.0°C, 0.300 wt percent AIBN, f_0 = 0.50, f_s = 0.00, t_f = 50.0 min, UA = 500.0, No Gel Effect, Variable Volume, Non-Isothermal
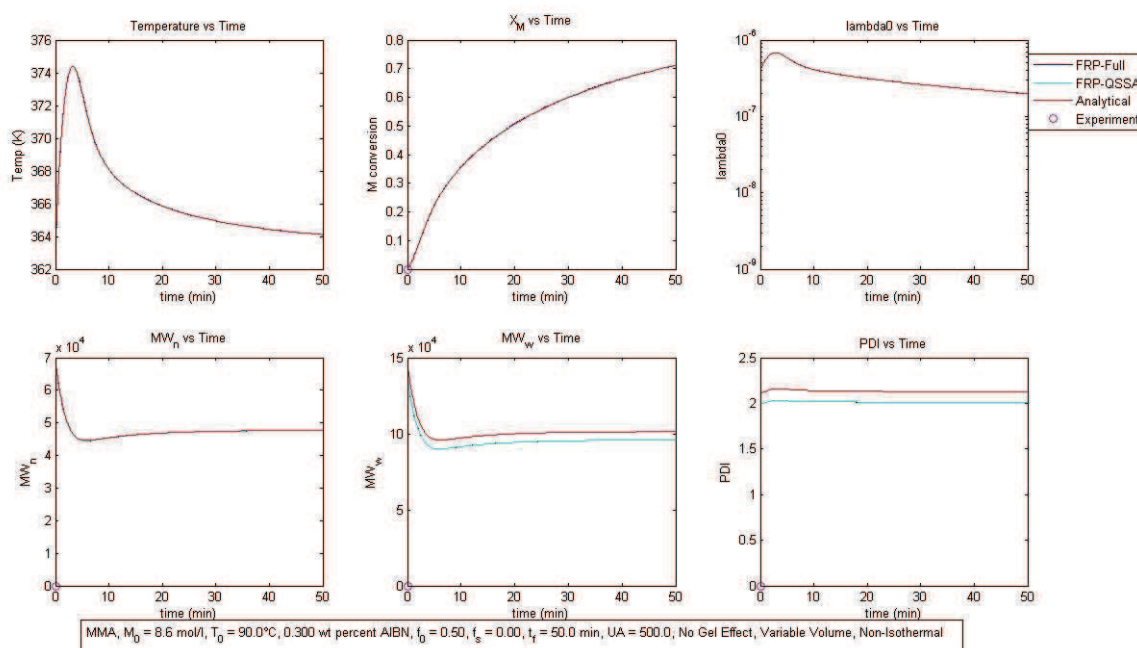
Fig. 4.4-2- MMA- Results obtained for temperature variation with $UA = 500 \, cal/min/K$ for no gel/glass/cage effect
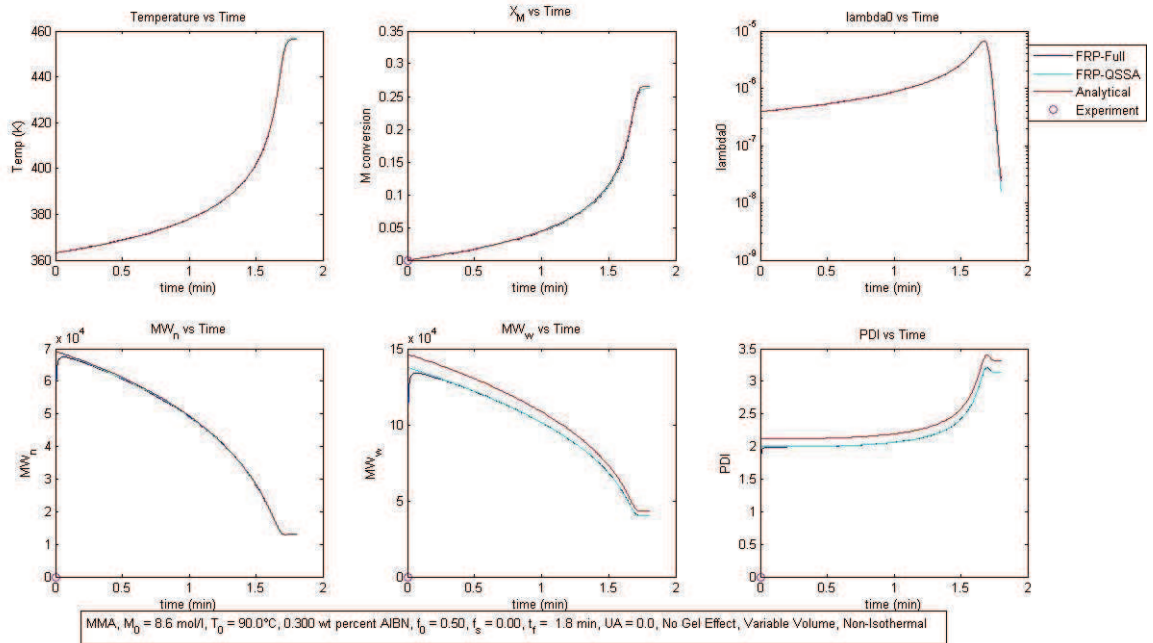
Fig. 4.4-3- MMA- Results obtained for temperature variation with $UA = 0\ cal/min/K$
(adiabatic) for no gel/glass/cage effect

Fig. 4.4-4 to Fig. 4.4-7 show the results for conditions implementing gel/glass effect using CCS model. Fig. 4.4-4 and Fig. 4.4-5 show the results for $UA = 1000\ cal/min/K$ whereas Fig. 4.4-6 and Fig. 4.4-7 show the results for adiabatic condition. Fig. 4.4-5 and Fig. 4.4-7 show the results for variation in K_t and K_{pr} with temperature change. f was held constant in this model. It can be observed that here too, AS matches excellently with NS predicted temperature profile and other variables.
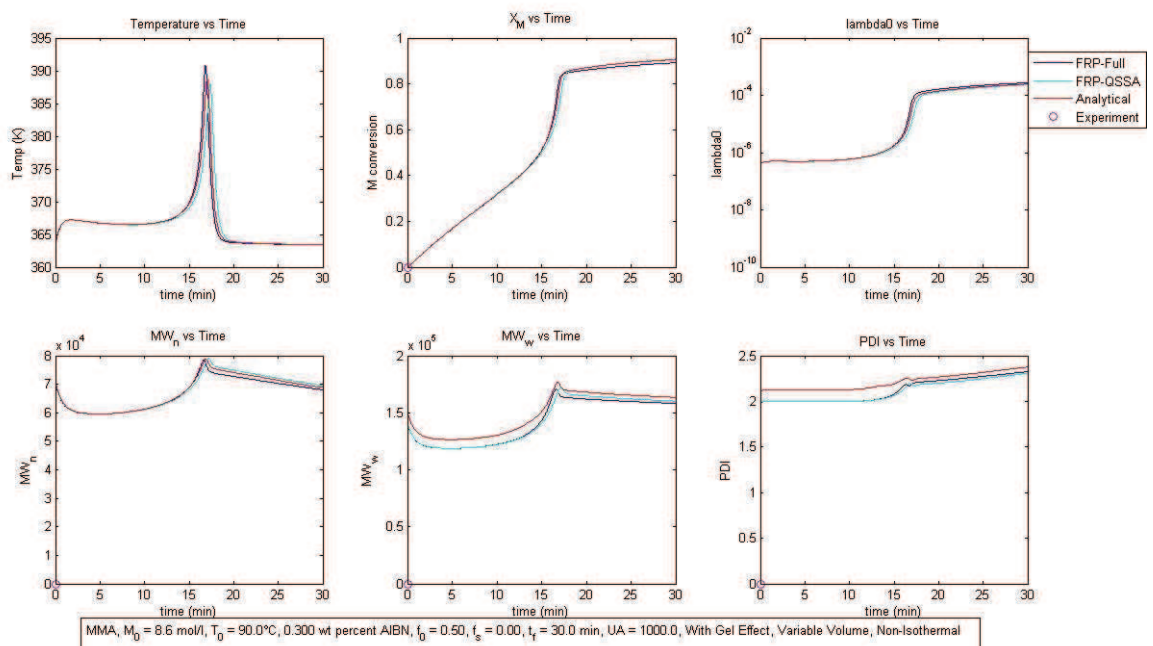
Fig. 4.4-4- MMA- Results obtained for temperature variation with $UA = 1000\ cal/min/K$
for gel/glass effect with CCS model
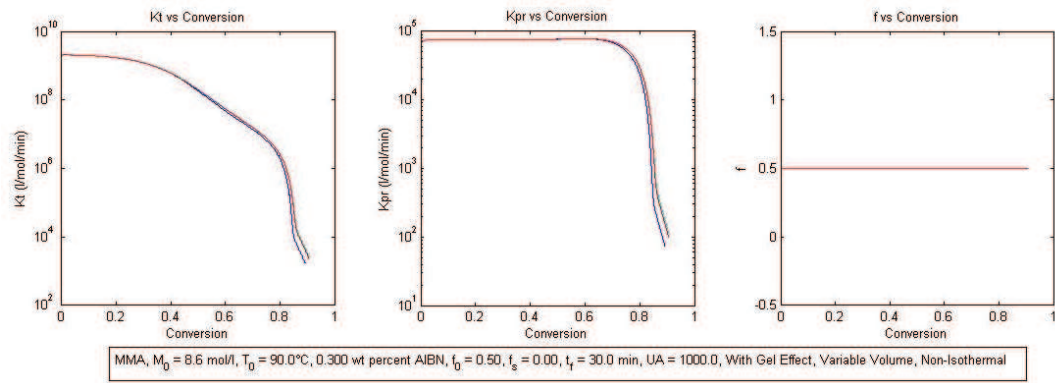
Fig. 4.4-5- MMA- Results obtained for K_t and K_{pr} for temperature variation with $UA = 1000 \ cal/min/K$ for gel/glass effect with CCS model
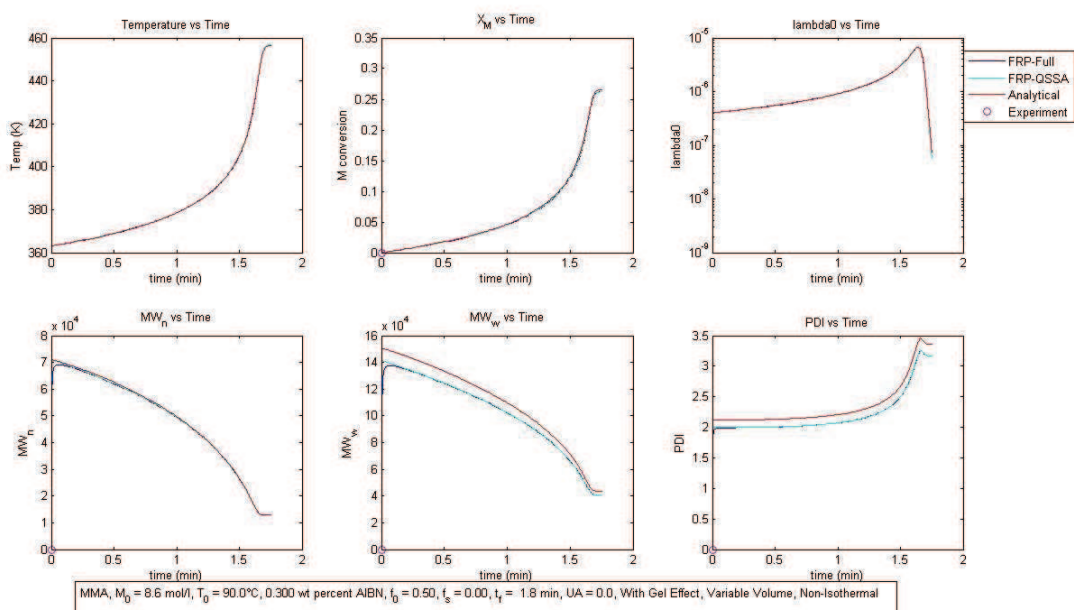
Fig. 4.4-6- MMA- Results obtained for temperature variation with $UA = 0 \ cal/min/K$ (adiabatic) for gel/glass effect with CCS model
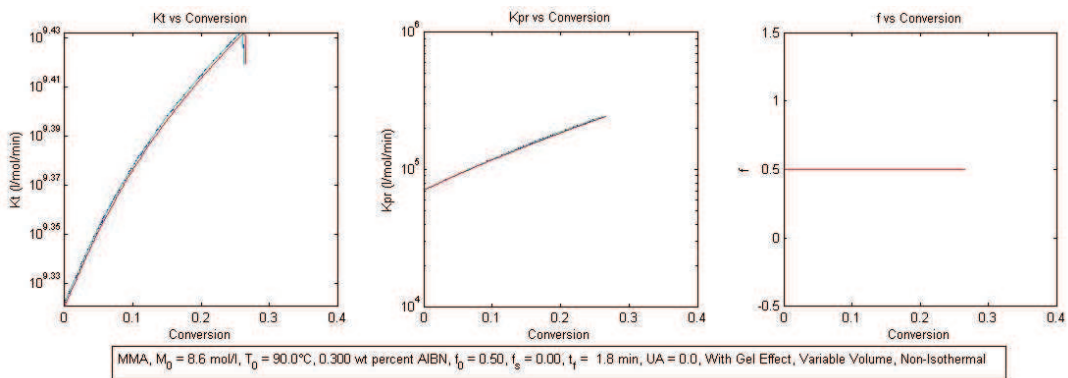
Fig. 4.4-7- MMA- Results obtained for K_t and K_{pr} for temperature variation with $UA = 0 \ cal/min/K$ (adiabatic) for gel/glass effect with CCS model

Fig. 4.4-8 to Fig. 4.4-11 show the results for the conditions implementing gel/glass and cage effect using AK model. Fig. 4.4-8 and Fig. 4.4-10 show the results for $UA = 5000 \, cal/min/K$ whereas Fig. 4.4-9 and Fig. 4.4-11 show the results for adiabatic condition. Fig. 4.4-9 and Fig. 4.4-11 show the results for variation in K_t, K_{pr} and f with temperature changes. Again, the results for AS match well with NS for temperature profile as well as for all other variables as shown in Fig. 4.4-1 to Fig. 4.4-11.
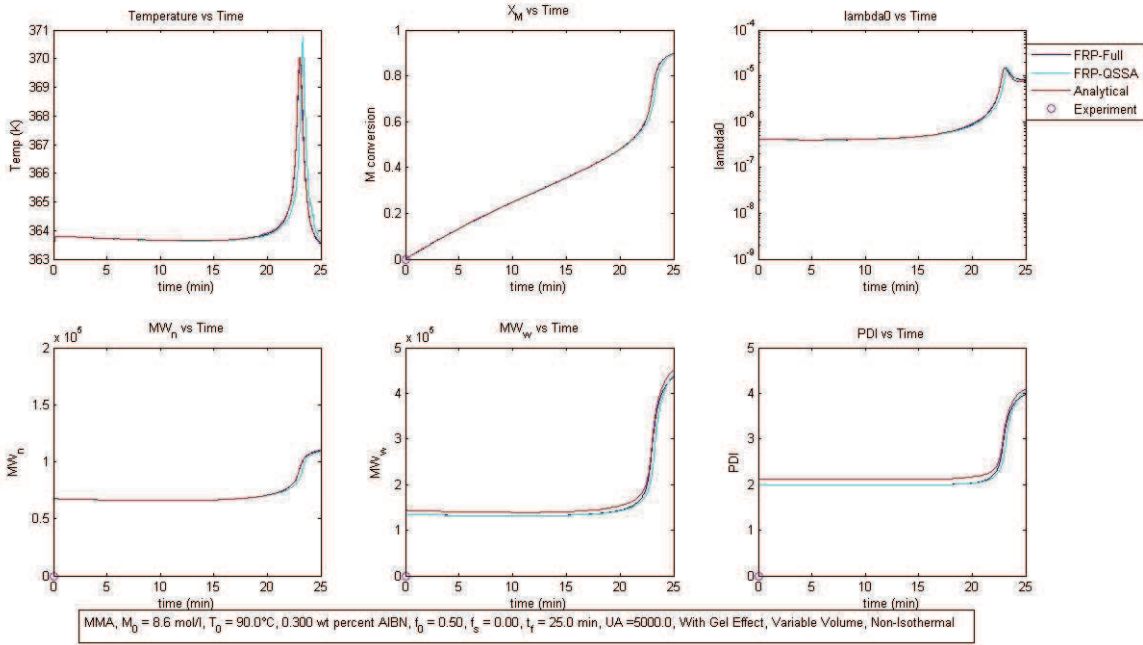
Fig. 4.4-8- MMA- Results obtained for temperature variation with $UA = 5000 \, cal/min/K$ with gel/glass/cage effect using AK model
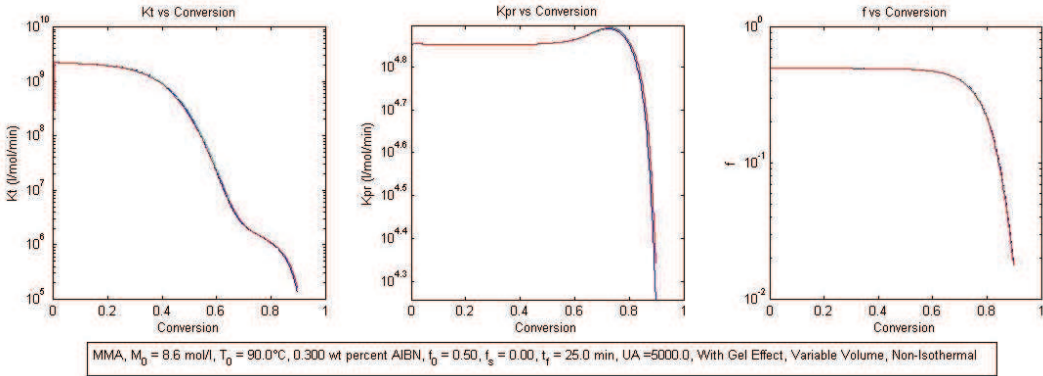
Fig. 4.4-9- MMA- Results obtained for K_t, K_{pr} and f for temperature variation with $UA = 5000 \, cal/min/K$ with gel/glass/cage effect using AK model
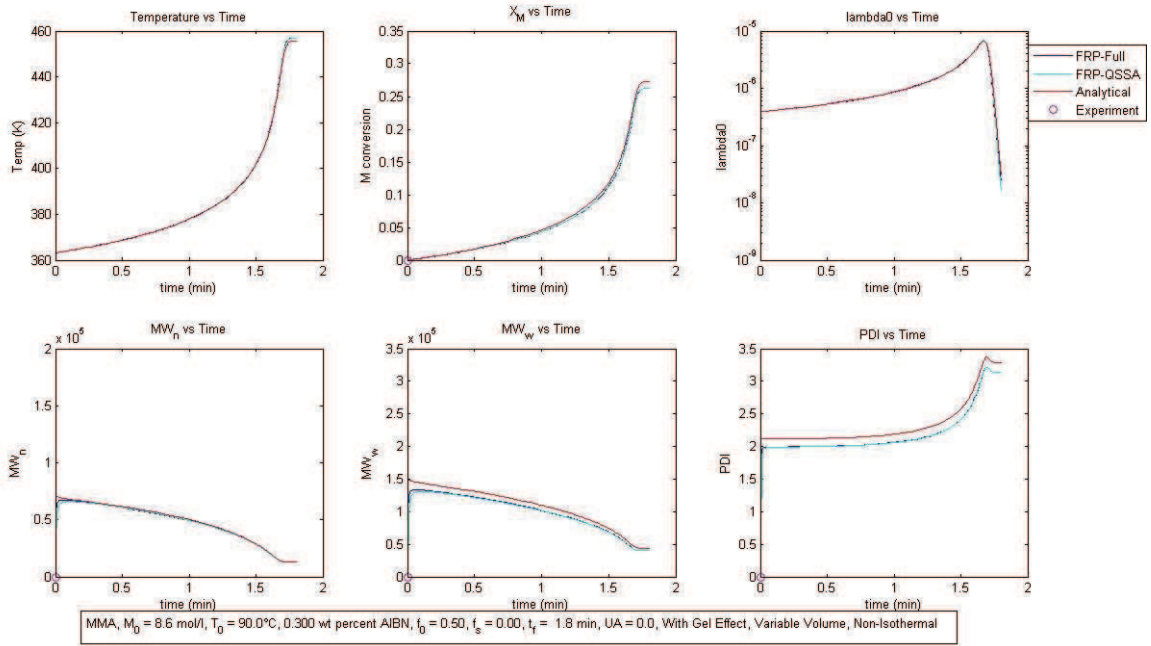
Fig. 4.4-10- MMA- Results obtained for temperature variation with $UA = 0 \ cal/min/K$ (adiabatic) with gel/glass/cage effect using AK model
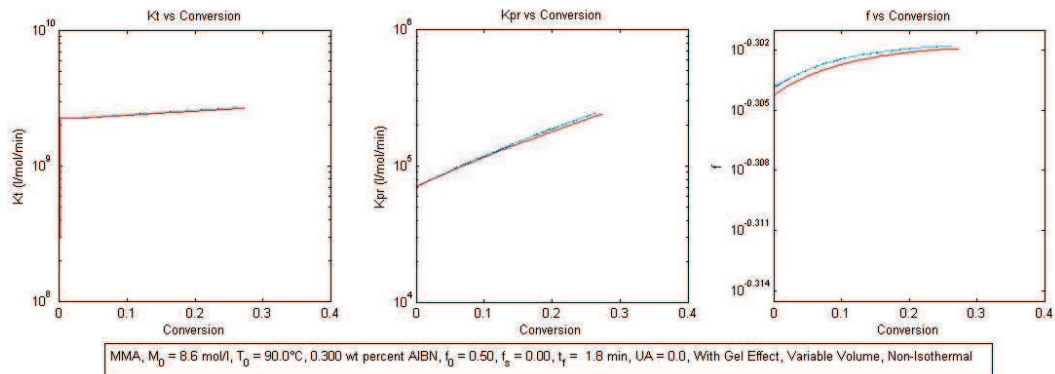
Fig. 4.4-11- MMA- Results obtained for K_t, K_{pr} and f for temperature variation with $UA = 0 \ cal/min/K$ (adiabatic) with gel/glass/cage effect using AK model

4.4.6   Discussion

All the non-isothermal results shown here are for three different cases from the AS complexity point of view, namely 1) without any gel/glass/cage effect, 2) with gel/glass effect using CCS model and 3) with gel/glass and cage effect using AK model. Case1 here represents AS in its original form[14] and the conditions represent situations before gel effect or under large dilution with solvent leading to no gel effect. Case2[15] and case3[16] represents higher conversion cases and their major differences arise from the complexity of modeling of diffusion coefficients for monomer, polymer and initiator. This affects the prediction of MW_w and PDI as shown in our previous work[15,16]. Most of similar work reported in the literature was accomplished using CCS model whereas this is probably the first time that AK model (using free volume theory) is being used to show non-isothermal results. It can be seen that

183

the results of NS matched quite well with AS as well as with each other in all the figures shown. However different heat transfer rates lead to different situations in terms of reactor temperature profile and parameters value and are discussed in the following. The particular adiabatic effect in all three aforementioned cases is discussed together later.

Fig. 4.4-1 to Fig. 4.4-2 shows the results for case1 mentioned above. In Fig. 4.4-1 & Fig. 4.4-2, UA decreases from $1000 \, to \, 500 \, cal/min/K$. It can be observed that the temperature maxima increase with decrease in heat transfer rate which is about $4°C$ in Fig. 4.4-1 and about $11°C$ in Fig. 4.4-2. This can be explained as follows: as the reaction takes place, heat is generated; due to the limitation of heat transfer rate, not all heat that is generated gets removed. So the remaining heat within the system increases its temperature. This has positive feedback on various kinetic rate coefficients and rate of reaction is increased leading to further increase of heat generation and this in turn increases temperature and so on. Meanwhile, due to increasing temperature, heat transfer rate is also increased due to increased thermal gradient. So at a particular temperature, heat removal rate is balanced by heat generation rate. This leads to stop any further rise in system temperature. Now as the reaction proceeds, monomer concentration decreases. This decreases the rate of reaction thus decreases the heat of generation. Depending on the actual decrease in rate of reaction, one can observe either the steep fall in system temperature or very slow fall. This continues till the conversion reaches to a level, actual value depending on system conditions, where gel effect take place. To that extent, auto-acceleration of the reaction takes place due to decrease in radical termination process which is due to increased viscosity of the reaction system. As a consequence, reaction rate increases quite fast thus increasing the heat generation. This, in the absence of proper heat transfer, increases the temperature of the system till it balances out with the heat removal rate. After gel effect, rate of reaction decreases quite rapidly due to the considerable decrease in monomer concentration and the increasing glass effect which slows down the reaction to the point where it just freezes. So in the absence of any further heat generation, the system temperature falls finally to heat sink temperature. The effect of temperature is almost proportional on molecular weight distribution, higher in Fig. 4.4-2 compared to that in Fig. 4.4-1. PDI is at about 2 in both figures signifying the increased importance of termination by disproportionation over termination by combination. PDI remains nearly constant as the variation in temperature is not very large and the effects on MW_n and MW_w are synchronized in such a way that the ratio remains constant.

Fig. 4.4-4 to Fig. 4.4-7 show the results for case2 as mentioned above. Here, in Fig. 4.4-4 and Fig. 4.4-5, the results for finite heat transfer rate, $UA = 1000 \, cal/min/K$ are shown whereas Fig. 4.4-6 and Fig. 4.4-7 show the results for adiabatic condition. It can be seen that due to implementing gel effect, the temperature rise is much higher compared to the case1 without gel effect. Besides this, it can be observed that there are two temperature maxima compared to the case1-without gel effect. Baillagou & Soong[1,8] had made the similar observation with same CCS model. They explained it by stating that the first maximum was due to degenerated runaway. It assumed that heat transfer was not sufficient enough to remove produced heat thus could not prevent temperature rise initially. But with temperature rise, heat transfer rate also rises (proportional to the difference between T and T_{bath}) and thus heat transfer rate

maintains and even lowers the temperature a little bit. The second maximum was due to gel effect. Baillagou & Soong[1,8] had not shown the K_t and K_{pr} profile which is shown here. Fall in K_t can be observed in Fig. 4.4-5 leading to gel effect. K_{pr} can also be observed in the same Fig. 4.4-5 going to low values thus leading to glass effect shown in Fig. 4.4-4. That is why the conversion almost got steady. Due to decrease in reaction, heat generation is reduced and because of increased temperature, heat transfer rate is also increased. Both these effects force the temperature to come down sharply and finally attain the heat sink temperature. The profile for MW_n and PDI is also similar to one obtained by Baillagou & Soong[8]. MW_n initially decreased due to increase in temperature, then rises slowly with increasing conversion and then increased again due to increased reaction/ conversion despite increasing temperature and then fell down a little with beginning of glass effect and decreasing temperature. The same happened with MW_w. As an overall consequence, PDI suddenly increased a little during gel effect and then increases slowly with time.

Fig. 4.4-8 to Fig. 4.4-11 show the results for the case3 mentioned above i.e. implementing gel/glass/cage effect using AK model. Fig. 4.4-8 and Fig. 4.4-9 show the results for $UA = 5000\ cal/min/K$ which are higher compared to previous cases considered. The results are different to Fig. 4.4-4 to Fig. 4.4-5 just explained above. The reason for delayed gel effect is that because of higher heat transfer, the temperature rise is less thus the conversion rate is lower compared to the case of $UA = 1000\ cal/min/K$. Thus, it takes more time to reach the conversion to cause gel effect. Besides this, the temperature rise is also less during the gel effect due to higher heat transfer rate. Unlike Fig. 4.4-5, in Fig. 4.4-9, the K_t and K_{pr} profile is different a little bit. K_t is more in-line with the prediction of Buback[19]. K_{pr} here, increases during gel effect instead of remaining constant probably because of increased temperature. The temperature now starts falling down due to two reasons- increased temperature increased heat transfer and decreasing reaction rate due to decreasing monomer concentration. This, in a synergetic effect with increasing viscosity due to higher conversion, decreases K_t sharply, thus inducing glass effect. Unlike to the previous case of constant initiator efficiency in CCS model, f decreases almost with K_{pr} as predicted by Zhu et al.[20] Since the temperature before the gel effect remains almost constant so not effect is seen on MW_n and MW_w and thus on PDI, they all remain flat; rising only during gel effect. PDI attains much higher value compared to low heat transfer rate case as shown in Fig. 4.4-4. This probably may not be compared. As shown in our previous work, AK model is better than CCS model for predicting MW_w and thus PDI. So it might be the case that CCS model in Fig. 4.4-4 is underestimating PDI.

Fig. 4.4-3, Fig. 4.4-6, and Fig. 4.4-10 represent the situation where adiabatic condition applies for each of the three cases mentioned above. Sufficiently before the gel effect, all the three cases should have the same results and adiabatic condition is one such situation. Looking carefully, we will observe that all three are same. The same results are for Fig. 4.4-7 and Fig. 4.4-11. This validates the mathematical formulation for each case indirectly. So now we can discuss any one of these figures without referring all of them separately. There are several important aspects to be noted from the results. In Fig. 4.4-10, the conversion graph shows that the final conversion is at about 0.26 for adiabatic condition which is quite low despite high

temperature. This can easily be explained by the fact that due to such large temperature rise and that too in such a short time, initiator decomposes too fast thus leaving the monomer unreacted. This condition is defined as dead-end by Baillagou & Soong[1]. The low conversion combined with high temperature rise leads to increase in K_t and K_{pr}. PDI rise is higher than the case of finite heat transfer, due to the large production of macroradicals upon initiator decomposition which favors termination reactions. MW_n and PDI profiles are similar to the ones presented by Baillagou & Soong[8]. Hence we have validated our results under similar conditions.

4.4.7 Conclusion

The results through Fig. 4.4-1 to Fig. 4.4-11 clearly showed that AS results match well with NS for all cases of different heat transfer rates as well as different models for gel/glass/cage effect. NS also matched with each other for all these conditions. These results clearly establish that the derived analytical solution (AS) is extremely flexible, versatile, adaptable and useful than the previous work by Venkateshwaran *et al.*[13] AS has proved its capability to be used in all practical situations using various models to simulate gel/glass/cage effect explicitly for covering the complete range of conversion. So instead of using 11 differential equations (eqn.(3-3 to 3-14)), only one differential equation (eqn.(3-14)) is required to be solved using AS for non-isothermal condition and none for isothermal condition. This all can be done without any loss of accuracy compared to detailed numerical solutions (NS) except may be at low temperature. NS has also shown to give similar results in all conditions despite the difference in implementing QSSA for eqn.(3-8)-eqn.(3-10) in FRP_QSSA compare to FRP_Full. Therefore one can only implement AS or possibly FRP_QSSA instead FRP_Full in CFD problems thus reducing the no. of variables to be solved and saving computer time unit.

4.4.8 References

1. Baillagou, P. E.; Soong, D. S., Major Factors Contributing to the Nonlinear Kinetics of Free-Radical Polymerization. *Chem Eng Sci* **1985**, *40* (1), 75-86.
2. Balke, S. T.; Hamielec, A. E., Bulk Polymerization of Methyl Methacrylate. *Journal of Applied Polymer Science* **1973**, *17*, 905-949.
3. Marten, F. L.; Hamielec, A. E., High-Conversion Diffusion-Controlled Polymerization of Styrene .1. *Journal of Applied Polymer Science* **1982**, *27* (2), 489-505.
4. McKenna, T. F.; Villanueva, A.; Santos, A. M., Effect of solvent on the rate constants in solution polymerization. Part I. Butyl acrylate. *J Polym Sci Pol Chem* **1999**, *37* (5), 571-588.
5. McKenna, T. F.; Villanueva, A., Effect of solvent on the rate constants in solution polymerization. Part II. Vinyl acetate. *J Polym Sci Pol Chem* **1999**, *37* (5), 589-601.
6. Achilias, D. S.; Kiparissides, C., Development of a General Mathematical Framework for Modeling Diffusion-Controlled Free-Radical Polymerization Reactions. *Macromolecules* **1992**, *25* (14), 3739-3750.
7. Keramopoulos, A.; Kiparissides, C., Development of a comprehensive model for diffusion-controlled free-radical copolymerization reactions. *Macromolecules* **2002**, *35* (10), 4155-4166.

8. Baillagou, P. E.; Soong, D. S., Molecular-Weight Distribution of Products of Free-Radical Non-Isothermal Polymerization with Gel Effect - Simulation for Polymerization of Poly(Methyl Methacrylate). *Chem Eng Sci* **1985**, *40* (1), 87-104.

9. Chiu, W. Y.; Carratt, G. M.; Soong, D. S., A Computer-Model for the Gel Effect in Free-Radical Polymerization. *Macromolecule*s **1983**, *16* (3), 348-357.

10. Ray, A. B.; Saraf, D. N.; Gupta, S. K., Free-Radical Polymerizations Associated with the Trommsdorff Effect under Semibatch Reactor Conditions .1. Modeling. *Polym Eng Sci* **1995**, *35* (16), 1290-1299.

11. Srinivas, T.; Sivakumar, S.; Gupta, S. K.; Saraf, D. N., Free radical polymerizations associated with the Trommsdorff effect under semibatch reactor conditions .2. Experimental responses to step changes in temperature. *Polym Eng Sci* **1996**, *36* (3), 311-321.

12. Sangwai, J. S.; Bhat, S. A.; Gupta, S.; Saraf, D. N.; Gupta, S. K., Bulk free radical polymerizations of methyl methacrylate under non-isothermal conditions and with intermediate addition of initiator: Experiments and modeling. *Polymer* **2005**, *46* (25), 11451-11462.

13. Venkateshwaran, G.; Kumar, A., Solution of Free-Radical Polymerization. *Journal of Applied Polymer Science* **1992**, *45* (2), 187-215.

14. Garg, D. K.; Serra, C. A.; Hoarau, Y.; Parida, D.; Bouquey, M.; Muller, R., Analytical Solution of Free Radical Polymerization: Derivation and Validation. **2014,** *to be submitted*.

15. Garg, D. K.; Serra, C. A.; Hoarau, Y.; Parida, D.; Bouquey, M.; Muller, R., Analytical Solution of Free Radical Polymerization: Applications-Implementing Gel effect using CCS model. **2014,** *to be submitted.*

16. Garg, D. K.; Serra, C. A.; Hoarau, Y.; Parida, D.; Bouquey, M.; Muller, R., Analytical Solution of Free Radical Polymerization: Applications-Implementing Gel effect using AK model. **2014**, *to be submitted*.

17. Achilias, D.; Kiparissides, C., Modeling of Diffusion-Controlled Free-Radical Polymerization Reactions. Journ*al of Applied Polymer Science* **1988,** *35* (5), 1303-1323.

18. Zielinski, J. M.; Duda, J. L., Predicting Polymer Solvent Diffusion-Coefficients Using Free-Volume Theory. *Aiche J* **1992,** *38* (3), 405-415.

19. Buback, M., Free-Radical Polymerization up to High Conversion - a General Kinetic Treatment. *Makromol Chem* **1990,** *191* (7), 1575-1587.

20. Zhu, S.; Tian, Y.; Hamielec, A. E.; Eaton, D. R., Radical Concentrations in Free-Radical Copolymerization of Mma/Egdma. *Polymer* **1990,** *31* (1), 154-159.

4.5 Chapter Summary

In this chapter, a fairly broad kinetic scheme of free radical polymerization (FRP) was considered. This kinetic scheme included the elementary steps of initiator dissociation and initiation, propagation, termination by combination and disproportionation, transfer to monomer, solvent and chain transfer agent (CTA). A mathematical model based on moment method was used. An analytical solution (AS) was derived applying the following simple assumptions: isothermal, homogeneous solution, homopolymerization in batch reactor under the variation of volume with monomer conversion. This AS was then rigorously tested and validated against two numerical solutions (NS) namely FRP_Full and FRP_QSSA. AS was also validated against experimental data, before the gel effect, whenever available. Experimental data consisted of four monomers, from the slowest to the fastest, two different initiators, different initiator and monomer concentrations, different solvent fractions and finally different temperatures. After validation against NS and experimental data under the conditions for which it was derived, AS applicability was extended to complete range of conversion by initially implementing gel and glass effects using CCS model and then AK model to accommodate further cage effect. After modeling all these 3 effects, AS has been validated against NS and experimental data again. Thereafter, it was extended for modeling temperature variation with all the models and effects mentioned above. Here again it was validated against published data. So, AS was finally found to give same results as that of NS under all conditions (except for low temperature).

Chapter5   CFD analysis of tubular microreactors

Preface

This chapter deals with CFD simulations of free radical polymerization (FRP) under flow in microreactors of different tubular geometries. The purpose of this chapter is to improve the modeling as well as simulation of FRP under the stated conditions. This chapter is divided into three sections.

In the first section, the problem regarding modeling the various chemical species as passive scalars and its probable solution is considered. CFD is based on conservation laws of mass, momentum and energy. But the chemical data are always presented in terms of moles. So the main problem arises from feeding the chemical data in mass form in CFD modeling. This creates problems especially for the kinetic rate coefficients. So a new transformation is worked out to derive dimensionless scalars that consist in parameters which can be fed in molar form. Obtained CFD modeling results are compared with published results.

In section two, using the new transformation developed in first section, two tubular microreactor geometries are studied for unmixed feed condition. The various fluid thermo-physical properties were modeled constant at first along with discrete variation of diffusion coefficients assumed to be same for all chemical species. The results are compared with published results. Then, variations in fluid thermo-physical properties like density, viscosity and thermal conductivity is considered and their impact on simulation results are evaluated.

In the last section, the work of section two is extended to mixed feed condition with one additional reactor geometry to analyze the reactor geometry and its effect on polymerization in a better way. In addition to model variation of fluid thermo-physical properties with discrete variation of diffusion coefficient, variation in diffusion coefficient is also modeled but with constant fluid thermo-physical properties.

This chapter is composed of the three following articles corresponding to the three aforementioned sections:

*(1) Garg D.K., C.A. Serra, Y. Hoarau, D. Parida, M. Bouquey, R. Muller, New transformation proposed for CFD simulation of free radical polymerization. Microfluid Nanofluid **2014**, to be submitted.*

*(2) Garg D.K., C.A. Serra, Y. Hoarau, D. Parida, M. Bouquey, R. Muller, Numerical investigations of different tubular microreactor geometries for the synthesis of polymers under unmixed feed condition. Microfluid Nanofluid **2014**, to be submitted.*

*(3) Garg D.K., C.A. Serra, Y. Hoarau, D. Parida, M. Bouquey, R. Muller, Numerical investigations of perfectly mixed condition at the inlet of free radical polymerization tubular micoreactors of different geometries. Microfluid Nanofluid **2014**, to be submitted.*

5.1 New Transformation Proposed for CFD Simulation of Free Radical Polymerization

5.1.1 Abstract

A new yet simple transformation for free radical polymerization (FRP) suitable for CFD simulations is proposed. Using this new transformation, the chemical data for chemical species concentration and kinetic rate coefficients can be fed in original molar form to CFD simulations while simulating chemical species as passive scalars. The expression for transformed reaction rate equations remains unchanged thus enabling an easy coding and debugging process. Significant errors that may arise from the use of chemical data in mass form instead of original molar form is also shown. The new transformation keeps all the advantages similar to Zhu transformation with the additional benefit of being more suitable for CFD simulations.

Keywords- CFD, free radical polymerization, simulation, transformation.

5.1.2 Introduction

In today's time, as the resources are becoming scarce, chemical industry needs to optimize its manufacturing processes, reactor design, operating conditions etc. This usually requires a lot of experiments and thorough analysis. This may consume a lot of physical resources and may be highly time consuming and costly especially for new emerging techniques. Even for well-established technologies, this may be costly as not all desired conditions could be performed in limited time and budget.

This problem could partly be overcome by modeling the process mathematically and then simulate it with dedicated software. The decrease in cost of computers, the increase in computing power along with past intensive researches aiming at developing efficient and rapid numerical methods, has increased industry interest towards modeling and simulation. Doing simulations on computers offers many advantages. It does not require any physical resource like reagents, equipment, manpower, etc. Many simulations can be run at the same time for different geometries of the equipment and/or different flow and reaction conditions. A lot more data is available from the simulation which could not possibly be available from physical experiment for practical reasons. Simulations on computers are much cheaper, faster and flexible compared to physical experiments.

However, the use of computers for simulations has its own limitations. It must be validated against the physical experimental data under similar conditions. To make the simulation better so as to match the physical reality, a good mathematical model of the process must be available. Sufficient computational capacity should also be available to solve the problem in a given time with the given complexity. Sometimes, the problem may be complex enough to require tremendous computational resources which may be beyond the reach of the researchers. So the complexity of the problem may be lowered to make it solvable under the available computation power.

One of the most common areas for modeling is flow. Computation fluid dynamics (CFD) deals with it. The mathematical equations to model flow are based on three conservation laws, namely law of conservation of mass, momentum and energy, in short Navier-Stokes equations. Various tools have been developed to simulate flows successfully under various conditions like in heat exchangers, mixers etc. Chemical reactions are also now being modeled extensively but should be so with flow as in many applications flow may significantly affect the result of any chemical reaction. Various commercial CFD software packages offer special chemistry package to incorporate chemical reactions with flow and heat transfer processes.

In such software packages, chemical species are usually modeled as passive scalar, i.e. they don't affect the flow condition with their movement. One of the problems modeling chemical reactions with flow is that chemical rates (generation terms) and chemical data for chemical species are presented in terms of moles which is not a conserved quantity. Since only mass is conserved, all the computation is in terms of mass. Hence, all quantities including scalars should be present in terms of mass so that conservation of mass can be applied to such species. This requires all the chemical data to be converted from molar form to mass form before being fed in the CFD software. The problem starts from converting the value of various kinetic rate coefficients of the elementary reaction steps to be modeled. For simple reaction steps where only one chemical species is present in a nth order reaction rate expression, the molecular weight of that chemical species can be used to convert the value of kinetic rate coefficient from molar to mass form. But if the reaction rate expression involves more than one species in a non-linear form, then it is difficult to choose which molecular weight or what combination of molecular weights of chemical species for converting the kinetic rate coefficient data from mole to mass form. Besides this, the output of the simulation has to be interpreted and may be required to be converted backward to molar form again for further analysis. Polymerization is one such area of chemical reactions where this problem is quite visible.

Nowadays, simulations and computers are being used extensively for the study and optimization of polymerization processes under various conditions[1-8]. For the current work, free radical polymerization (FRP) is considered. The mathematical model based on the moment method has been developed and used by various researchers successfully[1-3]. The form of equations does not give simple relationships between chemical species and reaction rates. The various chemical species concentrations and kinetic rate coefficients appearing in this model vary from each other by several orders of magnitude thus introducing a strong stiffness in the set of equations. This also leads to numerical errors during solving such quantities and much mathematical manipulations are required to keep the numerical error low enough to let the simulations converge.

In this work, a new simple transformation is proposed for FRP which will serve the following purposes:

1. To transform various chemical species concentrations (e.g. initiator, monomer etc.) into dimensionless forms to justify their use as passive scalars,

2. To transform various kinetic rate coefficients into dimensionless entities in terms of concentration. This will help in feeding the data in the original molar form,
3. To bring the value of these new parameters to same order so as to reduce the stiffness and numerical error arising from the large difference in their parent values.

5.1.3 Mathematical model for CFD
The mathematical model for CFD is given in section 3.2.9.

5.1.4 Model of FRP
The kinetic scheme used here is given in section 3.2.2. The related mathematical model is given in section 3.2.3.

5.1.5 New transformation
To apply the new transformation, some assumptions are required which are not very restrictive in nature and still retain the essence of the complete model. These assumptions are as follows:

1. Quasi-steady state assumption (QSSA) for live polymer radical chain lengths distribution, i.e. $\lambda_0, \lambda_1, \& \lambda_2$.

This assumption is fully valid before the gel effect sets in. However, in chapter-4, we have also shown that the model with or without using QSSA gave similar results when modeled properly.

Thus, application of QSSA leads to:

$$\lambda_0 = \sqrt{\frac{2fK_dI}{(K_{tc}+K_{td})}} = \sqrt{\frac{2fK_dI}{K_t}} \tag{4-36}$$

$$\lambda_1 = \lambda_0(\bar{L}+1) \tag{4-38}$$

$$\lambda_2 = \lambda_1(2\bar{L}+1) = \lambda_0(\bar{L}+1)(2\bar{L}+1) \tag{4-40}$$

where :

$$\bar{L} = L.\left(\frac{1-R_{MM}}{1+R_PL}\right) = L.\left(\frac{1-R_M}{1+R_PL}\right) \tag{4-34}$$

$$L = \frac{(K_p+K_{fm})M\lambda_0}{2fK_dI} = \frac{K_{pr}M\lambda_0}{2fK_dI} \tag{4-31}$$

2. We simplify the above two relationships using the following long chain assumption.

For $\bar{L} \gg 1$

$$\lambda_1 = \lambda_0\bar{L} \tag{4-43}$$

$$\lambda_2 = 2\bar{L}\lambda_1 = 2\bar{L}^2\lambda_0 \tag{4-44}$$

This assumption is quite reasonable as the value of $\bar{L}$ is quite large and thus this assumption does not introduce significant error in the model and its outcome.

Now the new transformation is as follows:

For concentration terms

For initiator, $I' = \dfrac{I}{I_0}$ (5-1)

For monomer, $M' = \dfrac{M}{M_0}$ (5-2)

For solvent, $S' = \dfrac{S}{S_0}$ (5-3)

For CTA, $A' = \dfrac{A}{A_0}$ (5-4)

For kinetic rate coefficients

$K_d' = K_d$ (5-5)

$K_p' = K_p\sqrt{I_0.M_0}$ (5-6)

$K_t' = K_t M_0$ (5-7)

So eqn.(5-1) to eqn.(5-7) constitutes the new transformations where all terms marked with (') are dimensionless in terms of concentration. All the transfer rate coefficients like transfer to monomer K_{fm}, transfer to solvent K_{fs}, and transfer to CTA K_{fa} are connected to K_p through eqn.(3-21) to eqn.(3-23), eqn.(3-26) to eqn.(3-30). Similarly, K_t is connected to K_{tc} & K_{td} through eqn.(3-19), eqn.(3-24) & eqn.(3-25).

Applying this transformation results into the following relationships between their dimensionless and dimensional forms:

$$\lambda_0' = \sqrt{\frac{2fK_d'I'}{K_t'}} = \sqrt{\frac{2fK_dI}{K_t}} * \frac{1}{\sqrt{I_0 M_0}} = \frac{\lambda_0}{\sqrt{I_0 M_0}}$$ (5-8)

$$L' = \frac{K_p'\lambda_0'M'}{2fK_d'I'} = \frac{K_p\lambda_0 M}{2fK_dI} * \left(\frac{I_0}{M_0}\right) = L\left(\frac{I_0}{M_0}\right)$$ (5-9)

Number average chain length, $DPn = \dfrac{\mu_1}{\mu_0} = \dfrac{\mu_1'}{\mu_0'}\left(\dfrac{M_0}{I_0}\right)$ (5-10)

Polydispersity Index, $PDI = \dfrac{\mu_0\mu_2}{\mu_1^2} = \dfrac{\mu_0'\mu_2'}{\mu_1'^2}$ (5-11)

As such, we have no theoretical basis to derive the new transformation for kinetic rate coefficients as suggested above. So proving the correctness of new transformation in the absence of theoretical basis is difficult. But we have used other means to prove its correctness. By applying these transformations in the mathematical model of FRP presented above along

with the aforementioned assumptions, few things can easily be observed. First observation is that, by applying the proposed transformation on the right hand side of the eqn.(3-11) to eqn.(3-13) for dead polymer chain lengths distribution first and taking out the common factor in each equation, we will obtain:

$$\mu_0' = \frac{\mu_0}{I_0} \tag{5-12}$$

$$\mu_1' = \frac{\mu_1}{M_0} \tag{5-13}$$

$$\mu_2' = \frac{\mu_2}{(M_0^2/I_0)} \quad - \tag{5-14}$$

which is the same form of the transformation proposed by Zhu[12].The only difference is that the latter transformation was applied to the whole equation whereas we have applied transformation to concentration terms and kinetic rate coefficients individually. This proves the correctness of our proposed new transformation. This also proves the claim of our new transformation about bringing the various chemical species values at the same order and thus helping in reducing stiffness and numerical error. So, in a way, one can say that this proposed transformation is a new way of achieving Zhu transformation but with an additional advantage of having kinetic rate coefficients dimensionless in terms of concentration and thus moles.

Second, the form of the equations before and after applying the transformation remains the same except for the fact that now the transformed terms are dimensionless in terms of concentration. This is a very significant advantage as this transformation does not introduce any new factor in the model in each or some equations to account for the transformation as with the case of Zhu transformations.. This helps in coding and debugging the equations as the same form of equation is retained.

5.1.6 Validation

The new transformation is validated for batch reactor condition against the analytical solution (AS) developed for batch reactor in our previous work for the same model. The above mentioned mathematical model constitutes the so-called FRP_QSSA in our previous work[9] with results from the application of the QSSA assumption. The transformation was then applied to CFD simulation of FRP in straight tube reactor (STR) with unmixed feed condition. This was done to match and validate the results using new transformation with published results under same conditions except for the fact that the published results had fed the data to simulations in mass form. The CFD geometry grid used was the same as by Mandal et al.[13] so no further mesh independency analysis was performed. An unstructured grid was used for straight tube as shown in Fig. 5.1-1 (a) and Fig. 5.1-1 (b). The operating conditions with kinetic data were taken to be same as that of Serra et al.[14] and the results were compared with the same like in Mandal et al.[13] paper. The details of the operating conditions and kinetic data Table 3-5, Table 3-1 & Table 3-3 respectively

(a)   (b)

(c)   (d)
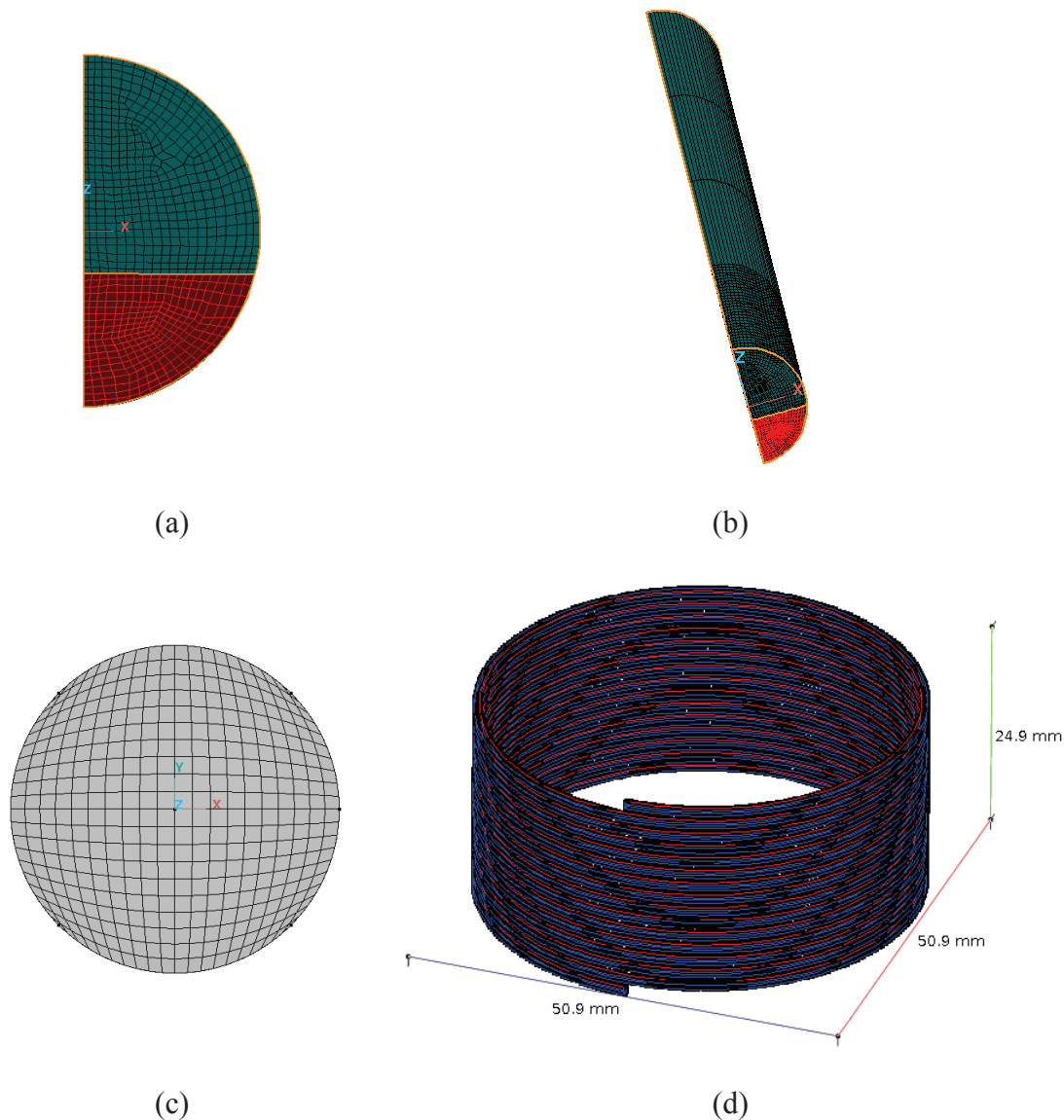
Fig. 5.1-1-(a) Unstructured mesh for STR[13] inlet, (b) volume grid of STR, (c) CTR inlet structured mesh and d) CTR volume grid used in this work

The no-slip boundary conditions for the velocities, i.e., $u_i = 0$, and the zero first derivative conditions for the scalars were imposed on the solid wall implying zero flux of scalars through the wall. The concentration and velocity profiles at inlet were modeled as flat profile. The fluids considered in the study were assumed to have similar properties and were modeled as Newtonian in nature. The wall of the pipe was maintained at constant temperature (isothermal condition). The numerical computation was found to be converged when the error residual added over all the computational nodes is $\leq 10^{-6}$ for pressure p, velocity u_i, and scalars.

Additional CFD simulations were performed and compared with experimental data[15] for benzoyl peroxide (BPO) initiated solution polymerization of styrene with 30% dilution in a coiled tube reactor (CTR). The details of the operating conditions and reactor are given in Table 5.1-1. The geometry of CTR is generated using CFD-GEOM of CFD-ACE+, an

established commercial CFD software package. The structure grid was used. A mesh independency analysis was done for fully mixed feed condition. The final mesh of inlet and volume grid of the CTR is shown in Fig. 5.1-1. The flow, heat and scalar modules of the CFD-ACE were used to model respectively: flow in the reactor, heat effects due to reaction and heat transfer through the fluid as well as across the reactor walls, and the modeling of the various chemical species as passive scalars with reaction rates as well as generation terms for respective scalars. Third order scheme was used for scalars spatial distribution to reduce the numerical diffusion. The steady-state was considered all through for the simulations.

Table 5.1-1-Experimental data for solution polymerization of styrene in CTR[15]

Type of Reactor Geometry	CTR
Length (m)	2.356
No. of turns	15
Pitch (m)	0.0016
Diameter (m)	0.0009
Diameter of coil (m)	0.05
Residence time (s)	9000
Initiator, concentration (mol/l)	BPO, 0.00937
Monomer, concentration (mol/l)	Styrene, 6.3
Temperature (K)	378.15
Diffusivity Coefficient (m^2/s)	1×10^{-10}

5.1.7 Results
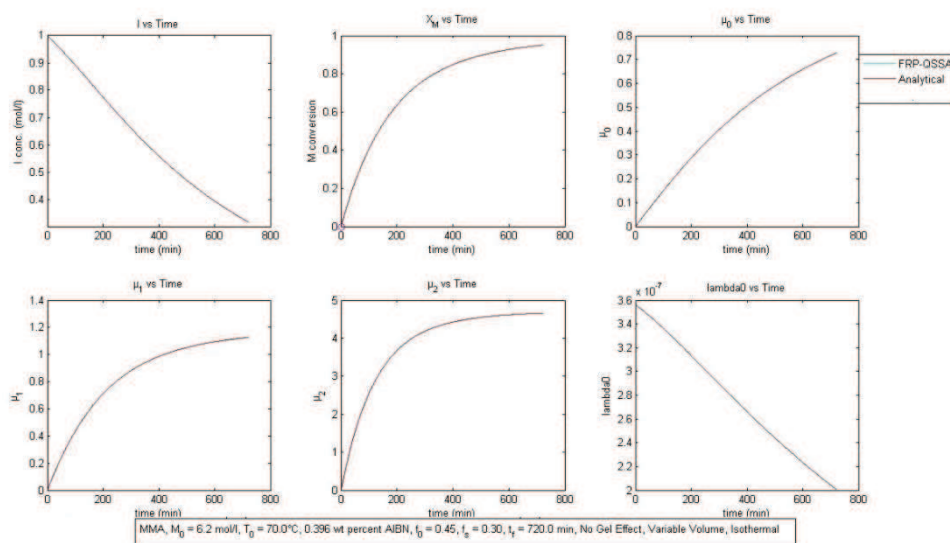
Fig. 5.1-2-Comparison between the analytical solution and FRP_QSSA numerical solution using new transformation

As can be seen in Fig. 5.1-2, results of AS match exactly with FRP_QSSA for all the variables shown for batch reactor. Another thing that can be observed is that all the variables except λ_0 which was not modeled as passive scalar, are of the same order as desired and expected. This validates that the new transformation are correct and also works for the AS.
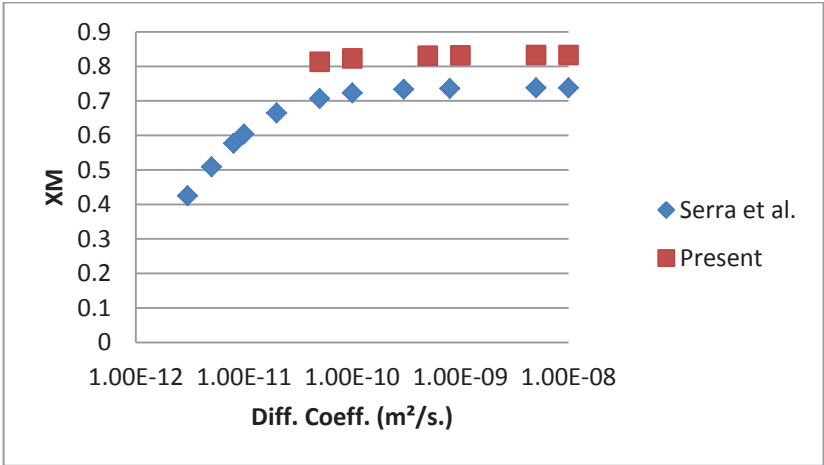
Fig. 5.1-3- Comparison for monomer conversion between present work and Serra *et al.*[14]
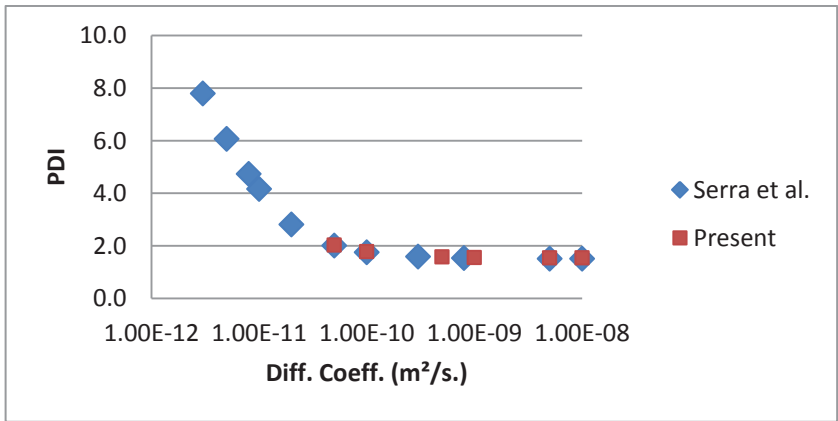
Fig. 5.1-4- Comparison for *PDI* between present work and Serra *et al.*[14]
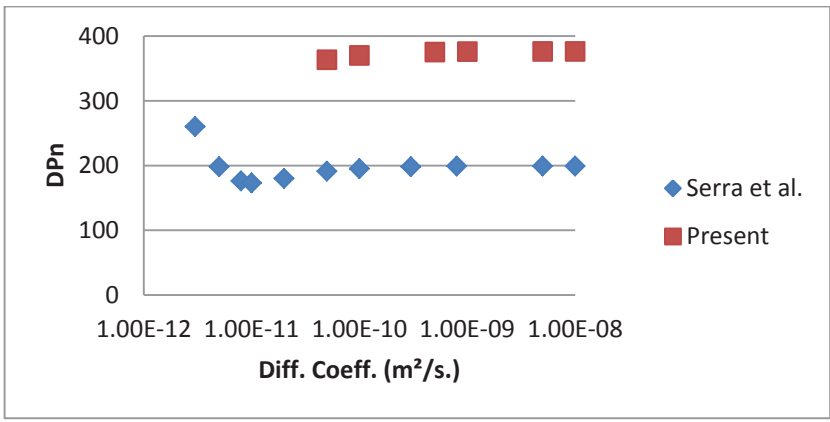
Fig. 5.1-5- Comparison for *DPn* (number average molecular weight) between present work and Serra *et al.*[14]

As can be seen in Fig. 5.1-3 to Fig. 5.1-5, the comparison for monomer conversion $(x_M), PDI$ and DPn has been made between current work and previous Serra *et al.*[14] work under same conditions of reactor, operating conditions and kinetic data for STR. The slight differences for x_M and large difference for DPn between the two set of results is observed in Fig. 5.1-3 and Fig. 5.1-4 respectively. But, for PDI in Fig. 5.1-5, the match is quite good. Detailed explanations are presented in discussion section.

Table 5.1-2- Comparison of experimental and simulation results for BPO-initiated polymerization of styrene in a CTR

	Experimental CTR	Simulation CTR
$T(°C)$	105	105
x_M	0.53	0.57
DPn	335	385
PDI	1.52	1.76
Time (*s*)	9000	9000

The Table 5.1-2 shows the results for the CFD simulation for mixed feed condition in CTR and compared with experimental data[15]. The simulation results matches satisfactorily with the experimental data under the simplified assumptions using the new proposed transformation.

5.1.8 Discussion

In this work, a new transformation was proposed For concentration terms, i.e. for initiator, monomer, solvent and CTA equations (eqn.(5-1) to eqn.(5-4)) to make them dimensionless. The transformation was also performed to eqn.(5-5)-to eqn.(5-7) and applied directly to the various kinetic rate constants instead of applying it to the complete equations of μ_0, μ_1, μ_2. However, despite the transformation, μ_0, μ_1 and μ_2 still have the same form as per the transformation proposed by Zhu[12] as can be seen in eqn.(5-12) to eqn.(5-14). So it proves the correctness of this new transformation. Moreover, Fig. 2 clearly shows that new transformation brings the order of magnitude of the various variables of interest to the same level as desired except for λ_0 which was not modeled as passive scalar.

Only molar form of data is required as shown through Fig. 5.1-2 where AS is compared with FRP_QSSA after applying the new transformation for both.

As we can see from eqn.(5-8) to eqn.(5-10), various terms like λ'_0, L' and DPn are not completely independent of initial values of initiator, I_0 and monomer, M_0 except for PDI. Since the final form of transformation for μ_0, μ_1, μ_2 is same in both Zhu[12] and new transformation PDI and DPn will have same relationship among μ_0, μ_1, μ_2. So one can wonder as to what is the importance of the initial concentration values on the final values of conversion, PDI and DPn as visible in the Fig. 5.1-3 to Fig. 5.1-5.

It can be seen that AS[9] for initiator concentration, i.e.

$$I = I_0 e^{-K_d \cdot t} \tag{4-134}$$

is of first order with respect to I, initiator concentration and only one concentration term is present. So applying the transformation of eqn.(5-1), I will become dimensionless in terms of concentration and units (mass or molar) and value of concentration term will have no effect on the solution of this I' (scalar1). Final value of I can simply be obtained by multiply it by I_0.

But this is not the case for M, monomer concentration. AS[9] for monomer concentration is

$$M = M_0 \exp\left[-\sqrt{\frac{8 f K_{pr}^2 I_0}{K_d K_t}} \cdot \left(1 - e^{\frac{-K_d \cdot t}{2}}\right)\right] \tag{4-136}$$

Eqn.(4-136) is first order in M but of complex order in I. So, after applying Zhu transformation[12] for monomer concentration (eqn.(5-2)) the dimensionless monomer concentration is injected into eqn.(3-4). It can be seen that the result is still dependent of I_0. So the value of I_0 depending on the units chosen (mass or molar) will have impact on evaluation of M' and ultimately on M. So this could be the possible reason for the discrepancy observed between monomer conversions as shown in Fig. 5.1-3.

As for DPn, as can be seen in eqn.(5-10), it is strongly dependent on the ratio of initial concentration values of both initiator and monomer. Besides this, the value of μ_1 will be dependent on the calculation of M. So the choice of units and thus the values (mass or molar) will definitely affect the final value of DPn. This could be the probable reason for the large discrepancy observed in Fig. 5.1-5. In case of PDI, as can be seen in eqn.(5-11), it is totally independent of initial values of initiator and monomer concentrations, so whatever may be the individual values of μ_0, μ_1, μ_2, the ratios as given in eqn.(5-11) will still give the same result as clearly visible in Fig. 5.1-4.

Besides this, the validation of the simulation results with experimental data also matches quite well as shown in Table 5.1-2. It is noteworthy that DPn simulated value matches perfectly with the experimental one[15]. So there should not be any doubt about the validity of the new transformation proposed in this work. In our opinion, the discrepancy between our current results and Serra $et\ al$ [14] is not because of any error in simulation. The discrepancy probably arose because of different modeling/transformations used by them compared to us, which affected the subsequent results. Their modeling affected the units as well as the numerical value of the initial concentrations of initiator and monomer. The new results, thus, should be seen as the outcome of improvement in the modeling (new transformation) rather than due to incorrect data or as error.

5.1.9 Conclusion
Chemical reactions are frequently modeled in CFD simulations. The chemical data need to be converted to mass form so as to satisfy the law of conservation of mass required for CFD simulations. This may not give correct results in all cases especially for polymerization reactions where most of reaction terms are not simple expression of just one chemical species concentration. This can lead to serious errors in simulation output and also in its analysis. However, the new transformation proposed in this work overcome this problem and was

exemplified by the modeling of the free radial polymerization (FRP). A good match was observed between the simulation results and experimental ones for the BPO initiated styrene polymerization. The new transformation does not have the only advantage of keeping the benefit of reducing the stiffness of the set of equations as originally proposed by Zhu[12] but is also well adapted for implementation in CFD software packages.

This section has clearly shown that significant errors are introduced by converting molar form of chemical data into mass form as required in CFD simulations. A new but simple transformation has been proposed which enables the data to be fed in original molar form while possessing all the advantages of established Zhu transformation. This new transformation will be used in next section to review the existing work of Mandal et al.[13] Their work was about evaluating two microreactor geometries namely coiled flow inverter reactor (CFIR) against straight tube reactor (STR) while simulating free radical polymerization with CFD for unmixed feed conditions. Effects of variation in density and viscosity with conversion with discrete variation of diffusion coefficient will be additionally studied.

5.1.10 References

1. Baillagou, P. E.; Soong, D. S., Major Factors Contributing to the Nonlinear Kinetics of Free-Radical Polymerization. *Chem Eng Sci* **1985**, *40* (1), 75-86.
2. Achilias, D. S.; Kiparissides, C., Development of a General Mathematical Framework for Modeling Diffusion-Controlled Free-Radical Polymerization Reactions. *Macromolecules* **1992**, *25* (14), 3739-3750.
3. Keramopoulos, A.; Kiparissides, C., Development of a comprehensive model for diffusion-controlled free-radical copolymerization reactions. *Macromolecules* **2002**, *35* (10), 4155-4166.
4. Baillagou, P. E.; Soong, D. S., Free-Radical Polymerization of Methyl-Methacrylate in Tubular Reactors. *Polym Eng Sci* **1985,** *25* (4), 212-231.
5. Cabral, P. A.; Melo, P. A.; Biscaia, E. C.; Lima, E. L.; Pinto, J. C., Free-radical solution polymerization of styrene in a tubular reactor - Effects of recycling. *Polym Eng Sci* **2003,** *43* (6), 1163-1179.
6. Chen, C. C., A Continuous Bulk-Polymerization Process for Crystal Polystyrene. *Polym-Plast Technol* **1994,** *33* (1), 55-81.
7. Chen, C. C., Continuous production of solid polystyrene in back-mixed and linear-flow reactors. *Polym Eng Sci* **2000,** *40* (2), 441-464.
8. Costa, E. F.; Lage, P. L. C.; Biscaia, E. C., On the numerical solution and optimization of styrene polymerization in tubular reactors. *Comput Chem Eng* **2003,** *27* (11), 1591-1604.
9. Garg, D. K.; Serra, C. A.; Hoarau, Y.; Parida, D.; Bouquey, M.; Muller, R., Analytical Solution of Free Radical Polymerization: Derivation and Validation. 2014, *to be submitted*.
10. Garg, D. K.; Serra, C. A.; Hoarau, Y.; Parida, D.; Bouquey, M.; Muller, R., Analytical Solution of Free Radical Polymerization: Applications-Implementing Gel effect using CCS model. **2014,** *to be submitted*.
11. Garg, D. K.; Serra, C. A.; Hoarau, Y.; Parida, D.; Bouquey, M.; Muller, R., Analytical Solution of Free Radical Polymerization: Applications-Implementing Gel effect using

AK model. **2014**, *to be submitted*.

12. Zhu, S. P., Modeling of molecular weight development in atom transfer radical polymerization. *Macromol Theor Simul* **1999,** *8* (1), 29-37.
13. Mandal, M. M.; Serra, C.; Hoarau, Y.; Nigam, K. D. P., Numerical modeling of polystyrene synthesis in coiled flow inverter. *Microfluid Nanofluid* **2011,** *10* (2), 415-423.
14. Serra, C.; Schlatter, G.; Sary, N.; Schonfeld, F.; Hadziioannou, G., Free radical polymerization in multilaminated microreactors: 2D and 3D multiphysics CFD modeling. *Microfluid Nanofluid* **2007,** *3* (4), 451-461.
15. Serra C., Sary, N.; Schlatter, G., A multiphysics approach of the styrene free radical polymerization modeling performed in different microreactors, In Proc. of Conference FemLab 2005, Paris (France), 15 November 2005.

5.2 Numerical investigations of different tubular microreactor geometries for the synthesis of polymers under unmixed feed condition

5.2.1 Abstract

Two tubular microreactor geometries, namely straight tube reactor (STR) and coiled flow inverter reactor (CFIR), were numerically considered with unmixed feed at their inlet for the synthesis of poly(methyl methacrylate) and poly(styrene) by free radical polymerization. A new transformation was used to feed CFD code with original molar forms of species concentrations and kinetic rate coefficients. Significant differences between the two types of reactor were observed. Compared to STR, CFIR was found to achieve higher number-average chain length (DPn) while keeping polydispersity index (PDI) lower. But the monomer conversion was slightly lower compared to STR. The modeling was then extended to include the variation in physical properties like density, viscosity and thermal conductivity to evaluate the effect on simulation results. Compared to constant one, varying fluid thermo-physical properties case results for monomer conversion and DPn were found to be on higher side with similar trend but for PDI, the values were found to be lower with different trend especially at lower diffusion coefficient. This emphasizes importance of implementing variation in flow properties instead of taking them constant in CFD simulations. A special case of increased mixing in STR at low diffusion coefficient for unmixed feed condition was also observed. The absence of this effect with constant density and viscosity condition clearly emphasizes the importance of implementing variation in density and viscosity for unmixed feed condition. CFIR was found to show better mixing compared to STR under similar conditions and thus allows achieving a better control over the molecular weight distribution and PDI of synthesized polymer over a wide range of diffusion coefficients under unmixed feed condition.

Keywords: Coiled flow inverter, microreactor, free radical polymerization, straight tube, unmixed feed, solution polymerization.

5.2.2 Introduction

Mixing is a very important aspect to be considered before designing any chemical reaction process[1]. In any reactor, improper mixing leads to decrease in the quality of product, lesser production, generation of waste products etc. Moreover, as the size of the reactor increases, the problem of mixing gets more crucial. The mixing can be accomplished in flow reactors either by active or passive methods[2]. The former are those where moving parts or external source of energy are provided to improve mixing within the reactor, e.g. stirring blades. Whereas in passive type, mixing is achieved through variations in fluid flow profile generated by geometry of the reactor. Active mixing requires huge amount of energy for ensuring desired level of mixing but may be necessary in cases where high level of mixing needs to be ensured all time, e.g. for highly viscous reacting fluids etc. Because of the presence of active/moving parts, maintenance cost is an additional burden. In some cases, active mixing may not be a good option, e.g. under highly corrosive or fouling environment where frequent maintenance is required which lowers the time productivity. On the other hand, passive mixing is quite simple compared to active one, it usually requires less energy input for

reaching the desired level of mixing. Since, the mixing is achieved due to complex flow profiles generated by specific reactor geometries, various complex geometries emerge achieving different level of mixing. However, none all geometries may not be good for commercial production[3].

To ensure the best mixing within the reactor, one simple option would be to have all the reactants mixed before the reaction starts. For batch reactors, all the reagents are usually added to the reactor, mixed using stirrers and then the temperature can be varied to promote the reaction. But for flow reactors, this is usually done separately. Mixing in large scale is ensured by forced convection but final mixing happens at molecular level only through diffusion which is a very slow process compared to convection. So to increase mixing, several methods are devised which bring various components near to each other. This can be achieved by increasing contact area between the two mixing fluids[4]. Another aspect that affects mixing is the dimensions of the reactor. By decreasing cross sectional dimensions, diffusion can become significant in increasing mixing despite being in laminar flow regime. This is the basis of micromixing and microreactor technology[2-4].

Normally, fluid properties are assumed to be constant for simplifying the modeling and in most of the chemical reactions, variation in density and viscosity is not significant. But for polymerization, the viscosity can vary by about 4-6 orders thus affecting the flow profile significantly. As a consequence, heat and mass transfers can be severely decreased hence affecting the macromolecular properties (i.e. molecular weight and polydispersity index (*PDI*)). This work is essentially an extension and improvement of the work done by Mandal *et al.*[5]. In that work, the authors had numerically modeled a tubular polymerization reaction of styrene (St) under unmixed feed condition. A new transformation is used which was developed in our previous work[6] to fed CFD code with original molar forms of species concentrations and kinetic rate coefficients instead of usual mass form. Variation in density, viscosity and thermal conductivity as a function of conversion are also modeled for the free radical polymerization (FRP) of methyl methacrylate (MMA). Results are compared with those for constant properties as in Mandal *et al.*[5] work. Additionally two types of tubular reactor were compared and evaluated for different chemical species diffusion coefficients.

5.2.3 Mathematical model for CFD
The mathematical model for CFD is given in section 3.2.9.

5.2.4 Model of FRP
The kinetic scheme given in section 3.2.2 is used in this work except for the steps for transfer to solvent and transfer to chain transfer agent. The mathematical model is given in section 3.2.3 is used appropriate to the kinetic scheme.

5.2.5 New transformation
The new transformation is presented in section 5.1.5.

5.2.6 Chemical and physical data

Chemical and kinetic data used for MMA and styrene are given in Table 3-1, for AIBN in Table 3-3 and for toluene in Table 3-4. For modeling variation in viscosity of MMA, equations are given in 3.2.5.2.

5.2.7 Operating conditions of reactor

The reaction conditions are given in Table 3-5.

5.2.8 Methodology

The geometries studied are the same as used by Mandal *et al.*[5] The same files for the simulations are used in this study so no mesh independency test was done. The reaction conditions were taken to be same as that taken by the authors Mandal in their work for St. For the case of MMA, all conditions remain same as for St. 5 passive scalars were used defining different chemical species. Scalar1 represent initiator concentration whose generation term was defined by eqn.(6). Similarly, scalar2 represent monomer concentration with eqn.(7), scalar3-scalar5 are for μ_0, μ_1 & μ_2 thorough eqn.(11)-(13) respectively. Diffusion coefficient was taken to be same for all these chemical species (scalars1-5 in CFD simulation). Third order spatial scheme was used for all scalars to reduce the numerical diffusion. Instead of these five scalars as used by the authors, two additional scalars were taken in the current work. They modeled non-reacting diffusing and non-diffusing tracer each. Non-reacting diffusing tracer scalar was denoted as scalar6 and non-reacting non-diffusing tracer as scalar7. For non-diffusing tracer, the diffusion coefficient was taken to be 1×10^{-20} for all simulations. For the diffusing tracer, the diffusion coefficient was taken to be the same as that for all chemical species. It was also modeled as solvent when variation in physical properties was modeled.

The diffusion coefficient was varied discretely for the simulations (Table 3-5) whereas other physical properties like density, viscosity, thermal conductivity and specific heat were kept fixed to their value reported in Table 3-5 for both MMA and styrene. In another set of simulations on MMA, density, thermal conductivity and fluid viscosity were varied by using the expressions given in Table 3-1 and in section 3.2.5.2.

The simulations were assumed to be converged when the residual error ratio reduced below 10^{-8} for all the variables. Velocity and concentration profiles were modeled flat at the inlet. The inlet temperature was taken to be 27°C (ambient temperature). No-slip at walls, zero flux for all the scalars across the wall and isothermal condition at wall were taken as boundary conditions. Unstructured meshing was used for both straight tube reactor (STR) and coiled flow inverter (CFIR) reactor as shown in Fig. 3-1. The monomer was fed from the bigger cut of inlet and initiator with solvent was fed from smaller (30%) cut of inlet. Inlet values for scalars are as follows:

Table 5.2-1- Scalars values at reactor inlet for unmixed condition.

	70% cut	30% cut
Scalar1	0	1
Scalar2	1	0
Scalar3-5	0	0
Scalar6-7	0	1

For running simulation, CFD-ACE was used and CFD-VIEW was used for post-processing.

To prevent wrong calculation of viscosity based on monomer conversion, following scheme was used. In any cell, if the scalar6 (solvent as non-reacting diffusing tracer) is 1, i.e. only solvent is present, then volume fraction of monomer in that cell was taken to be 0. If scalar6 value is zero, i.e. the solvent is absent, then the monomer conversion and volume fraction are to be obtained for bulk polymerization. For all other cases, monomer conversion and volume fraction were calculated for solution polymerization with constant dilution factor as 0.3.

5.2.9   Results and discussion

By optimizing different relaxation parameters, we have been able to get the simulations converged faster (mostly in about 150-3000 iterations depending on diffusion coefficient) with much lower residual error ratio values and with an extended range of diffusion coefficient values compared to Mandal *et al.*[5] Furthermore, the new transformation was applied successfully and all data was fed in molar form only.

Fig. 5.2-12 to Fig. 5.2-3 shows the results regarding monomer conversion, *DPn and PDI* respectively for both STR and CFIR obtained in this work and compared with Mandal *et al.*[5]
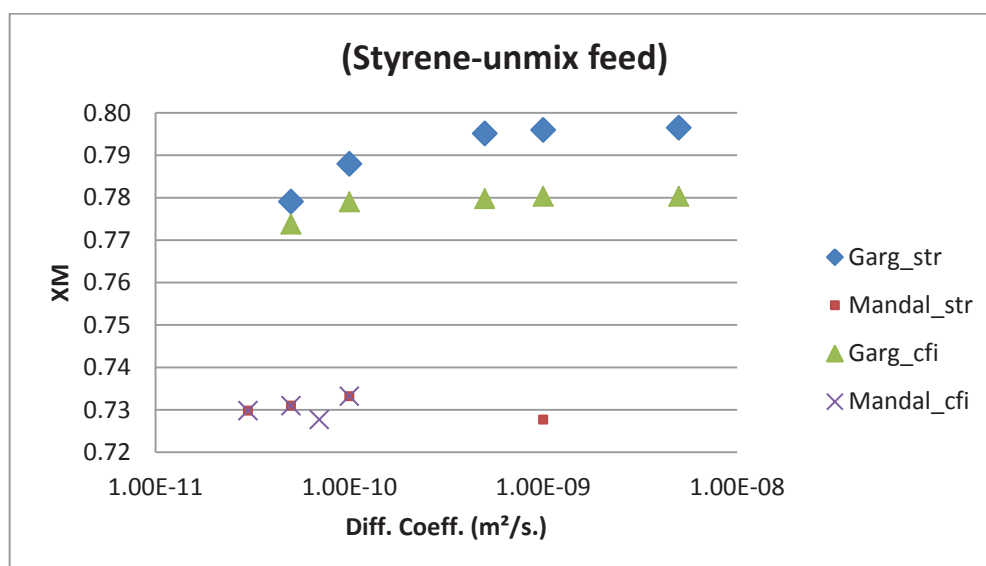
Fig. 5.2-1-Variation of St conversion (x_M) with diffusion coefficient for the case of constant fluid thermo-physical properties.

In Fig. 5.2-1, it can easily be seen that monomer conversion has been calculated higher for both STR and CFIR in current work compared to Mandal *et al.*[5] This result is in accordance with the results obtained in our previous work on the new transformation. The difference is due to the effect of the initial value and units of monomer and initiator concentrations as well kinetic rate constants which have been properly accounted by the new transformation while introducing significant error when entered in mass form.

Besides this, the monomer conversion is predicted consistently higher for STR compared to CFIR in our work. This can be understood by looking at the inlet feed condition. Since the two reactant streams (solvent + initiator and monomer) are fed to the reactor in unmixed

condition (Fig. 3-1c), they can only be mixed with flow. Since the initiator is mixed with solvent and not with monomer, so monomer and solvent need to diffuse in opposite regions to have any reaction. In STR, the mixing operates solely because of diffusion process, so the concentration of monomer remains high which favors a rapid polymerization rate. Thus higher monomer concentration leads to higher conversion[12]. In CFIR, the mixing is enhanced by inversion of secondary flow (Dean Vortices) caused due to bend at regular intervals in curved geometry (helical shape)[13]. Although the secondary flows will be very small but they will still improve mixing for inviscous fluid as shown by Vanka *et al.*[14]. This along with diffusion process lowers the monomer concentration for reaction and thus lower conversion is achieved. But this higher conversion in STR does not come without problem. Due to poor mixing in STR, DP_n and PDI would be affected in negative way and their results will be discussed while discussing the results for Fig. 5.2-2 and Fig. 5.2-3 respectively.

The monomer conversion in Fig. 5.2-1 can also be observed to be increasing with increasing diffusion coefficient and then remains nearly constant for high diffusion coefficients. This is because increasing diffusion coefficient increases the mixing process by diffusion and hence after a certain value of diffusion coefficient for a given reactor dimension and velocity (as given by Peclet number), mixing remains same and concentration remains uniform throughout the cross-section. For STR, the variation in monomer conversion from low value of diffusion coefficient to high value is quite significant compared to CFIR. This clearly shows the improved internal mixing benefit of CFIR over STR for monomer conversion even at low values of diffusion coefficient.

On the other hand, the results obtained by Mandal *et al.*[5] do not show significant differences for monomer conversion between STR and CFIR. Moreover, due to smaller range of diffusion coefficient values in their simulations, no trend could be figured out.
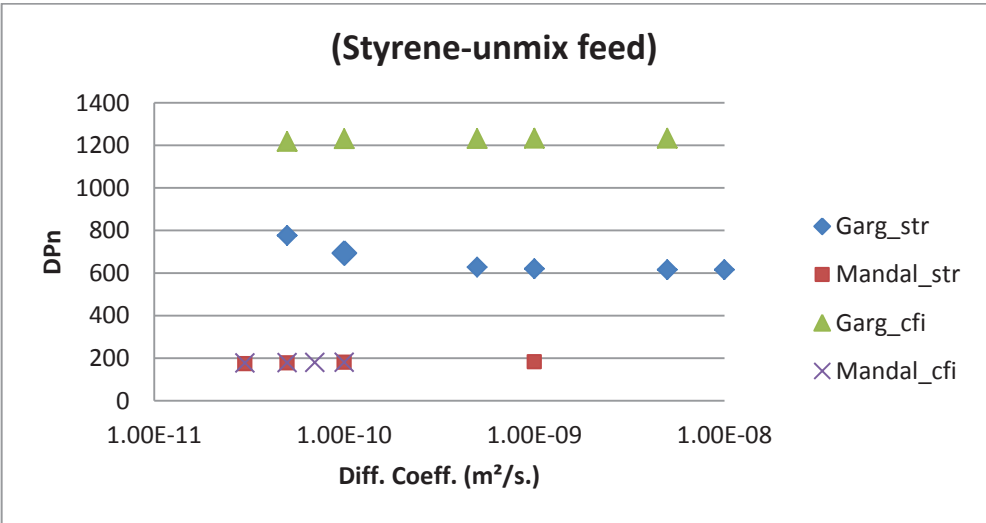
Fig. 5.2-2 Variation of polystyrene number-average chain length with diffusion coefficient for the case of constant fluid thermo-physical properties.

Fig. 5.2-2 shows the results for DPn. Again, we can observe that the DPn in our work for both STR and CFIR are predicted higher compared to those obtained by Mandal *et al.*[5] It is

also on the same line as shown in our previous work about the new transformation. Here significant observation about the values of *DPn* for CFIR compared to STR for the same range of diffusion coefficient can be observed. The values of *DPn* for CFIR are nearly twice as much compared to STR. This is a significant improvement over STR. Besides this, for CFIR, the value of *DPn* is nearly constant for the whole range whereas for STR, it increases for low values of diffusion coefficient. As already explained earlier regarding the mixing process in STR, this results is straightforward and predictable. CFIR is proved again to have much better control on *DPn* compared to STR for same range of variation of diffusion coefficients.
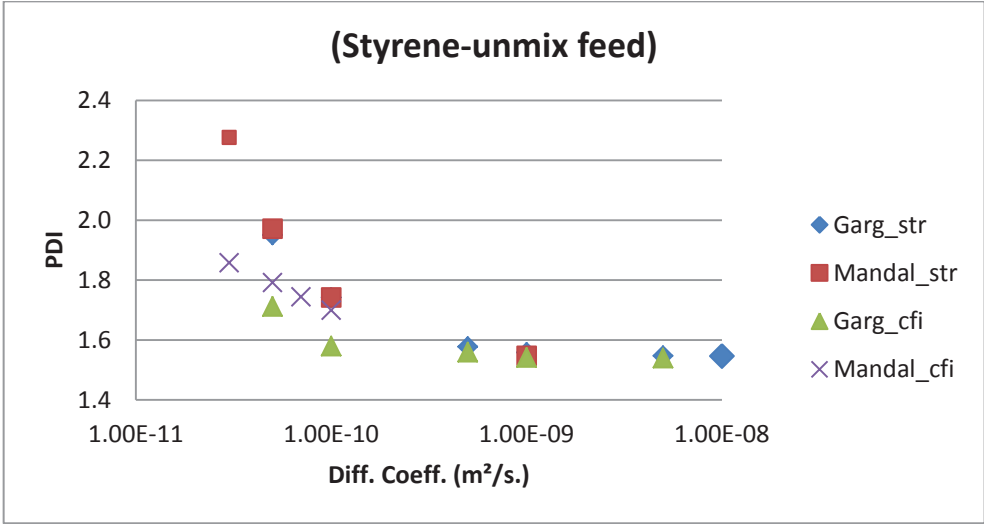
Fig. 5.2-3 Variation of polystyrene polydispersity index with diffusion coefficient for the case of fluid constant physical properties.

Fig. 5.2-3 actually proves that the results shown in our current work are in right direction. This can be inferred from the matching of *PDI* in case of STR for high diffusion coefficients between our work and that of Mandal *et al.*[5]. Indeed, as *PDI* is independent of units of initial concentration values of initiator and monomer, it can be said that *PDI* is transformation independent. So if the modeling in our work had been wrong, then this matching would not have occurred.

It can be seen that *PDI* predicted for CFIR is lower than STR in both our and Mandal *et al.*[5] works. This is due to improved mixing as explained earlier. It can also be seen that *PDI* predicted in current work remains nearly constant for a larger range of diffusion coefficients. Besides this, variation in PDI values is much less compared to STR for the same range of diffusion coefficient. For higher diffusion coefficient, *PDI* for both STR and CFIR is nearly same. This again is due to improved mixing resulting from higher diffusion coefficients and hence peclet numbers. This result demonstrates the improved control over *PDI* by CFIR compared to STR under similar conditions.

Fig. 5.2-1 to Fig. 5.2-3 clearly presented the significant improvements gained in current work compared to previous work by Mandal *et al.*[5] under same conditions. Current work has been able to show in a better manner with more clarity the superiority of CFIR over STR.

Now, we will see the results for MMA simulated under similar conditions in Fig. 5.2-4 to Fig. 5.2-8. These results have been obtained for constant as well as with variation in density, viscosity and thermal conductivity with discrete variation of diffusion coefficient (as mentioned in methodology- section (5.2.8)) to observe the impact of these physical properties on flow and thus on mixing. In each figure, the data is presented for both STR and CFIR for both constant and variable fluid thermo-physical properties.
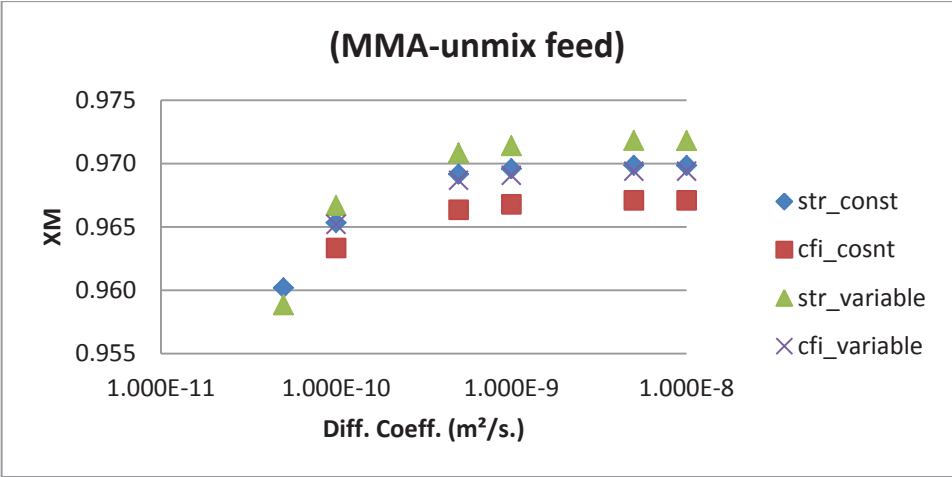
Fig. 5.2-4- Variation of MMA conversion (x_M) with diffusion coefficient for constant as well as variable fluid thermo-physical properties.

Fig. 5.2-4 shows the results for monomer conversion. Similar to results obtained for styrene, here too, the conversion in STR is predicted to be more compared to CFIR. This observation is same for both cases of constant and variable fluid thermo-physical properties. It can also be observed that predictions for monomer conversion are shifted to higher values for variable fluid thermo-physical properties compared to constant ones. Thus introducing variation in fluid thermo-physical properties does affect the monomer conversion prediction significantly as it accounts for the mixing effect in a better way.
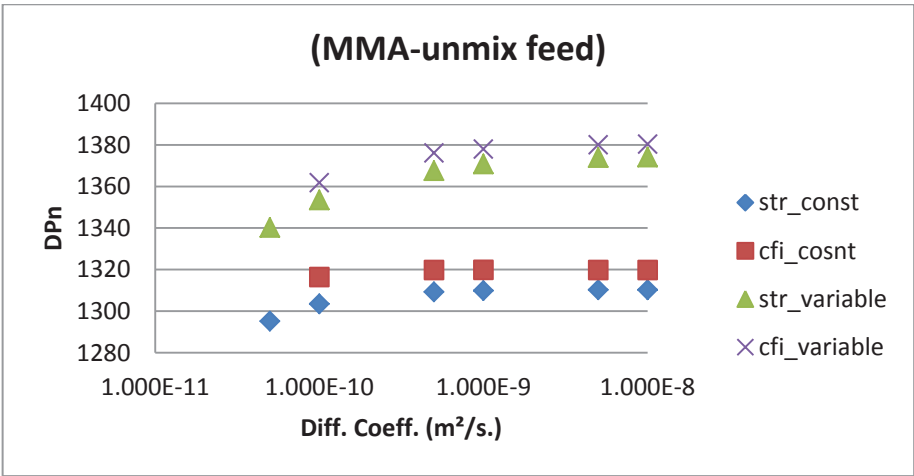
Fig. 5.2-5- Variation of poly(methyl methacrylate) number-average chain length with diffusion coefficient for constant as well as variable physical properties.

Fig. 5.2-5 shows the results for *DPn*. Here, the predictions for variable fluid properties are higher and better compared to the case of constant one. Besides this, the results for CFIR are better than STR whether fluid thermo-physical properties are considered constant or variable. Moreover, for both CFIR and STR, *DPn* increases when diffusion coefficient increases. This could be due to low mixing at lower diffusion coefficient which further decreases because of increased viscosity with conversion.
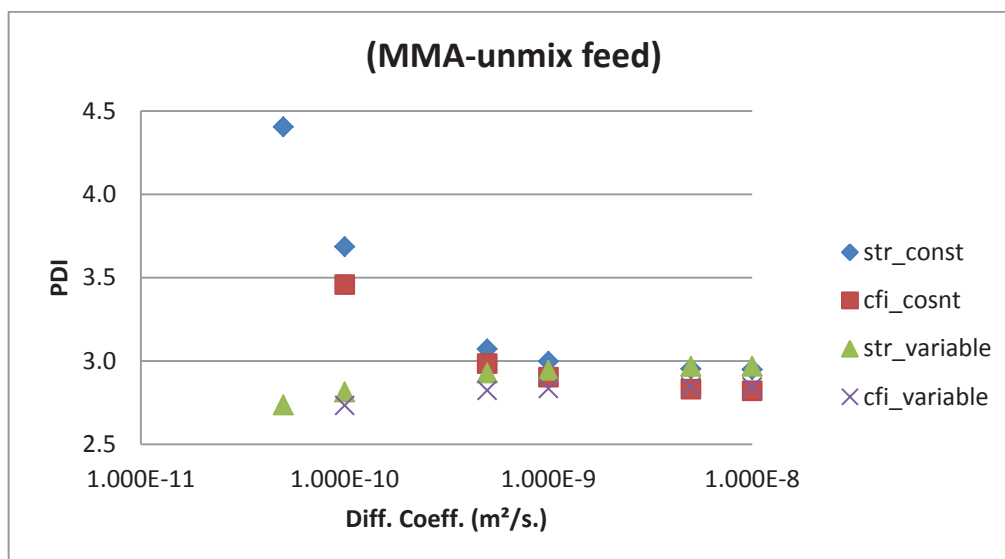
Fig. 5.2-6- Variation of poly(methyl methacrylate) polydispersity index with diffusion coefficient for constant as well as variable physical properties.

Fig. 5.2-6 shows the results for *PDI*. It shows the most significant difference between constant and variable fluid thermo-physical properties cases. For constant parameters, *PDI* is increasing for both STR and CFIR when diffusion coefficient is decreasing. Similar trend was reported earlier for STR for constant physical property case[5,15]. Whereas, for variable parameters, *PDI* decreases on decreasing diffusion coefficient value. This result seems to be unexpected. Ivleva *et al.*[16] have discussed the conditions under which chemical reactions promote mixing in unstirred reactor. They have discussed some cases. In one case they had discussed about increased mixing due to natural convection arising due to spatial temperature variation. This spatial temperature variation arises out of non-uniformity in exothermic reaction and cooling of the reactor through walls. Another case is about the case of "critical mixing" when the substance is near critical point. Here large changes in density, temperature and concentration can occur and thus can increase mixing due to large fluctuations induced. Another case discussed is about increased mixing due to chaotic behavior in the chemical reaction where several elementary steps are included and they may proceed in a chaotic way spatially. So in our case, when both the situations of unmixed feed condition as well as variation of fluid thermo-physical properties are looked together, this may look straightforward. The probable explanation is as follows. Due to decreased diffusion coefficient, the diffusion of monomer and solvent into each other is reduced. Thus, reaction is more non-uniform across the cross-section of the reactor. This leads to non-uniform conversion across the cross-section as well as axially. Since the viscosity is a function of

conversion through volume fraction of monomer and polymer (eqn.(3-63)-(3-67)), this will lead to non-uniformity of viscosity across the cross-section according to the conversion. This when combined with variation in density due to conversion (density will increase due to polymer formation) will affect the flow and flow profile and will bend the streamlines increasing local mixing. This will improve mixing even in STR.

This can also explain the increased mixing rate of scalar7 (non-reacting non-diffusing tracer) at lower diffusion coefficients compared to higher diffusion coefficients as shown in Table 5.2-2. Scalar7 cannot mix by diffusion due to its very low diffusion coefficient. So it can only mix due to convective process. At higher diffusion, the mixing between solvent and monomer is improved and thus the variation in density and viscosity across the cross-section is less and hence the flow profile remains nearly unchanged. Thus, in absence of any convective flow across cross-section, it remains unmixed and non-diffused at high diffusion coefficients. The broadening of scalar7 concentration at the mixing interface in STR is due to coarser mesh used.

In CFIR, the scalar7 profile looks same but maximum and minimum concentration values as shown in respective graphs are different. CFIR with variable fluid thermo-physical properties shows much mixing of scalar7 at all diffusion coefficient values by having much lower difference between maximum and minimum values of concentration. This shows that CFIR improves mixing even for highly non-diffusing components and at such a low Reynolds number (0.06 at reactor inlet).

Table 5.2-2-Scalar7 distribution at reactor outlet.

Diffusion coefficient (m²/s)	STR		CFIR	
	Constant parameters	Variable parameters	Constant parameters	Variable parameters
5×10^{-11}				
1×10^{-10}				
5×10^{-10}				
1×10^{-9}				
5×10^{-9}				
1×10^{-8}				

213
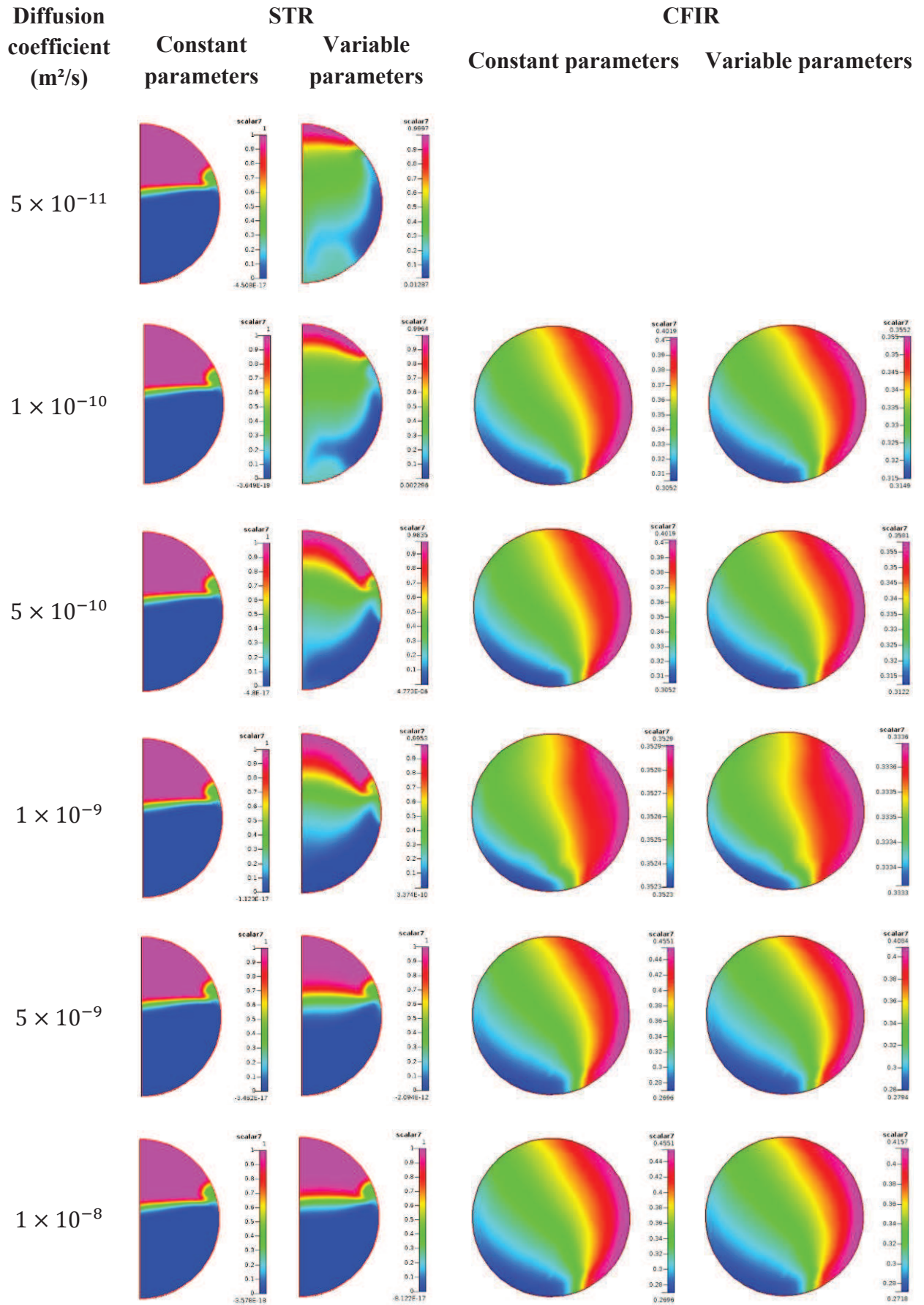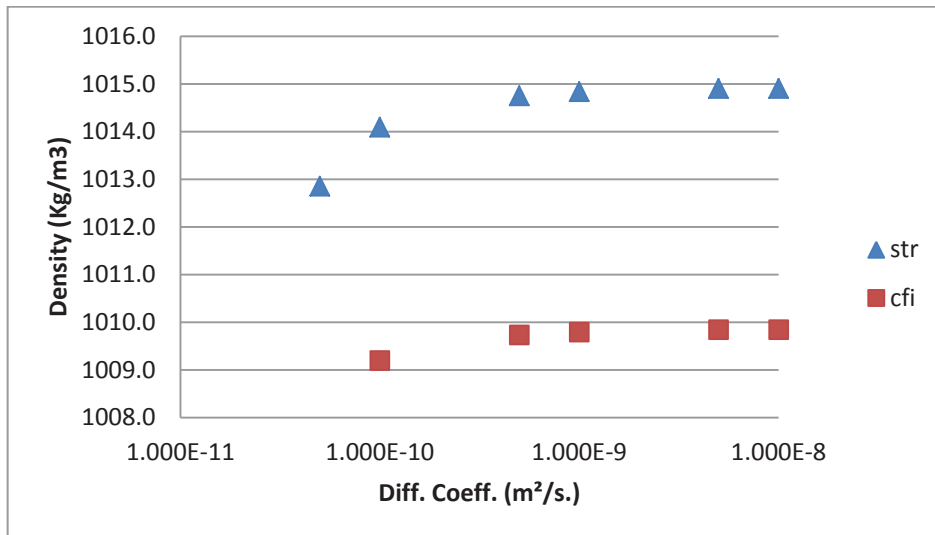
Fig. 5.2-7- Variation of fluid density with diffusion coefficient
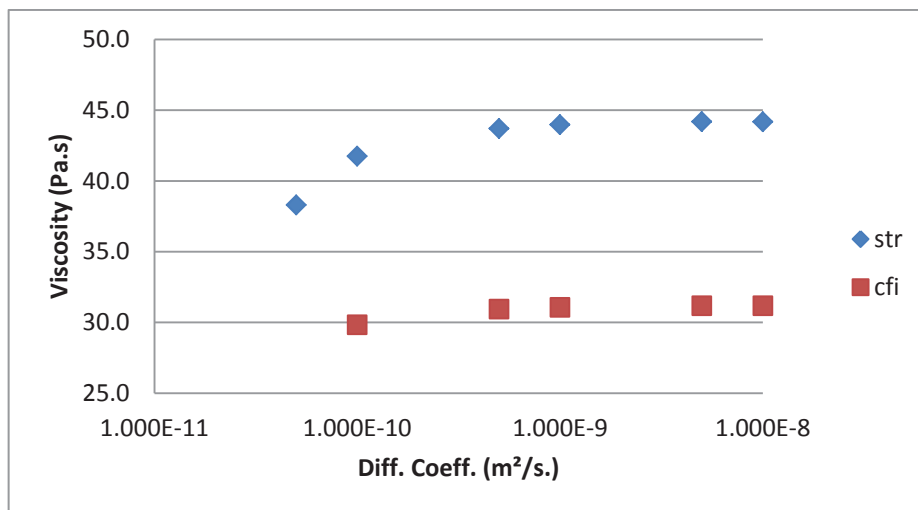
Fig. 5.2-8- Variation of fluid viscosity with diffusion coefficient.

Fig. 5.2-7 & Fig. 5.2-8 show the variation of fluid density and viscosity respectively at the reactor outlet for both STR and CFIR. The trend can easily be related to increased conversion with diffusion coefficient as shown in Fig. 5.2-4. Higher conversion means higher density and viscosity. The viscosity was found to rise by 6 orders from inlet to outlet during the simulations. The density and viscosity distribution at outlet can also be seen in Table 5.2-3 for both STR and CFIR at different diffusion coefficients.

Higher density and viscosity can be observed near wall. This is due to the fact that no-slip boundary condition was applied at wall. So residence time was higher near the wall. This led to higher conversion at wall compared to the center of the tube. The same can be observed by scalar2 distribution at outlet as shown in Table 5.2-4. The distribution of density as well as viscosity can be observed to be much more uniform in CFIR compared to STR proving that the mixing in CFIR is much better than STR.

214

Table 5.2-3- Density and viscosity at reactor outlet
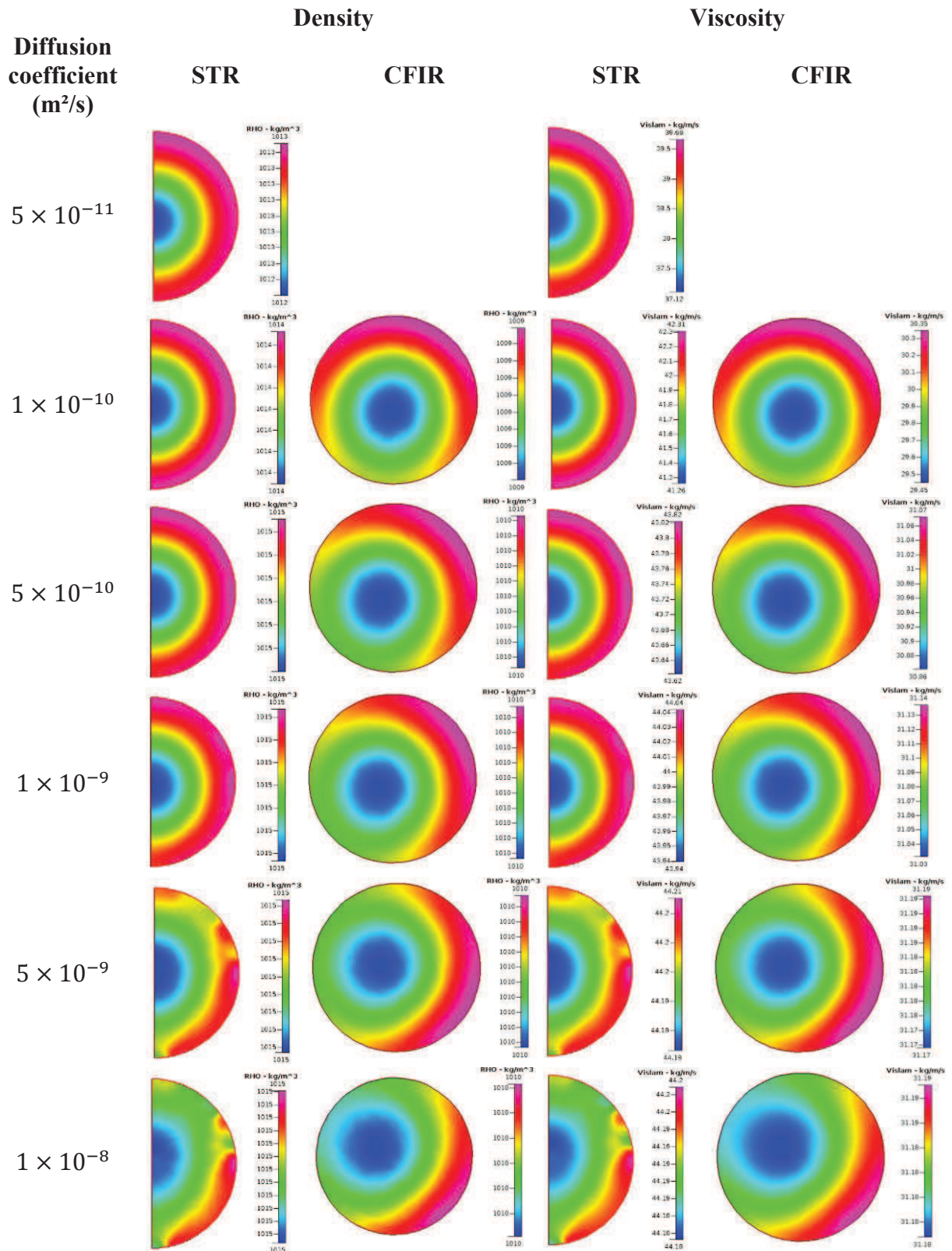
Despite huge variation in viscosity and moderate changes in density, no significant variation of thermal conductivity was observed across cross-section. The temperature variation across the cross section differs only by 0.1K even after varying physical properties. No additional

graph or figure regarding temperature is shown here in the absence of any significant variation of temperature across cross-section Thus truly isothermal condition was observed even during high viscosity variation and density changes. So, modeling thermal conductivity as constant would be a good assumption without affecting any results. But flow properties like density and viscosity have significant impact on the results of the simulations.

Table 5.2-4 shows the scalar2 (monomer concentration) distribution at the outlet for both STR and CFIR with and without variation in fluid thermo-physical properties. The profile looks similar but the difference between maximum and minimum for the concentration is lower for CFIR compared to STR. This highlights one again that local mixing is higher in case of variable physical properties.

Table 5.2-4- Scalar2 distribution at reactor outlet

Diffusion coefficient (m²/s)	STR		CFIR	
	Constant parameters	Variable parameters	Constant parameters	Variable parameters
5×10^{-11}				
1×10^{-10}				
5×10^{-10}				
1×10^{-9}				
5×10^{-9}				
1×10^{-8}				
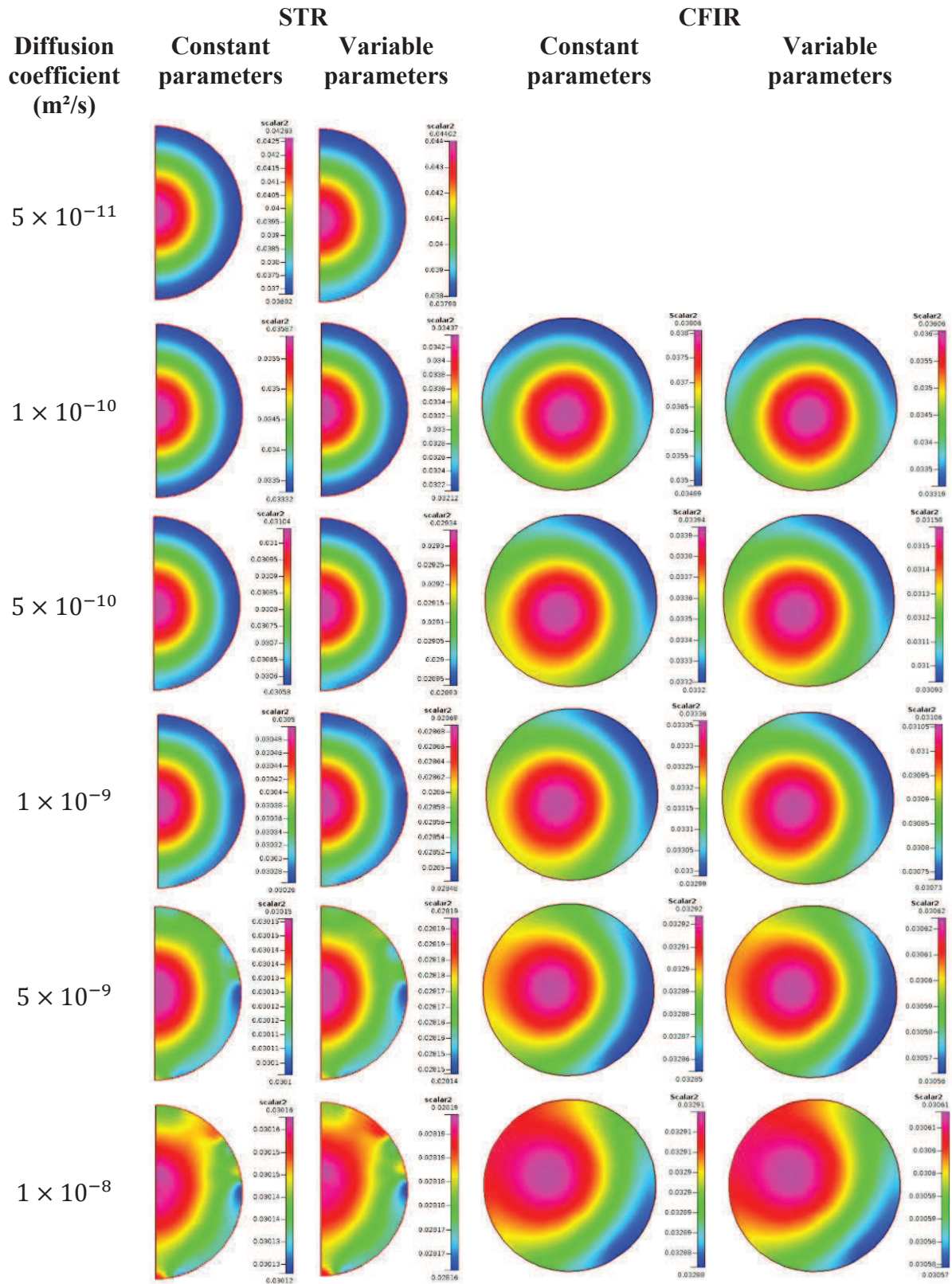
Table 5.2-5 shows the scalar6 profile at the outlet of STR and CFIR for both varying and constant fluid thermo-physical properties. Scalar6 represents non-reacting diffusing tracer. It's mixing increases with increasing system diffusion coefficient and thus it becomes uniformly

spread throughout the cross section even for STR. This was in contrast to the profile of scalar7 which is non-diffusing. This shows that due to its small size, complete mixing can be achieved in STR even with diffusion process only. This is against the normal observation for large sizes tubular flow where such cross-sectional mixing requires flow to be in turbulent range. Another interesting observation is that CFIR achieves the complete mixing for scalar6 at even lower diffusion coefficient compared to STR despite having same dimensions and operating conditions. This shows again the better mixing capabilities of CFIR over STR.

Table 5.2-5-Scalar6 distribution at reactor outlet

Diffusion coefficient (m²/s)	STR		CFIR	
	Constant parameters	Variable parameters	Constant parameters	Variable parameters

218
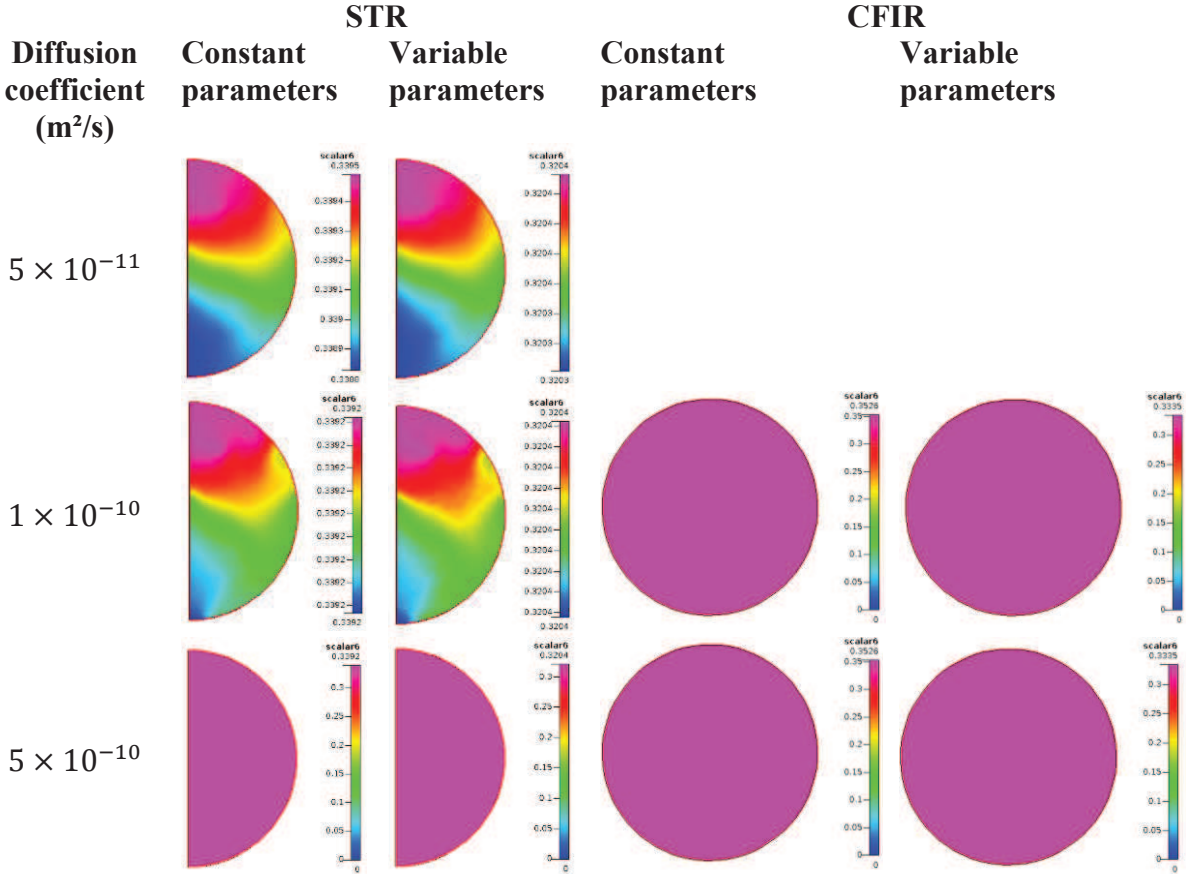
5.2.10 Conclusion

Free radical polymerization was modeled and simulated in two different microtubular geometries namely straight tube reactor (STR) and coiled flow inverter reactor (CFIR) under unmixed feed condition. New transformation proposed in an earlier paper[6] which allows feeding chemical species concentration and kinetic rate coefficients in molar form instead of mass form was applied. Results were first compared with the existing work of Mandal *et al.*[5]obtained for styrene and for constant fluid thermo-physical properties (density, viscosity, thermal conductivity). Significant differences between the works were observed. Compared to Mandal *et al.*[5], current work predicted higher conversion and higher number average chain length (*DPn*) for both STR and CFIR while keeping polydispersity index (*PDI*) lower for CFIR. But prediction for *PDI* was same due to transformation. Compared to STR, CFIR showed much higher *DPn* with lower *PDI*. But the monomer conversion was slightly lower compared to STR.. The modeling was then extended to include the variation in fluid thermo-physical properties. MMA was selected for this and the results were evaluated under the conditions similar to those applied for styrene. Compared to constant one, varying fluid thermo-physical properties case, results for monomer conversion and *DPn* were found to be on higher side with similar trend but for *PDI*, the values were found to be lower with different trend especially at lower diffusion coefficient. A special case of increased mixing in STR at low diffusion coefficient for unmixed feed condition was observed when variation in viscosity and density was modeled. This effect cannot be observed with constant density and viscosity condition. This clearly emphasizes the importance of implementing variation in density and viscosity for unmixed feed condition. CFIR was found to have a much better mixing capability and thus has the possibility to promote a better control over *DPn and PDI* of the produced polymer compare to STR under similar conditions for unmixed feed condition. Thermal conductivity variation and temperature variation across the cross section of the tube were found to be negligible even in the case of variable fluid thermo-physical properties. Hence thermal conductivity can be modeled as constant without any significant effect on the results. Reaction can be assumed to be isothermal for all purposes under microreactor conditions.

CFIR seems to be a promising reactor design and needs to be further evaluated. In next section, mixed inlet condition will be considered to investigate if further improvement in control over macromolecular characteristics can be achieved. Comparison between CFIR and STR, while considering continuous (and not discrete) variation in chemical species diffusion coefficient, will be performed.

5.2.11 References

1. Levenspiel, O., Chemical Reaction Engineering. John Wiley & Sons, New York, third edition, 1999.
2. Hessel, V.; Lowe, H.; Schonfeld, F., Micromixers - a review on passive and active mixing principles. *Chem Eng Sci* **2005,** *60* (8-9), 2479-2501.
3. Suh, Y. K.; Kang, S., A Review on Mixing in Microfluidics. *Micromachines-Basel* **2010,** *1* (3), 82-111.
4. Bockhorn, H.; Mewes, D.; Peukert, W.; Warnecke, H.-J., *Micro and Macro Mixing: Analysis, Simulation and Numerical Calculation*. Springer-Verlag Berlin Heidelberg: Berlin, Heidelberg, 2010.
5. Mandal, M. M.; Serra, C.; Hoarau, Y.; Nigam, K. D. P., Numerical modeling of polystyrene synthesis in coiled flow inverter. *Microfluid Nanofluid* **2011,** *10* (2), 415-423.
6. Garg, D. K.; Serra, C. A.; Hoarau, Y.; Parida, D.; Bouquey, M.; Muller, R., New Transformation Proposed for CFD Simulation of Free Radical Polymerization. **2014,** *to be submitted.*
7. Garg, D. K.; Serra, C. A.; Hoarau, Y.; Parida, D.; Bouquey, M.; Muller, R., Analytical Solution of Free Radical Polymerization: Derivation and Validation. 2014, *to be submitted*.
8. Keramopoulos, A.; Kiparissides, C., Mathematical Modeling of diffusion-controlled free-radical terpolymerization reactions. *Journal of Applied Polymer Science* **2003,** *88* (1), 161-176.
9. Keramopoulos, A.; Kiparissides, C., Development of a comprehensive model for diffusion-controlled free-radical copolymerization reactions. *Macromolecules* **2002,** *35* (10), 4155-4166.
10. Baillagou, P. E.; Soong, D. S., Free-Radical Polymerization of Methyl-Methacrylate in Tubular Reactors. *Polym Eng Sci* **1985,** *25* (4), 212-231.
11. Shoulberg, R. H.; Shetter, J. A., The thermal conductivity of poly(methyl methacrylate). *J. of Appl. Polym. Sci.*, **1962**, *23*(6), 32-33.
12. Cortese, B.; Noel, T.; de Croon, M. H. J. M.; Schulze, S.; Klemm, E.; Hessel, V., Modeling of Anionic Polymerization in Flow With Coupled Variations of Concentration, Viscosity, and Diffusivity. *Macromol React Eng* **2012,** *6* (12), 507-515.
13. Saxena, A. K.; Nigam, K. D. P., Coiled Configuration for Flow Inversion and Its Effect on Residence Time Distribution. *Aiche J* **1984,** *30* (3), 363-368.
14. Vanka, S. P.; Luo, G.; Winkler, C. M., Numerical study of scalar mixing in curved channels at low Reynolds numbers. *Aiche J* **2004,** *50* (10), 2359-2368.
15. Serra, C.; Schlatter, G.; Sary, N.; Schonfeld, F.; Hadziioannou, G., Free radical polymerization in multilaminated microreactors: 2D and 3D multiphysics CFD modeling. *Microfluid Nanofluid* **2007,** *3* (4), 451-461.
16. Ivleva, T. P.; Merzhanov, A. G.; Rumanov, E. N.; Vaganova, N. I.; Campbell, A. N.; Hayhurst, A. N., When do chemical reactions promote mixing? *Chem Eng J* **2011,** *168* (1), 1-14.

5.3 Numerical investigations of perfectly mixed condition at the inlet of free radical polymerization tubular microreactors of different geometries

5.3.1 Abstract

Three microtubular geometries were considered for the numerical simulation of methyl methacrylate free radical polymerization (FRP) with mixed feed condition, namely straight tube reactor (STR), coil tube reactor (CTR) and coiled flow inverter reactor (CFIR). The effect of variation of fluid properties (density, viscosity and thermal conductivity) with reaction along with discrete variation of chemical species diffusion coefficient was studied first. Then, one case of varying diffusion coefficient with constant fluid thermo-physical properties was simulated. All the three reactors were found to give similar results. However, significant differences were found for the prediction of monomer conversion, number average chain length and polydispersity index (PDI) whether fluid thermo-physical properties were considered constant or not. Non constant case gave systematically lower values for the above mentioned properties.. Results clearly show the importance of modeling the variation in fluid flow properties with respect to monomer conversion. Constant thermal conductivity and isothermal reactor condition were found to be good assumption as temperature varied quite few within reactor cross section. CFIR was shown to have chaotic flow even at very low inlet Reynolds number (0.06) for both viscous (i.e. for variable fluid thermo-physical properties) and non-viscous flow conditions resulting in an efficient internal mixing which in turn allows achieving the best control over macromolecular characteristics.

Keywords: Coiled flow inverter, microreactor, free radical polymerization, straight tube, unmixed feed, solution polymerization, methyl methacrylate, chaotic advection.

5.3.2 Introduction

Since mixing has profound impact on polymerization and polymer product properties[1], its effect was required to be studied for extreme conditions of completely unmixed as well as completely mixed feed conditions at inlet of continuous-flow reactor. The effect of unmixed feed condition has already been investigated numerically by some researchers[2,3]. This work is made for mixed feed condition and is in continuity with our earlier work4 focused on unmixed feed condition. In this previous work, a new transformation5 was used which allowed feeding the CFD code with molar form of chemicals species concentration and kinetic rates coefficient instead of mass form. It was found to significantly reduce errors and hence improves the modeling. Moreover, fluid flow properties like density and viscosity were also modeled with respect to monomer conversion and compared with the constant fluid thermo-physical properties modeling. The discrete variation of diffusion coefficient assumed to be same for all chemical species was imposed and its effect was observed on several variables like monomer conversion, polydispersity index (PDI) and number-average polymer chain length (DPn). Two reactor geometries namely straight tube (STR) and coiled flow inverter (CFIR) reactors were considered. Significant differences were found in the prediction of monomer conversion, number average chain lengths and PDI after modeling variations in density and viscosity compared to constant density/viscosity ones. Viscosity was found to rise

by about 6 orders from inlet to outlet and have profound impact on flow profiles. As a consequence mixing due to convective flow was severely affected. But a case of increased convective mixing at low diffusion coefficient was observed which could not be simulated using constant fluid properties. Thermal conductivity was also modeled as function of monomer conversion but no significant variation in its value was observed. The temperature profile across cross-section was indeed found to be uniform even under the varying density and viscosity condition. CFIR was found to perform better with more control over polymer properties (lower PDI, higher DPn) compared to STR under similar operating conditions for unmixed feed.

To evaluate even more precisely the promising CFIR with the hope to improve the polymerization modeling further, this study considers now the case of mixed feed condition for the polymerization of methyl methacrylate (MMA). To study and evaluate the systematic improvement in mixing and control of polymer properties like PDI and number-average chain lengths (DPn) due to reactor geometry, three different tubular microreactor geometries are taken for study. All three reactors could be considered as passive mixers[6], i.e. no external stimulus (e.g. stirrer, ultrasound etc.) is used to promote mixing. The first reactor geometry considered is the straight tube (STR, Fig. 1b) which relies only on mixing by mass diffusion. Second is the coil tube reactor (CTR, Fig. 1d) which take benefit from secondary flows arising from its curvature to increase mixing[7-10]. The third reactor geometry is the CFIR (Fig. 1f) which was found to significantly increase internal mixing in unmixed feed condition owing to 90° bends placed at regular intervals along a normal CTR[11].

The importance of modeling fluid properties like density and viscosity over simulation results was observed in our previous work with unmixed feed condition[4]. To evaluate its importance for mixed feed condition, same methodology is adopted. First set of modeling involves constant fluid properties with discrete variation of chemical species diffusion coefficient. Second set includes the variation of density, viscosity and thermal conductivity with respect to monomer conversion along with discrete variation of diffusion coefficient. Finally, the third set models the variation of diffusion coefficient using free volume theory[12-14] keeping fluid thermo-physical properties constant.

5.3.3 Mathematical model for CFD
The mathematical model for CFD is given in section 3.2.9.

5.3.4 Model of FRP
The kinetic scheme given in section 3.2.2 is used in this work except for the steps for transfer to solvent and transfer to chain transfer agent. The mathematical model is given in section 3.2.3 is used appropriate to the kinetic scheme.

5.3.5 New transformation
The new transformation is presented in section 5.1.5.

5.3.6   Chemical and physical data

Chemical and kinetic data used for MMA and styrene are given in Table 3-1, for AIBN in Table 3-3 and for toluene in Table 3-4. For modeling variation in viscosity of MMA, equations are given in 3.2.5.2.

5.3.7   Operating conditions of reactor

The reaction conditions are given in Table 3-5. The reactor data for each type of reactor geometry used are given in Table 3-6.

5.3.8   Meshing

The details of meshing are given in section 3.2.10. Fig. 3-2 shows the structure meshing used in this work for each reactor geometry.

5.3.9   Numerical modeling

Five chemical species represented by eqn.(3-3), eqn.(3-4), eqn.(3-11) to eqn.(3-13) were modeled as passive scalars denoted as scalar1 to scalar5 respectively. CFD-ACE+, a reputed commercial CFD software, was used for CFD simulation. The spatial distribution of velocity and all the five scalars were taken to be 3rd order so as to improve the accuracy and to reduce the numerical diffusion in the simulations. CGS+Preconditioner solver was selected for velocity and all 5 scalars whereas AMG solver was selected for pressure. SIMPLEC algorithm was used for solving pressure equation. During mesh independency test, several variations in relaxation parameters were also made and their effect on convergence and rate of convergence were observed. The values of relaxation parameters chosen were found to speed up the rate of convergence thus reducing the time required for simulation. The values chosen for relaxation parameters were found to reduce the residual error ratio to levels below 10^{-8} and thus improving the accuracy of simulations. Furthermore, this was achieved in less number of iterations.

To evaluate the effect of variation of fluid thermo-physical properties over constant values, two such sets of simulations were conducted. One set was carried out keeping the fluid variables like density, viscosity etc. as constant with discrete variation of diffusion coefficient as an easiest case. The second set models the variation of density, viscosity and thermal conductivity.

Finally, variation in diffusion coefficients was modeled using equations given in section 3.2.8.

In this article, the effect on various reaction parameters like monomer conversion (X_M), *PDI* and *DPn* with discrete variation in diffusion coefficient of chemical species is studied. During discrete variation of diffusion coefficient, it was assumed same for all the scalars in a given simulation. The case of variable diffusion coefficients was also studied but was modeled while keeping fluid thermo-physical properties constant. When varying diffusion coefficients, first two scalars representing initiator in solvent and monomer, were considered to have same diffusion coefficient and thus calculated using eqn.(3-111). For rest three scalars, diffusion coefficient were considered same and calculated using eqn.(3-112) as these scalars represent polymer molecules.

The simulations were assumed to be converged when the residual error ratio reduced below 10^{-8} for all the variables. Velocity profile was taken to be parabolic and concentration profiles were modeled flat at the inlet. The inlet temperature to the reactor was taken to be same as inside the reactor i.e. 70°C. No-slip at walls, zero flux for all the scalars across the wall and isothermal condition at walls were taken as boundary conditions. Scalar1 and scalar2 are taken to be 1 and scalar3 to scalar5 are taken to be 0 at inlet. To run simulation, CFD-ACE was used while CFD-VIEW was utilized for post-processing.

5.3.10 Methodology

The analytical solution of the set of differential equations constituting the mathematical model of the polymerization reaction is derived for ideal conditions, i.e. isothermal, well mixed batch reactor, in our previous work for a batch reactor[17]. The given set of mathematical model (eqn.(3-3)-(3-14)) was simulated for well-mixed isothermal batch reactor and transient analysis of STR was done. Its results were matched with the results obtained by analytical solution and they matched perfectly. The results are shown in Fig. 5.3-1 with dimensionless variables in terms of concentration. The graph obtained here is for Styrene. For details about its chemical data, please refer to our previous work.[4,5]
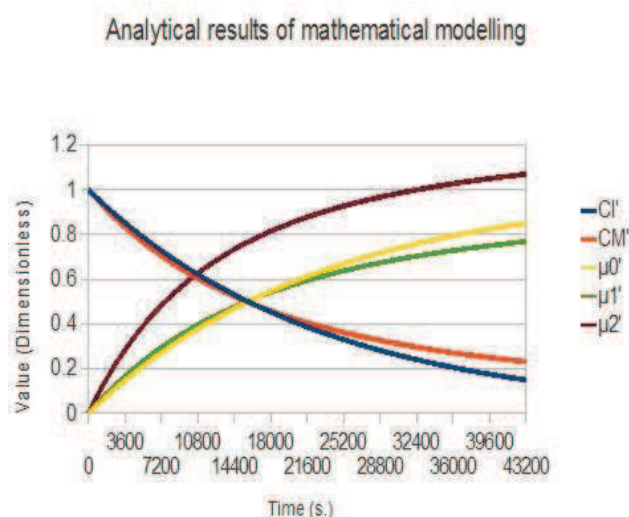
Fig. 5.3-1:Comparison of simulated mathematical model for well mixed isothermal batch reactor with the analytical solution for the same conditions.

The batch reactor results are theoretically applicable for the plug flow condition also. This was used to validate the coding for STR geometry. The plug flow was simulated using CFD in STR geometry by applying moving wall boundary condition with fully mix inlet for concentration and flat profile for velocity at inlet. The results compared to analytical solution for batch reactor (equivalently for plug flow in terms of length) are given in Table 5.3-1.

Table 5.3-1- Comparison of the analytical solution and the simulation of plug flow reactor.

	Analytical solution	Plug flow simulation
Conversion, x_M	0.770093	0.770024
PDI	1.53879	1.53873
DPn	372.981	372.968

224

The fully mixed feed with 30% dilution by solvent at inlet was taken for all the cases. The results matches excellently with analytical solution obtained for the same reactor conditions. Thus, both batch type reactor as well as plug flow type reactor simulations validates the correctness of the implementation of the equations within the software for simulation along with the correct implementation of the new transformation.

5.3.11 Mesh independency test

The process of mesh independency is given in detail in section 3.2.11. The results of mesh independency are given in Table 3-7. The final mesh selected for each reactor geometry based on mesh independency test, is given in Table 3-8.

5.3.12 Results and discussion

For constant fluid thermo-physical properties case, the convergence was obtained for discrete variation of diffusion coefficient over a large range of values ranging from 1×10^{-12} to 1×10^{-8} m^2/s for all the three reactor geometries under study. The value of diffusion coefficient chosen remained constant during a given simulation. For variable fluid thermo-physical properties case, the convergence could be obtained for limited values of diffusion coefficient, in 5 cases for STR and just in 3 cases each for CTR and CFIR. Varying diffusion coefficient could only be converged for the case of constant fluid thermo-physical properties case.
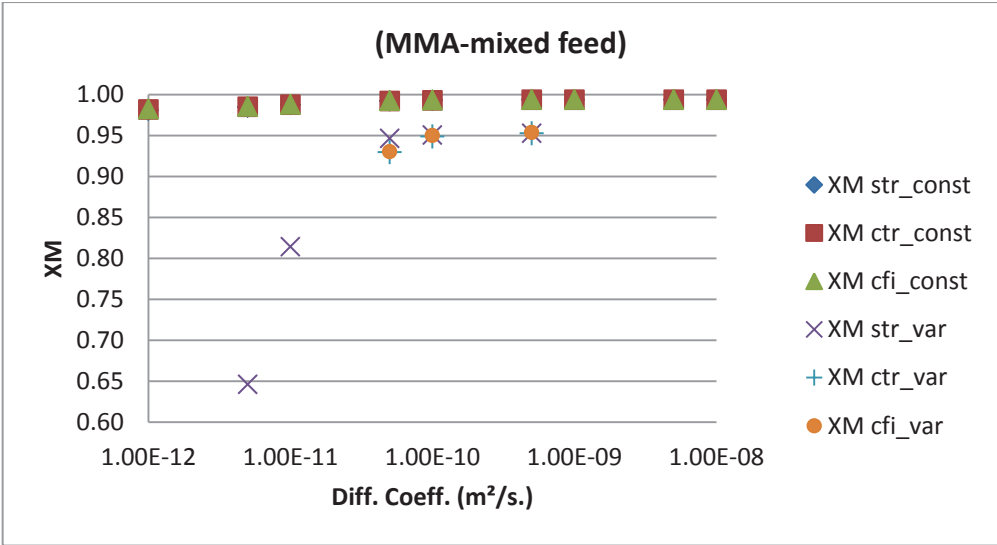
Fig. 5.3-2- Monomer conversion (x_M) results for STR, CTR and CFIR for constant and variable fluid thermo-physical properties.

Fig. 5.3-2 shows some important results. All the three reactor geometries are showing results similar to each other for both cases of constant and variable fluid thermo-physical properties. This can probably be due to mixed feed condition which lowers the requirement for mixing within the reactor compared to unmixed condition as shown in our previous work[4,5] and other published results[2,3]. The values of x_M predicted for the variable fluid properties case are lower compared to the one predicted for constant case. Besides this, for constant physical properties case, the variation in x_M value is not much over the complete range of variation of diffusion coefficient. Contrary to this, for variable fluid thermo-physical properties case, there is a

severe decrease in conversion with decrease in diffusion coefficient. This seems to be more realistic as decrease in diffusion coefficient will decrease mixing. In absence of proper mixing, most of the monomer present in central portion of the flow remains underutilized as it experiences less residence time due to higher velocity in and around center of tube. This clearly establishes the importance of modeling variation in flow properties over constant one.
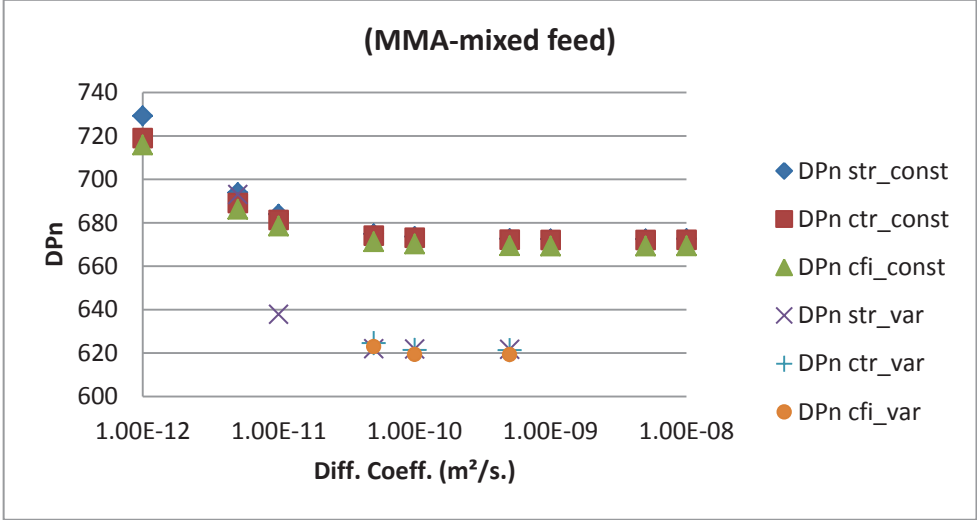
Fig. 5.3-3- DPn results for STR, CTR and CFIR for constant and variable fluid thermo-physical properties.

Fig. 5.3-3 shows the results for DPn and exhibits qualitatively similar results as for Fig. 5.3-2 except that DPn increases as diffusion coefficient decreases. In FRP, DPn decreases with increasing monomer conversion. Decreased diffusion coefficient had decreased monomer conversion also as seen in Fig. 5.3-2. So, lower conversion due to lower diffusion coefficient made DPn to rise. Here again the prediction for DPn are lower in case of variable properties case compared to constant properties case.
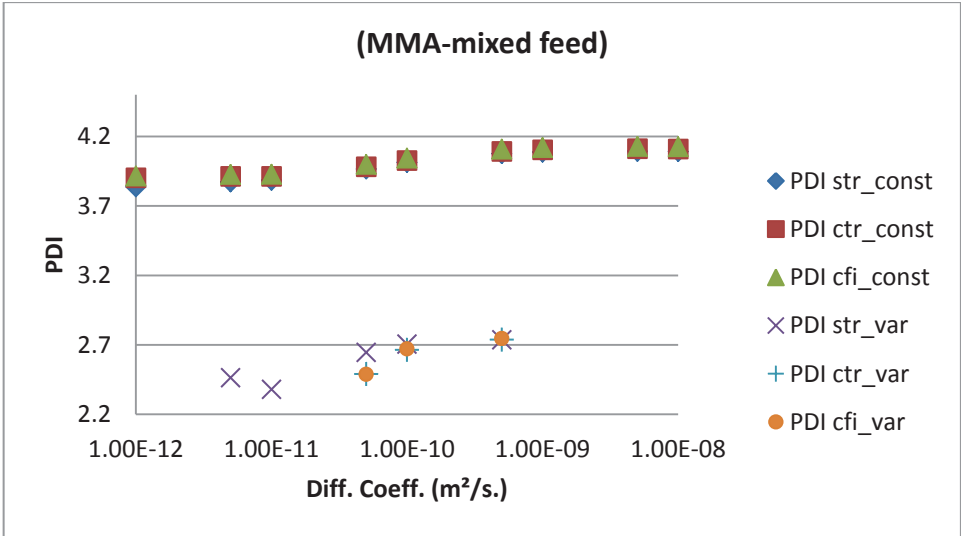
Fig. 5.3-4- PDI results for STR, CTR and CFIR for constant and variable fluid thermo-physical properties.

Fig. 5.3-4 shows the results qualitatively similar to the ones already shown. Here again the results for all the three reactor geometries match with each other quite well for both the cases of constant and variable fluid thermo-physical properties. The predictions of variable properties case are significantly lower than for the constant property case. *PDI* being one of the most important parameters determining the quality of the polymer product, its realistic prediction is of practical importance and is highly desirable. Besides this, unlike previous results for *DPn*, where the prediction difference was not great for constant and variable properties case, difference here is by about 70%.
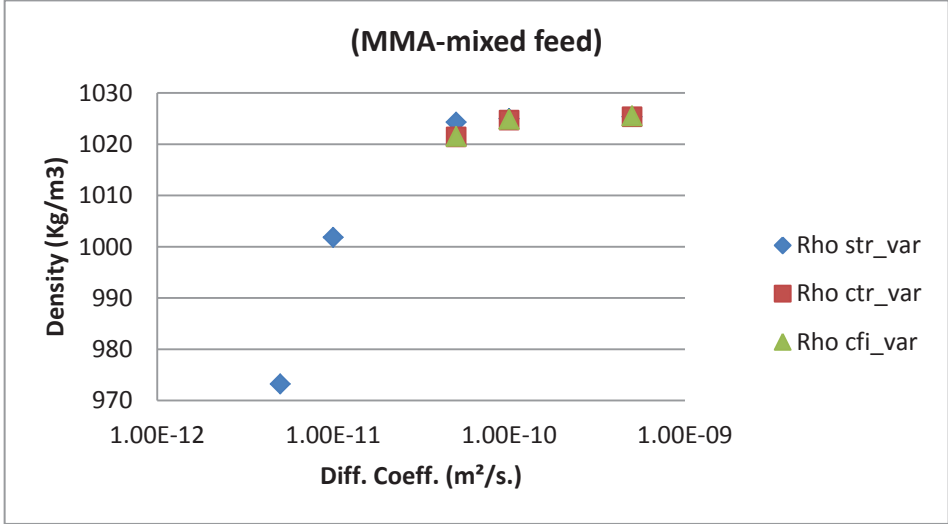
Fig. 5.3-5- Density results for STR, CTR and CFIR for variable fluid thermo-physical properties.

Fig. 5.3-5 shows the variation of density with diffusion coefficient for variable fluid thermo-physical properties case. The increase in density with increase in diffusion coefficient is understandable from the point of view of corresponding conversion as shown in Fig. 5.3-2.
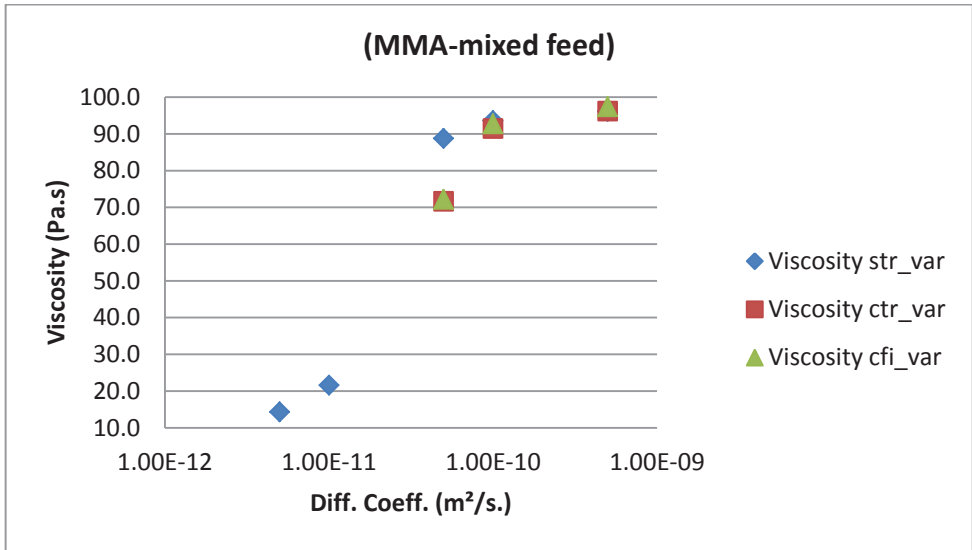
Fig. 5.3-6- Viscosity results for STR, CTR and CFIR for variable fluid thermo-physical properties.

Fig. 5.3-6 shows the results for viscosity variation. This is the most important property in the polymerization reactions which changes by about 4-6 orders for full conversion. Besides this, significant change in viscosity can affect the flow profile as well as thus mixing and heat removal. Viscosity was found to be increased by 6 orders (inlet viscosity at 70°C being equal to $4.38 \times 10^{-4}\ Pa.s$) in our simulations. The viscosity at outlet increases with increase in diffusion coefficient. This is because of increasing conversion and thus more polymer fraction in the system thus higher viscosity. This increases pressure drop across the reactor too. Variation of viscosity, pressure drop and density is shown in Fig. 5.3-7 to Fig. 5.3-9.

Diffusion Coefficient (m²/s)	Viscosity	Pressure drop	Density
5×10^{-11}			
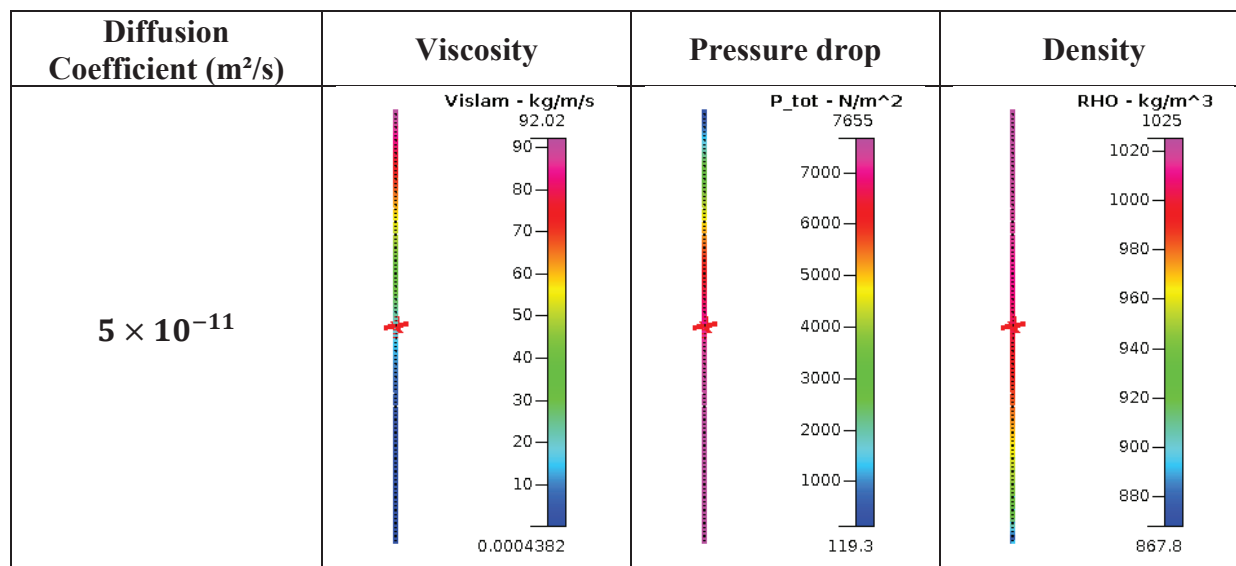
Fig. 5.3-7-Viscosity, pressure drop and density variation throughout the volume of STR

Diffusion coefficient (m²/s)	Viscosity	Pressure drop	density
5×10^{-11}	Vislam - kg/m/s 76.53 70 60 50 40 30 20 10 0.000374	P_tot - N/m^2 5435 5000 4500 4000 3500 3000 2500 2000 1500 1000 500 2.641	RHO - kg/m^3 1022 1020 1000 980 960 940 920 900 880 863.7
1×10^{-10}	Vislam - kg/m/s 94.13 90 80 70 60 50 40 30 20 10 0.000374	P_tot - N/m^2 7899 7000 6000 5000 4000 3000 2000 1000 3.288	RHO - kg/m^3 1025 1020 1000 980 960 940 920 900 880 863.7

Fig. 5.3-8- Viscosity, pressure drop and density variation throughout the volume of CTR

229

Diff. Coeff. (m²/s)	5×10^{-11}	1×10^{-10}
Viscosity		
Pressure drop		
Density		
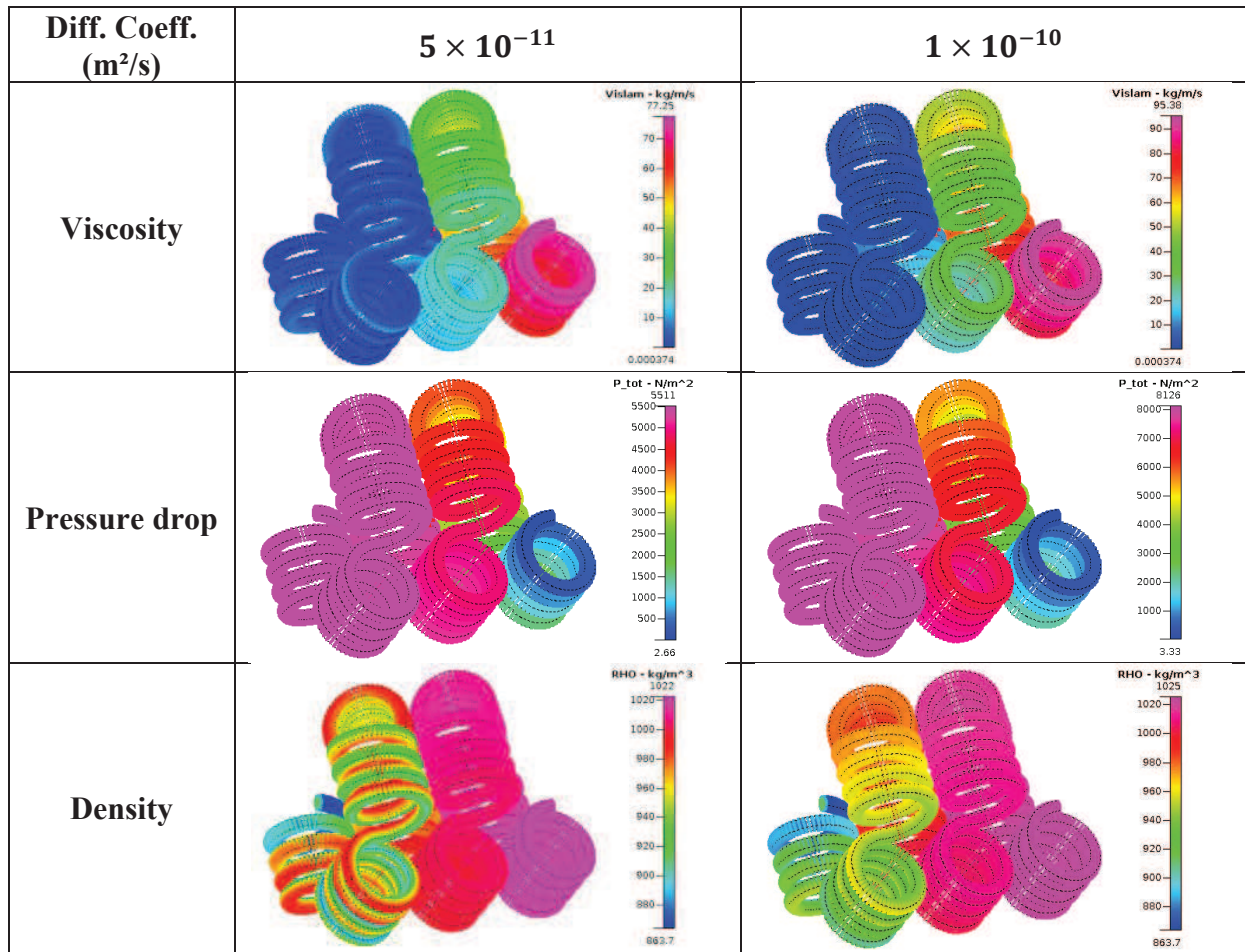
Fig. 5.3-9- Viscosity, pressure drop and density variation throughout the volume of CFIR

The results for variable diffusion coefficient with constant fluid thermo-physical properties are summarized below in Table 5.3-2.

Table 5.3-2-Results for variable diffusion coefficient with constant physical properties.

	STR	CTR	CFIR
x_M	0.905	0.909	0.910
PDI	2.59	2.62	2.62
DPn	693	685	683

Here we can observe that the results for conversion and PDI are more near to the one predicted by using variable fluid thermo-physical properties with discrete variation of diffusion coefficient. Only DPn is predicted higher and more near to constant physical fluid property case. Again the results are nearly same for the three reactor geometries.

Despite huge variation in viscosity and moderate changes in density, no significant variation of thermal conductivity was observed. The temperature variation across the cross section differs only by 0.1 K even after varying fluid thermo-physical properties. Thus truly isothermal condition was observed even during high viscosity variation and density changes. So, modeling thermal conductivity as constant would be good assumption without affecting

any results. However, properties like density and viscosity have significant impact on the results of the simulations as aforementioned.

For visualizing the impact of variation in density and viscosity on flow profile inside reactor, massless tracer particles were used. They were injected at various places uniformly spaced at the inlet. The results are presented for STR, CTR and CFIR.

Particles location

$D = 5 \times 10^{-11} \, m^2/s$, constant

$D = 5 \times 10^{-11} \, m^2/s$, variable
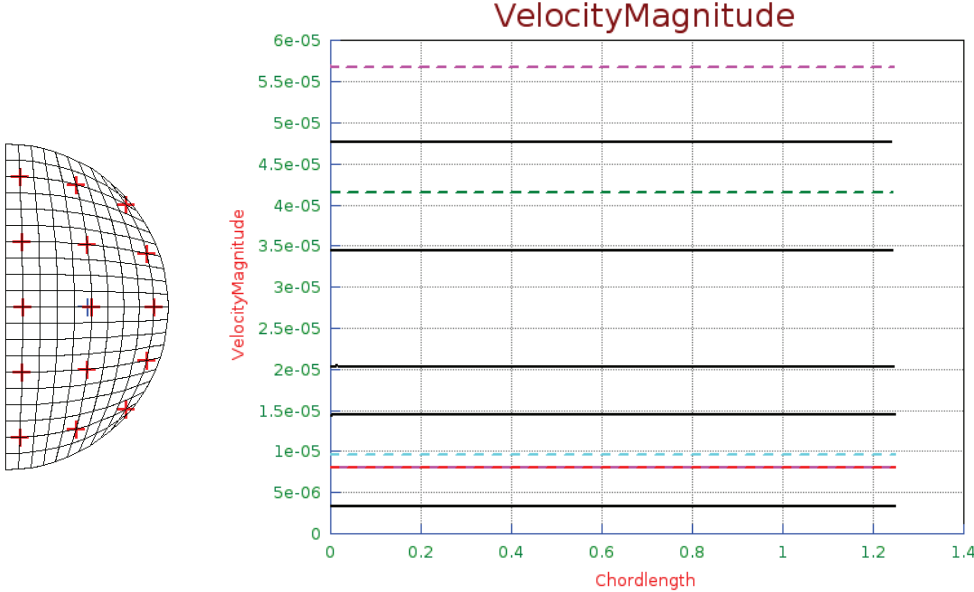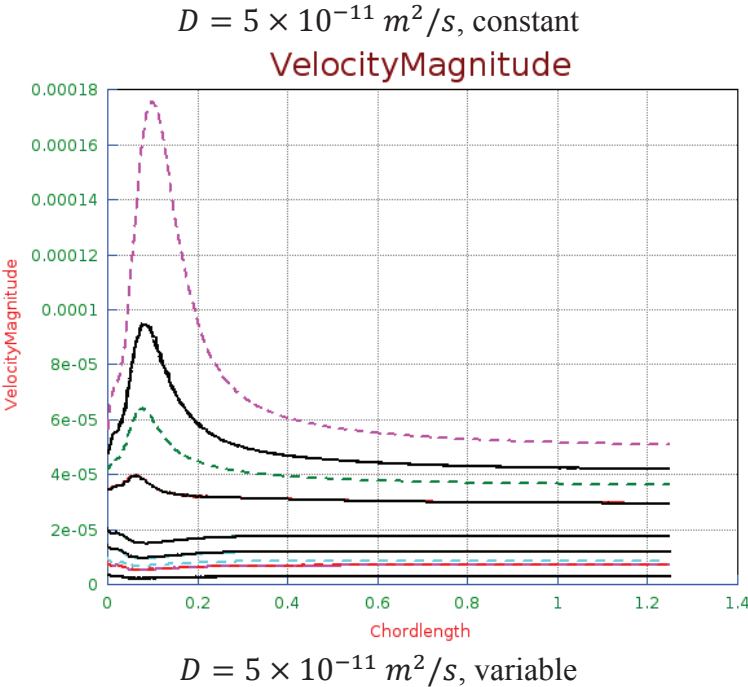
Fig. 5.3-10-Velocity profile of massless tracer particles in STR for constant or variable fluid thermo-physical properties and at a given value of diffusion coefficient.

In Fig. 5.3-10, on x-axis, chord-length represents the distance along the flow from the reactor inlet whereas y-axis represents velocity magnitude of the tracer particle experienced by it at

each point along its trajectory in the flow. Different velocities for different particles are due to parabolic velocity profile imposed at inlet. It can easily be seen that for constant fluid property case, the particles went in straight streamlines as expected. For variable density and viscosity case, the streamlines bends due to variation in density and viscosity as shown in Fig. 5.3-11. This bending of streamlines occurs because of following reason. As the fluid enters the STR, reaction starts. But the residence time is more near the wall due to no-slip boundary condition. This leads to higher conversion near the wall. Thus viscosity and density increases near the wall. This constricts the flowing cross section and hence acceleration for the central flow and deceleration for the flow near the wall initially. Meanwhile at the same cross-section, the reaction mixture sees less residence time and hence less conversion. Due to this, there is less viscosity but as it continues to experience more residence time, conversion increases and thus increases its viscosity and density. This leads to its deceleration. But still there is no mixing due to convective process as no particle crosses other's path.
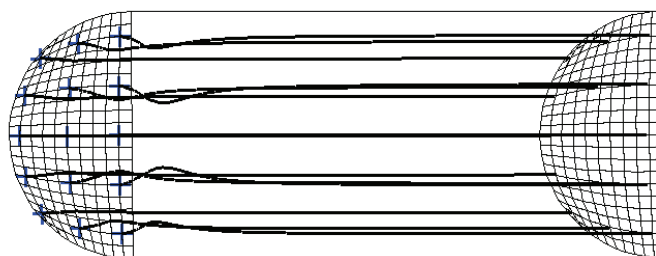
Fig. 5.3-11-Streamlines of tracers in STR variable fluid thermo-physical properties (left is inlet with blue dots for tracers origin and right is outlet of STR)

For CTR and CFIR, such is not the case. In Fig. 5.3-12 for CTR, the velocity profiles for various particles along the flow are quite random for both constant and variable density/ viscosity cases because of secondary flow induced due to curvature. The velocity profile for all the particles narrows down to a small range for constant density/viscosity case. This gets further narrowed down for variable density/ viscosity case. The velocity fluctuations also got lowered for variable density/viscosity case. The streamlines of the tracer particles can be seen in Fig. 5.3-12. Different diffusion coefficients show different velocity profiles. This can be explained as follows. Different conversion is achieved for different diffusion coefficient and thus different viscosity and density present spatially along the flow. Due to no-slip boundary condition, the residence time is higher and thus leads to higher conversion. This increases viscosity near the wall. Along the reactor, this envelop of viscosity increases towards the center from the wall. Thus only a block type flow is there with cross-section being decreased along the flow. This can be observed in Fig. 5.3-13 (b) and (c). The same observation was made by Baillagou et al.[20] too. No particle reached the wall for constant viscosity/density case as no particle reached zero velocity. This implies that particles starting from different positions at inlet do not reach the wall because at wall, the velocity would be zero. Since they are modeled as particles so they cannot move once they reach the wall. But these particles represent volume packets in real flow. So, these particles reaching wall means those volume packets with different residence time will move to wall in real flow. When they will reach

wall, they will displace the volume from there. This will bring another volume packet to main-stream with higher residence time. This, thus, will improve mixing. So the absence of any points reaching wall implies poor mixing near the walls in CTR. For variable density/viscosity case, some particles do reach zero velocity pointing improved mixing. Thus variable density/ viscosity modeling shows improved mixing.

Particles location $\qquad$ $D = 5 \times 10^{-11} \ m^2/s$, constant

$D = 5 \times 10^{-11} \ m^2/s$, variable $\qquad$ $D = 1 \times 10^{-10} \ m^2/s$, variable
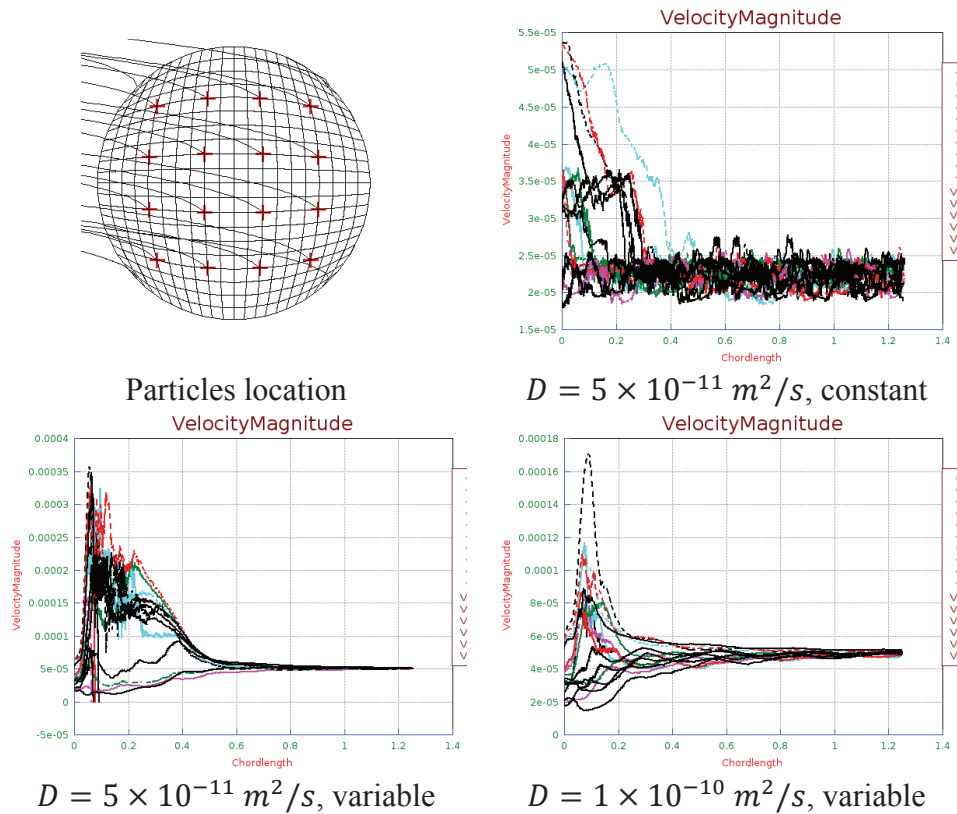
Fig. 5.3-12- Velocity profile of massless tracer particles in CTR for constant or variable fluid thermo-physical properties and at two different values of diffusion coefficient
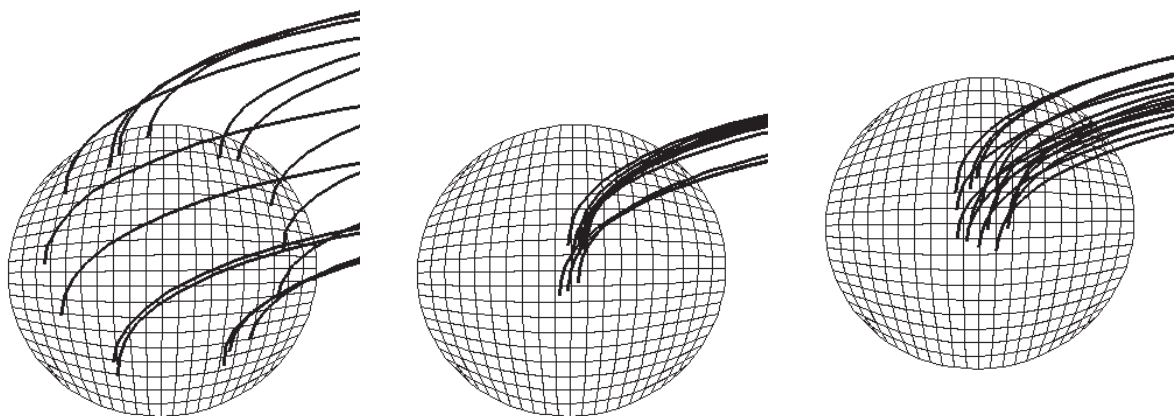
(a) $5 \times 10^{-11} \ m^2/s$, constant (b) $5 \times 10^{-11} \ m^2/s$, variable (c) $1 \times 10^{-10} \ m^2/s$, variable

Fig. 5.3-13-Streamlines of tracers at CTR outlet for a) constant, b) variable, $D = 5 \times 10^{-11} m^2/s$., c), variable, $D = 1 \times 10^{-10} \ m^2/s$. fluid thermo-physical property cases.

For CFIR as shown in Fig. 5.3-14, the results are different compared to CTR. CFIR is a chaotic device[11]. The chaos being introduced by the 90° bend at regular intervals as shown in Fig. 3-1 and Fig. 3-2.

Particles location

$D = 5 \times 10^{-11} \ m^2/s$, constant

$D = 5 \times 10^{-11} \ m^2/s$, variable

$D = 1 \times 10^{-10} \ m^2/s$, variable
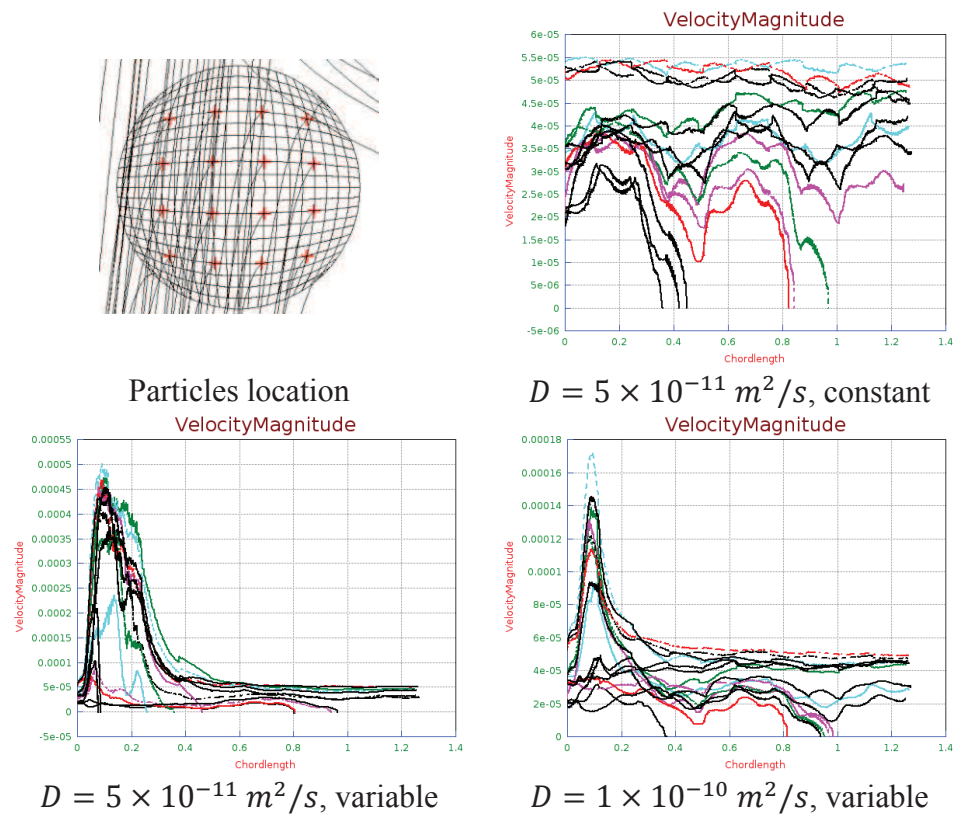
Fig. 5.3-14- Velocity profile of massless tracer particles in CFIR for constant or variable fluid thermo-physical properties and at two different values of diffusion coefficient.
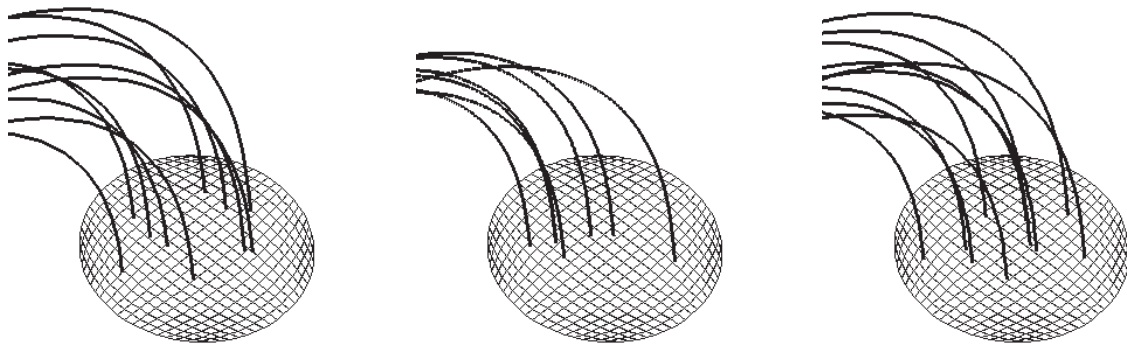
(a) $5 \times 10^{-11} \ m^2/s$, constant   (b) $5 \times 10^{-11} \ m^2/s$, variable   (c) $1 \times 10^{-10} \ m^2/s$, variable

Fig. 5.3-15-Streamlines of tracers at CFIR outlet for a) constant, b) variable, $D = 5 \times 10^{-11} m^2/s.$, c), variable, $D = 1 \times 10^{-10} \ m^2/s.$ fluid thermo-physical property cases..

So, despite having the same location at the inlet as was in CTR, the velocity profile is totally different for different massless tracer particles. Each bend changes the velocity profile despite such a low inlet Reynolds number which decreases along the path in variable density/viscosity case. This is quite remarkable from the fact that due to this phenomenon,

even at such a low Reynolds number and thus low Dean number, more particles reach to the wall starting from first to second bend itself. This points out improved mixing capability of CFIR. Thus less particles reach the outlet as can be seen in Fig. 5.3-15. The number of particles reaching outlet decreased for low diffusion coefficient and increased for high diffusion coefficient as well as for constant fluid properties case.

$$D = 5 \times 10^{-11} \; m^2/s, \text{constant}$$

$$D = 5 \times 10^{-11} \; m^2/s, \text{constant}$$

$$D = 5 \times 10^{-11} \; m^2/s, \text{variable}$$
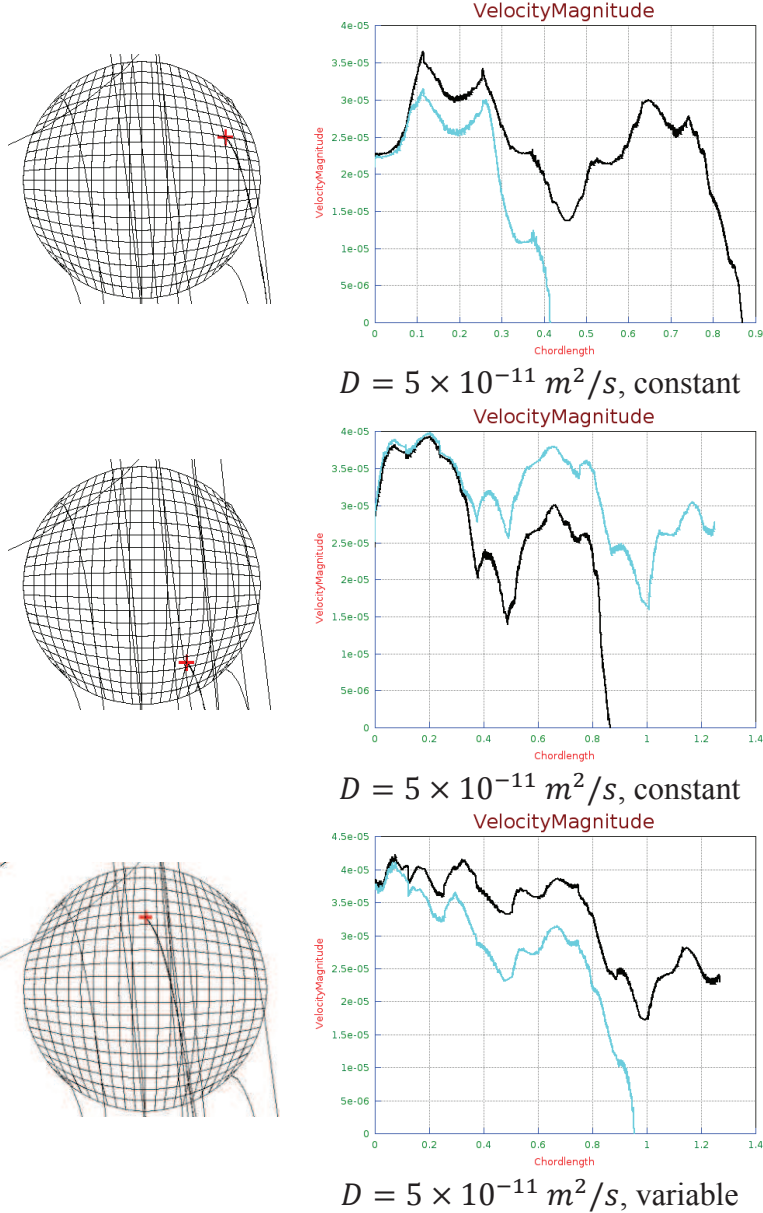
Fig. 5.3-16- Results showing chaotic trend for two nearly spaced particles at CFIR inlet.

In chaotic advection[23-25], two particles, even if they are very close to each other at the beginning start moving along the flow but follow totally different paths ultimately. This has been shown in Fig. 5.3-16 for both constant and variable density and viscosity cases. This is consistent with the published results that a non-viscous 3D flow can be chaotic[23] provided certain conditions are followed. The first column shows the location of the points at inlet whereas the second column shows the velocity profile along the path. For non-chaotic flow, the two massless tracer particles placed very near to each other follow the same path and

hence see almost the same velocity profile. The first row shows the case for constant density/velocity for the two tracer particles reaching the wall at two different distances. In the second, one of them reaches the wall while other reaches the outlet. Same result is shown for variable density/viscosity case in last row.

5.3.13 Conclusion

The effects of variation of fluid thermo-physical properties with discrete variation of diffusion coefficient were studied. Three microreactor geometries were taken with mixed feed condition. One case of varying diffusion coefficient with constant physical properties was also studied. The results were compared and found to have significant differences. The viscosity was found to vary by 6 orders from inlet to outlet after modeling its variation. Under the given condition of reactor dimensions and operating conditions, all three reactors tend to give same results whether fluid thermo-physical properties were kept constant. It was found that constant fluid thermo-physical properties modeling predicted all the desired polymer characteristics at higher values especially *PDI* and X_M compared to the modeling which considers variation in fluid thermo-physical properties. The trend of X_M was also found to be different in both these cases. For the case of varying diffusion coefficient with constant fluid thermo-physical properties, the predictions were near to the one modeling variation in fluid thermo-physical properties except for *DPn*. The variation in thermal conductivity was not found to be significant and hence can safely be assumed constant for all practical purposes. The temperature was also found to be uniform throughout the cross section even for variable density and viscosity condition. Thus, the reaction can safely be assumed to be isothermal under the given dimensions and operating conditions.

The CFIR was also shown to exhibit chaotic effect even at such a low Reynolds number of 0.06 at the reactor inlet. The study clearly established the importance of modeling the flow properties, namely density and viscosity along with diffusion coefficient. CFIR seems to be promising as a microreactor but to evaluate it, a good modeling is required. This should include complete variation of fluid thermo-physical properties with varying diffusion coefficient which may hopefully improve the simulation results further.

5.3.14 References

1. Kim, J. Y.; Laurence, R. L., The mixing effect on the free radical MMA solution polymerization. *Korean J Chem Eng* **1998,** *15* (3), 273-286.
2. Mandal, M. M.; Serra, C.; Hoarau, Y.; Nigam, K. D. P., Numerical modeling of polystyrene synthesis in coiled flow inverter. *Microfluid Nanofluid* **2011,** *10* (2), 415-423.
3. Serra, C.; Schlatter, G.; Sary, N.; Schonfeld, F.; Hadziioannou, G., Free radical polymerization in multilaminated microreactors: 2D and 3D multiphysics CFD modeling. *Microfluid Nanofluid* **2007,** *3* (4), 451-461.
4. Garg, D. K.; Serra, C. A.; Hoarau, Y.; Parida, D.; Bouquey, M.; Muller, R., Numerical investigations of different tubular microreactor geometries for the synthesis of polymers under unmixed feed condition. **2014,** *to be submitted.*

5. Garg, D. K.; Serra, C. A.; Hoarau, Y.; Parida, D.; Bouquey, M.; Muller, R., New Transformation Proposed for CFD Simulation of Free Radical Polymerization. **2014,** *to be submitted.*

6. Hessel, V.; Lowe, H.; Schonfeld, F., Micromixers - a review on passive and active mixing principles. *Chem Eng Sci* **2005,** *60* (8-9), 2479-2501.

7. Kumar, V.; Aggarwal, M.; Nigam, K. D. P., Mixing in curved tubes. *Chem Eng Sci* **2006,** *61* (17), 5742-5753.

8. Berger, S. A.; Talbot, L.; Yao, L. S., Flow in Curved Pipes. *Annu Rev Fluid Mech* **1983,** *15*, 461-512.

9. Dean, W. R.; Hurst, J. M., Note on the motion of fluid in a curved pipe. *Philosophical Magazine Series 7* **1927**, *4*(20), 77-85.

10. White, C. M., Streamline Flow through Curved Pipes. *Proc. R. Soc. Lond. A* **1929**, *123*, 645-663.

11. Saxena, A. K.; Nigam, K. D. P., Coiled Configuration for Flow Inversion and Its Effect on Residence Time Distribution. *Aiche J* **1984,** *30* (3), 363-368.

12. Ramesh, N.; Davis, P. K.; Zielinski, J. M.; Danner, R. P.; Duda, J. L., Application of Free-Volume Theory to Self Diffusion of Solvents in Polymers Below the Glass Transition Temperature: A Review. *J Polym Sci Pol Phys* **2011,** *49* (23), 1629-1644.

13. Vrentas, J. S.; Duda, J. L., Diffusion in Polymer-Solvent Systems .2. Predictive Theory for Dependence of Diffusion-Coefficients on Temperature, Concentration, and Molecular-Weight. *J Polym Sci Pol Phys* **1977,** *15* (3), 417-439.

14. Vrentas, J. S.; Duda, J. L., Diffusion in Polymer - Solvent Systems .1. Re-Examination of Free-Volume Theory. *J Polym Sci Pol Phys* **1977,** *15* (3), 403-416.

15. Mandal, M. M.; Serra, C.; Hoarau, Y.; Nigam, K. D. P., Numerical modeling of polystyrene synthesis in coiled flow inverter. *Microfluid Nanofluid* **2011,** *10* (2), 415-423.

16. Serra, C.; Schlatter, G.; Sary, N.; Schonfeld, F.; Hadziioannou, G., Free radical polymerization in multilaminated microreactors: 2D and 3D multiphysics CFD modeling. *Microfluid Nanofluid* **2007,** *3* (4), 451-461.

17. Garg, D. K.; Serra, C. A.; Hoarau, Y.; Parida, D.; Bouquey, M.; Muller, R., Analytical Solution of Free Radical Polymerization: Derivation and Validation. 2014, *to be submitted*.

18. Keramopoulos, A.; Kiparissides, C., Mathematical Modeling of diffusion-controlled free-radical terpolymerization reactions. *Journal of Applied Polymer Science* **2003,** *88* (1), 161-176.

19. Zielinski, J. M.; Duda, J. L., Predicting Polymer Solvent Diffusion-Coefficients Using Free-Volume Theory. *Aiche J* **1992,** *38* (3), 405-415.

20. Baillagou, P. E.; Soong, D. S., Free-Radical Polymerization of Methyl-Methacrylate in Tubular Reactors. *Polym Eng Sci* **1985,** *25* (4), 212-231.

21. Achilias, D. S.; Kiparissides, C., Toward the Development of a General Framework for Modeling Molecular-Weight and Compositional Changes in Free-Radical Copolymerization Reactions. *J Macromol Sci R M C* **1992,** *C32* (2), 183-234.

22. Brandrup, J., Polymer Handbook. Eds.Brandrup, J. & Immergut, E. H. 1966, Interscience Publishers, New York.

23. Aref, H., Stirring by Chaotic Advection. *J Fluid Mech* **1984,** *143* (Jun), 1-21.

24. Aref, H., Chaotic Advection of Fluid Particles. *Philos T Roy Soc A* **1990,** *333* (1631), 273-288.

25. Aref, H., The development of chaotic advection. *Phys Fluids* **2002,** *14* (4), 1315-1325.

5.4   Chapter Summary

This chapter deals with CFD aspects of modeling and simulation of free radical polymerization (FRP) under flow condition in different tubular microreactor geometries. The geometries under study are straight tube reactor (STR), coil tube reactor (CTR) and coiled flow inverter reactor (CFIR). Section5.1 proposes a new transformation to make all kinetic rate coefficients dimensionless in terms of concentration along with individual chemical species terms. This avoids the data to be fed in mass form and retains the form of data in original molar form. Moreover, the proposed transformation possesses all the advantages of Zhu transformation which allow reducing the stiffness of the set of equations arising from the different chemical species mass balances. The results were obtained using this new transformation and compared with published simulated data under similar conditions and also with experimental data. The new transformation was found to improve the predictions of number-average chain length (DPn), making them near to reality. Thus, the new transformation proposed is more suitable for CFD simulations of FRP. The use of this new transformation was then extended in section-5.2 to study the case of unmixed feed condition for two different microreactor geometries (STR and CFIR) with constant fluid thermo-physical properties and discrete variation of chemical species diffusion coefficients assumed to be same for all species. Results were compared with published results and use of new transformation was found to give higher conversion, DPn and lower polydispersity index (PDI) values. Variation of fluid thermo-physical properties like density, viscosity and thermal conductivity was implemented with discrete variation of variation of diffusion coefficient. Again the results were found to predict higher conversion, DPn and lower PDI compared to constant fluid thermo-physical property case. Convective mixing was also found to increase at lower diffusion coefficient under unmixed feed condition which could not be observed under constant fluid thermo-physical properties conditions. This work was then extended in section-5.3 to mixed feed condition. One more reactor geometry (CTR) was added under study to evaluate the effect of geometry in a better way. A single case of varying diffusion coefficient with constant fluid thermo-physical properties was also carried out. The predictions for variable fluid properties were found to be consistently lower for all the polymer properties like monomer conversion, number-average chain lengths and PDI. The use of varying diffusion coefficient improves the result predictions.

Chapter6   Conclusion and Perspectives

6.1 Conclusion

This thesis aimed at improving modeling and simulation of free radical polymerization (FRP) in batch as well as in flow reactors. These improvements were then used for evaluating three tubular microreactor geometries under different feed conditions at very low Reynolds numbers (1 and below). The modeling for FRP considered successively for constant fluid thermo-physical parameters and their variation with monomer conversion. Resulting effects on simulation results were observed and compared with published experimental data for different monomers. Study of effects of diffusion by varying diffusion coefficient discretely as well as continuously was also performed. The three tubular microreactor geometries included straight tube reactor (STR), coil tube reactor (CTR) and coiled flow inverter reactor (CFIR). The feed condition at microreactor inlet was either considered unmixed or perfectly mixed.. Several monomers from the slower to the faster were considered during this study: styrene (St), methyl methacrylate (MMA) for both batch and flow reactors, butyl acrylate (BuA) and vinyl acetate (VAc) only for batch reactors.

In pursuit of above goals, a generalized explicit analytical solution (AS) of free radical homo-polymerization (FRP) was obtained for the case of variable volume, bulk/solution polymerization, homogeneous and isothermal batch reactor. The reaction steps included initiation, propagation, transfer to monomer, transfer to solvent, transfer to chain transfer agent (CTA), termination by combination and disproportionation. The mathematical model was based on the method of moments. It was found that R_F and $\bar{L}$ appearing in AS for the stage without gel (Phase-I) were similar to the two parameters β and γ^{-1} given by Soh $et\ al.$[1], which affect the gel and glass phase (Phase-II to IV). Furthermore, AS has shown that those two parameters actually affected all the four phases of the reaction and have physical meaning and importance too. Two other parameters, R_L and R_T, appearing naturally in AS were similar to the ones given by Zhu $et\ al.$[2] for the prediction of gel effect. Unlike previously thought, it has also been found that it was only the energy equation which is the actual source of stiffness in the current model without gel/glass effect. It has also been shown why and how much the energy equation was sensitive to temperature variation as well as to time and conversion. AS has been validated against numerical solutions as well as experimental data before the onset of gel effect for four different cases of monomer-polymer systems. This AS explains the reasons why it is easier to correlate and predict MW_n by empirical or semi-empirical methods but same approach fails in predicting MW_w, hence polydispersity index (PDI). The analytical solution required only physical and chemical data of the given monomer/polymer system. There was no correlational adjustable parameter. Only initiator efficiency needed to be adjusted only once to match the experimental data and then remained constant for the monomer/polymer system. AS is quite handy and the only inputs required are time and initial temperature. It can easily be implemented in any computer program or simple excel sheet unlike previous models[3]. This AS has the potential to be used in various practical applications like model based process control, CFD simulations etc.

In its original form, AS was limited in its application to the conversions below gel effect. The practical use of AS could have been extended to full range of monomer conversion after implementing gel and glass effects using Chiu, Carratt & Soong (CCS) model[4]. The time

steps were kept constant during simulation for evaluating AS and they were shown to work well despite the stiffness of the equation. The results thus presented in this work, proved again the superiority of our analytical solution over the one given by Venkateshwaran et al.[3] under the similar conditions of simulating gel effect using CCS model under isothermal condition.

Limitations regarding CCS model were overcame by replacing it with the more evolved Achilias & Kiparissides (AK) model[5] which is a natural extension of CCS model. AK model uses free volume theory for diffusion effects and thus is able to implement cage effect (decrease in initiator efficiency) too. It also incorporates the chain length effect on termination kinetic rate coefficients. The results for AS incorporating AK model were improved in comparison to CCS model and were in good agreement with the experimental data as well as numerical solutions. This exhibited a good flexibility of AS with respect to incorporating explicitly different models of gel/glass and cage effects. We think that it would be possible to improve the results by explicitly incorporating better models as and when available in future or to use our AS for developing new models.

Later AS was used to simulate non-isothermal effects. The conditions involved finite heat transfer rate and adiabatic condition, i.e. no heat transfer. The results were obtained by solving energy balance differential equation which received its inputs from AS when incorporating CCS and AK models. The results were compared with numerical solutions and were in good agreement with published data. With this, AS was finally proved to be better in comparison to earlier work by Ventakeshwaran et al.[3] in all respect.

AS was thus able to demonstrate its versatility, flexibility and usability for the conditions for which it was derived as well as to those for which it was not applicable directly including non-isothermal conditions. By incorporating different models explicitly, AS extended its usage to complete range of conversion.

Then, CFD aspects of modeling and simulation of free radical polymerization (FRP) under flow condition in different tubular microreactor geometries were considered. A new code was written to generate CFIR of any desired characteristic including pitch, number of turns, number of bends etc. it works well for any type of structured mesh like butterfly, square mesh etc.

Integration of chemical reaction with CFD was performed by modeling chemical species as passive scalars and their reaction rates as generation terms. Passive scalar is a massless quantity which does not affect the flow profile. Use of such passive scalars is quite usual in CFD simulations. But all the quantities that are modeled in CFD have to fulfill the law of conservation of mass. So the data corresponding to passive scalars and their generation term need to be fed in mass form. But the data for chemical species (modeled as passive scalars) and their generation terms (reaction rates) are to be found in the form of molar form. Its conversion from molar to mass form poses certain problems and can lead to errors in the simulation results and analysis. A new transformation was proposed to make all kinetic rate coefficients dimensionless in terms of concentration along with individual chemical species terms. This avoids the data to be fed in mass form and retains the form of data in original molar form. The new transformation also kept the original form of equations for generation

terms intact and hence enabled easy coding and debugging. Moreover, this new transformation possesses all the advantages of Zhu transformation in reducing the stiffness of the set of equations[6]. The results were obtained using the new transformation and compared with the published data of Serra *et al.*[7] for STR under similar conditions and also with experimental data for CTR. The new transformation was found to improve the predictions bringing them near to reality. Thus, this new transformation is more suitable for CFD simulations of FRP.

The case of unmixed feed condition to STR and CFIR was taken for study. The new transformation was applied with constant fluid thermo-physical properties and discrete variation of diffusion coefficient to mimic the effect of viscosity. The results were then compared with published results of Mandal *et al.*[7] under similar conditions and significant differences were found between the two. The current work predicted higher conversion and higher number-average chain lengths (DPn) for both STR and CFIR while lower PDI for CFIR. The new results for STR and CFIR clearly demonstrated the superiority of CFIR over STR under unmixed fix condition in controlling the quality of the polymers but with a slightly less monomer conversion compared to STR. Variation of density, viscosity and thermal conductivity were then modeled still keeping the discrete variation of diffusion coefficient. The results were significantly different from the constant fluid thermo-physical properties case. They predicted monomer conversion and DPn on higher side while predicting lower values as well as a different trend for PDI. Again CFIR was found to have a better control compared to STR over polymer characteristics. A special case of increased mixing in the absence of any mechanical mixing in STR at low diffusion coefficient was observed. It was due to flow direction variation arising from of non-uniform viscous effect for unmixed flow condition compounded with low diffusion coefficient. This effect could not be observed in constant fluid thermo-physical properties case. This clearly emphasized the importance of modeling the variation of density and viscosity for FRP in flow reactors for unmixed feed condition. Thermal conductivity variation and temperature variation across the cross-section were found to be negligible. Hence constant thermal conductivity and isothermal condition can be assumed under the microreactor conditions, reducing the complexity of simulations without introducing any significant error in the simulation results.

In the end, the effects of mixed feed condition at the inlet of different microreactor geometries were considered. Here CTR was also included to observe the effect of the gradual variation in geometry over various parameters of polymerization. Strategy similar to unmixed feed conditions was conducted, i.e. one case with constant fluid thermo-physical properties and another with variable properties both with discrete variation of diffusion coefficient. Again the results were found to be different for the two cases. Variable fluid thermo-physical properties case predicted lower values of all the polymer characteristics like monomer conversion, DPn and PDI. The trend of monomer conversion was also found to be different in both cases. For the case of constant fluid thermo-physical properties, monomer conversion remained almost constant throughout the variation of diffusion coefficient whereas for the case of variable fluid thermo-physical properties, it decreased with the decrease in diffusion coefficient. All the three reactor geometries gave similar results to each other under both

conditions of constant and variable fluid thermo-physical properties. One simulation of varying diffusion coefficient using free volume theory was made. Its results were near to variable fluid properties case except for *DPn*. Again variations in thermal conductivity and temperature were found to be negligible and hence can be assumed to be constant for mixed feed condition. CFIR was shown to demonstrate chaotic advection even at such a low Reynolds numbers of $O(0.1)$ for both viscous and non-viscous flow.

Thus clear improvements in CFD simulations were made by using the new transformation. Importance of modeling variation in density and viscosity for mixed and unmixed feed condition was demonstrated. One simulation of modeling variation in diffusion coefficient was also made mimicking the real behavior of chemical species diffusion to some extent. CFIR seems to be a promising reactor design under microreaction conditions.

6.1.1   References

1. Soh, S. K.; Sundberg, D. C., Diffusion-Controlled Vinyl Polymerization .1. The Gel Effect. *J Polym Sci Pol Chem* **1982,** *20* (5), 1299-1313.
2. Zhu, S.; Hamielec, A. E., Gel Formation in Free-Radical Polymerization Via Chain Transfer and Terminal Branching. *J Polym Sci Pol Phys* **1994,** *32* (5), 929-943.
3. Venkateshwaran, G.; Kumar, A., Solution of Free-Radical Polymerization. *Journal of Applied Polymer Science* **1992,** *45* (2), 187-215.
4. Chiu, W. Y.; Carratt, G. M.; Soong, D. S., A Computer-Model for the Gel Effect in Free-Radical Polymerization. *Macromolecules* **1983,** *16* (3), 348-357.
5. Achilias, D. S.; Kiparissides, C., Development of a General Mathematical Framework for Modeling Diffusion-Controlled Free-Radical Polymerization Reactions. *Macromolecules* **1992,** *25* (14), 3739-3750.
6. Zhu, S. P., Modeling of molecular weight development in atom transfer radical polymerization. *Macromol Theor Simul* **1999,** *8* (1), 29-37.
7. Serra, C.; Schlatter, G.; Sary, N.; Schonfeld, F.; Hadziioannou, G., Free radical polymerization in multilaminated microreactors: 2D and 3D multiphysics CFD modeling. *Microfluid Nanofluid* **2007,** *3* (4), 451-461.
8. Mandal, M. M.; Serra, C.; Hoarau, Y.; Nigam, K. D. P., Numerical modeling of polystyrene synthesis in coiled flow inverter. *Microfluid Nanofluid* **2011,** *10* (2), 415-423.

6.2 Perspectives

6.2.1 Modeling of simultaneous variation of density and viscosity with diffusion coefficient

It is hoped that the modeling of diffusion coefficient variation with simultaneous variation in fluid thermo-physical properties will further improve the results. But it requires much finer meshing to get the simulations converged and higher computational power and time. With this also comes the problem of tuning various relaxation parameters for various variables to make the simulations converged as well as to speed up the convergence. Its validation with experimental data will also be required.

6.2.2 Modeling of gel, glass and cage effect

Once the above mentioned goal is achieved, the next step would be to incorporate gel, glass and cage effect using AK model. This will bring the simulations much near to reality. But it will pose several problems related to convergence, stability and related meshing fineness of the grid, that needs to be tackled. Its validation with experimental data needs to be done at the end.

6.2.3 Optimization of CFIR microreactor

CFIR has been shown to be a promising microreactor design. It has also been shown to have chaotic advection. Chaotic advection is a very important type of flow as it improves mixing without any additional energy requirement unlike turbulent flows. Thus, CFIR geometry, i.e. pitch, number of bends, number of coils in between each bend, curvature ratio etc., needs to be optimized for increasing chaotic flow using the above developments made. The code developed in this thesis to generate CFIR of any characteristic will be very useful to generate different variations in design and their respective simulations. The conditions under which optimizations can be sought may vary from types of monomer and operating conditions (i.e. Reynolds number, temperature, feed condition etc.).

6.2.4 Extension to other polymerization methods

As closely related, this work should be easily extended to controlled/'living' radical polymerization methods (ATRP, NMP, RAFT). These methods offer an unique chemical advantage for controlling polymer characteristics as they have been designed to reduce termination rates in order to improve control over molecular weight and molecular weight distribution. Thus it will be probably much interesting to model and simulate such methods in the aforementioned microreactors to combine chemical and process advantages.

Articles

(1) Garg D.K., C.A. Serra, Y. Hoarau, D. Parida, M. Bouquey, R. Muller, Analytical Solution of Free Radical Polymerization, Derivation and Validation. Macromolecules **2014,** *to be submitted.*

(2) Garg D.K., C.A. Serra, Y. Hoarau, D. Parida, M. Bouquey, R. Muller, Analytical Solution of Free Radical Polymerization, Applications- Implementing Gel effect using CCS method. Macromolecules **2014***, to be submitted.*

(3) Garg D.K., C.A. Serra, Y. Hoarau, D. Parida, M. Bouquey, R. Muller, Analytical Solution of Free Radical Polymerization, Applications- Implementing Gel effect using AK Model. Macromolecules **2014***, to be submitted.*

(4) Garg D.K., C.A. Serra, Y. Hoarau, D. Parida, M. Bouquey, R. Muller, Analytical Solution of Free Radical Polymerization, Applications- Implementing Non-isothermal Effect. Macromolecules **2014***, to be submitted.*

(5) Garg D.K., C.A. Serra, Y. Hoarau, D. Parida, M. Bouquey, R. Muller, New transformation proposed for CFD simulation of free radical polymerization. Microfluid Nanofluid **2014***, to be submitted.*

(6) Garg D.K., C.A. Serra, Y. Hoarau, D. Parida, M. Bouquey, R. Muller, Numerical investigations of different tubular microreactor geometries for the synthesis of polymers under unmixed feed condition. Microfluid Nanofluid **2014***, to be submitted.*

*(7) Garg D.K., C.A. Serra, Y. Hoarau, D. Parida, M. Bouquey, R. Muller, Numerical investigations of perfectly mixed condition at the inlet of free radical polymerization tubular micoreactors of different geometries**. Microfluid Nanofluid* **2014***, to be submitted.*

Conferences

Oral Communications

1. Dhiraj K. Garg, Yannick Hoarau, C. Serra, Numerical modeling of polymerisation reaction in CFI, CFM 2011, XXème Congrès Français de Mécanique, 28 août - 02 sep 2011, Besançon, France.

2. D.K. Garg, Y. Hoarau, C.A. Serra, D. Parida, Numerical investigations of different microreactor geometries for the synthesis of polymers, CHISA 2012, 20th International Congress of Chemical and Process Engineering, 25-29 août 2012, Prague, Czech Republic.

3. D.K. Garg, Y. Hoarau, C.A. Serra, D. Parida, Numerical modeling of polymerization reactions in different tubular microreactor geometries, ISCRE22, 22nd International Symposium on Chemical Reaction Engineering, 02-05 sep 2012, Maastricht, The Netherlands.

4. D.K. Garg, Y. Hoarau, C.A. Serra, D. Parida, Flow improving polymerisation reactions in coil flow inverter, EFMC9, 9th European Fluid Mechanics Conference, 09-13 sep 2012, Rome, Italy.

5. D.K. Garg, Y. Hoarau, C.A. Serra, D. Parida, Numerical simulation of polymerization reactions in tubular microsystems: effect of reactor geometry, WPPRE 2012, 1st Working Party on Polymer Reaction Engineering, 11-13 oct 2012, Lyon, France.

6. D.K. Garg, Y. Hoarau, C.A. Serra, D. Parida, Analytical solution of FRP for constant volume, isothermal, well mixed batch reactor and its application, WPPRE 2013, 2nd Working Party on Polymer Reaction Engineering, 24-26 mai 2013, Hamburg, Germany.

7. D.K. Garg, Y. Hoarau, C.A. Serra, D. Parida, Derivation of analytical solution for the Free Radical Polymerization reaction conducted in a constant volume, isothermal, well mixed batch reactor and its applications to CFD modeling, WCCE9, 9th World Congress of Chemical Engineering, 18-23 août 2013, Seoul, South Korea.

Posters

1. Dhiraj Garg, Y. Hoarau, C. Serra, D. Parida, Numerical modeling of polymerisation reactions in straight tube and coiled flow inverter (CFI) Reactors, SoMaS 2011, Summer school in soft matter, 10-15 juillet 2011 Mittelwihr, France.

2. D. Parida, C.A. Serra, Y. Hoarau, D.K. Garg, Improvement of the control of polymer architechtures by means of a coil flow inverter microreactor, ISCRE22, 22nd International Symposium on Chemical Reaction Engineering, 02-05 sep 2012, Maastricht, The Netherlands.

3. D.K. Garg, Y. Hoarau, C.A. Serra, D. Parida, Analytical solution of FRP for constant volume, isothermal, well mixed batch reactor and its application, 11th Workshop on Polymer Reaction Engineering, 21-24 mai 2013, Hamburg, Germany.

Awards
ISCRE Poster Award for poster titled, "Improvement of the control of polymer architechtures by means of a coil flow inverter microreactor" authored by D. Parida, C.A. Serra, Y. Hoarau, D.K. Garg, ISCRE 22, 22nd International Symposium on Chemical Reaction Engineering, 02-05 sep 2012, Maastricht, The Netherlands.

Dhiraj Kumar GARG

Numerical modeling and simulation of polymerization reactions in Coiled Flow Inverters

Résumé

L'objectif de ce travail fut d'améliorer la modélisation et la simulation de la polymérisation radicalaire dans des réacteurs continus et discontinus. Une solution analytique explicite généralisée (AS) fut obtenue dans le cas de la polymérisation en masse/solution, homogène et isotherme menée dans un réacteur fermé de volume variable. Les différentes étapes considérées furent l'initiation, la propagation, le transfert au monomère, au solvant, à un agent de transfert de chaîne, la terminaison par combinaison et dismutation. Différents modèles rendant compte des effets de gel, de vitrification et de cage ont également été considérés. AS a été validée avec succès par comparaison avec des solutions numériques et des données expérimentales de la littérature. Par ailleurs, AS a été étendue à des conditions pour lesquelles elle ne fut pas originellement développée comme par exemple des conditions non isothermes. La polyvalence et la flexibilité de AS sur l'ensemble de l'échelle de conversion du monomère furent ainsi démontrées. Ensuite, pour élargir encore plus son champ d'application, AS fut utilisée dans des simulations numériques (CFD). Une nouvelle transformation très simple a été proposée afin d'adimensionnaliser les constantes cinétiques en terme de concentration. Cela a permis de rentrer dans les simulations les données chimiques sous leur forme originale en mole et de faciliter ainsi le codage et le débogage du code de calcul. Cette transformation a ensuite été utilisée pour évaluer trois géométries tubulaires de microréacteur, un réacteur tubulaire droit (STR), à géométrie hélicoïdale (CTR) et à inversion de flux (CFIR), dans des conditions d'alimentation différentes (fluides d'entrée non ou parfaitement mélangés) et à de très faibles nombres de Reynolds (<1). La modélisation a été réalisée avec des paramètres constants ou variables des propriétés physiques du fluide sous écoulement (densité, viscosité et conductivité thermique) ainsi qu'en variant de manière discrète les coefficients de diffusion. Leurs effets sur les résultats de simulation ont été observés et comparés avec les données expérimentales publiées pour 4 monomères différents et furent en très bon accord. Les résultats pour le cas d'un mélange parfait furent indépendants de la géométrie des microréacteurs. Le CFIR semble être le réacteur le plus prometteur puisque, dans les conditions de microréaction étudiées, il a permis le meilleur contrôle des caractéristiques du polymère synthétisé.

Mots-clés : polymérisation radicalaire, modélisation, solution analytique, simulation, microréacteur, inversion de flux, modèle CCS, modèle AK, mécanique des fluides numérique

Abstract

This thesis aimed at improving the modeling and simulation of free radical polymerization (FRP) in batch as well as in flow reactors. A generalized explicit analytical solution (AS) was obtained in case of variable volume, bulk/solution polymerization, homogeneous and isothermal batch reactor. The reaction steps included initiation, propagation, transfer to monomer, transfer to solvent, transfer to chain transfer agent (CTA), termination by combination and disproportionation. Different models of gel, glass and cage effects were also implemented explicitly. AS was validated against numerical solutions as well as published experimental data and was found in good agreement. Furthermore, its applicability was extended to conditions for which AS was not derived, i.e. non-isothermal conditions. The versatility and flexibility of AS over the complete range of monomer conversion were thus demonstrated. Then, to broaden its applications range even more, AS was used in CFD simulations. A new and simple transformation was proposed to make kinetic rate coefficients dimensionless in terms of concentration. This enabled chemical data to be fed in molar form to CFD modeling. It also enabled easy coding and debugging by keeping the original form of generation terms intact. The results were found to be improved after validation against experimental data. This transformation was then used for evaluating three tubular microreactor geometries, namely straight tube reactor (STR), coiled tube reactor (CTR) and coil flow inverter reactor (CFIR), under different feed conditions (unmixed or perfectly mixed) at very low Reynolds numbers (<1). The modeling for FRP was performed with constant or variable fluid physical parameters (density, viscosity and thermal conductivity) along with discrete variation of diffusion coefficients. Their effects on simulation results were observed and compared with published experimental data for 4 different monomers and were found to match perfectly. Results for mixed feed condition were found to be independent of microreactor geometry. CFIR seems to be the most promising reactor design under microreaction investigated conditions as it allowed the best control over polymer characteristics.

Keywords: free radical polymerization, modeling, analytical solution, simulation, microreactor, coil flow inverter, CCS model, AK model, CFD